TURBULENCE AND TURBULENT TRANSPORT IN SEDIMENT-LADEN OPEN-CHANNEL FLOWS

by

Dennis Anthony Lyn

W. M. Keck Laboratory of Hydraulics and Water Resources
Division of Engineering and Applied Science
CALIFORNIA INSTITUTE OF TECHNOLOGY
Pasadena, California

Report No. KH-R-49

December 1986

Turbulence and Turbulent Transport in Sediment-laden Open-Channel Flows

by

Dennis Anthony Lyn

Project Supervisor:

Norman H. Brooks
James Irvine Professor of
Environmental and Civil Engineering

Supported by

The National Science Foundation (Grants CEE-7920311, MSM-8611127)
James Irvine Professorship

W. M. Keck Laboratory of Hydraulics and Water Resources
Division of Engineering and Applied Science
California Institute of Technology
Pasadena, California

Report No. KH-R-49 December 1986

Copyright ©1986 by Dennis A. Lyn
All rights reserved

Acknowledgements

A number of people have contributed, directly or indirectly, to the work reported here. Prof. N.H. Brooks, my advisor, suggested the general field of sediment transport as an impossible area of research, instantly seducing the innocent, and generally allowed me the freedom to go on my own wild goose chases. Vito Vanoni provided constant encouragement even when he was not, perhaps, in total agreement with all of my ideas. Jim Skjelbreia, Dimitri Papantoniou, and Panos Papanicolaou helped signally in the areas involving instrumentation, data acquisition and computing hardware. The presence of Peter Goodwin, my co-conspirator in sediment-transport intrigues, substantiated my suspicion that somebody else besides myself was still interested in sediment-transport research. Cathy van Ingen got me started on the nuts-and-bolts of experimental work, and bequeathed the essential data acquisition software. Comments on an early draft of some of the ideas in Chap. 3 by Profs. D. Coles and J. Imberger were also useful. The general critique of Prof. J. List should also be acknowledged. The artisans of the Hydraulics Lab shops, Elton Daly, Rich Eastvedt, Joe Fontana, and Leonard Montenegro, facilitated experimental work, not only by their technical prowess, but also by their agreeable character. Jeff Zelt, my fellow Canadian, introduced me to the beauties of TEX, thereby delaying the completion of this document by, at least, a couple of years.

A possibly harrowing experience was made certainly bearable, at times pleasurable, by those with whom I came into daily contact (in addition to those already noted above): Joan (pronounced Jo-anne) Mathews, Rayma Harrison, Gunilla Hastrup, Bob Koh, Jin Jwang Wu, Liyuan Liang, Chi Kin Ting, Imad Hannoun, and of course my office mates, the departed Pratim Biswas and the still (and for

some time to come) present Kit Yin Ng (pronounced ?).

Financial support for the work reported here was provided by the National Science Foundation through grant CEE-7920311 until 1983, and grant MSM-8611127 for 1986, and by discretionary funds from the James Irvine Professorship. The author received personal support during the period 1981-82 in the form of a Haagen-Smit/Tyler Fellowship, and during the period 1982-85 from the National Science and Engineering Research Council of Canada in the form of post-graduate fellowships. This report is essentially identical to the thesis submitted by the author in September, 1986 in partial fulfillment of the requirements for the degree of Doctor of Philosophy.

Lastly, I would like to dedicate this work to my mother, whose example of stoicism and perseverance stood me in good stead during the frustrations of research.

This report was submitted to the California Institute of Technology
in December 1986 as a thesis in partial fulfillment of the requirements
for the degree of Doctor of Philosophy in Environmental Engineering Science.

Table of contents

Abstract

Some aspects of turbulence in sediment-laden open-channel flows are examined. A conceptual model based on similarity hypotheses rather than the traditional mixing-length closures is proposed. It is argued that, over a wide range of laboratory conditions, the main effect of the suspended sediment on the flow is confined to a layer near the bed. *If* such a distinct layer can be discerned, then this is separated from the outer flow by an inertial subregion in which the mean-velocity profile is approximately logarithmic, with an associated von Kàrman constant of ≈ 0.4, i.e., the *same* value as in single-phase flows. It is further shown that power-law profiles may be derived from general similarity arguments and asymptotic matching. These implications contrast with those of previous models in which changes in the mean-velocity profile are supposed to occur throughout the flow or primarily in the flow far from the bed. Length and concentration scales appropriate to sediment-laden flows are suggested.

An experimental study was also undertaken. Both the saturated case, in which a sand bed was present, and the unsaturated case, in which a sand bed was absent, were investigated. The study was restricted to nominally flat beds, composed of three well sorted sands (median grain diameters ranged from 0.15 mm to 0.24 mm). A two-component laser-Doppler-velocimetry system was used for velocity measurements. Suction sampling was used to measure local mean concentrations. The major points of the conceptual model are supported by the experimental results. Higher-order statistics of the velocity field were found to exhibit little evidence of any effect on the outer flow, supporting the view that the effect of the suspended sediment is felt primarily in the inner region. This contrasts with the predictions of recent models that propose an analogy between sediment-laden flows and weakly stable density-stratified flows.

List of Tables

List of figures

Notation

Symbol	Definition
	Roman symbols
a	reference point in Rouse suspended-load profile
b	width of flume
$B_i,\ B_o$	additive constants in inner and outer log-law
$c,\ \langle c \rangle$	local mean concentration, depth-averaged concentration
$c_a,\ c_0$	mean concentration at a reference point, y = a, and at the bed, y = 0
$c_h,\ c_s$	outer and inner concentration scales
$c_{s\infty}$	general function of w_{s0}/u_*, an asymptotic form of c_s
$-\overline{c'v'}$	net upwards flux of sediment due to turbulent transport
$C_1,\ C_1',\ C_2,\ C_3$	integration constants
$d,\ d_{50}$	median grain diameter
E	estimate of sample statistic for any length of averaging time
E_∞	estimate of true statistic for an infinite averaging time
ΔE	relative error in estimate of sample statistic
$\mathcal{E}$	general function of w_{s0}/u_* associated with the concentration profile in the intermediate region
$\mathcal{E}_h$	general function of w_{s0}/u_* associated with the outer concentration scale
$\mathcal{E}_s$	general function of w_{s0}/u_* associated with the inner concentration scale
f	general inner similarity solution
$f_1,\ f_2$	functions of only a single variable, used in separation of variables
f_D	estimate of friction factor, $8u_*^2/\langle u \rangle^2$
$\langle\langle f_D \rangle\rangle$	estimate of friction factor, $8gr_hS/\langle\langle u \rangle\rangle^2$

$\langle\langle f_D \rangle\rangle_{sw}$	same as $\langle\langle f_D \rangle\rangle$, but incorporating a sidewall correction (Brooks, 1954)
$(f_D)_B$	friction factor for equilibrium-bed upper regime flows predicted from a formula of Brownlie (1981)
$(f_D)_{cw}$	friction factor for a corresponding clear-water flow with the same $Re = 4\langle u \rangle r_h/\nu$ and relative roughness, $d_{50}/4r_h$
F	general outer similarity solution
Fr	Froude number, $\langle u \rangle/\sqrt{gh}$
F_u, F_v	normalized power spectrum of horizontal and vertical velocity fluctuations
$\mathcal{F}_1$, $\mathcal{F}_2$	general relations between dimensional variables
g	gravitational constant
h	depth of flow
H	hole size, used in quadrant analysis (appendix A.1)
J	quadrant (1,2,3,or 4) in $u' - v'$ plane
k	characteristic height of roughness elements
k_1	one-dimensional wavenumber related to the frequency, n, by $k_1 = 2\pi n/u$
l	general inner length scale
l_K	Kolmogorov length scale, $(\nu^3/\varepsilon)^{1/4}$
l_m	mixing-length
l_s	inner length scale specific to sediment-laden flows
l_ν	viscous length scale, ν/u_*
L_C	length scale implicit in bulk Richardson number of Coleman (1981), $u_*^2/g(s-1)c_0$
L_s	Monin-Oboukhov length scale defined by Itakura and Kishi (1980), $u_*^3/\kappa w_s g(s-1)\langle c \rangle$
$\mathcal{L}$	general outer length scale
n	frequency coordinate of power spectrum
P	local mean pressure
P_f, P_s	power parameters used in Einstein-Chien correlation
Q	bulk discharge of flow
q_*	constant boundary heat flux in the atmospheric surface layer
r	general dependent variable
r_h	hydraulic radius

r_*	general scale for the dependent variable, r
r_ξ, r_η	inner and outer scales for the dependent variable, r
$\langle R_s \rangle$	a Richardson number for sediment-laden flows based on depth-averaged quantities, h/L_s
Ri_C	bulk Richardson number defined by Coleman (1981), $y_{\max}/L_C$
Re	appropriate Reynolds number, usually $4\langle u \rangle r_h/\nu$
Re_k	roughness Reynolds number, $u_* k/\nu$
Re_*	Reynolds number based on shear velocity, $u_* h/\nu$
s	relative density of the sediment
S	bed slope
t	time coordinate
Δt	the mean time between velocity realizations by the LDV system
$(\Delta t)_I$	the mean time used in regularly sampling the linearly interpolated signal derived from the original LDV data
T	temperature
T_*	temperature scale used in Monin-Oboukhov theory of the atmospheric surface layer
$-T'v'$	turbulent heat flux in Monin-Oboukhov theory
T_{avg}	averaging time for statistics
$\mathcal{T}$	operator used in matching argument
u, $\langle u \rangle$, $\langle\langle u \rangle\rangle$	local, depth-averaged, area-averaged velocity
$\tilde{u}'$	instantaneous horizontal velocity
$u_{\max}$	maximum local mean velocity
u_s	velocity parameter used to collapse velocity profile
u_*	shear velocity
$\sqrt{u'^2}$	root mean square of horizontal velocity fluctuations
$u'^3/(\sqrt{u'^2})^3$	skewness of the horizontal velocity fluctuations
$u'^4/(\sqrt{u'^2})^4$	flatness of the horizontal velocity fluctuations
$(u'^2)_I$, $(v'^2)_I$	mean square of the horizontal and vertical velocity fluctuations, computed from the linearly interpolated, regularly sampled time series derived from the original time series
$-u'v'$	kinematic Reynolds stress
$[u'v']_J$	contribution of velocity fluctuations in the J^{th} quadrant to the Reynolds stress

$\sqrt{(u'v')'^2}$	root mean square of the Reynolds stress fluctuations
$(u'v')'^3/(\sqrt{(u'v')'^2})^3$	skewness of the Reynolds stress fluctuations
$(u'v')'^4/(\sqrt{(u'v')'^2})^4$	flatness of the Reynolds stress fluctuations
v	mean vertical velocity
$\tilde{v}'$	instantaneous vertical velocity
$\sqrt{v'^2}$	root mean square of vertical velocity fluctuations
$v'^3/(\sqrt{v'^2})^3$	skewness of the vertical velocity fluctuations
$v'^4/(\sqrt{v'^2})^4$	flatness of the vertical velocity fluctuations
$\sqrt{w'^2}$	root mean square of the lateral velocity fluctuations
w_s	settling velocity of sediment in a turbulent suspension
w_{s0}	settling velocity of an isolated particle in a stagnant fluid, defined by a standard drag curve
W_0	wake coefficient for the velocity profile
W_c	general wake function for the concentration profile
W_{c0}	restricted wake function for the concentration profile
x	streamwise coordinate
y	vertical coordinate
$y_{\max}$	point at which the maximum mean velocity, u_{mqx}, occurs
y^+	vertical coordinate scaled by the viscous length scale, y/l_ν
Δz	deviations from the mean bed elevation
Z	exponent in the concentration power-law
Z_R	Rouse exponent in suspended-load profile
Z_h	exponent in the wake-component of the concentration profile

Greek symbols

$\hat{\alpha}$	dimensionless parameter important in both the inner and outer region with respect to the velocity profile
$\alpha_i,\ \alpha_o$	dimensionless parameters important only in either the inner or the outer region with respect to the velocity profile

β_i, β_o	dimensionless parameters important only in either the inner or the outer region with respect to the concentration profile
$\hat{\beta}$	dimensionless parameter important in both the inner and the outer region with respect to the concentration profile
β_s	reciprocal of the turbulent Schmidt number used in traditional eddy-diffusivity models of vertical turbulent transport
γ	ratio of outer to inner length scales, $\mathcal{L}/l$
Δ_s	non-dimensionalized sediment inner length scale, $g(s-1)l_s/u_*^2$
ϵ_s	eddy-diffusivity of vertical sediment transport
ε	rate of dissipation of turbulent kinetic energy
Φ, Φ_1, Φ_2	general functions of a single variable
κ, κ_s	von Kàrman constant in clear-water and in sediment-laden flows
λ_1, λ_2, λ	exponents used in the matching argument
ν	kinematic viscosity
η	outer coordinate
Π	general function of w_{s0}/u_*
Π_h, Π_s	general dimensionless relation for the outer and inner scales
ρ_w, ρ_s, ρ_m	density of water, the sediment, and the mixture
ρ_0, $\rho_{y_{max}}$	density of the water-sediment mixture at the bed and at the elevation, $y = y_{max}$ (used by Coleman (1981))
$\langle\rho\rangle$	depth-averaged density of the suspension
σ	dummy variable
σ_g	geometric standard deviation of grain-size distribution
$\sigma_{\Delta t}$	standard deviation of the time interval between velocity realizations
θ_{ij}	the angles at which the laser beams intersect at the probe volume
τ	mean local shear stress
ξ	inner coordinate
ξ_s	inner coordinates specific to sediment-laden flows
Ξ, Ξ_∞	general and asymptotic functional form of correlation for Δ_s

1. Introduction

Suspended particles are found in large-scale turbulent geophysical flows. In many cases, these particles are of no dynamic significance and the turbulence may be studied independently of the presence of particles. In some cases, notably in flows in natural alluvial channels, the presence of suspended particles may exert a sufficiently strong influence on the flow so as to invalidate its treatment as a passive contaminant. The present work is aimed at examining more closely the interaction between a mostly dilute suspension of sediment with the turbulent flow that transports it. Although the interest is mainly fundamental, this work may have implications for solutions to practical problems in the hydraulics of rivers, reservoirs and estuaries.

Sediment-laden flows pose several problems. A rigorous characterization of multiphase flows is difficult. Their diluteness has raised questions concerning the justification of the traditional continuum description. On the other hand, a kinetic description would seem to present overwhelming difficulties. Compounding the difficulty of treating two phases is the turbulent nature of the flow. A modest aim would be a reliable description of the mean field such as has been achieved for the classic shear flows of a homogeneous fluid. Two coupled fields, the velocity

and the concentration fields, must be considered. This coupling has traditionally been underemphasized even though it must be important if it is believed that the presence of suspended sediment has any significant effect on the turbulent flow. Although its heterogeneity is due to the presence of two phases, the sediment-laden flow, with its vertical variation of sediment concentration, has motivated a recurring analogy to a weakly stable density-stratified flow. Such an analogy is attractive in its intuitive appeal and offers the possibility of exploiting a large literature on stably-stratified turbulent flows.

The concept of asymptotic similarity has been central in the development of useful solutions to problems in turbulent flows but has found little or no systematic application to sediment-laden flows. This may be partly explained by the historical dominance of mixing-length models, carried over from single-phase flow problems. Of probably equal importance, however, is that such solutions are most naturally found in simple flows with a limited number of well-defined length and velocity scales. Sediment-laden flows are not simple in that appropriate scales are not known, or are thought to be too many in number to be reduceable to any simple form. In spite of this, a similarity approach has the advantage of being rather general because it avoids detailed dynamic considerations. This may be particularly desirable in the case of a two-phase flow in which even the correct balance equations may be in dispute.

A number of fundamental questions are prompted by the different aspects of sediment-laden flows. In view of the uncertainties regarding continuum assumptions and the correct equations of motion, can a macroscopic, as against a kinetic, formulation be developed to describe the mean fields? It will be argued that a similarity approach may provide a basis for a macroscopic description which does

not rely on detailed physical models. Also, because it is a turbulent wall-bounded flow, the question of its similarities to and differences from the more well-known homogeneous-fluid flows may be raised. Of particular interest in this regard is the multiple-scales nature that is known to be important for homogeneous-fluid flows. The possibility of a tractable model offered by the analogy to density-stratified flows raises the further question: to what extent, if any, is such an analogy valid for sediment-laden flows? This study will focus on these three questions.

The difficulties posed by sediment-laden flows are not confined to the theoretical or conceptual plane; experimental problems are many, particularly where information regarding the fluctuating field is concerned. Traditional probes such as are used in hot-film-anemometry must be physically delicate in order to satisfy frequency-response requirements. Sediment-laden flows, however, present a harsh environment for which a more robust probe is necessary. In this study, the more recently established laser-Doppler velocimetry (LDV) technique is used. Its optical probe is immune to physical wear, incurs no calibration drift, and is capable of an adequate frequency response. Problems of interpretation of data due to the presence of particles other than tracer particles do accompany this use of the LDV technique. The pragmatic approach taken here has been to interpret the measurements, keeping in mind a possible reduced reliability in regions of high sediment concentration. In such regions, the LDV technique is severely limited in any case because of the attenuation of both incident and scattered light.

In view of the coupled nature of the problem, it would be desirable experimentally to treat the velocity and the concentration fields on an equal footing. Unfortunately, the availability of more sophisticated velocity-measuring instruments results in a disproportionate amount of information on the velocity field

compared to the concentration field. An additional problem associated with the concentration field is the ill-defined nature of fluctuating quantities, a consequence of the uncertainties of the continuum description. This study, in common with previous studies, is limited then to the mean concentration field, which is determined by the traditional suction-sampling technique.

Although it is hoped that this work has implications for river hydraulics, it examines a rather idealized flow. Only flows uniform in the streamwise direction, at least over the working section, are considered. These include both flows in which a sand bed exists in equilibrium with the suspension, i.e., equilibrium-bed flows, and flows in which no such sand bed exists, i.e., starved-bed flows. As interest is on the effect of suspended sediment on turbulence, the equilibrium-bed experiments are restricted to beds that are nominally flat. Although natural sands are used in the experiments, the sands are well sorted, and thus highly uniform in size distribution compared to that typically found in natural channels. The size range is also above that in which cohesion between particles would be important, so that effects of cohesion are not considered.

A critical review of the traditional and the more recent approaches to describing the mean fields is given in Chap. 2. A conceptual framework for thinking about the mean fields in sediment-laden flows is developed in Chap. 3. The ideas of multiple scales, asymptotic matching, and similarity are crucial in this development. Appropriate length, velocity, and concentration scales are suggested.

A description of the apparatus and instrumentation used in the experimental part of this work may be found in Chap. 4. Results of sieve analyses of the sand grains used are also presented. Experimental design is discussed in terms of the type of experiments performed, the constraints limiting the range of experimental

conditions obtainable, and the statistical requirements for representative turbulence characteristics. The procedure followed in performing experiments is also outlined.

Experimental results are presented and discussed in Chaps. 5-7. Both the mean and the fluctuating fields of clear-water flows, i.e., those with no suspended sediment, are considered first. These results form the basis for comparison with results in sediment-laden flows. The results for the mean fields in sediment-laden flows are then considered with interest being centered on the range of validity of the various proposed models. Finally, the fluctuating velocity field, as characterized by its statistics, is examined.

2. Background and literature review

2.1 A review of previous theoretical work

2.1.1 Uniform fully developed open-channel flow without sediment

Consider a steady, turbulent, open-channel, gravity-driven flow of depth, h, uniform in the mean-flow direction (the x-direction), over a smooth surface of infinite extent, inclined at a slope, S. A definition sketch is given in Fig. 2.1.1. The longitudinal momentum equation reduces to

$$\frac{\tau(y)}{\rho_w} = -\overline{u'v'} + \nu\frac{du}{dy} = u_*^2(1 - y/h), \tag{2.1.1}$$

where $\tau(y)/\rho_w$ is the shear stress, $-\overline{u'v'}$ is the Reynolds stress, ν is the kinematic viscosity, u_* is the shear velocity, h is the depth of flow, and ρ_w is the density of water. For convenience, time-averaged quantities will not be denoted with an overbar. In the bulk of the flow, where viscous effects are negligible, the shear stress is primarily carried by the Reynolds stresses, which should then follow a linear profile. The classical solution to the closure problem posed by Eqn. 2.1.1 is the mixing-length hypothesis of Prandtl. This hypothesis relates the fluctuating velocites, $\tilde{u}'$ and $\tilde{v}'$, *and* their correlation, to the mean-velocity gradient and a

length scale, the so-called mixing length, taken to be proportional to the distance from the wall. This leads to a prediction of a logarithmic velocity profile in a region where $-u'v' \approx u_*^2$.

Fig. 2.1.1 Definition sketch

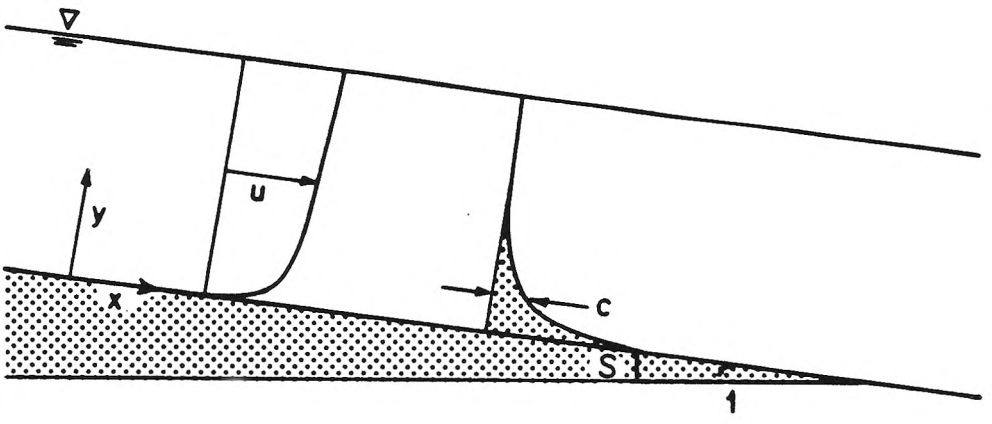

In traditional hydraulics, the logarithmic profile is often held to describe the entire flow field (except in the viscous sublayer) in an open channel. In velocity-defect form, the velocity profile is then described by

$$\frac{u - u_{\max}}{u_*} = \frac{1}{\kappa} \ln \frac{y}{h}, \tag{2.1.2}$$

where κ is a "universal" constant, the von Kàrman constant, with a value in homogeneous flows of ≈ 0.4 (Daily and Harleman, 1966; Schlichting, 1979), and $u_{\max}$ is the maximum mean velocity attained in the flow. A number of workers have more recently argued that, from mixing-length arguments, the logarithmic behavior can be justified only for a restricted region near the bed, e.g., $y/h \leq 0.2$, and

that, for $y/h \geq 0.2$, a correction to the logarithmic function is necessary. Coleman and Alonso (1983) suggested the use of the wake-function that was originally proposed by Coles (1956) to describe turbulent boundary-layer flow. Eqn. 2.1.2 would therefore be revised to

$$\frac{u - u_{\max}}{u_*} = \frac{1}{\kappa}\left[\ln\frac{y}{h} - 2W_0\cos^2\left(\frac{\pi}{2}\frac{y}{h}\right)\right], \tag{2.1.3}$$

where W_0 is the wake coefficient, which should be constant for sediment-free open-channel flows. In the next chapter, an alternate approach, based on multiple scales and asymptotic matching, as distinct from mixing-length arguments, is discussed.

2.1.2 Sediment-laden flows: the mean-velocity profile

Eqn. 2.1.1 is only approximately true for sediment-laden flows. Mean-momentum balance requires that

$$\frac{d\tau}{dy} = -\rho_m(y)gS, \tag{2.1.4}$$

where $\rho_m(y)$ is the local mean density of the fluid-sediment mixture at an elevation, y, and g is the gravitational constant. In terms of the local mean volume concentration, $c(y)$ (by which we shall always mean the volume of sediment per volume of mixture), ρ_m may be expressed as

$$\rho_m(y) = (1 - c(y))\rho_w + \rho_s c(y), \tag{2.1.5}$$

ρ_w and ρ_s being the densities of the water and the sediment respectively. Integration of Eqn. 2.1.4, with Eqn. 2.1.5 and the boundary condition, $\tau(h) = 0$, leads to an expression for the local stress

$$\frac{\tau(y)}{\rho_w} = ghS\left(1 - \frac{y}{h}\right) + g(s-1)S\int_y^h c(y)dy, \tag{2.1.6}$$

where s is the relative density of the sediment. The local stress in sediment-laden flows is seen to be greater than the corresponding clear-water flows of the same S and h by a contribution due to the presence of sediment. The maximum value of the latter is seen to be $g(s-1)Sh\langle c\rangle$, where $\langle c\rangle \equiv (\int_0^h c(y)dy)/h$ is the depth-averaged concentration. In most cases, $\langle c\rangle \ll 1$, and the correction to the clear-water stress profile due to the presence of sediment can be neglected, as is done hereafter.

Vanoni(1946) observed that, although the distribution of mean velocity in sediment-laden open-channel flows could be described by Eqn. 2.1.2, the value of κ necessary to agree with the estimated u_*, to be denoted by κ_s, was significantly smaller than that found in clear-water flows. Vanoni speculated that this was due to damping of turbulence by the presence of suspended sediment. A similar speculation in a related context is found in Saffman(1962), in a study of the hydrodynamic stability of dusty gases. That the logarithmic profile still seemed applicable was interpreted as some justification for a mixing-length model. The apparent reduction in κ would then be interpreted as implying a reduced mixing length or a reduction in the scales of turbulent motion.

Einstein and Chien (1955) proposed a heuristic correlation, based on energy arguments, to predict the variation of κ_s. This involved the ratio of the mean power required to maintain the sediment in suspension, P_s, to the overall power expended by the flow, P_f. The former is found to be

$$P_s = w_s g(s-1)\langle c\rangle h, \tag{2.1.7}$$

where w_s is a characteristic settling velocity of the turbulent suspension. The power expended by the flow is

$$P_f = gh\langle u\rangle S, \tag{2.1.8}$$

where $\langle u \rangle \equiv (\int_0^h u(y)dy)/h$ is the depth-averaged velocity. It is noted that the ratio, P_s/P_f, is proportional to the parameter, $\langle R_s \rangle$, defined as $\langle R_s \rangle \equiv g(s-1)w_s\langle c \rangle h/u_*^3$. This may therefore be interpreted as a suspension Richardson number based on depth-averaged quantities, analogous to that used in characterizing density-stratified flows. The correlation is reproduced in Fig. 2.1.2. Although a crude trend may be discerned, a large scatter is evident, with values of P_s/P_f differing by an order of magnitude being associated with the same value of κ (or κ_s in our notation). Although the quality of the data is uncertain, the fact that κ_s attained values less than 0.2, nevertheless, indicates that a significant effect is due to the presence of sediment. In the development of this correlation, however, the appropriateness of a variable κ_s or even Eqn. 2.1.2 was not questioned. A possible explanation for the large scatter is that, at least in some of these flows, Eqn. 2.1.2 was inadequate.

If the traditional approach is considered as more than an empirical fitting procedure, then it implies a qualitative view of the effects of sediment on the turbulent flow. Since the log law is presumed valid throughout the flow, a reduction in the von Kàrman constant affects the velocity profile throughout the flow. The effects of the sediment, according to the traditional view, are global in nature.

In the western literature, the possible importance of a buoyancy effect was already pointed out by Barton and Lin (1955). They noted that the Einstein-Chien parameter, although not originally intended as such, could be interpreted as a Richardson number. The meteorological analogy also inspired the analysis of Hino (1963), who developed an analytical expression for the variation of κ_s from mixing-length concepts. The explicit analogy between thermal stratification and sediment

Fig. 2.1.2 The Einstein-Chien correlation for κ_s (from Vanoni, 1977)

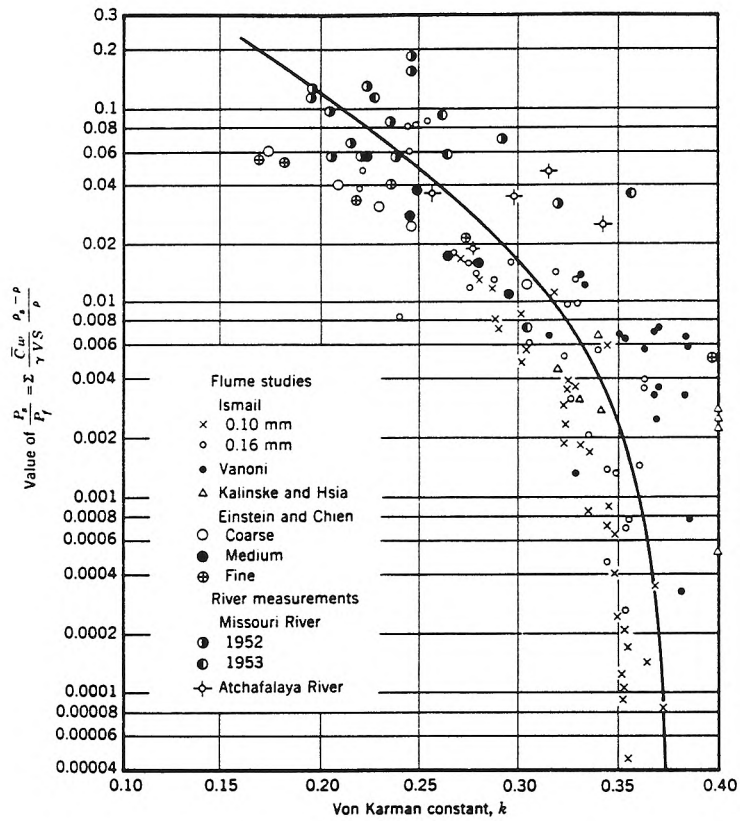

suspension may, however, have been first pointed out by Barenblatt(1953). Its physical motivation may be seen from Eqn. 2.1.5. Because of a vertical variation in local mean concentration, an effective vertical variation in local mean mixture density results; the flow may thus be considered to be density-stratified. Further, since the mean concentration increases as the bed is approached, the density of the mixture increases in the same way; the effective stratification is stable. The speculation of Vanoni (1946) concerning the possible damping of turbulence due to the presence of suspended sediment is qualitatively consistent with the analogy to density-stratified flows. In the latter, vertical turbulent transport is inhibited,

leading to a reduction in the scales of turbulent motion and a larger mean-velocity gradient for given u_*.

The explicit use of the Monin-Oboukhov formalism to describe particulate turbulent flows appears in Monin and Yaglom (1971), Lumley (1976) and Itakura and Kishi (1980), albeit with rather different definitions for the Monin-Oboukhov length scale. Itakura and Kishi (1980) studied specifically open-channel flows with alluvial sands and suggested that an appropriate Monin-Oboukhov scale would be $L_s \equiv u_*^3/[\kappa w_s g(s-1)\langle c\rangle]$. The relation to the Einstein-Chien parameter is evident. The log-linear velocity-defect profile proposed by Itakura and Kishi, based on their Monin-Oboukhov approach, may be viewed simply as the use of a linear wake function.

The straightforward application of the Monin-Oboukhov theory to sediment-laden open-channel flows faces several criticisms. The original theory was based on constant, externally imposed momentum and scalar fluxes. The importance of these assumptions lies in the possibility, for non-constant fluxes, of defining length scales other than L_s, e.g., a local length scale based on dc/dy, thereby invalidating the simple similarity hypothesis that the mean profiles are functions only of (y/L_s). Since the momentum flux varies linearly with distance from the wall, the possible importance of the depth, h, particularly if $h/L_s \leq O(1)$, as is often the case, cannot be discounted. In the case of the sediment flux, this criticism has greater force because of the large gradients often observed in sediment-concentration profiles. An attendant difficulty is the definition of an appropriate Monin-Oboukhov length scale. The wall heat flux, q_*, in the atmospheric surface layer is assumed externally imposed and constant. For the sediment-laden flow, little is known of the concentration at the boundary; indeed, this is generally internally determined.

The use of $\langle c \rangle$ as a characteristic concentration may have little justification, since the deviation of $c(y)$ from $\langle c \rangle$ may be quite large. In this connection, Vanoni and Nomicos (1960) argued that the Einstein-Chien parameter should be modified by replacing $\langle c \rangle$ with a concentration close to the bed. This debate raises the question of appropriate concentration scales in sediment-laden flow.

In contrast to the traditional view, the Monin-Oboukhov interpretation retains the universality of κ and accounts for the deviation from the log profile by a correction term, linear in y/L_s. A similar argument has been advanced by Coleman (1981), who proposed that the effects of suspended-sediment may be better parametrized using the wake-function of Eqn. 2.1.4. Whereas in homogeneous-fluid flows, the wake-coefficient, W_0, has a constant value, say 0.2 in open-channel flows, it may, according to Coleman, vary in sediment-laden flows. A correlation is proposed between this coefficient and a gross flow Richardson number, defined as $R_C \equiv g y_{\max}(\rho_0 - \rho_{y_{\max}})/\langle\rho\rangle u_*^2$, where $y_{\max}$ is the elevation where the maximum velocity is found, ρ_0 and $\rho_{y_{\max}}$ are the mixture densities at $y = 0$ and $y = y_{\max}$, and $\langle\rho\rangle$ is the depth-averaged mixture density. Of some practical relevance in the use of this correlation is the difficulty in obtaining an accurate estimate of ρ_0, or equivalently, the concentration, c_0, at the bed. Coleman obtained estimates by simple extrapolation, a dubious procedure in view of the large concentration gradients near the bed.

Two conceptual points may be raised. The wake-coefficient characterizes what may be termed the outer flow, i.e., the region where the wake function is non-negligible. It is, however, correlated with a hybrid parameter, essentially $y_{\max}/L_C = y_{\max}/(u_*^2/g(s-1)c_0)$ in the context of sands, made up of an outer length scale, $y_{\max}$, and a concentration scale, c_0, more characteristic of the inner

region. The resemblance to the Einstein-Chien parameter as modified by Vanoni and Nomicos (1960) should be noted. This hybrid parameter may be justified if c_0 is the only concentration scale, much as u_* is the only velocity scale. This remark is clarified in the following chapter. The second point is related and concerns the magnitude of Ri_C. As estimated by Coleman from his starved-bed experiments, these attain values up to 200. If Ri_C is interpreted in analogy to density-stratified flows, such large magnitudes indicate extremely stable flows, in which turbulence should be practically extinguished. This is evidently not the case, as shear must remain important in order to sustain the suspension. The relation to the first point is seen in that one reason for the large magnitudes is the use of c_0 as a concentration scale. Alternate scales, e.g., $\langle c \rangle$, would result in much smaller values of Ri_C.

Conceptually, both the approach of Itakura and Kishi (1980) and that of Coleman (1981) are identical, differing only in the specific wake functions and the specific correlations (or equivalently, length scales) used. They both argue that, in the region, $y/L_s \ll 1$ or $y/L_C \ll 1$ (presumably, $y/h \ll 1$ also), boundary shear dominates and the effects of stratification are negligible, with the result that the flow in this region should resemble a clear-water flow. In particular, the velocity gradients in this region should be the same for both clear-water and sediment-laden flows if u_* is constant. Only in the outer region, $y/L_s = O(1)$ or $y/L_C = O(1)$ (and $y/h = O(1)$), are the effects of stratification felt. The effects of sediment may therefore be considered localized in that they should be observed only in the outer region.

Whether the velocity profile is best represented by a pure log law with $\kappa_s < \kappa$, or with a log-wake law (where the wake function may be either linear or $\cos^2$) with a variable wake-coefficient, is still being debated. In spite of some qualitative

similarity such as the idea of turbulence damping, the traditional and the more recent approaches ultimately diverge. The former's use of a pure log law with a variable κ_s implies a view in which the structure of turbulence is changed radically throughout the flow. In the latter's view, the suspension affects primarily the outer flow, such that, near the bed, where the wake function is insignificant, the structure of turbulence remains essentially unchanged from that of a clear-water flow.

2.1.3 Sediment-laden flows: the mean-concentration profile

The mean-concentration profile is also to be determined in the sediment-laden flow problem. The traditional view has not been seriously challenged. This view has been based on the equation,

$$-c'v' + w_s c = 0, \tag{2.1.9}$$

found, for example, in Monin and Yaglom(1971), Lumley(1976), and Vanoni(1977). *One* interpretation of this equation is that it expresses the balance between the net turbulent upward flux of sediment and the downward flux due to gravitational settling.

The difference is noted between Eqn. 2.1.9 and the equation governing the temperature field in the atmospheric surface layer, i.e., the problem for which the Monin-Oboukhov theory was originally developed. In that case, the relevant equation is

$$-T'v' = q_*, \tag{2.1.10}$$

where T' is the fluctuating temperature. Whereas Eqn. 2.1.10 provides an unambiguous temperature scale because q_* is constant, Eqn. 2.1.9 provides no intrinsic scale for c. Further, the relevant momentum equation is $-u'v' = u_*^2$ (i.e., the same

as Eqn. 2.1.1 for $y/h \ll 1$). The similarity between momentum and temperature equations suggests that the mean-velocity and temperature profiles are similar, as indeed they are found to be. In the contrasting case of sediment-laden flows, the difference between the concentration equation, Eqn. 2.1.9, and the momentum equation, Eqn. 2.1.1, points to a radical difference between concentration and velocity profiles. The difference in the structure of the governing equations is an indication that sediment-laden flows may differ substantially from flows treated by the Monin-Oboukhov theory.

The closure problem posed by Eqn. 2.1.9 may be resolved by a mixing-length hypothesis (Lumley, 1976; Vanoni, 1977). Unlike the model for the velocity profile, namely, $-u'v' = (l_m du/dy)^2 = u_*^2$, where $l_m = \kappa_s y$ is the mixing length, the model traditionally used for the concentration profile is the somewhat inconsistent

$$\begin{aligned} -c'v' &= \beta_s (l_m \frac{du}{dy})^2 \frac{dc/dy}{du/dy} \\ &= \beta_s u_*^2 (1 - y/h) \frac{dc/dy}{u_*/\kappa_s y}, \end{aligned} \tag{2.1.11}$$

where β_s is the reciprocal of a turbulent Schmidt number. Thus, the actual stress profile, rather than the constant stress profile of the velocity model, is used. It may be noted that some have suggested, on empirical grounds, using the actual stress profile for the velocity model also (Montes and Ippen, 1971; Bradshaw, 1976; Schlichting, 1979). The result of the traditional model is the Rouse suspended-load equation (Rouse, 1937);

$$\frac{c}{c_a} = \left(\frac{1 - y/h}{y/h} \frac{a/h}{1 - a/h} \right)^{Z_R}, \tag{2.1.12}$$

where the Rouse parameter is defined as $Z_R \equiv w_s/\beta_s \kappa u_*$, and c_a is a reference concentration at an elevation, $y = a$, where a is often taken to be $a = 0.05h$. Like

the log law, this solution cannot be valid at $y = 0$, since it predicts an infinite concentration. A satisfactory answer to the question of the lower limit of validity of Eqn. 2.1.12 has yet to be given, the most well-known being perhaps the suggestion of Einstein (1950) that this should be within a few grain-diameters from the bed.

It has been implicitly recognized that Eqn. 2.1.12 does not adequately agree with experimental results. In practice, it is used mainly to describe the profile in the lower part of the flow, it being argued that the sediment concentration, and hence the error, is often negligible in the upper part of the flow. Nevertheless, more recent work that have emphasized the the two-layer nature of the problem may be seen as attempts to improve on the traditional model. Constant eddy diffusivities in the outer flow have been recommended by Coleman (1969) and van Rijn (1984) on purely empirical grounds. The latter proposed a composite eddy diffusivity in which the traditional eddy diffusivity is used below $y/h = 0.5$, and a constant eddy-diffusivity is used above, with the constraint that it be continuous at $y/h = 0.5$. Thus, in the upper half of the flow, the maximum eddy diffusivity of the traditional model is used. If the estimated Z_R for the van Rijn model and the traditional model are the same, the former predicts larger concentrations in the upper half of the flow than the latter. In the van Rijn model, the reference level is distinct from the dividing line between the inner and the outer flow and is situated near the bed.

A multiple-scales model may also be approached via scaling arguments. It has been argued (Batchelor, 1965; Lumley, 1976; McTigue, 1981) that, near the bed, the only relevant velocity scale is u_*, and the only relevant length scale is y. The eddy-diffusivity of vertical sediment transport, ϵ_s, must then scale like $\epsilon_s \sim u_* y$, with the result that the solution near the bed is a power law. Note

that Eqn. 2.1.12 reproduces this in the limit, $y/h \ll 1$. McTigue(1981), following Batchelor(1965), suggested further that the only relevant scale in the outer flow is h. Thus, $\epsilon_s \sim u_* h$, i.e., a constant eddy diffusivity.

The analogy with density-stratified flows, previously emphasized in connection with the velocity profile, has not yet had any significant impact on the treatment of the concentration profile. Itakura and Kishi (1980), in their Monin-Oboukhov approach, simply used an eddy diffusivity based on their suggested velocity profile. This seems contrary to the spirit of the similarity approach of the original Monin-Oboukhov theory, in which the temperature profile is obtained with an argument parallel to that used to obtain the velocity profile, without invoking any eddy-diffusivity models.

A more thorough going interpretation in terms of the stratified-flow analogy is found in the theory of Barenblatt(1979) (also cited in Monin and Yaglom, 1971). This differs in several respects from the traditional approach and motivates some of the ideas to be developed in the next chapter. A system of five equations, including Eqn. 2.1.9 and a turbulent kinetic energy balance in which the stratified-flow analogy is explicitly made, is examined. The analysis is limited to the case where the flow has absorbed the maximum possible amount of sediment. A general solution to the system is not sought; rather, it is asked whether and under what conditions self-similar solutions are possible. Such solutions are found possible provided $w_s/\kappa u_* < 1$ (note κ, and not κ_s, is used in this criterion). The self-similar velocity profile is found to be logarithmic with what may be interpreted as an effectively reduced κ_s, while the corresponding concentration profile is a power-law profile with exponent, -1. It is argued that these are the only possible self-similar solutions. These solutions imply that the self-similar state is characterized

by a constant flux Richardson number, $[g(s-1)c'v']/[u'v'(du/dy)]$. A constant flux Richardson number is also found in flows treated by the standard Monin-Oboukhov theory; these are, however, highly stable rather than weakly stable flows.

As a heuristic balance equation, Eqn. 2.1.9 may be satisfactory; whether it can be justified more rigorously has been questioned. In an experimental study using the LDV technique, van Ingen(1981) was prompted to ask whether any physical meaning can be attached to the correlation, $-c'v'$, representing the net upward turbulent flux of sediment. This questions the blithe acceptance of the continuum assumption. Hinze(1972) notes that this assumption places severe restrictions on a problem; in particular, the average separation distance between particles should be at least an order of magnitude smaller than the Kolmogorov length scale, $l_K \equiv (\nu^3/\varepsilon)^{1/4}$, where ε is the rate of turbulent kinetic energy dissipation. The additional assumption of diluteness imposes even more severe restrictions. Since the typical sand-grain diameter is of the order of or greater than l_K, the continuum assumption in sediment-laden flows of rivers should not be taken lightly.

Over what length scales *is* it possible to define a concentration? Lumley(1976) estimates that, for an accuracy of 10% in the definition of a local particle density, 3000 particles in a characteristic volume are necessary. For a fairly high concentration of 0.005, and a grain diameter of 0.15mm, this requires a characteristic volume of $\approx 1\text{cm}^3$. In the laboratory where $l_K \sim 0.1\text{mm}$, the length scale over which a concentration can be defined is significantly larger than l_K. Because the fluctuating concentration field can be defined only on scales much larger than the significant scales of the fluctuating velocity field, the correlation, $-c'v'$, has questionable physical meaning in the context of alluvial sediment-laden flows. Thus,

the effort, made for example by mixture theorists (Drew, 1975; McTigue, 1981), to derive equations like Eqn. 2.1.7 using continuum-type assumptions in which correlations between concentration and velocity fluctuations appear, seems inappropriate for this particular class of problems. The difficulty may be avoided, as in the approach of Batchelor (1965), who started directly from a gradient-transport model without reference to any correlations. The gradient-transport assumption is, however, itself not above question.

2.2 Experimental results

2.2.1 Mean-field results

In the literature on open-channel flows without sediment, the limitations of the purely logarithmic velocity profile and the necessity for a wake-type correction have become increasingly apparent. The specific wake-function of Coles (1971) appears to be gaining wide acceptance. There is wide scatter, however, in the reported values of the W_0, ranging from 0 to 0.25 in experiments of Nezu and Rodi (1986), and from 0 to 0.48 in results examined by Coleman and Alonso (1983).

In the investigation of the velocity profile in sediment-laden flows, a number of experimentally-related factors contribute to the controversy between traditional and recent approaches. An accurate estimate of the wall shear, independent of any assumptions about the velocity profile, is complicated by a finite width and by differences in the roughness of the bed and the sidewalls. Since the determination of κ (or κ_s) depends on u_*, this introduces error in the estimate of κ. Experimental procedure plays a role also in that, a velocity profile is often obtained from a relatively small number of points (8–12). The performance of the standard

instrument, the pitot-static probe, in proximity to solid boundaries has also been a source of doubt.

The criticism of Coleman (1981) with respect to the early practice of fitting a logarithmic curve to the entire flow is justified. Re-examination of the early work reported, e.g., by Vanoni(1946) and Vanoni and Nomicos (1960), shows that measurements made very near the bed were weighted less in the fitting of the logarithmic profile. If these had been given more weight, the estimates of κ_s would be typically revised upwards. In a re-examination of some data of Vanoni (1946), Coleman determined a $\kappa = 0.5$ by fitting the logarithmic curve to the near-bed measurements in both a clear-water and a sediment-laden flow. In their defense, this early practice may reflect an implicit judgement of the reliability of near-bed measurements, which, from the high value of κ found for even a clear-water flow, may be well founded. The justice of Coleman's criticism does not necessarily invalidate the traditional hypothesis, although it certainly throws doubt on it.

The experiments on which Coleman(1981) based his wake-function correlation may, in turn, be criticized for the small width-to-depth ratio of 2. Three-dimensional effects due to the sidewalls may be important. Such effects would be of greatest importance in the outer flow, precisely the region in which it is claimed that the effects of the suspension are primarily felt. Two points may, however, be noted. The aspect ratio was kept approximately constant in all of his experiments, so that the effects of the sidewalls should be approximately the same in all the experiments, unless these effects depend strongly on sediment concentration. Also, the few near-bed measurements, which should be less influenced by three-dimensional effects, indicated a value of $\kappa \approx 0.4$, which was independent of sediment concentration. Nevertheless, the reliability of near-bed measurements

with a pitot-tube and the statistical significance of a logarithmic fit over two or three points is questionable.

Although less controversy has surrounded the concentration profile, similar experimental problems exist. The traditional suction-sampling technique introduces a sampler into the flow. In an equilibrium-bed flow, the reliability of near-bed measurements is uncertain because of possible local local scour of the bed induced by the sampler. Even in starved-bed flows where this is not a problem, measurements cannot be made at the bed because of the finite size of the sampler. The accuracy in measuring local mean concentration that may be expected of such a technique is, perhaps at best, 10%, compared to an accuracy of perhaps 1% in a mean-velocity measurement. The tedious procedure has probably also contributed to the fact that fewer data are available on point concentrations.

As noted earlier, it has been traditional practice to place more weight on near-bed measurements in trying to apply the Rouse equation, Eqn. 2.1.10. This may have again reflected concern about the reliability of measuring the small concentrations in this region, and also possible effects of a slight non-uniformity of the grain-size distribution. The evidence presented in support of the more recent approaches has been rather meager. Both Itakura and Kishi (1980) and McTigue (1981) gave a comparison of theory and experiment for only a single experiment.

The experimental evidence regarding the mean profiles may therefore be considered inconclusive with both traditional and recent approaches open to criticism. The possibility should not be ruled out, particularly with respect to the velocity profile, that *both* approaches may be valid, each for a different range of conditions.

2.2.2 Results on the fluctuating velocity-field

One of the earliest studies of the fluctuating velocity field was reported by Elata and Ippen (1961), who used an impact-tube pressure transducer to measure

longitudinal velocity fluctuations in a flow transporting neutrally buoyant particles of a single size. They reported a decrease in κ_s (which has since been questioned by Coleman (1981)), and an increase in turbulence intensity with increasing particle concentration. They, therefore, disputed the speculation of Vanoni (1946) that the presence of sediment damped turbulence, and suggested that the structure of turbulence was altered by the presence of the additional solid surface of the sediment. The major effect was, nevertheless, obtained in flows with volume concentrations (up to 0.3) an order of magnitude or more larger than those to be considered in the present work. Particle-particle interactions would undoubtedly be of more significance in their work. These experiments could also be criticized for the non-uniformity of the flow.

Smaller concentrations, up to 0.03, of slightly negatively buoyant particles were again studied by Bohlen (1969), who measured the three velocity components in a silicone-oil, open-channel flow using hot wire probes. While his results showed the same trend with increasing concentration as those of Elata and Ippen (1961), the magnitudes of the measured intensities may be questioned. Typically, as the wall is approached, the following scaling is usually found: $\sqrt{u'^2}/u_* \sim 2$, $\sqrt{w'^2}/u_* > \sqrt{v'^2}/u_* \sim 1$. Bohlen's data, including a particle-free flow, consistently showed all turbulence intensities to be less than u_*.

The LDV technique offers an alternative that avoids the difficulties of introducing a physical probe into the flow. The work of van Ingen (1981,1983a) investigated a sediment-laden, open-channel flow with a predominantly flat equilibrium bed. A single sand size was used, and only the longitudinal velocity component was measured. A slight increase in $\sqrt{u'^2}/u$, compared with clear-water flow, was observed. It was cautioned, however, that the slight increase in $\sqrt{u'^2}/u$ might

not be statistically significant in view of the scatter in results reported by other workers. Tsuji and Morikawa (1982) used a single-component LDV technique also in studying air flow in a pipe, with a suspension of particles of two sizes. They did not, however, analyze velocities in terms of the log-law. Longitudinal turbulence intensities relative to the bulk mean speed, $\sqrt{u'^2}/\langle u \rangle$, were found to *decrease* with increasing concentration of small particles, $d = 0.2$mm (pipe diameter, 30.5mm), and to *increase* for large particles, $d = 3.4$mm. The implications of this study for the present work are not clear in view of two essential differences between particulate airflow in a pipe and sediment-laden open-channel flows, namely, the density ratio and the geometry.

2.3 Summary

Both the traditional and the more recent approaches to the description of the two mean fields and to the interpretation of experimental results are open to criticism. The recent more explicit analogy to density-stratified flows in the treatment of the velocity profile has been discussed. A trend away from a reliance on the the mixing-length closures towards the adoption of an approach based more on similarity ideas may be seen in the application of the Monin-Oboukhov theory and, to a lesser extent, in the wake-coefficient correlation.

In contrast, both the traditional and the more recent treatments of the concentration profile remain tied to a vertical balance equation, whose conceptual foundations have been questioned. The stratified-flow analogy has been seen to have had little impact. This asymmetry in the conceptual approach to the description of the two mean fields may be attributed to the traditional implicit decoupling of the velocity from the concentration field. In the next chapter, an attempt is made to follow more systematically and thoroughly a similarity approach, which treats the two mean fields in parallel but different ways.

3. Similarity and sediment-laden flows

3.0 Introduction

The preceding review highlighted the controversies surrounding the description of the mean fields. To clarify some of these issues and to develop an alternative conceptual framework for thinking about sediment-laden flows, a discussion of the concepts of self-similarity, multiple scales, and asymptotic matching is given. The similarity approach to wall-bounded turbulent shear flows can be formalized in an argument originally given by Izakson (1937) and Millikan (1939). An outline of the conventional argument, following Tennekes and Lumley (1980), is given. Since the concepts of multiple scales and asymptotic matching are important in homogeneous flows, it is natural to ask to what extent they apply to sediment-laden flows. *If* these concepts may be applied to the velocity profile in sediment-laden flows, how do they apply to the concentration profile? A naive generalization of the conventional matching argument to the case of the concentration profile concludes that the profile follows a logarithmic law. This is contrary to experimental evidence. A more appropriate generalization is developed such that asymptotic matching may result in either a power law or a log law. A two-stage similarity model for sediment-laden flows is then developed, using this generalization.

The discussion regarding sediment-laden flows is restricted to a simplified case. Unless otherwise specified, a suspension in equilibrium with a sand bed is assumed. The bed itself, though deformable, is assumed to be flat and statistically stationary, and to be composed of sand grains perfectly uniform in density and size. Temperature effects are not considered. All variables are assumed homogeneous in the streamwise direction.

3.1 The conventional matching argument

A general law of the wall may be expressed as

$$\frac{u}{u_*} = f(y^+, \alpha_i), \tag{3.1.1}$$

where $y^+ \equiv y/l_\nu$, $l_\nu \equiv \nu/u_*$, and α_i is a dimensionless parameter, relevant only in the inner region, e.g., a roughness Reynolds number, $Re_k \equiv k/l_\nu$, k being the characteristic height of the roughness element. Similarly, a general velocity-defect law is considered, namely,

$$\frac{u - u_{\max}}{u_*} = F(\eta, \alpha_o), \tag{3.1.2}$$

where $\eta \equiv y/h$, and α_o is a dimensionless parameter relevant only in the outer region, e.g., the bulk Richardson number proposed by Coleman (1981). Following Tennekes and Lumley (1980) and the standard practice in multiple-scales analysis (Kevorkian and Cole, 1981), we consider the inner variable, y^+, and the outer variable, η, to be essentially independent. An asymptotic matching of the velocity gradients is then proposed. From Eqn. 3.1.1,

$$\frac{du}{dy} = \frac{u_*}{l_\nu}\frac{df}{dy^+}, \tag{3.1.3}$$

while from Eqn. 3.1.2,

$$\frac{du}{dy} = \frac{u_*}{h}\frac{dF}{d\eta}. \tag{3.1.4}$$

In an intermediate region, $y^+ \to \infty$, $\eta \to 0$, Eqns. 3.1.3-3.1.4 are assumed to match asymptotically, such that

$$\frac{u_*}{h}\frac{dF}{d\eta} = \frac{u_*}{l_\nu}\frac{df}{dy^+}. \tag{3.1.5}$$

Multiplication by y/u_* then reveals

$$\eta\frac{dF}{d\eta} = y^+\frac{df}{dy^+}. \tag{3.1.6}$$

For given parameters, α_o and α_i, the two sides of Eqn. 3.1.6 (which should, strictly speaking, be interpreted as an asymptotic relation) depend on different variables and so must be equal to a constant, independent of η or y^+. This matching constant, traditionally denoted by $1/\kappa$, is independent of either α_o or α_i, since these are relevant only in their respective regions. In this limited analysis, the matching constant is universal in the sense that the asymptotic limit, $Re_* \equiv h/l_\nu \to \infty$, has been taken in obtaining the constant, such that it must be independent of Re_*. The matching solution in the intermediate region, $l_\nu \ll y \ll h$, is obtained by integrating Eqn. 3.1.6 to give, in inner coordinates,

$$f(y^+) = \frac{1}{\kappa}\ln y^+ + B_i(\alpha_i), \tag{3.1.7}$$

where the constant of integration, B_i, may depend on α_i, but not on Re_*. Similarly, in outer coordinates, the matching solution is expressed as

$$F(\eta) = \frac{1}{\kappa}\ln\eta + B_o(\alpha_o). \tag{3.1.8}$$

Although the above analysis considered the special case where the inner length scale is l_ν, nothing in the analysis depends on this choice. The same result would be obtained for any other inner scale, l, provided that the disparity in scales exists. Further, the matching constant should remain the same. Consider a case where $l_\nu \ll l \ll h$, and matching occurs in $l \ll y \ll h$, with a matching constant, $1/\kappa'$. If l decreases, the matching constant does not vary. In the asymptotic limit, where $l/l_\nu \to O(1)$, matching can be obtained with either y^+ or y/l as the inner coordinate, so that the matching constant must be the same, i.e., $1/\kappa$. A familiar example is the case of flow over a fully rough surface, in which case, k is the appropriate inner scale rather than l_ν, and a $\kappa \approx 0.4$ still characterizes the logarithmic velocity profile.

What conclusions can be drawn in a case where a dimensionless parameter, $\hat{\alpha}$, that is relevant in both inner and outer regions exists? The above matching analysis can still be applied but a "universal" matching constant cannot be deduced. The possibility that the matching constant varies with this parameter cannot be excluded.

3.2 A generalization of the conventional matching argument

The traditional approach to describing the mean-concentration profile has been based on the balance equation, Eqn. 2.1.9, and an eddy-diffusivity model. Since similarity laws are familiar in the context of the velocity field, can such similarity concepts provide an alternative framework for discussing the concentration profile? In particular, are there equivalents to the law of the wall and the velocity-defect law for the concentration field? Can a matching argument be found to deduce a plausible concentration profile in some matching region? The conventional

matching argument is not restricted to the velocity field but can be applied to any dependent variable. A straightforward application of the conventional matching argument with concentration instead of velocity as the dependent variable yields a logarithmic profile for the concentration profile in the intermediate matching region. This is not a trivial result, since the temperature field in a weakly stable atmospheric surface layer, as treated by the Monin-Oboukhov theory, exemplifies this result. Such a logarithmic behavior is not observed in sediment-concentration profiles. The conventional matching can, however, be formally generalized in a heuristic manner such that it admits not only log-law profiles but also power-law profiles in the matching region.

Assume that two disparate length scales, l and $\mathcal{L}$, exist and are important in two distinct flow regions, i) $y/l = O(1)$, $y/\mathcal{L} \ll 1$, and ii) $y/l \gg 1$, $y/\mathcal{L} = O(1)$. A general inner law for a dependent variable, r, may be expressed formally as

$$\frac{r}{r_*} = f\left(\frac{y}{l}, \frac{y}{\mathcal{L}}\right) \tag{3.2.1}$$

where r_* is an appropriate scale. An outer law can be similarly expressed as

$$\frac{r}{r_*} = F\left(\frac{y}{l}, \frac{y}{\mathcal{L}}\right). \tag{3.2.2}$$

The scale, r_* is assumed to be common to both regions (like u_*). As in the conventional argument, the variables, $\xi \equiv y/l$ and $\eta \equiv y/\mathcal{L}$, are treated as essentially independent in the asymptotic limit, $\mathcal{L}/l \to \infty$. With a view to matching the gradient, Eqns. 3.2.1-3.2.2 may be differentiated with respect to y to give

$$\frac{dr}{dy} = r_* \left[\frac{1}{l}\frac{\partial f}{\partial \xi} + \frac{1}{\mathcal{L}}\frac{\partial f}{\partial \eta}\right], \tag{3.2.3}$$

and

$$\frac{dr}{dy} = r_* \left[\frac{1}{l}\frac{\partial F}{\partial \xi} + \frac{1}{\mathcal{L}}\frac{\partial F}{\partial \eta}\right]. \tag{3.2.4}$$

These are to be matched in an intermediate region, $\xi \to \infty$, $\eta \to 0$, such that

$$\frac{1}{l}\frac{\partial f}{\partial \xi} + \frac{1}{\mathcal{L}}\frac{\partial f}{\partial \eta} = \frac{1}{l}\frac{\partial F}{\partial \xi} + \frac{1}{\mathcal{L}}\frac{\partial F}{\partial \eta}. \tag{3.2.5}$$

Multiplication by y converts this asymptotically valid equation to a relation expressible in terms of only ξ and η, i.e.,

$$\xi\frac{\partial f}{\partial \xi} + \eta\frac{\partial f}{\partial \eta} = \xi\frac{\partial F}{\partial \xi} + \eta\frac{\partial F}{\partial \eta}. \tag{3.2.6}$$

The conventional argument relies on the separability of both sides of Eqn. 3.2.6; both f and F should be such that the operation, $\mathcal{T}\Phi$, where $\mathcal{T} \equiv \xi\partial/\partial\xi + \eta\partial/\partial\eta$, results in a separation of variables. If this were the case, then division by the appropriate factor would result in an equation of expressions, each of which is dependent on its own variable and so must be constant. A class of particular solutions which may be useful is found where f (or F) is itself separable; i.e.,

$$f = f_1(\xi)f_2(\eta). \tag{3.2.7}$$

This results in

$$\mathcal{T}f = \xi f_1'(\xi)f_2(\eta) + \eta f_1(\xi)f_2'(\eta). \tag{3.2.8}$$

From this, it is clear that the separability condition is that

$$\eta f_2'(\eta) = \lambda_1 f_2(\eta), \tag{3.2.9}$$

where λ_1 is an undetermined constant, with the simple solution

$$f_2(\eta) \propto \eta^{\lambda_1}. \tag{3.2.10}$$

Instead, therefore, of the general relations, Eqns. 3.2.1-3.2.2, we assume that

$$\frac{r}{r_*} = \eta^{\lambda_1}\Phi_1(\xi), \tag{3.2.11}$$

$$\frac{r}{r_*} = \xi^{\lambda_2}\Phi_2(\eta). \tag{3.2.12}$$

The form of Eqns. 3.2.11-3.2.12 was chosen such that the special case treated by the conventional argument is included when $\lambda_1 = \lambda_2 = 0$. The matching condition, Eqn. 3.2.5, then results in

$$\frac{\xi\Phi_1' + \lambda_1\Phi_1}{\xi^{\lambda_2}} = \frac{\eta\Phi_2' + \lambda_2\Phi_2}{\eta^{\lambda_1}} = C_1, \tag{3.2.13}$$

where C_1 is the matching constant. The general equation to be satisfied by Φ_1 and Φ_2 is of the form

$$\sigma\Phi'(\sigma) + \lambda_1\Phi(\sigma) = C_1\sigma^{\lambda_2}. \tag{3.2.14}$$

In the special case where $\lambda_1 = \lambda_2 = 0$, the classical result is obtained. The general solution of Eqn. 3.2.14 is

$$\Phi(\sigma) = C_1'\sigma^{\lambda_2} + C_2\sigma^{-\lambda_1}, \tag{3.2.15}$$

where $C_1' = C_1/(\lambda_1 + \lambda_2)$. In the overlap layer, the profile may, therefore, be expressed in terms of inner coordinates as

$$\frac{r}{r_*} = \left(\frac{l}{\mathcal{L}}\right)^{\lambda_1}\left[C_1'\xi^{\lambda_1+\lambda_2} + C_2\right]. \tag{3.2.16}$$

This may be put in more insightful form by defining a new scale for the inner region, $r_\xi \equiv r_*(l/\mathcal{L})^{\lambda_1}$, and denoting $(\lambda_1 + \lambda_2)$ as λ, with the more compact result,

$$\frac{r}{r_\xi} = C_1'\xi^{\lambda} + C_2. \tag{3.2.17}$$

In a similar fashion, with the additional definition, $r_\eta \equiv r_*(\mathcal{L}/l)^{\lambda_2}$, the outer-solution form of the profile in the overlap layer is

$$\frac{r}{r_\eta} = C_1'\eta^{\lambda} + C_3. \tag{3.2.18}$$

Not surprisingly, the form of Eqn. 3.2.18 is similar to the classic log law with the substitution of the power-law for the log-law. A significant difference, however, is that, rather than having a common scale, as first assumed, for both the inner and outer layer, two disparate scales are found to be necessary. Since the dependent-variable scales must satisfy the relation,

$$\frac{r_\xi}{r_\eta} = \left(\frac{l}{\mathcal{L}}\right)^\lambda, \tag{3.2.19}$$

and it is assumed that $l \ll \mathcal{L}$, these must be disparate scales, unless $\lambda = 0$, as in the conventional argument.

The development, though formal and heuristic, is quite general in that it does not depend on any particular inner or outer scales but requires only that the inner scale and the outer scale are disparate. Moreover, although the discussion has been in the context of wall-bounded flows, it may be applied much more generally. Thus, results for the downstream evolution of free turbulent flows such as buoyant jets, as well as for other wall-bounded turbulent flows, such as a turbulent boundary layer on the verge of separation, may be viewed from this general perspective. The classic logarithmic profile is thus seen as a special degenerate case in which only a single velocity scale is relevant for both inner and outer regions, imbedded in a much broader range of profiles.

The remarks previously made in the context of the log-law profile should also apply to the power-law profile. In particular, if a dimensionless parameter, $\hat{\beta}$, is relevant in both inner and outer regions, then all of the the constants involved in the profile, including the exponent, λ, may vary with this parameter. It is implied here that any such dimensionless parameter must remain finite in the limit, $\mathcal{L}/l \gg 1$. In this connection, the power-law profile may be interpreted generally

as an example of what Barenblatt and Z'eldovich (1972) have termed "self-similar solutions of the second kind" (also Barenblatt, 1979). The exponent, λ, may be regarded as an eigenvalue in the sense that only for certain values of λ can the inner and outer solutions, which are determined by the boundary conditions, be matched. In cases where closed equations can be investigated analytically, e.g., the Guderley solution of the blast-wave problem in gas dynamics (Whitham, 1974), the eigenvalue aspect of λ is revealed clearly. In that example, λ is seen to possess a continuous spectrum that depends on the ratio of specific heat capacities, a dimensionless parameter relevant on both sides of the singular characteristic.

3.3 Another approach to a generalized matching argument

Another approach to the conventional argument, closer to the original treatment, is preferred by some workers. This approach, exemplified by that taken in Monin and Yaglom (1971), may also be used to obtain an equivalent generalized matching argument. Although it leads to a less general result, it is convenient to assume, from the start, a disparity in scales. We begin, therefore, with

$$\frac{r}{r_\xi} = f(\xi), \tag{3.3.1}$$

$$\frac{r}{r_\eta} = F(\eta), \tag{3.3.2}$$

and ask under what conditions these can be matched? In the overlap region, r is assumed to match, so that

$$r_\xi f(\eta\gamma) - r_\eta F(\eta) = 0, \tag{3.3.3}$$

where $\gamma \equiv \mathcal{L}/l$. Letting

$$\frac{r_\xi}{r_h} = g(\gamma) \tag{3.3.4}$$

gives a functional equation for g,f, and F,

$$g(\gamma)f(\eta\gamma) - F(\eta) = 0. \tag{3.3.5}$$

Taking the derivative with respect to γ, we obtain

$$g'(\gamma)f(\eta\gamma) + \eta g(\gamma)f'(\eta\gamma) = 0. \tag{3.3.6}$$

Multiplication by γ reveals the possibility of separation of variables such that

$$\frac{\gamma g'(\gamma)}{g(\gamma)} = \frac{\chi f'(\chi)}{f(\chi)} = \lambda, \tag{3.3.7}$$

where λ is the separation constant, and the group, $\eta\gamma$, has been relabelled as χ. The solution of Eqn. 3.3.7 results in a power law as expected. Note, however, that there is no additive constant, differing from the previously obtained result. This is a consequence of the assumption of disparate scales from the beginning.

Eqn. 3.3.7 for f may be expressed in terms of the original variables, r and y, as

$$\frac{y}{r}\frac{dr}{dy} = \lambda. \tag{3.3.8}$$

A familiar physical argument in the context of the velocity profile and the log law is that there exists a region in which y is the only relevant length scale. From the perspective of multiple scales, this may be more precisely stated as the existence of a region, $l \ll y \ll \mathcal{L}$. In the case of a power law, we may say that, in addition, in this same region, r itself is the only relevant scale, or more precisely, $r_\xi \ll r \ll r_\eta$. Eqn. 3.3.8 is then interpreted as an extension of the familiar scaling argument rather than arising from a matching argument.

3.4 Implications for sediment-laden flows

3.4.0 Introduction

It has been shown that a power-law profile with a variable exponent, as well as the conventional logarithmic profile, may be deduced from general assumptions regarding the existence of similarity laws and of disparate scales. The Rouse suspended-load equation, Eqn. 2.1.12, tends asymptotically, as $\eta \to 0$, to

$$c \sim \eta^{-Z_R}, \tag{3.4.1}$$

i.e., a power law with a variable exponent. This suggests that the arguments of the preceding sections may be used to obtain a description of the mean-concentration profile without appealing to either a vertical balance equation, a mixing-length or an eddy-diffusivity hypothesis. Can similarity concepts provide a flexible alternative as the basis of a conceptual framework? What assumptions are necessary for such an approach to give plausible results? An answer to this question is developed in two stages. Basic similarity hypotheses are stated in the first stage and their implications developed. At this stage, specific physical content is minimized by not specifying length and concentration scales. The implications remain general and compatible with a variety of more specific physical models. At the second stage, we consider two specific models as embodied in *particular* choices of length and concentration scales, one corresponding to the analogy to stably stratified flows, and the other motivated from a more general dimensional analysis.

3.4.1 Similarity hypotheses and implications

The following basic hypotheses are made:

H1. A two-layer structure exists in which an inner region of extent, l_s, can be distinguished from an outer region, whose scale is the depth of flow, h.

H2. As far as the velocity profile is concerned,

a) a single common velocity scale, u_*, characterizes both the inner and the outer regions, and

b) no dimensionless parameter is relevant in the outer region.

H3. As far as the concentration profile is concerned,

a) two disparate concentration scales, c_s and c_h, exist, and

b) a dimensionless parameter, $\hat{\beta}$, is relevant in both the inner and the outer regions.

H4. In each region, asymptotic similarity in the inner and the outer variables prevails.

In mathematical form, these may be stated in terms of inner similarity laws;

$$\frac{u}{u_*} = f(\xi_s; \alpha_i), \tag{3.4.2}$$

$$\frac{c}{c_s} = g(\xi_s; \hat{\beta}, \beta_i), \tag{3.4.3}$$

and of outer similarity laws;

$$\frac{u - u_{\max}}{u_*} = F(\eta), \tag{3.4.4}$$

$$\frac{c}{c_h} = G(\eta; \hat{\beta}), \tag{3.4.5}$$

where $\xi_s \equiv y/l_s$.

From these fairly general yet restrictive hypotheses, what can be deduced? If it is believed that the presence of sediment may noticeably affect the velocity profile, then, from H1, it must be concluded that l_s cannot be either l_ν or d_{50}. Otherwise, the velocity profile would be essentially identical to the clear-water case. This does not preclude the possibility that l_ν or, more likely, d_{50}, may be important in some region of the flow, e.g., very near the bed. The two-layer

assumption applies to the region of flow that we are interested in and which we can investigate experimentally. It supposes then that other possible length scales are much smaller than l_s. We also leave open the possibility that, under certain conditions, the extent of the inner region may grow so as to render the inner region indistinguishable from the outer region. This region of extent, l_s, may be loosely interpreted as that to which the effects of the presence of sediment are confined.

The possibility of a power-law velocity profile is eliminated by H2a, which argues in favor of a logarithmic profile with an associated von Kàrman constant of ≈ 0.4, i.e., the *same* as in clear-water flows. It should be emphasized that, as is made clear in the matching argument, such a profile is asymptotically approximate for $l_s/h \ll 1$ and should be observed only in a limited intermediate region, $l_s \ll y \ll h$. If cases exist where $l_s \sim h$, then these simple hypotheses are no longer sufficient to give a definite result; a logarithmic profile may or may not be observed. From H2b, it is deduced that the wake component of the velocity profile remains the same as in clear-water flows. This is a simplifying hypothesis, which may be relaxed.

The existence of two disparate concentration scales allows the possibility of a power-law profile, as argued in the preceding sections. As in the case of the velocity profile, such an asymptotic profile should be found only in a intermediate region. The assumption in H1 that only two length scales, l_s and h, are important *in* the region under consideration implies that the inner length scales of the velocity and the concentration profiles are the same. This may be motivated by the belief in a strong coupling between the the mean- velocity and concentration fields. It may also be viewed as a weak form of a Reynolds analogy between vertical sediment and momentum transport. The existence of a dimensionless parameter, $\hat{\beta}$, that is

relevant in both inner and outer regions for the concentration profile only permits the possibility of an exponent that may vary with this parameter.

From fairly general hypotheses, fairly definite conclusions have been drawn. To some extent, these hypotheses were tailored to fit qualitative experimental evidence. The description of the concentration profile by a power law with a variable exponent, deduced from our hypotheses, has essentially reproduced the traditional result in the asymptotic case, $\eta \ll 1$, or that based on a direct eddy-diffusivity model with $\epsilon_s \sim u_* y$. In the case of the velocity profile, however, the conclusions drawn differ significantly from those of previous approaches. It has been argued that the effects of the presence of sediment may be confined to a layer near the bed, of extent l_s. The traditional model argues that these effects are observed throughout the depth of flow. The more recent models based on the stratified-flow analogy argue that these effects are primarily found in the outer region of the flow. Although it can reproduce some old results, the proposed approach is distinct from previous approaches. It is also more flexible in that it recognizes the possibility of cases where effects of sediment may be felt throughout the flow ($l_s \sim h$).

Whether the hypotheses on which the similarity approach is based are any less questionable or any more fruitful than previous hypotheses may be debated. What we consider to be the advantages are that

i) there is no reliance on balance equations whose justification is questionable;

ii) there is no reliance on mixing-length or eddy-diffusivity hypotheses;

iii) the velocity and the concentration fields are treated in parallel as befits a coupled problem, with no priority being assigned to the velocity field, the

coupling between the two fields appearing in a general way, in that a common inner length scale is assumed;

iv) the assumptions, implicit in simple mixing-length models, and thus often overlooked, are clarified, e.g., the limited extent of the region where a logarithmic profile should be observed, and

v) the use of a similarity treatment imbeds the sediment-laden flow problem in a general scheme which has been used to treat a large number of other turbulent flows.

3.4.2 A wake component in the concentration profile

The term "wake component" is a misnomer in the context of open-channel velocity profiles because the strict analogy with a wake flow in the outer region fails. More generally, the wake component may be interpreted, and is so interpreted throughout this work, as reflecting the effect of the bounding free surface. The spatial extent of such an effect is uncertain; experimentally, it is found in clear-water flows that, above, say $\eta = 0.2$, the effect is noticeable in the velocity profile. Because the origin of such an effect, as interpreted here, is so general, it seems highly likely that a wake effect will be observed in sediment-laden flows. Indeed, we have previously argued that, where $l_s/h \ll 1$, the wake component for the velocity field will remain largely unchanged in importance from that found in clear-water flows.

Consistent with its presence in velocity profiles, a wake effect must also be considered a possibility in the concentration profile. The matching argument makes explicit that the power-law can be justified only for $\eta \ll 1$, and, presumably, becomes increasingly invalid as $\eta \to 1$. The adoption of a constant eddy diffusivity in the outer region may be viewed as an attempt to characterize better the wake

component. Instead of the traditional reliance on eddy diffusivity concepts, and the use of the vertical-balance equation, a simpler approach, more consistent with similarity concepts, is proposed. This is the use of a wake function for the concentration profile also, therefore paralleling the treatment of the velocity profile. It is suggested that a general profile, valid for the matching and the outer regions, be of the form,

$$\frac{c}{c_h} = \eta^{-Z} W_c(\eta;\hat{\beta}), \tag{3.4.6}$$

where $W_c(\eta;\hat{\beta})$ satisfies the asymptotic conditions,

$$W_c \to 1, \qquad \text{as} \quad \eta \to 0, \tag{3.4.7}$$

$$W_c \to 0, \qquad \text{as} \quad \eta \to 1. \tag{3.4.8}$$

This last condition, based on the grounds that the concentration should vanish at the free surface, may be debated but is adopted for convenience. Eqn. 3.4.6 can be expressed in a more suggestive form by taking the logarithm,

$$\frac{\log c - \log c_h}{Z} = -\log\eta + \frac{1}{Z}\log W_c\left(\eta;\hat{\beta}\right). \tag{3.4.9}$$

By analogy with the treatment of mean-velocity profiles, it is proposed that a useful form of the concentration wake function, W_c, may be

$$\log W_c(\eta;\hat{\beta}) = Z_h(\hat{\beta}) \log W_{c0}(\eta), \tag{3.4.10}$$

where the restricted wake function, W_{c0}, is independent of the parameter, $\hat{\beta}$, and Z_h plays the role of a wake coefficient. Beyond this level of simplification, the choice of W_{c0} is arbitrary within the above asymptotic constraints. A particularly

simple choice of W_{c0} that allows easy comparison with the traditional result is proposed; namely,

$$W_{c0} = (1 - \eta). \tag{3.4.11}$$

Our general profile, valid for $y/l_s \gg 1$, may be expressed as

$$\frac{c}{c_h} = \eta^{-Z}(1 - \eta)^{Z_h}. \tag{3.4.12}$$

This is seen to differ from the traditional suspended-load equation in at least two important respects. A concentration scale with some physical significance replaces the simple reference concentration. Secondly, the traditional model would insist that $Z_h \equiv Z$, while the present approach permits the two exponents to differ. A non-dimensional eddy diffusivity may be associated with the profile, Eqn. 3.4.12; namely,

$$\frac{\epsilon_s}{w_s h} = \frac{1}{c}\frac{dc}{d\eta} = \frac{\eta(1-\eta)}{Z}\left[1 + \frac{\eta(1 - Z_h/Z)}{1 - \eta(1 - Z_h/Z)}\right]. \tag{3.4.13}$$

If Z is identified with Z_R, the factor in square brackets distinguishes the present from the traditional eddy diffusivity. Depending on whether $Z_h/Z < 1$ or $Z_h/Z > 1$, the former will be larger or smaller than the latter.

An alternate choice of W_{c0} is such that

$$\log W_{c0} = \eta, \tag{3.4.14}$$

which leads to an exponential decay in the outer region and is consistent with a constant eddy diffusivity in that region. This does not satisfy the condition given by Eqn. 3.4.8.

3.4.3 An inner length scale for sediment-laden flows

It should be emphasized again that the above results rest on comparatively few physical assumptions because the length scale, l_s, the concentration scales, c_s

and c_h, and the parameter, $\hat{\beta}$, have yet to be specified. In the present study, we will not be concerned with the dimensionless parameters, α_i, β_i, since these are of secondary importance. The above basic similarity structure is therefore compatible with a variety of more specific physical models. The validity or invalidity of any of the more detailed physical assumptions does not affect the validity of the basic structure. To obtain more specific results, however, more specific assumptions, which will determine the scales, are necessary.

Two familiar inner length scales for sediment-laden flows have been implicitly or explicitly suggested by previous workers, namely, the viscous scale, l_ν (Itakura and Kishi, 1980; Coleman, 1985), and the grain diameter, d_{50} (Einstein, 1950; Elata and Ippen, 1961). The viscous scale is not peculiar to sediment-laden flows and needs no further comment. As a possible inner scale, the grain diameter presents a number of different aspects. At the simplest level, it provides a roughness height, which, again, is not peculiar to sediment-laden flows. It is also associated with the concept of bed-load transport put forward by Einstein (1950), who argued that a transitional layer with thickness scaled by d_{50} exists between the bed and the suspension. The grain diameter should thus be interpreted in terms of a saltation height, characterizing the elevation to which a saltating particle rises. Yet another interpretation of d_{50} as length scale was offered by Elata and Ippen (1961), in their study with neutrally buoyant particles. They argued that neutrally buoyant suspended particles are capable of directly affecting turbulence primarily at scales that are comparable to the particle size. Since typical grain sizes are of the same order of magnitude as or larger than the Kolmogorov scale, there would exist a range of scales within which interaction between sand grains and turbulence may occur. Moreover, since smaller scales become more important

as the bed is approached, the effect of suspended particles should be primarily in the flow near the bed. Another inner length scale, which was suggested by Coleman (1969), may also be mentioned. It is the displacement thickness of the actual sediment-laden channel flow. The motivation for this suggestion was not given and the displacement thickness may be regarded as an *ad hoc* empirical scale. Even in the theory of turbulent boundary layers where this length scale is of more use, it is considered more of an outer scale than an inner scale being defined in terms of an integral over the entire boundary layer.

Our viewpoint is closest in spirit to that of Elata and Ippen, which focuses on the effect on turbulence and is consistent with a multiple-scales interpretation of wall-bounded turbulent shear flows. We argue, however, that, in the case of sedimenting particles with a non-negligible settling velocity, it is not clear that the grain diameter remains the only important physical parameter, since the settling velocity may be equally important or perhaps even dominant. Indeed, we have already concluded from our basic similarity model that if the presence of sediment does markedly affect the velocity profile, then d_{50} cannot be identical to l_s.

A general relation between the physical parameters relevant in the inner region may be expressed as

$$\mathcal{F}_1(l_s,\, u_*,\, d_{50},\, g(s-1),\, \nu) = 0, \tag{3.4.15}$$

where l_s may be considered the dependent variable and the other parameters are independent, externally imposed variables. It has been assumed that h is irrelevant in the inner region, and so has been excluded from consideration. More convenient forms of Eqn. 3.4.15 may be obtained by replacing one of the independent parameters by other equivalent parameters. In particular, since the standard

drag curve for a single sphere, falling under gravity at its terminal settling velocity, w_{s0}, in a stagnant flow, relates the parameters, $g(s-1)$, d_{50}, ν, and w_{s0}, then the latter may be substituted in Eqn. 3.4.15 for any of the other three. The motivation for such a substitution stems from the use of a settling velocity, w_s (to be distinguished from w_{s0}), in the traditional treatment of the concentration profile. The inclusion of w_{s0} in the "basis" parameters allows an easy comparison with the traditional result. Because w_{s0} is defined from the standard drag curve, it unambiguously characterizes the particle and the fluid and is independent of the flow. Its use as a "basis" parameter thus avoids the conceptual problem, encountered in previous approaches based on the flux of settling particles (e.g., in the use of Eqn. 2.1.9), of determining the actual settling velocity, w_s, in a turbulent suspension. The latter would, strictly speaking, vary with local concentration as well as on the turbulence intensity (at least).

In the case where $l_s \gg l_\nu$, it is reasoned that a more appropriate representation of Eqn. 3.4.15 is

$$\mathcal{F}_2(l_s,\, u_*,\, d_{50},\, g(s-1),\, w_{s0}) = 0. \tag{3.4.16}$$

Viscous effects are thus assumed to be important in this inner region only insofar as they affect the grains, and not as they arise from the bottom boundary. From dimensional considerations, Eqn. 3.4.16 may be expressed as

$$\Delta_s \equiv \frac{g(s-1)l_s}{u_*^2} = \Xi\left(\frac{w_{s0}}{u_*},\, \frac{g(s-1)d_{50}}{{w_{s0}}^2}\right). \tag{3.4.17}$$

This grouping was chosen in order to separate in Ξ, the effects of the flow, as characterized by u_*, and the effects of the particle, as characterized by d_{50} and

w_{s0}. For constant d_{50} and w_{s0}, then, it is expected that Δ_s will depend solely on w_{s0}/u_*.

Can Eqn. 3.4.17 be simplified in asymptotic cases? As w_{s0}/u_* becomes large, there will no longer be any sediment in suspension and, presumably, no effect will be observed in the mean-velocity field. This suggests that $l_s \to 0$ in such a case, and other length scales, such as d_{50} or l_ν, that are the relevant inner scales for sediment-free flows regain their importance. At the other extreme, the case where $w_{s0}/u_* \to 0$ is complicated by questions of saturation (is the suspension in equilibrium with the bed?) and of possible changes in the basic nature of the flow (are there non-Newtonian effects?). An intermediate case, in which w_{s0}/u_* remains finite but $l_s \gg d_{50}$, may, however, be of interest. It is reasonable to hypothesize that, in this case, d_{50} ceases to be a relevant parameter *in* the region, $y/l_s \geq O(1)$. This permits the simplification of Eqn. 3.4.17 to

$$\Delta_s = \Xi_\infty \left(\frac{w_{s0}}{u_*} \right), \tag{3.4.18}$$

or, in terms of l_s, to

$$l_s = \frac{u_*^2}{g(s-1)} \Xi_\infty \left(\frac{w_{s0}}{u_*} \right). \tag{3.4.19}$$

Not surprisingly, perhaps, l_s, as defined by Eqn. 3.4.19, resembles the length scales previously defined by Itakura and Kishi (1980) and implicitly by Coleman (1981). One significant difference is that a concentration scale is not explicitly involved in Eqn. 3.4.19. For a suspension in equilibrium with a sand bed, the mean-concentration field is internally determined by hydraulic and grain parameters. This differs from the stably stratified atmospheric surface layer, where a heat flux is externally imposed. The appropriate length scale for equilibrium-bed flows should be definable entirely in terms of hydraulic and grain parameters. In this

respect, l_s resembles more closely a length scale that was proposed by Monin and Yaglom (1971), who omitted, however, any dependence on the settling velocity.

The approaches of Itakura and Kishi (1980), Coleman (1981), and Monin and Yaglom (1971) are all associated with the simple analogy to weakly stable, density-stratified flows. Their respective length scales should be interpreted as length scales above which the effects of stratification become important. The fact that the first two involve a concentration scale is characteristic of the stratified-flow analogy. In contrast, the length scale, l_s, is interpreted, by hypothesis, as a scale, *below* which the effects of the sediment are confined.

The difficulty for experimental work in this formulation lies in that the length scale is here defined only in terms of an unknown function, Ξ or Ξ_∞. This contrasts with familiar length scales, e.g., $l_\nu = \nu/u_*$, or the roughness height, k, which are known functions of known parameters. The unknown function must be determined from experiments. This determination presumes, however, an operational definition of l_s, such as the point at which the velocity-defect profile begins to deviate from the velocity-defect profile for clear-water experiments. The precision of such an operational definition is likely to be less than satisfactory.

3.4.4 Concentration scales

Various choices for inner and outer concentration scales would be consistent with the basic similarity model of §3.4.1. We first examine the implication based on the analogy to density-stratified flows. This implication is found to be too restrictive to describe the range of experimental results. This choice is, therefore, abandoned in favor of a more general model.

The effects of stratification are associated with buoyancy. In particular cases, the buoyancy flux or gradient may be a more convenient parameter. The local

buoyancy or submerged weight in a sediment-laden flow is $g(s-1)c$. A characteristic buoyancy for the outer or the inner region may be expressed as $g(s-1)c_h$ or $g(s-1)c_s$, where c_h and c_s are concentration scales for the outer and the inner regions. A distinctive feature of the analogy to stratified flows is seen to be the grouping of the reduced gravity, $g(s-1)$, and a characteristic concentration into a single term, e.g., $g(s-1)c_h$. If the buoyancy flux is taken as the more convenient parameter, such a grouping necessarily arises also.

On dimensional grounds, the stratified-flow analogy leads, therefore, to the following scaling for the outer region,

$$g(s-1)c_h h \sim u_*^2 \mathcal{E}_h \left(\frac{w_{s0}}{u_*}\right), \tag{3.4.20}$$

where it has been assumed that ν and d_{50} are of no direct importance. If the stronger assumptions, $\mathcal{E}_h \sim u_*/w_{s0}$, $w_{s0} \sim w_s$, and $c_h \sim \langle c \rangle$ are made, then this scaling may be used to motivate the Einstein-Chien (1955) parameter, and by extension, the Monin-Oboukhov scale proposed by Itakura and Kishi (1980). These previous approaches implicitly assume a single concentration scale. In the multiple-scales context, the scaling provides a possible definition of an outer concentration scale, namely,

$$c_h = \frac{u_*^2}{g(s-1)h} \mathcal{E}_h \left(\frac{w_{s0}}{u_*}\right). \tag{3.4.21}$$

An inner concentration scale may be symmetrically defined by

$$c_s = \frac{u_*^2}{g(s-1)l_s} \mathcal{E}_s \left(\frac{w_{s0}}{u_*}\right), \tag{3.4.22}$$

where l_s may be defined generally, though not necessarily, by Eqn. 3.4.17. *If* these scalings are appropriate, then it might be expected that $\mathcal{E}_h$ and $\mathcal{E}_s$ are $O(1)$ if

$w_{s0}/u_* = O(1)$. A matching of the scales in an overlap region requires, according to the condition, Eqn. 3.2.19, that

$$\frac{c_h}{c_s} \sim \left(\frac{h}{l_s}\right)^{-1}. \tag{3.4.23}$$

Eqn. 3.4.23 may also be obtained if it is assumed that $\mathcal{E}_h \sim \mathcal{E}_s$ rather than the stronger assumption that each is separately $O(1)$.

A power-law matching is therefore consistent with scales motivated by a stratified-flow analogy only if the exponent is -1. This may also be concluded from a more direct dimensional argument. If it is assumed that the mean-concentration profile is determined by the parameters, $g(s-1)c$, y, u_*, and w_{s0}, then a dimensional argument gives

$$g(s-1)c = \frac{u_*^2}{y}\Pi\left(\frac{w_{s0}}{u_*}\right). \tag{3.4.24}$$

As emphasized in §3.3, implicit in this dimensional scaling argument is the assumption that $l_s \ll y \ll h$, implying that the only relevant length scales are y and $u_*^2\Pi/g(s-1)c$. This result was previously obtained by Barenblatt (1979), following a more elaborate line of reasoning. To the extent that this simple stratified-flow analogy is accepted in the description of the mean-velocity profile, it is inconsistent to accept a power-law variation near the bed with an exponent different from -1, as was proposed by Itakura and Kishi (1980) in their Monin-Oboukhov approach.

A concentration profile varying precisely with y^{-1} is rarely observed in the laboratory. A possible explanation is that the conditions obtaining in typical laboratory flows do not satisfy the Barenblatt (1979) criterion, i.e., $w_s/\kappa u_* < 1$, for the existence of self-similar solutions. A practical difficulty in assessing Barenblatt's result is that his analysis assumes a constant-stress layer or, equivalently, an infinitely deep flow in which the effect of an outer length scale is everywhere

negligible. In a flow of finite depth, the self-similar power-law profile, like the log-law profile, is expected to be valid only in an intermediate region. The operational definition of this intermediate region, which may not be of large extent, may therefore influence the determination of the exponent. Nevertheless, some experimental results, e.g., Brooks (1954), indicate that a -1 power law is not necessarily observed even when the Barenblatt criterion is satisified.

Two choices are possible: i) abandoning the simple analogy to stratified-flows, or ii) abandoning the possibility of a self-similar solution. The simple analogy to stratified-flows is abandoned as the less drastic course. The stratified-flow analogy is characterized by the grouping of $g(s-1)$ and c into a single group, $g(s-1)c$; more generally, these parameters may be considered as two *independent* groups. This may be motivated on general grounds by the hypothesis that the presence of particles may affect the flow by other more important means besides buoyancy. Dimensional reasoning, then, gives for the concentration scales,

$$\Pi_h \left(\frac{g(s-1)h}{u_*^2}, c_h, \frac{w_{s0}}{u_*} \right) = 0, \tag{3.4.25}$$

$$\Pi_s \left(\frac{g(s-1)l_s}{u_*^2}, c_s, \frac{w_{s0}}{u_*} \right) = 0. \tag{3.4.26}$$

By itself, this takes us no further than before. Are there, however, concentration scales definable from these dimensionless groups that would be consistent with a more general power-law profile? Since the choice of Eqns. 3.4.21-3.14.22 led to Eqn. 3.4.23 and the -1 power law, another choice may be thereby motivated; namely,

$$c_h = \left[\frac{u_*^2}{g(s-1)h} \mathcal{E}_h \left(\frac{w_{s0}}{u_*} \right) \right]^Z, \tag{3.4.27}$$

$$c_s = \left[\frac{u_*^2}{g(s-1)l_s} \mathcal{E}_s \left(\frac{w_{s0}}{u_*} \right) \right]^Z, \tag{3.4.28}$$

where the exponent, Z, can depend only on a dimensionless parameter which is relevant in both the inner and outer flow regions. This choice of concentration scales is consistent with a power-law profile with a variable exponent, Z, since the ratio of c_h and c_s gives

$$\frac{c_h}{c_s} \sim \left(\frac{l_s}{h}\right)^Z . \tag{3.4.25}$$

Already, in the original Eqns. 3.4.21-3.4.22, as well as in the revised Eqns. 3.4.27-3.4.28, it has been assumed that the dimensionless parameter, w_{s0}/u_*, is relevant in both inner and outer regions. It is proposed, then, that the exponent, Z, is a function of this parameter only; i.e.,

$$Z = Z(\hat{\beta}) = Z\left(\frac{w_{s0}}{u_*}\right), \tag{3.4.29}$$

In the intermediate region, the above scales imply a concentration profile of the form,

$$c \approx \left[\frac{u_*^2}{g(s-1)y}\mathcal{E}\left(\frac{w_{s0}}{u_*}\right)\right]^Z . \tag{3.4.30}$$

It may also be noted that the simple asymptotic expression for l_s, Eqn. 3.4.18, leads to a corresponding asymptotic form for c_s, namely,

$$c_s = c_{s\infty}\left(\frac{w_{s0}}{u_*}\right). \tag{3.4.31}$$

3.4.5 Starved-bed flows and higher-order statistics

A subtle assumption that has not been stressed is that the suspension is saturated, being in equilibrium with a sand bed. The notion of saturation should be interpreted with reference to a specific sand grain. The fact that the mean fields are internally determined by the hydraulic and the grain parameters in the equilibrium case simplifies the problem. It permits the elimination of, at least,

one additional parameter which would be necessary to characterize the degree of unsaturation in a starved-bed regime where a sand-bed is not present. Indeed, what parameter, if only one is necessary, would be most appropriate is an interesting question which seems not to have been explicitly posed before. Given the parameters necessary for determining the saturated case, i.e., u_*, h, w_{s0}, d_{50}, and $g(s-1)$, what is the minimum information necessary to determine the unsaturated case? A possible answer is a point concentration at a reference location. Should, then, the reference location be fixed, e.g., at $\eta = 0$ or at $\eta = 0.05$, or should it vary with flow parameters, e.g. at l_s, the inner-length scale under equilibrium conditions? Another possibility is the depth-averaged concentration. In the Monin-Oboukhov approach of Itakura and Kishi (1980) and the wake-coefficient approach of Coleman (1981) applied to starved-bed flows, it is implicitly assumed that only a single additional parameter is necessary, e.g., the depth-averaged concentration, $\langle c \rangle$, or the bed concentration, c_0. Although it seems likely that one concentration measurement may determine a concentration scale, it is uncertain that it will determine concentration scales. It is seen, then, that the starved-bed case may be more complicated conceptually than the equilibrium case, opening a whole host of questions which have not been examined before.

Similarity hypotheses should also, strictly speaking, apply to higher-order statistics of a turbulent flow. Typically, however, these tend to exhibit more scatter and less similarity. Although this may be attributed to the greater experimental error associated with estimates of higher-order statistics, it may also be speculated that the requirements, in terms of the appropriate dimensionless number, e.g., the Reynolds number, may be more stringent. Even if only a very approximate similarity is achieved in the higher-order statistics, the concept of multiple scales

and the associated idea of rescaling may still be important in interpreting higher-order statistics. To some extent, these higher-order statistics, particularly the turbulence intensities, may be used to support the similarity hypotheses. In the less controversial case of homogeneous flows, it is now generally accepted that u_* is the sole velocity scale in the problem, even though *historically* there may have been debate about this. That the turbulence intensities, and hence the turbulent kinetic energy, scale with u_* or u_*^2, may be interpreted as giving further support to the hypothesis that u_* *is* the only velocity scale in the problem. *If*, in sediment-laden flows, it is also found that intensities scale with u_*, the same interpretation may be applied.

3.5 Summary and implications for experiments

A new conceptual model, based on similarity hypotheses rather than on traditional mixing-length closures, has been developed. It has been shown that the conventional matching argument used to deduce a logarithmic profile may be generalized to deduce a power law profile. This generalization allows the parallel treatment of velocity and concentration profiles entirely from general similarity hypotheses, without invoking a vertical balance equation. In addition to the purely procedural novelty, the suggested similarity model can reproduce traditional results, and has some novel implications for the velocity profile. It assumes that there is an inner region near the bed of extent, l_s, which is scaled neither by l_ν nor d_{50}, where the effect of sediment is largely confined. Thus, in the region, $y \gg l_s$, the velocity-defect profile should be identical to that found in clear-water flows. *If* there exists a distinct region, $l_s \ll y \ll h$, then the velocity profile in this region should be logarithmic with a von Kàrman constant of ≈ 0.4, the same as

in clear-water flows. In approximately the same region, the concentration profile should be described by a power law with a possibly varying exponent. Like the velocity profile, the concentration profile should also exhibit a wake component, reflecting the effect of the free-surface boundary. These general implications are all experimentally testable.

Although definite conclusions can be drawn from the basic similarity model, it does not completely characterize the mean profiles because it does not specify length and concentration scales. It is, therefore, compatible with a variety of more detailed physical assumptions, which would be embodied in specific choices of these scales. Scales based on the simple analogy to density-stratified flows were found to lead to results that were too restrictive. This analogy was therefore abandoned in favour of more general scales obtained from a more general dimensional analysis. These were, however, found only in terms of unknown functions which must be experimentally determined. The physical model also implies that the exponents, characterizing the asymptotic power law and the concentration wake function, should be correlated only with the ratio, w_{s0}/u_*.

4. Experimental details

4.1 Experimental apparatus

4.1.1 The open-channel flume

The experiments were carried out in an open-channel flume, shown in Fig. 4.1.1, approximately 13m (40ft) long and 26.67cm (10.5in) wide. Discharge is circulated by an axial-flow pump with variable-speed drive through a 10.2cm (4in)-diameter return pipe. A calibrated venturi section in the return pipe was used to measure the bulk flow rate. The flume is mounted on a tiltable truss such that its slope may be continuously varied. Observations were taken at a section $\approx$ 9m from the channel entrance, where glass windows permitted the use of the laser-Doppler-velocimetry (LDV) technique. The flume bottom was found initially to exhibit slight but measurable and localized non-uniformities, which were reflected in departures from strictly uniform flow conditions. This was attributed to modifications made to the flume truss in order to accommodate the carriage on which the LDV system was mounted. Adjusting mounting screws partially corrected these but tended to introduce new slight non-uniformities.

Fig. 4.1.1 Schematic diagram of open-channel flume

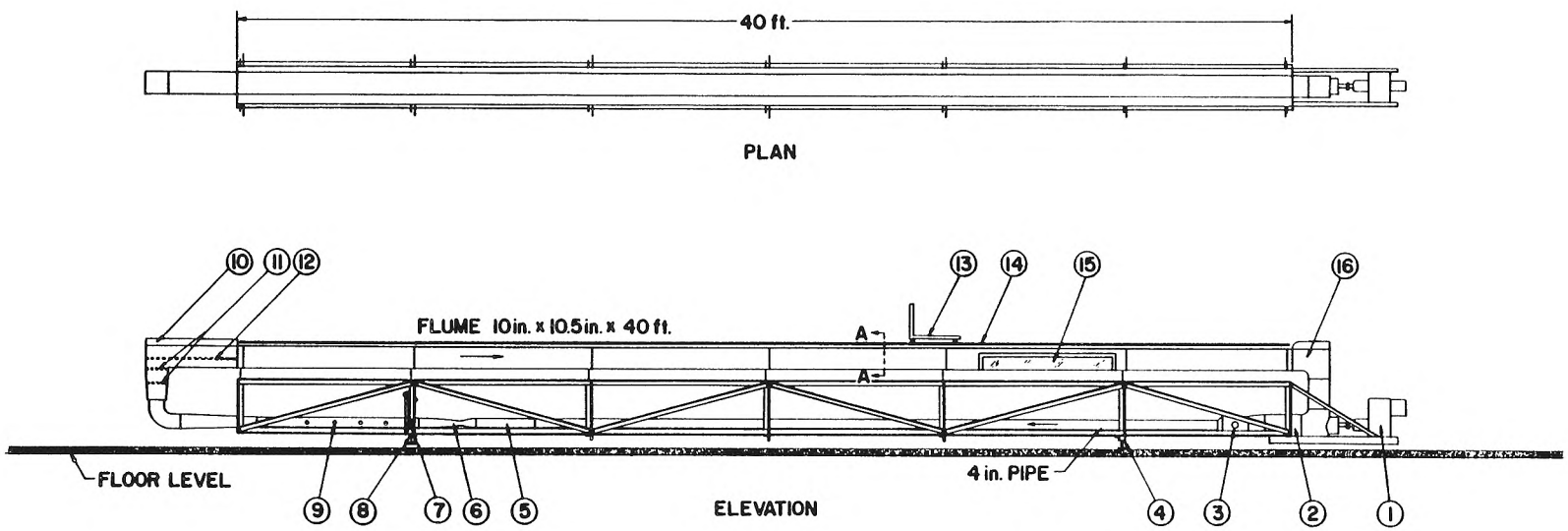

The bare flume is not perfectly smooth but rather is covered by an epoxied layer of fine sand, estimated to be of diameter, 0.15mm, or less. The flume sidewalls had no such layer and so were smoother, although some roughness stemmed from uneven or cracking paint. A slight flow disturbance could be noted at the junctions of the smooth glass windows and the sidewalls. In order to reduce entrance effects, coarse rectangular grids were placed horizontally in the vertical portion of the inlet box. A short ($\approx$ 6cm in length) honeycomb section at the entrance was used to straighten the flow. In some cases, this was raised from the bottom in order not to inhibit bed-load transport. Free-surface disturbances near the channel entrance due to the honeycomb were damped by placing a coarse wire mesh horizontally at approximately the level of the free surface. Another coarse wire mesh, placed vertically, was used as a downstream control, after which the flow fell freely into the outlet box. In cases where the downstream control was found unnecessary for achieving nominally uniform flow over the working section, it was removed altogether. Precision rails ran the length of the flume such that an instrument carriage carrying a point gauge could be freely moved along the flume.

4.1.2 The sediment sampler

Measurements of local concentration were made by the conventional suction-sampling procedure, in which a fixed quantity (here, 1 litre) of the suspension is drawn off isokinetically from the flow. The sampler is a 0.25 in o.d., 0.18 in i.d., brass tube bent at right angles, with a flattened tip, as shown in Fig. 4.1.2. The dimensions of the flattened tip were small enough so that a reasonable spatial resolution was obtained and yet large enough that, for the sand sizes investigated, i.e., up to 0.25 mm, sand grains were not inhibited from entering the sampler. The sampler is mounted on the instrument carriage and can be vertically positioned

to within 0.2 mm. A siphon arrangement, using 0.3 in tygon tubing, was used to provide the appropriate suction. Because of the possibility of deposition of sand in the siphon system, care was taken to minimize the length of tubing used and to maintain the tubing at a steep inclination by having the sampling bottle as near to the sampler as possible.

Fig. 4.1.2 Schematic diagram of the sediment sampler

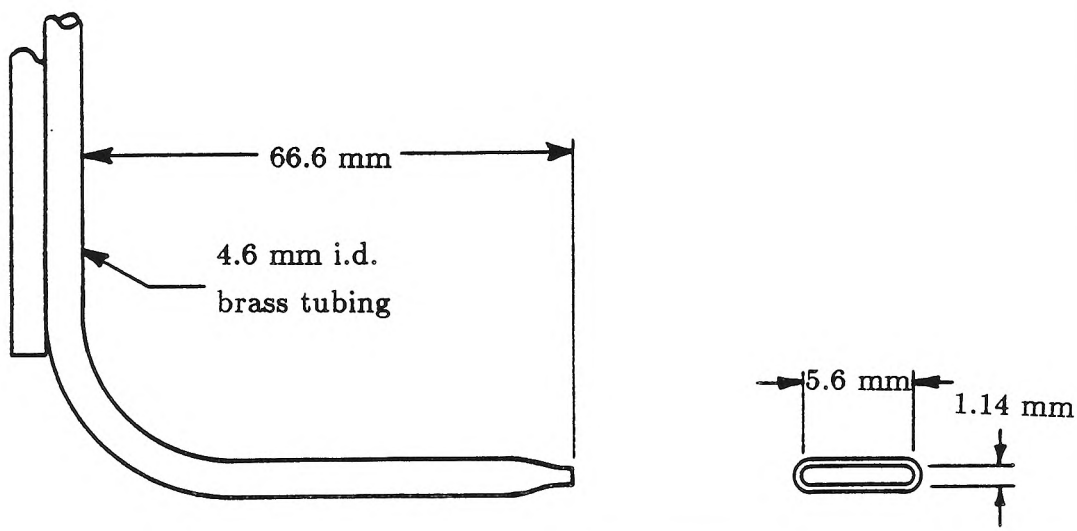

4.1.3 The laser-Doppler velocimeter (LDV) system

The basic LDV system, shown schematically in Fig. 4.1.3, used in this study was originally developed by van Ingen (1981) for use in sediment-laden flows. It is operated in the so-called real-fringe (or differential-doppler or single-particle-scattering) mode, since this allows the possibility of analyzing the doppler burst due to a single scattering particle, whether tracer or sediment. Its components may be divided into three subsections: 1) the transmitting optics, 2) the receiving optics, and 3) the electronic signal-processing system. The first was substantially

modified in detail from the original system used by van Ingen in order that two-component measurements could be made. The other subsections suffered only minor, if any, changes.

A schematic diagram of the transmitting optics is shown in Fig. 4.1.4. A 200 mW Lexel argon-ion laser, model 75.-2, tuned to the single green line (wavelength, 514.5 nm), is the light source. The beam from the laser is passed through two cube beamsplitters to produce three beams of differing intensities, one of which is perpendicular to the plane formed by the other two. Each beam is then frequency-shifted by passage through its own Bragg cell (oscillation frequency, $\approx$ 40MHz), then steered by means of a coated mirror in the desired direction. The resulting, nominally parallel, beams form a right isosceles triangle with its base horizontal, the length of each side being adjustable within certain limits. Parallelism was checked by directing the beams at a distant target ($\approx$ 40 m) and seeing that the distance between beams remained, within tolerance, constant at any section. van Ingen (1981) found that the typically elongated probe volume of the LDV system was susceptible to noise in sediment-laden flows and recommended the use of large ($\approx 20°$) intersection angles. For measurements on the flume centerline, such angles implied large beam separations, and, if a single focussing lens is to be used, a very large lens. Indeed, the beam separation at the base of the isosceles triangle actually used was $\approx$ 18 cm. The three-beam configuration was chosen in order to allow measurements closer to the bottom without compromising on the large intersection angles. The upper beam is masked if only the horizontal velocity component is to be measured.

The three parallel beams hit the convex face of a plano-convex lens (400 mm focal length, 250 mm diameter) at points equidistant from the axis of the lens,

Fig. 4.1.3 The laser-Doppler velocimetry system

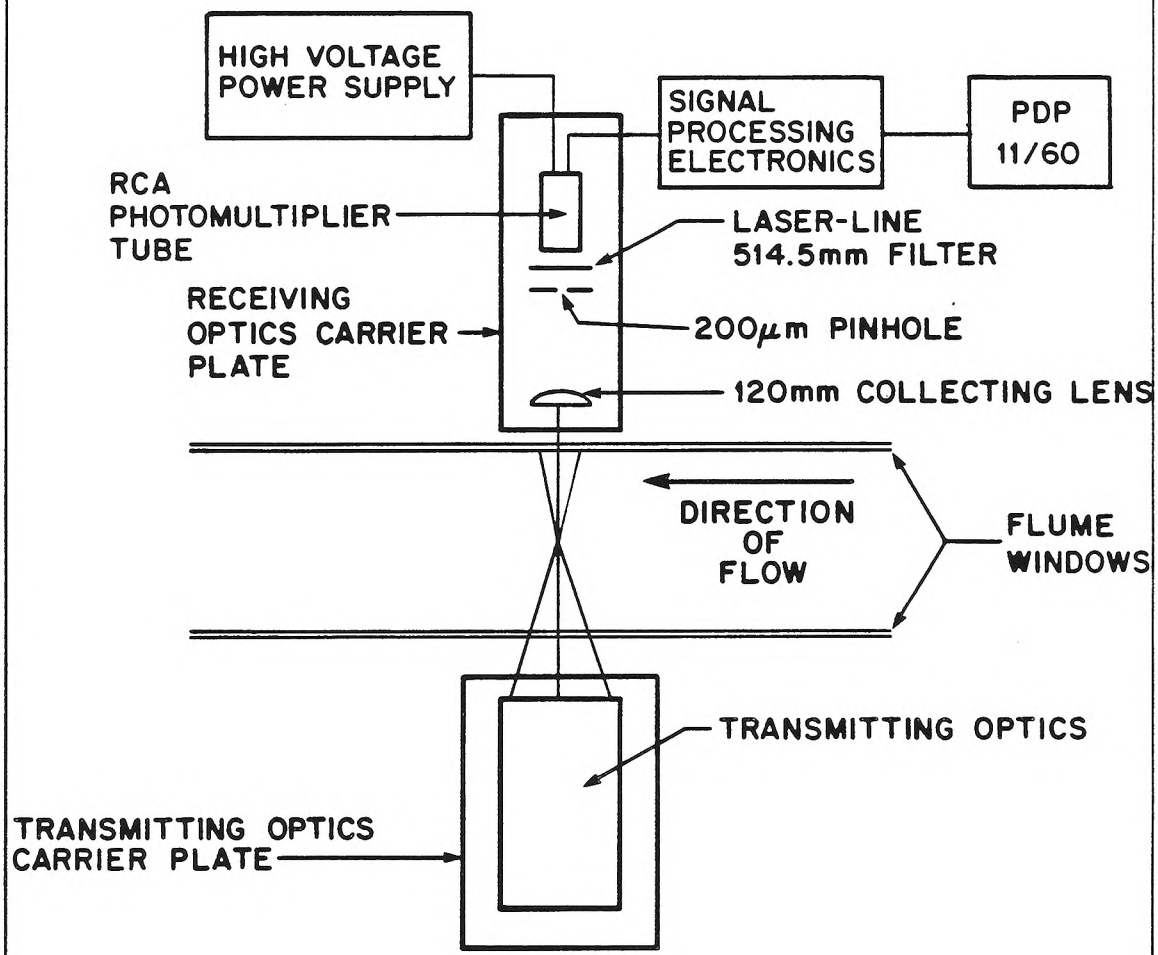

Fig. 4.1.4 Transmitting optics of LDV system

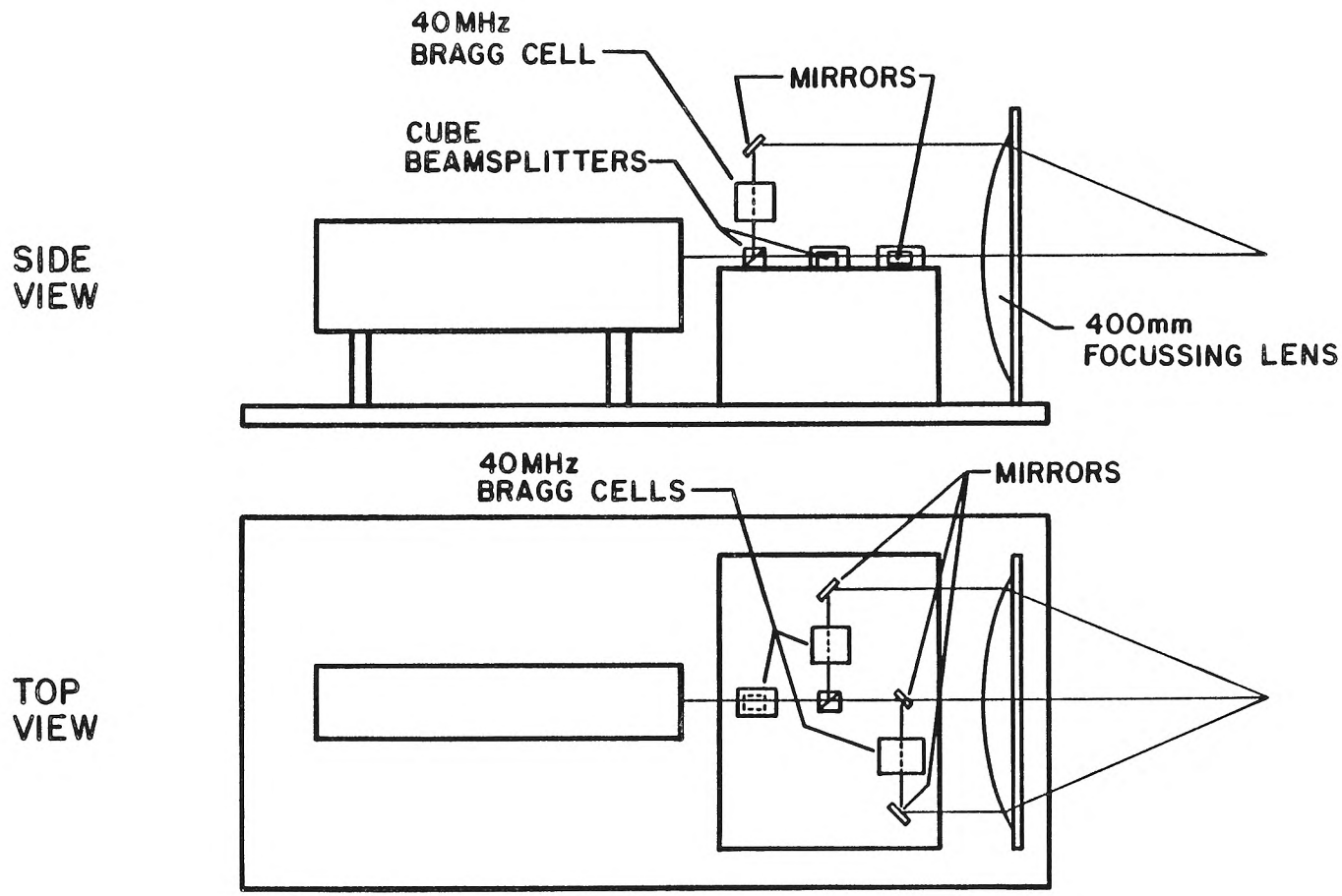

and are thus focused to a common focal volume. The system is also designed such that the three beams travel approximately equal optical path lengths. Slight adjustments were made to the mirrors to improve the coincidence of the beams at the crossing. Fig. 4.1.5 is a diagram of the resulting beam configuration. The approximately ellipsoidal common focal volume is estimated to have a minor diameter of $\approx$ 0.33 mm. The basic intersection angle, θ_{13}, between beams 1 and 3, was measured to be $24.12° \pm 0.10°$ in air. The angles, θ_{12}, and θ_{23}, were then determined from the geometry to be $18.06° \pm 0.08°$. In the flow, these angles would be reduced to 17.00° and 12.76° because of the larger refractive index of water. The major diameter of the probe volume was, therefore, estimated to be $\approx$ 2.2mm. In this configuration, the three pairs of beams can measure the instantaneous velocities, u (beams 1 and 3), $(u+v)/\sqrt{2}$ (beams 1 and 2), and $(u-v)/\sqrt{2}$ (beams 2 and 3). In this study, only the latter two are used when both velocity components are desired, while only the first is used when only the horizontal component is measured. A comparison of the u-statistics determined from two-component and one-component measurements offers a check on the geometrical consistency of the optical system.

The light scattered by the passage of particles (both sand grains and tracers) through the probe volume is collected by a single 120 mm focal length, 100 mm diameter plano-convex lens, with its convex face towards the beam intersection. Its optical axis is aligned so that it coincides with that of the transmitting lens. For two-component measurements, this results in a direction of collection oblique to the two pairs of beams involved and therefore a loss in light-collection efficiency. For measurements close to the flume bottom, a significant fraction of the collecting

Fig. 4.1.5 Configuration of laser beams

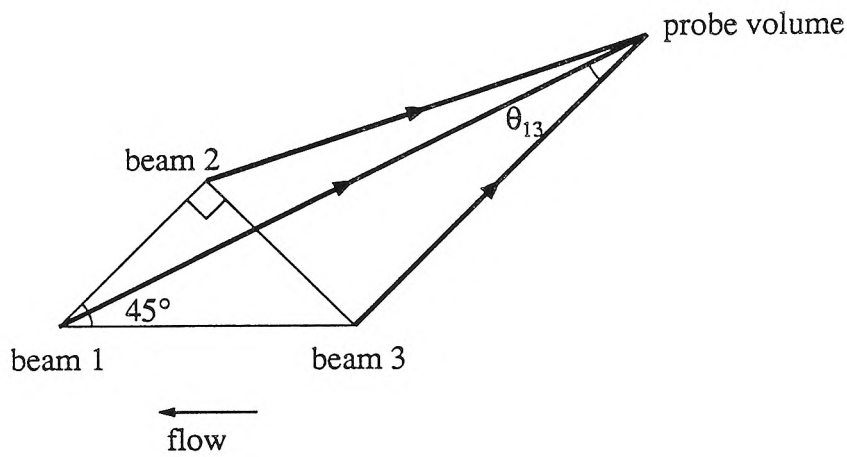

lens is further masked from the probe volume by the flume, contributing further to a reduction in light collected. The collecting lens is focused onto a photomultiplier module, consisting of a 200μm pinhole, which acts as a spatial filter, a 0.5145μm laser-line filter, and the photocathode of an RCA8645 photomultiplier tube (PMT). The unscattered laser beams are masked. The distances between the probe volume and the collecting lens and between the latter and the pinhole were adjusted to give a good signal. A magnification, estimated to be ≈ 1.2, was thus obtained.

Both transmitting and receiving optics were mounted on a special carriage, consisting of an aluminium box beam supported by four precision screw jacks, all of which passed beneath the flume structure. The jacks are manually driven and permit vertical positioning of the probe volume, accurate to within 0.2mm. The jacks themselves are supported by vibration isolators, Firestone Model IX84D Air Mount, to isolate the optical system from floor vibrations due primarily to the recirculating pump.

The PMT output is directly coupled to a preamplifier, constructed at the base of the PMT. A further consequence of large intersection angles used is the large frequencies (including the Bragg shift) encountered (0.4–1.3 MHz). The preamplifier used previously by van Ingen (1981,1983b) was found inadequate for this wide frequency range, and was replaced by another developed by D. Lang. Although the new preamplifier showed a marked improvement in performance and was found adequate for the present purposes, a gradual rolloff at frequencies beyond $\approx$ 800 kHz was noted. When two velocity components are to be measured simultaneously, the frequency shift resulting from each of the three Bragg cells is chosen such that three distinct frequencies are detected by the PMT, corresponding to the three pairs of beams. Only two of the three provide independent information. The frequencies are isolated by mean of analogue band-pass filtering, using high roll-off (24db/octave) Kronhite infinitely variable filters, model 3202.

Because of the use of electronic filtering for isolation (rather than, e.g., optical separation), it is necessary for the frequencies to be widely separated. The large magnitudes of the frequencies, as well as the roll-off characteristics of the preamplifier, however, restricted the choice of frequencies. It was finally decided to choose frequency shifts such that, under typical flow conditions, the frequencies present in the signal were $\approx$ 0.6 MHz, $\approx$ 1.2 MHz, and $\approx$ 1.8 MHz. The highest frequency, which suffered the most from preamplifier rolloff, was not used. Some difficulty was encountered in isolating the 1.2 Mhz signal, because its amplitude tended to be one-half or less of the 0.6 MHz signal. The use of two sets of filters in series was found necessary to obtain a reasonable 1.2 Mhz signal, while only one was used for the 0.6 Mhz signal. In the case of one-component measurements, interference effects were not an issue. Moreover, since only a single frequency is

to be measured, the constraint due to the frequency response of the preamplifier is relaxed. The chosen frequency shift for one-component measurements resulted in frequencies of $\approx$ 1 MHz. The signal-to-noise ratio achieved in both cases was typically 15–20 db in the clear-water experiments.

The filtered signal serves as input to a counter processor whose basic logic is shown schematically in Fig. 4.1.6, taken from van Ingen (1983b) to which reference is made for more details than are given below. The processor logic was aimed at i) distinguishing Doppler signals from noise, ii) determining the frequency of the Doppler signal, and iii) distinguishing between individual successive Doppler signals. A threshold level for the signal amplitude, below which a signal is considered to be noise, provides a first-level distinction between a valid Doppler signal and noise. The threshold level may also be used in a secondary role as a means of controlling the data rate by changing the effective measuring volume, since large-amplitude signals are associated with the comparatively rarer passage of particles through the central portion of the probe volume.

The frequency of the Doppler signal is determined by measuring the time required for a preset number of zero-crossings to occur, given that the signal amplitude remains above the threshold level. A limitation on the accuracy of the measurement is the clock frequency, which, in the present system, was 20 Mhz. Because of the high frequencies involved, the use of a faster clock was considered. This would, however, have meant that a large number of other components of the electronic system that could not operate reliably at much faster clock rates would have to be replaced. The other means of increasing accuracy, that of specifying a larger number of zero-crossings, was used instead. The use of a larger number

Fig. 4.1.6 Digital logic of the counter processor (from van Ingen, 1983b)

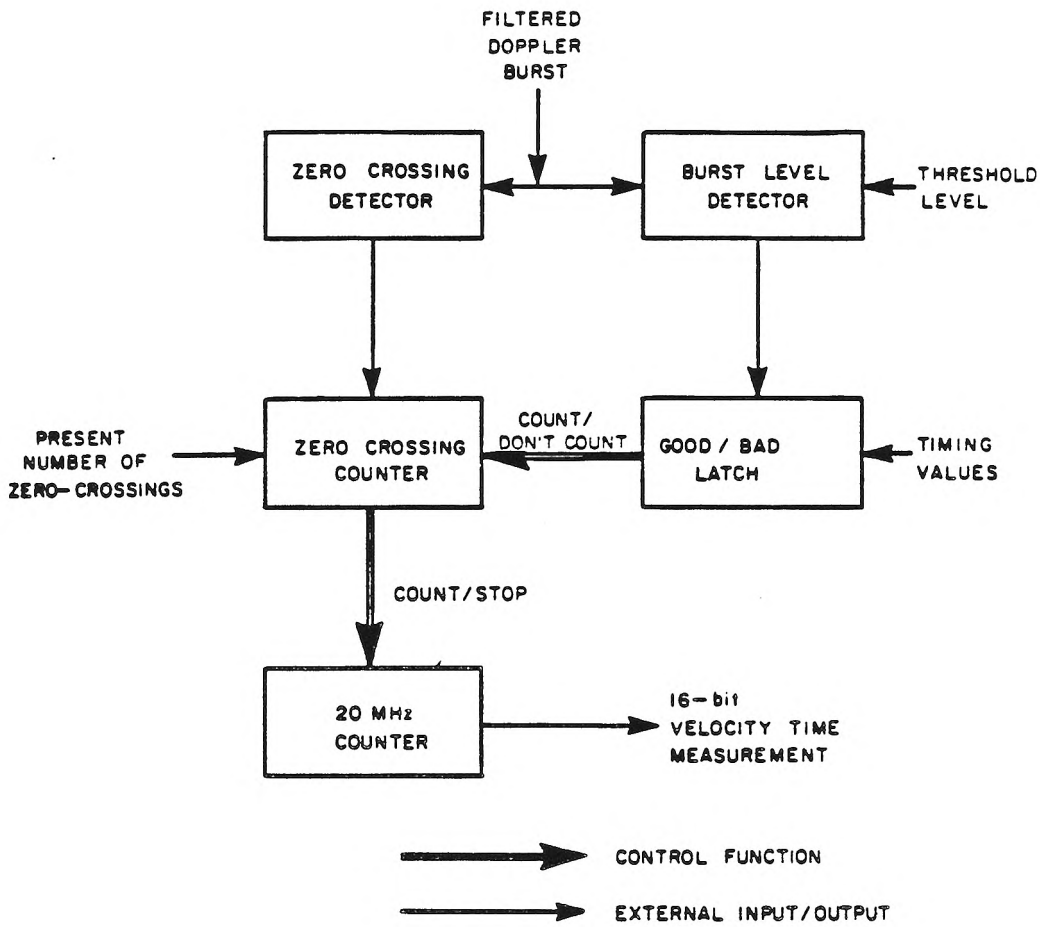

of zero-crossings, together with the threshold level, should also sharpen the distinction between noise and an actual Doppler signal, with resultant higher-quality data .

If the preset number of zero-crossings has been achieved, then all counters are cleared and the processor waits for another doppler burst. The distinction between successive Doppler signals is made by a timing circuit, with an adjustable time constant, chosen to be longer than the minimum time between two zero-crossings, but shorter than the minimum time between two successive Doppler bursts. In this way, if the preset number of zero-crossings has been achieved, the timing circuit will detect the end of the doppler burst, so that only a single velocity realization is obtained from a single doppler burst. For the present study, the time constants were chosen as 3.2μs and 2.5μs for the "slow" and the "fast" channels.

It should be noted that only a zero crossing is checked, and there is no check on the sequence of events surrounding a zero crossing, such as would be provided by using two threshold levels symmetric about the zero level, and then checking that the signal crosses the threshold levels in the appropriate sequence. The present logic of the counter may then be open to a type of error resulting in spurious zero-crossing counting. In order to minimize such an occurrence, an additional validation procedure, based on checking the regularity of the Doppler signal, is used. Besides the time required for a preset number of zero crossings to be achieved, the time required for approximately half of this preset number to be achieved is also reported. The consistency of the two times is then checked during the data analysis, and the realization is discarded if a certain tolerance (approximately half the mean time necesary for a single crossing) is not met.

In addition to the signal from which Doppler frequencies are obtained, another signal is derived from the raw signal by low-pass filtering at 10 kHz. This provides information concerning the pedestal of the Doppler burst, which depends on the intensity of the scattered light reaching the photocathode. As such, the passage through the measuring volume of sand grains, which are typically two orders of magnitude larger than tracer particles, should be associated with large pedestal amplitudes. These are compared to a number (here, four) of reference voltages, using a comparator circuit, and so may be placed in any of five size classes, the boundaries of which are defined by the reference voltages. This should provide a method of distinguishing between sand grains and tracer particles.

In practice, it was found that a sharp distinction could not be made. A wide variation of pedestal amplitudes was observed even under clear-water conditions. Unfortunately, much the same variation was observed in sediment-laden flows. This may be attributed, to some extent, to the attenuation both of the laser beams and the scattered light in a suspension. This also introduced a further complication since the vertical variation in sediment concentration resulted in a vertical variation in attenuation. Another source of vertical variation is the masking effect as either of the two boundaries, i.e., the free surface or the bed, is approached, since the collecting angle of the receiving lens may be significantly reduced. Further problems arise from the possibility of sand grains grazing the measurement volume and also, perhaps, from the irregular shape of sand grains, which may provide multiple small scattering sites rather than the single large site usually considered in idealized LDV studies.

Because of these many uncertainties, which do not seem susceptible to definite calibration, it was decided that the comparator circuit be used to minimize the

contamination of tracer-particle data by sand-grain data rather than to detect sand grains. From the five pedestal-amplitude classes obtained with the four reference voltages (chosen as 0.4 V, 0.8 V, 1.2 V, 1.6 V), only the class of the smallest amplitude, i.e, those below 0.4 V, was used for computing turbulence statistics. These reference voltages were used uniformly for all experiments. This was done since there seemed little rational basis for any alternative scheme. Further, it may be argued that the great majority of velocity realizations will be due to the tracer particles. The computed statistics will therefore not be especially sensitive to an occasional error in mistaking a sand grain for a tracer particle. On the other hand, if information on grain velocities is wanted, then the smaller sample of sand-grain velocity realizations will be very sensitive to contamination from tracer-particle velocities.

The above considerations apply, in general, to each individual channel separately. For two-component measurements, the signals of the two components must satisfy the requirements, e.g., the threshold level, simultaneously. In this sense, the conditions for the two-component measurements are more stringent and result typically in a reduced data rate. Zero crossings for two-component measurements were chosen as 41/80 and 17/32 (where the first number gives that used in the validation procedure as a regularity check and the second number gives that used in actual determination of the doppler frequency), corresponding to the high and the low frequencies to be measured. A 25/48 zero crossing was specified for one-component measurements. This may be compared to the 5/8 scheme, quoted in standard references (Drain, 1980; Durst et al., 1981). Besides the increased counting accuracy, two other reasons for setting a larger number of zero crossings may be cited. The use of the pedestal to distinguish between tracer particles and sand

grains should be more effective if the particle passes through the central portion of the measuring volume. Setting a large number of zero-crossings should aid, then, in minimizing the contamination of fluid-velocity measurements by grain-velocity measurements. Moreover, the large frequency shifts, 900 kHz and 300 kHz, used to obtain widely separated doppler frequencies, artificially inflated the actual Doppler frequencies of $\approx$ 300 kHz. The fluctuating part of the measurement, which is one of the main concerns of this study, forms a relatively small part of the measurement, and greater than usual counting accuracy is necessary to capture this.

The processor is digitally interfaced with a PDP-11/60 minicomputer. The results of the counter for each individual realization are transmitted digitally using a true handshake process. Each realization is made up of three (one-component measurement) or five (two-component measurement) words, consisting of the times for the check and the actual zero-crossings for each component, as well as the time of measurement. These are written on to either an RL05 removable disk or a DSD 880 fixed disk in 1024-word buffers.

A summary of the LDV characteristics is given in Table 4.1.1.

4.2 Experimental considerations

4.2.1 Experimental constraints

The modelling of the natural river in all its complexity is beyond the scope of laboratory investigation and undesirable, since interpretation of results is greatly complicated. Since attention is to be focused on the effect of suspended sediment on turbulence, this study is restricted to cases where the so-called "flat-bed"

Table 4.1.1 LDV system characteristics

	beams 1–2	beams 1–3	beams 2–3
probe volume diameter (μm)	328	328	328
probe volume length (mm)	3	2	3
intersection angle in water (°)	12.76	17.00	12.76
fringe spacing (μm)	1.16	0.88	1.16
frequency shift difference, 2-comp (MHz)	0.3	1.2	0.9
frequency shift difference, 1-comp (MHz)	–	0.5	–
number of zero crossings, 2-comp	17/32	–	41/80
number of zero crossings, 1-comp	–	25/48	–

regime is achieved. In the case of unsaturated or "starved-bed" flows, where an equilibrium sand bed does not exist, this restriction is automatically satisfied, since the bed is the flume bottom, which may be considered flat. Where a sand bed does exist, the flat-bed regime is achieved only under a rather narrow range of experimental conditions. The flatness of a bed should, however, be considered in relation to the other length scales of the problem. If the amplitude of the bed forms is sufficiently small relative to the depth of flow, and their horizontal extent is sufficiently long, it is usually classified as a flat-bed flow even if small departures from the ideal flat bed can be measured.

While restriction of the study to the starved-bed cases is convenient in practice, and, thus, has often been the case, the study of the equilibrium or saturation cases is attractive for several reasons. As mentioned previously, the existence of a saturation point, where local concentration cannot be exogenously increased for given hydraulic and grain parameters, distinguishes equilibrium sediment-laden flows from the type of density-stratified shear flows treated by the classic Monin-Oboukhov theory. This saturation limit seems then to be physically significant

in light of attempts to exploit the analogy with density-stratified flows. The conceptual simplicity of the equilibrium-bed case relative to the starved-bed case, discussed previously, also argues for an examination of the former.

A related question about starved-bed cases concerns its characterization. The existence of a saturation point suggests that the description of a starved-bed case be given in terms of, or relative to, the saturated case. If the latter is known, then this presents no problem. However, since little is known quantitatively of the saturated case, its investigation seems necessary. Finally, it should not be forgotten that the equilibrium case does occur naturally, although only under a relatively narrow range of conditions for a flat bed. It might even be argued that, for certain conditions, the results for a flat bed may be applicable qualitatively, and, perhaps, with simple modifications, quantitatively, to beds that are not flat.

The decision to deal solely with flat beds, both in equilibrium and starved-bed cases, placed one type of restriction on possible experimental conditions; another restriction involved the depth of flow, particularly in relation to the width of the flume. A major criticism of the work of Coleman (1981) was the small width-to-depth ratio (b/h) of 2 that was used. Other well-known experiments, e.g., Brooks (1954) ($b/h = 3-4$), Einstein and Chien (1955) ($b/h = 2-4$), have been performed with rather small aspect ratios in order that a larger number of measurements can be made at smaller relative depths, y/h. This advantage is counterbalanced, however, by the possible importance of three-dimensional effects, such as secondary currents, which may complicate the experimental results and their interpretation. Unfortunately, it is not clear, in general, what minimum width-to-depth ratio is necessary to obviate three-dimensional effects on measurements on the centerline of the flume. This issue is particularly unclear in the case of flows with a sidewall

roughness different from the bottom roughness, as would be the case with an equilibrium bed. Further, the effect of sidewalls should decrease as the free surface recedes. It was decided somewhat arbitrarily to perform experiments only with aspect ratios greater than or equal to 4, thereby giving a maximum depth of $\approx$ 6.6 cm. Such a depth (or smaller) accommodates a reasonable number of measurements without being obviously open to the criticism of too small an aspect ratio. Although the use of wider flume would have helped in this regard, it would also have aggravated the problem of the attenuation of the laser beams and the scattered light in the suspension, and probably, the noise in the Doppler signals.

To facilitate interpretation of results, particularly in problems where the relevant dimensionless groups are controversial, it is desirable to vary only a single parameter and keep all others constant in any specific experiment. The above restrictions, however, render this goal infeasible. For example, if a flat bed is achieved with given shear velocity, u_*, and depth, h, as well as with given grain size, d_{50}, then it is highly unlikely that, with the same u_* and h, but larger d_{50}, the bed will remain flat. In general, u_* must also be increased as d_{50} is increased. It may also happen that, for sufficiently large d_{50}, a flat bed may not be achievable if h is to be kept constant. A similar result is also likely to occur if h and d_{50} are to be kept constant, while u_* is increased. The range of conditions under which a flat bed can be achieved has been examined in Hill et al. (1969) and, somewhat more fully, in Vanoni (1974), and some crude empirical results are available. Because of the constraints on the depth, and because it is relatively easy to maintain and verify a constant depth, the other parameters were varied rather than the depth. Nevertheless, experiments were conducted at two different depths, $h \approx$ 6.5cm, and $h \approx$ 5.7cm, with respective aspect ratios of 4 and 4.7.

These depths were also satisfactory with respect to other considerations. Deposition of sand in the return pipe at the low bulk-flow rates associated with small depths did not pose any problems. The entrance length for turbulent, open-channel flows is usually given in terms of the depth of flow (Yalin and Karahan, 1981). In the case of equilibrium beds, it was found that the bed itself had a substantial associated entrance length, typically at least 4m, which was necessary before it approached its asymptotic equilibrium. As such, the relevant origin with respect to the full development of turbulence should then be the beginning of the equilibrium bed, rather than the actual channel entrance. While the ratio of the distance to the observation point from the channel entrance to the depth, for $h = 6.5$cm, was greater than 140, which is more than adequate, the ratio of the distance to the observation point from the beginning of the equilibrium bed was more like 70, which is perhaps just adequate.

4.2.2 Sand-grain characteristics

In practice, it is convenient to vary d_{50} and find the appropriate u_* to achieve a flat bed rather than vice versa. While u_* may be varied continuously, sands are only available at discrete levels of d_{50}. It has also been argued that the important characteristic of a sand grain, at least in relation to suspension effects, may be the settling velocity, w_{s0}, rather than d_{50}, and the important parameter is the ratio, w_{s0}/u_*. A further advantage of varying d_{50} rather than u_* is the wider variation in w_{s0}/u_* obtainable, since w_{s0} is relatively sensitive to d_{50}. On the other hand, because the concentration profile also depends sensitively on w_{s0}/u_*, care should be taken to obtain a dense, in addition to wide, variation in w_{s0}/u_*. The inevitable gradation in even well sorted natural sands limits, however, the denseness that can

be obtained, although this is compensated partially by the necessary accompanying variation in u_*. A further constraint on w_{s0} is imposed by the use of the LDV technique. At point concentrations of 10^{-3} (2.65g/l) or greater, the effectiveness of the LDV technique in measuring turbulent fluctuations, particularly when two velocity components are desired, is seriously reduced. As long as such concentrations are confined to a narrow region of the flow, and reliable measurements can be made outside of this region, this situation can be tolerated. As w_{s0}/u_* is decreased and local concentrations are increased, a point is reached where reliable turbulence measurements are not possible with the present LDV system.

Five sand sizes were tried in the course of this study, with d_{50} ranging from 0.1 mm to 0.35 mm, with a corresponding range in w_{s0} of 0.8 cm/s to 5 cm/s. The smallest was found, for a typical u_* of 3.5 cm/s, to result in concentrations too high for reliable measurements by the LDV technique. The largest size, on the other hand, was found incompatible with a flat-bed condition for the imposed depth of flow. Only three sand sizes were therefore used in this study. The size distribution of each, from sieve-analysis, is shown in Fig. 4.2.1, and the characteristic parameters of each are given in Table 4.2.1.

Table 4.2.1 Sand-grain characteristics ($T = 21°$)

	Sand 1	Sand 2	Sand 3
median grain diameter, d_{50} (mm)	0.15	0.19	0.24
gradation, σ_g	1.12	1.20	1.18
settling velocity, w_{s0} (cm/s)	1.6	2.3	3.1

Fig. 4.2.1 Grain-size distribution of sands used

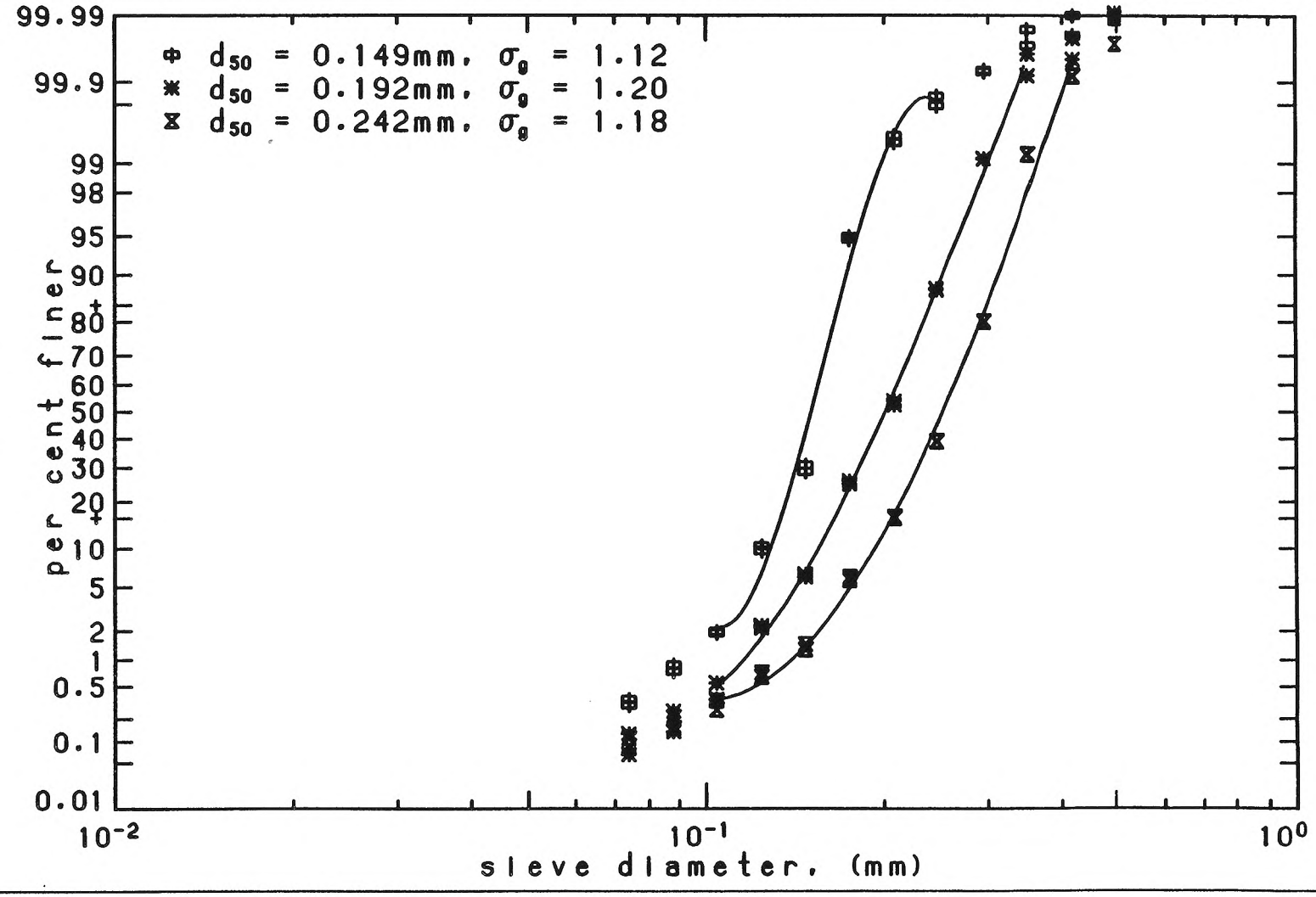

4.2.3 Starved-bed experiments

In addition to experiments with beds in equilibrium with the suspension, starved-bed experiments were also performed. These served the double purpose of further studying the effect of the suspension on turbulence characteristics and also of examining the approach to equilibrium. Because of the latter aim, the majority of the starved-bed experiments were performed under approximately the same conditions as the equilibrium-bed experiments. Starved-bed experiments were restricted to only a single sand size, the 0.19 mm sand. Equilibrium-bed experiments were performed first so that the results for these were used to guide the choice of the degrees of saturation at which the starved-bed experiments were performed. In one set of starved-bed experiments, conditions were used under which an equilibrium bed had not been previously achieved. This set, investigating the approach to equilibrium under high-transport conditions, was limited by the degree of saturation at which reliable results could be obtained by the LDV technique.

4.2.4 Clear-water experiments

Flows without sediment, i.e., clear-water flows, were also studied for several reasons. The performance of the LDV system, under the "ideal" conditions afforded by such flows, in measuring turbulence characteristics can be checked since an abundant literature describing results in homogeneous wall-bounded flows exists and may be used as a basis for comparison. In particular, the logarithmic velocity profile is well established and a value of 0.4 for the von Kàrman constant, κ, is generally accepted. Not all uncertainties, however, originate from the instrumentation. Because the width-to-depth ratios used were rather marginal, questions were raised as to its effect. Whether or not this effect is exacerbated

by the presence of suspended sediment is debatable, but some indication of its general effect may be investigated using clear-water flows alone. The questions concerning the wake component in open-channel flows and the magnitude of the wake coefficient and the expected scatter, have not yet been definitively settled in the literature. With regard to higher-order turbulence statistics, while a great many studies of the horizontal turbulence intensities may be found, relatively few give any information on the statistics of vertical motion, and fewer still on even higher-order statistics which may be of interest, such as the intensity of the Reynolds stresses. Even in published results, some scatter exists, which may be attributed to differences in instrumentation or in flow conditions. It may be argued that a more precise evaluation of the effect of suspended sediment on turbulence is made from a comparison of results from clear-water flows and sediment-laden flows under approximately the same flow conditions and obtained by the same instrumentation. Thus, the clear-water flows studied approximated the conditions of the sediment-laden flows.

4.2.5 Instrumentation and statistical considerations

The resolution of an instrument limits the scope of the investigation. As has already been noted, the probe diameter of the LDV system is $\approx$ 0.3mm for the minor axes and $\approx$ 2mm for the major axis. Although these may be reduced by the use of beam expanders, it is not clear that a reduction in probe volume would be advantageous in sediment-laden flows, with sand-sizes larger than the minor diameter. For the flows studied, estimates of the turbulence scales are listed in Table 4.2.2.

Table 4.2.2 Relevant length and time scales

Scales (μm or ms)	
outer length scale, h	60000 μm
viscous length scale, ν/u_*	30
Kolmogorov length scale	100
sand-grain diameter, d_{50}	200
probe volume diameter	300
sediment-sampler opening	1200
fringe spacing	1
outer time scale, h/u	100 ms
viscous time scale, ν/u_*^2	30
time resolution of LDV	0.5

A discussion of the temporal resolution of the LDV system is complicated by the nature of the sampling process in the single-particle-scattering mode of operation. Unlike the continuous signal from a hot-film anemometer or some LDV systems, the signal depends on the passage of a tracer particle through the measurement volume such that the sampling is highly irregular in time. The sampling rate, then, can be characterized only in a statistical sense. Care should, however, be taken in identifying this mean sampling rate (hereafter termed simply, data rate) with the conventional regular-sampling rate, e.g., in the application of the sampling theorem. A high data rate has the advantage that time integrals may be used in evaluating the signal statistics (Dimotakis, 1976) without sampling bias, and that reconstruction of the signal using interpolation may be performed with some confidence. A data rate of over 500 Hz has been achieved in one-component measurements in clear water, indicating the relatively fast response time of the LDV system. For the desired averaging times, however, high data rates result in

large amounts of data and an increased computational burden. More important, while such data rates may be achievable in clear-water flows, drastically lower rates are achieved in the noisier sediment-laden flows. In some such flows, data rates as low as 1 Hz were accepted. Data rates were, then, not limited by the LDV system itself but by the control parameters, e.g., threshold levels and the number of zero crossings. Since clear-water results are to be compared with sediment-laden flows, and since the spatial resolution is relatively coarse, high data rates were considered inappropriate and so more modest data-rate goals were specified.

Although it has been found in clear-water flows that relatively little energy resides in scales with frequencies beyond 25Hz (Raichlen, 1967; Blinco and Partheniades, 1971), the low data rates obtainable in sediment-laden flows limit the usefulness of spectral analysis. The irregular sampling, besides presenting problems in statistical bias to be discussed below, also renders a direct use of the fast Fourier transform (FFT) impossible, so that, if this is to be used, the data must be interpolated to obtain a regularly sampled record. In this work, spectral estimates are obtained from the raw, irregularly sampled record, linearly interpolated at a frequency somewhat below the mean data rate, using the FFT algorithm. These estimates should, therefore, be interpreted with some circumspection.

More emphasis has been placed on statistics, such as central moments, which are not constrained by the sampling theorem or the availability of a fast algorithm. To obtain stable statistical estimates, however, a sufficient length of record must be taken. In this regard, the analogy between a continuous time series with an integral scale and a sequence of independent random events is helpful (Lumley and Panofsky (1964); George, Jr., 1978). The integral scale provides a time scale, and points separated by more than two integral scales may be regarded as independent

events. As such, the familiar rule that the error in the estimate varies inversely as the square root of the number of independent measurements may be adapted. From this simple analysis, the length of record required for the estimate of the Reynolds stress to be within 5% of the actual Reynolds stress (assuming only statistical errors) is $\sim$ 3200 integral time scales. This is based on an estimate of the rms of the Reynolds stress, which is typically 200% of the mean. In the present study where the outer time scale, taken to be the same as the integral scale, is $\sim$ 0.1 s, this implies a length of record of $\sim$ 320 s. This may be compared to the length of record required for the same error in the estimate of the mean velocity which by the same analysis is found to be $\sim$ 2 s (assuming an rms of 15% of the mean). These estimates assumed that at least one point is sampled in each independent segment, i.e., a data rate of at least 5 Hz. At lower data rates, each point is independent and the requirement should be given in terms of the total number of points in the sample. For the example of the Reynolds stress, 1600 points would be deemed necessary. This discussion of averaging times has implicitly assumed regular sampling. The situation with irregular sampling is less clear but should not drastically change the estimates.

Associated with the question of irregular sampling is the problem of sampling bias (McLaughlin and Tiederman, 1973; Dimotakis, 1976; Buchhave et al., 1979). Because sampling depends on the passage of tracer particles through the measuring volume, more samples are taken at larger instantaneous flow rates through the measurement volume, assuming a distribution of tracer particles uncorrelated with velocity. Thus, a bias towards a higher mean velocity will result if the conventional method of estimating the mean, which assumes regular sampling, is used. Higher-order statistics are also affected, since the probability density distribution becomes

more positively skewed and somewhat narrower. Although various bias-correction schemes may be adopted, this study ignores this issue. One reason for this is uncertainty about the effect of the presence of suspended sediment on sampling bias. Further, since the comparison is made between clear-water and sediment-laden turbulence, this amounts to assuming that the suspension does not introduce any significant statistical bias over and above that encountered in clear-water flows. Also, errors due to sampling bias are expected to be less important in wall-bounded flows, where rms velocity fluctuations tend to be 5%-15% of the mean velocity.

4.3 Experimental procedure

4.3.1 Procedural considerations

A major concern of the experiment was to obtain a detailed characterization of the variation of turbulence statistics with distance from the wall. This meant a relatively large number of measurements at different vertical positions for each experiment. Earlier experimental work usually measured mean velocities at 8-12 points in the laboratory and even fewer in the field. In the present series of experiments, velocity measurements were taken at as many as 27 points, and at least 17 points, and these were chosen such that more points were taken as the bed was approached. Measurements of mean concentration were made at slightly fewer points, usually 15-20, being limited by the resolution of the suction-sampler. A further advantage of a dense observation scheme is the easier identification of outliers or spurious points, which are, therefore, weighted more appropriately if any kind of data-fitting is attempted.

In order to obtain stable averages, particularly for higher-order statistics, an averaging time of over 150 s was used for velocity records in the upper part of the

flow. This was gradually increased as the bed was approached, since turbulence intensities increased in that direction. In sediment-laden flows, for points near the bed, the constraint for statistical stability no longer rested on averaging time, because of the very low data rate, but rather depended on the number of velocity samples. A minimum of 1000 points in a velocity record was used as a criterion. In extreme cases, this might result in an averaging time of over 20 minutes. For concentration measurements, at least two 1-liter samples obtained from suction sampling, were taken at each point. The elapsed time for each sample was dictated by the isokinetic requirement, and for typical flow conditions, varied from 4-7 minutes, increasing as the bed is approached. Averaging times for both velocity and concentration measurements were, therefore, comparable being of the order of 1500-4000 integral time scales.

The desire for a large number of observations in the vertical, in view of the time taken for each velocity or concentration measurement, meant that a single experiment could not be completed in one sitting. In order to minimize the drift of experimental conditions, it was decided, after some initial experiments, that even a complete velocity or concentration profile could not be obtained in a single run. Moreover, interest in the mean velocity profile in the upper part of the flow, because of the predictions of the stratified-fluid analogy, and the limited vertical range of movement of the LDV system when operated to measure two velocity components, dictated that two independent sets of velocity measurements, a one-component set and a two-component set, should be made. These could be used to check on the consistency of the LDV system performance. The majority of experiments were therefore performed in six runs or sittings, two runs each for the two-component, the one-component and the concentration measurements, usually

in that chronological order. Typically, the points in the vertical obtained for the first and second runs were interleaved. This provided an additional check, not only of the consistency of the results, but also of the reproducibility of the flow conditions, since the water was usually changed completely for each run. Changing the water was necessary for sediment-laden flows because the water tended to become more cloudy with time, with an attendant decrease in signal-to-noise ratio for the LDV system. The total time during which measurements were made in a single run ranged from 2–4 hours.

It should be mentioned that there was not a rigid and uniform adherence to the above scheme for all experiments. In the early experiments with the smallest sand (d_{50} = 0.15 mm), complete profiles were taken at a single sitting. Even in these cases, however, interleaving of observations in two scans was used, such that they may be considered essentially as two separate runs performed at a single sitting. In the last clear-water and starved-bed experiments at the smaller depth, fewer measurement points in the vertical, as well as a faster data rate, permitted complete profiles in a single sitting with no interleaving.

4.3.2 Experimental preliminaries

When the desired flow conditions had been prescribed, the flow was set up. For the equilibrium-bed flows, 20–30 kg of sand from the laboratory sand library was placed in the flume, and washed. A flat-bed, uniform-flow condition was then achieved by a trial-and-error iteration in adjusting discharge and bed slope. Once achieved, the depth was fine-tuned. Typically, the bed, in the vicinity of the measuring station, had a thickness of 3–5 mm (i.e. $\approx$ 20 grain diameters), with a crust-like surface. Ripples tended to form at the flume corners and extended some 3–5 cm inward. After the flow had been essentially set up, it was run for periods

of 4–8 hrs for a few days in order to confirm the stability of the flow conditions. These periods were also often used to check the LDV system parameters such as the data rate and the threshold levels. For starved-bed flows, sand was added and the local concentration measured at one or two points. If the measured concentration was considered appropriate, considering the number of starved-bed experiments planned for those conditions, and considering, if available, the concentration for the equilibrium-bed case, then no more sand was added. Compared to the sediment-laden flows, the clear-water flows were easily set up and require no comment.

Before any measurements were taken, the flow was allowed to run for some time to establish a steady state. For clear-water and starved-bed experiments, this might be as short as 1 hr, while for equilibrium-bed experiments, this period might be over 4 hrs. Immediately prior to the beginning of making measurements for each run, a survey of the water-surface elevation in at least a 5 m vicinity of the observation point was taken with the point gauge. For equilibrium-bed experiments, the survey began at ≈ 5 m from the channel entrance in order to allow the bed to reach its fully-developed state. The temperature of the flow and the bulk flow rate were also noted. The equivalent information was also taken at the end of each run. In addition, for the equilibrium-bed cases, a survey of the bed elevation was taken after the flow had been stopped. The still-water level, corresponding to the particular flume slope, was known from a previous measurement. The energy slope was computed from the averaged measured water-surface elevation and the still-water level and the bulk flow-rate, while the bed slope (not necessarily the same as the flume slope) was computed from the measured bed elevations and the still-water level. In clear-water and starved-bed flows, differences between the bed slope and the energy slope were less than 3%. On the other hand, differences

might be as large as 5% for equilibrium-bed runs, although difficulties in defining a mean water-surface elevation because of small surface waves might be cited. The slopes given in the results are the averages of the energy and the bed slope.

4.3.3 Velocity and concentration measurements

Only centerline velocities were measured in this study. During a run, velocity measurements were begun in the upper part of the flow. The LDV carriage was then progressively lowered for each subsequent point. To aid in the choice of control parameters such as threshold levels and filter settings, short velocity records were often obtained, analyzed, and discarded prior to obtaining an actual record. Of prime concern were the validity rate and the associated data rate. For clear-water runs, validity rates were typically over 90% for 2-component measurements and over 95% for 1-component measurements. In sediment-laden flows, these rates were typically reduced by 5%. This may be compared to a rate of 50–60% suggested in Drain (1980) as the minimum acceptable. In the present study, it was found that validity rates lower than 80% may be adequate for mean velocities, but they are usually inadequate for reliable Reynolds stress measurements. It should be cautioned, however, that high validity rates do not guarantee good results. Raising threshold levels had a positive effect on validity rates, but beyond a certain point, this was more than offset by the adverse effect on data rates. Typically, these levels, once set, were not changed during a run, although in a few cases where the data rates were at a minimum, e.g., as the bed is approached in a sediment-laden flow, the levels might be lowered in order to improve the data rate. For the same reason, another option that was sometimes used was to increase the laser power. These options were used with caution since they also tended to increase the probability of noise in the data.

In 1-component measurements, the effect of filter bandwidth on either validation rate or data rate was not significant, provided it was appropriately centered. Because of the additional source of signal interference and also the limited choice in the working frequency ranges, the validation rate was more susceptible to filter-bandwidth effects in 2-component measurements. This restricted somewhat the dynamic range that could be set. With a Doppler frequency range of 200–350 kHz (excluding the Bragg shift), from positions near the bed to the upper part of the flow, the signal was band-filtered with cutoffs of $\approx$ 100–150 kHz, usually symetrically set about the mean frequency. In terms of the rms fluctuations, which were $\approx$ 10% or less, the cutoffs gave a dynamic range of 4–5 times the rms fluctuations. Because of the significant variation in mean Doppler frequency during a run, the filter settings were varied accordingly.

Prior to the measurement of concentration, the 1-liter bottles to be used for sampling were filled with water, which would be used to replace the sample and maintain a constant-water level. The mean velocity profile, obtained previously from LDV measurements, was used to compute the time necessary to fill the 1-liter bottle, assuming isokinetic conditions. The siphon was then adjusted, guided by timing 100 ml samples, to achieve the desired sampling time. The difference between actual and desired sampling time was typically less than 5%. Some deposition of sand in the sampling tubing at larger concentrations could be noticed. Provided a steady state is achieved in the sampler, this does not introduce significant error in the sampling if the isokinetic condition is maintained. After allowance of time for the sediment in the sample to settle, the sample was decanted and filtered, even while sampling at other points was being conducted. All filtered samples were then dried in an oven overnight and weighed on an electronic balance the following day.

5. Clear-water experiments

5.0 Introduction

Clear-water experiments were performed in order to evaluate the performance of the LDV system, to provide a basis for comparison with sediment-laden flows, and to develop consistent procedures for analyzing observed data. Four different runs were made under hydraulic conditions roughly similar to those that characterize the sediment-laden flows. Table 5.0.1 lists the flow conditions for these runs.

Table 5.0.1 Conditions for clear-water flow experiments

Experiment	C-1	C-2	C-3	C-4
depth, h (cm)	6.54	6.53	5.75	5.69
hydraulic radius, r_h (cm)	4.39	4.38	4.02	3.99
aspect ratio, b/h	4.06	4.06	4.68	4.68
slope, S ($\times 10^{-3}$)	2.06	2.70	2.96	4.01
bulk discharge, Q (l/s)	10.84	12.66	10.77	12.66
temperature, T (°C)	18.7	21.3	21.0	21.3

5.1 Mean profiles

5.1.1 Mean stress profiles

Because of its direct influence on the mean field and its use in estimating u_*, the Reynolds-stress profile is here considered as a mean quantity even though it is computed from the fluctuating part of the velocity field. The dimensional Reynolds-stress profiles are shown in Fig. 5.1.1a. The scatter is perhaps more than one would like, but not unexpected. More significant is a decay far from the wall, suggesting that a point of zero shear is attained below the free surface. The estimation of u_* is thus further complicated, since the linear stress profile of the idealized two-dimensional flow does not strictly apply. A falling-off of $-u'v'$ below $\eta = 0.1$ may also be noted, which is attributed to measurement error, since the Reynolds stress should remain dominant until very near the boundary.

To estimate u_*, it is argued that three-dimensional effects are localized and should diminish in importance as the bottom is approached. There, the stress profile should approximate more closely the idealized stress profile. A linear fit is therefore performed in a region, $0.1 \leq \eta \leq 0.4 - 0.5$, with the constraint that the stress vanish at $\eta = 1$. The upper limits of 0.4 and 0.5 were used for the lower and the higher aspect-ratio flows, respectively. The lower limit was relaxed in the case of experiment C-4, where an unlikely low value of $-u'v'$ was found at $\eta = 0.106$ and so was excluded from the fit.

The stress profiles, normalized by ${u_*}^2$, obtained from this fit are shown in Fig. 5.1.1b. In this plot, the influence of the sidewalls as the free surface is approached is more clearly seen. The first two experiments, performed at the smaller aspect ratio, depart consistently more from the linear profile for $\eta \geq 0.4$. Also drawn on Fig. 5.1.1b, are lines assuming an error in the estimate of u_*^2 of

Fig. 5.1.1 Reynolds-stress profiles: a) dimensional, b) normalized by u_*^2

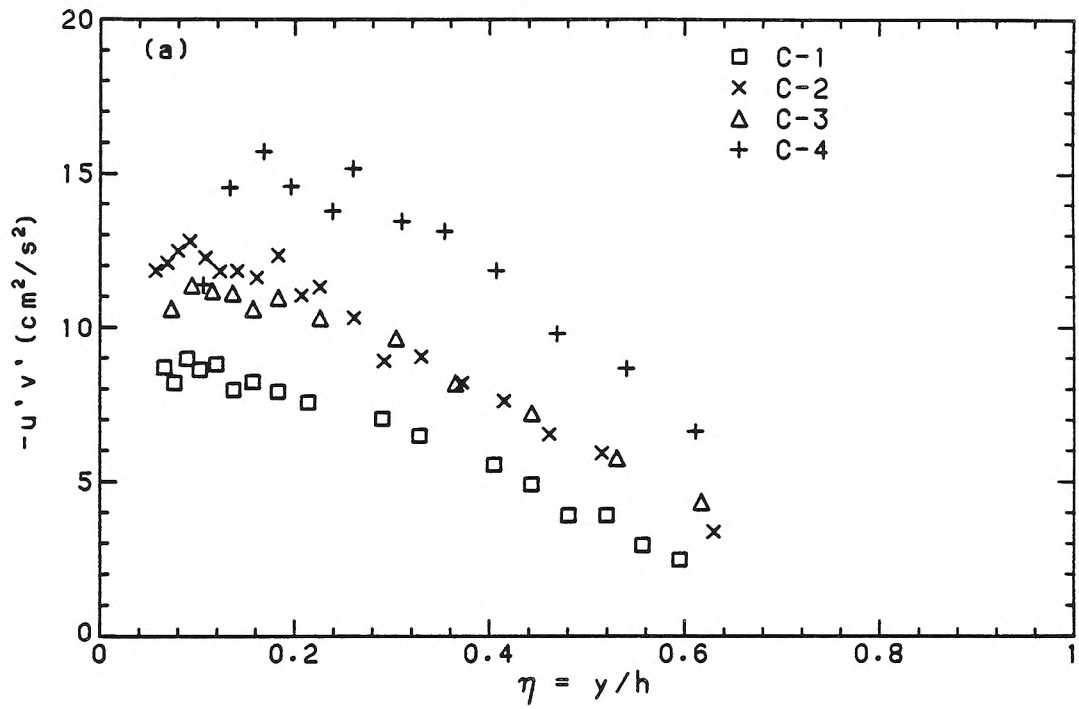

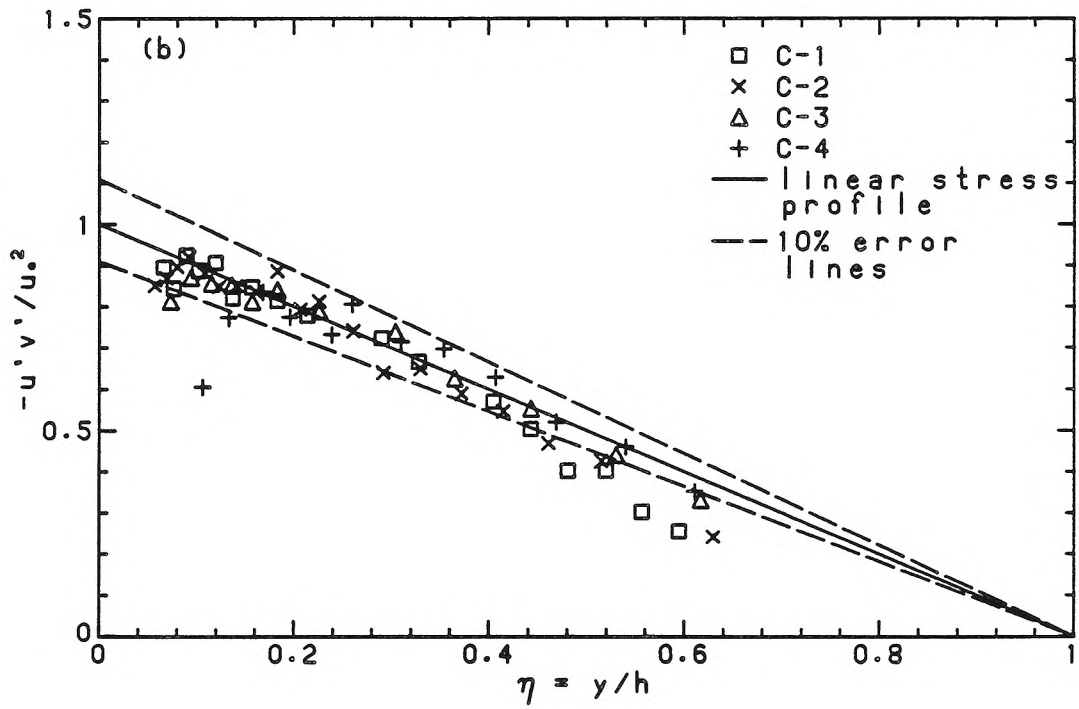

$\pm 10\%$. These are seen to envelop most of the data points for $\eta \leq 0.4$. It is believed then that the fitting procedure gives an estimate of u_*, with at most $\pm 5\%$ error (probably better), assuming that the Reynolds-stress measurements may be believed. This is supported by the good agreement between the value of u_* estimated from the Reynolds-stress measurements and that obtained from the logarithmic profile, assuming $\kappa = 0.405$. A comparison of these is given in Table 5.1.1, together with estimates from an empirical correlation, applicable to smooth-boundary, finite-width channels, developed by Knight et al. (1984). Also compared are estimates assuming an idealized two-dimensional flow, where $u_* = \sqrt{ghS}$, and assuming an averaged wall shear, such that $u_* = \sqrt{gr_hS}$.

Table 5.1.1 Comparison of estimates of u_* (cm/s): clear-water experiments

Experiment	C-1	C-2	C-3	C-4
Reynolds stress estimate	3.11	3.73	3.61	4.33
log-law estimate	3.26	3.78	3.60	4.19
Knight et al. correlation	3.13	3.59	3.61	4.20
$\sqrt{ghS}$	3.63	4.16	4.08	4.75
$\sqrt{gr_hS}$	2.98	3.40	3.41	3.97

5.1.2 Velocity profiles

In Fig. 5.1.2a, the dimensional velocity profiles from the direct one-component measurements are plotted according to the traditional hydraulic practice. This presentation has the advantage of not involving a troublesome estimate of the shear velocity, u_*, as well as giving a more concrete picture of the experimental conditions. Three features of these profiles may be pointed out: i) a logarithmic

Fig. 5.1.2 a) Dimensional velocity profiles
b) Consistency of 1-component, 2-component and pitot-tube results

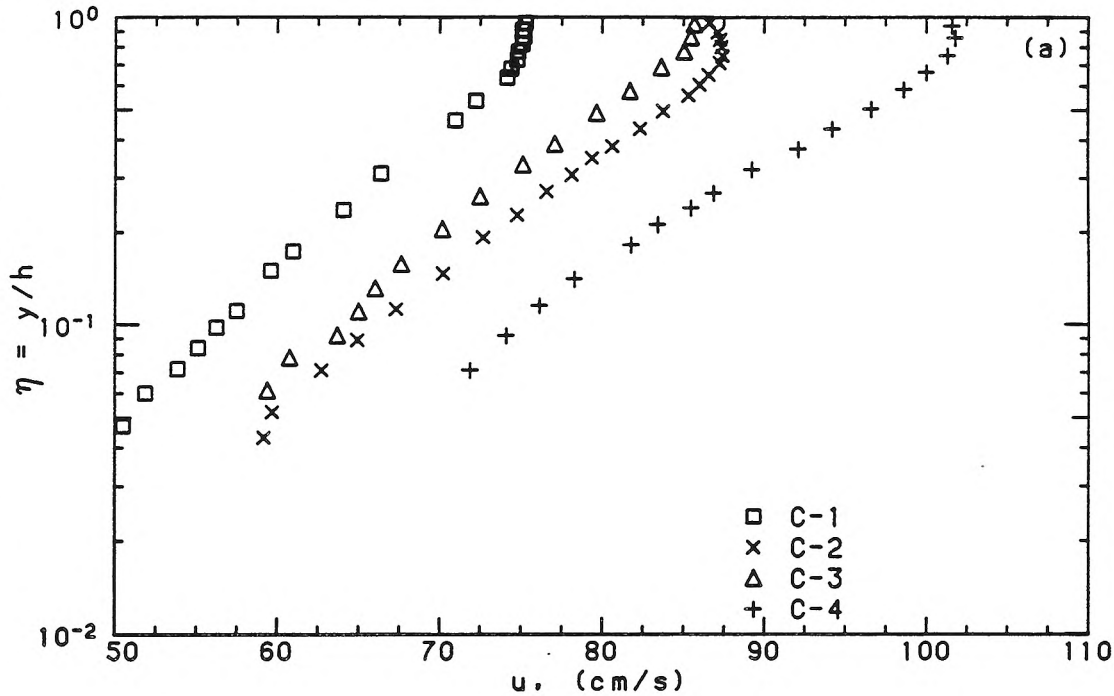

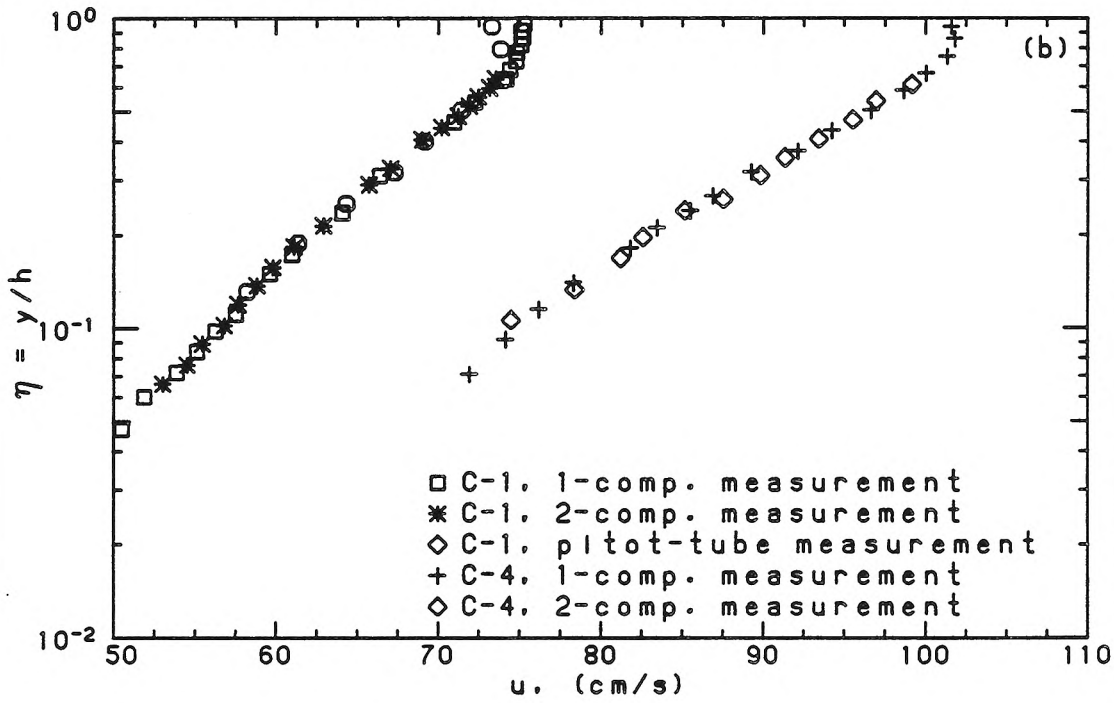

variation of u for small η, ii) a noticeable deviation from the logarithmic asymptote for $\eta = O(1)$, and iii) a maximum velocity, $u_{\max}$, which does not occur at the free surface, $\eta = 1$. The first feature is generally accepted in hydraulic practice. The complementary second feature has only recently been emphasized in the hydraulic literature. The last feature is also well known and is often attributed to the effect of sidewalls, inducing secondary currents. This would be consistent with what was seen previously in the Reynolds-stress profiles.

Fig. 5.1.2b compares the profiles in two cases obtained by simultaneous two-component measurements and by the more direct one-component measurements. The agreement is seen to be quite acceptable and indicates that, so far as the measurement of mean horizontal velocity is concerned, the geometrical consistency of the optical system is adequate. In one case, measurements by an uncalibrated Pitot tube were also taken, and again agree well with the LDV results except very near the free surface, a result which may have been expected. In view of this agreement, further analyses of the mean-velocity profiles, e.g., fitting to standard profiles, are performed only for the direct one-component measurements since these are available for the entire flow region. Moreover, the treatment of other statistics will make no distinction between one- and two-component results.

Velocity profiles in viscous coordinates using the estimated values of u_* are given in Fig. 5.1.3. Fitting points in the region, $\eta \leq 0.2$ (corresponding to $y^+ \leq 500$), to a semi-logarithmic profile may then be performed to determine κ and the additive constant, B, for each flow. The values so obtained for κ agree very well with the generally accepted value of 0.40–0.41. The low value for experiment C-1 may be quite plausibly attributed to a 5% error in the estimation of u_*, as well as to statistical fitting error.

Fig. 5.1.3 Velocity profiles in viscous coordinates

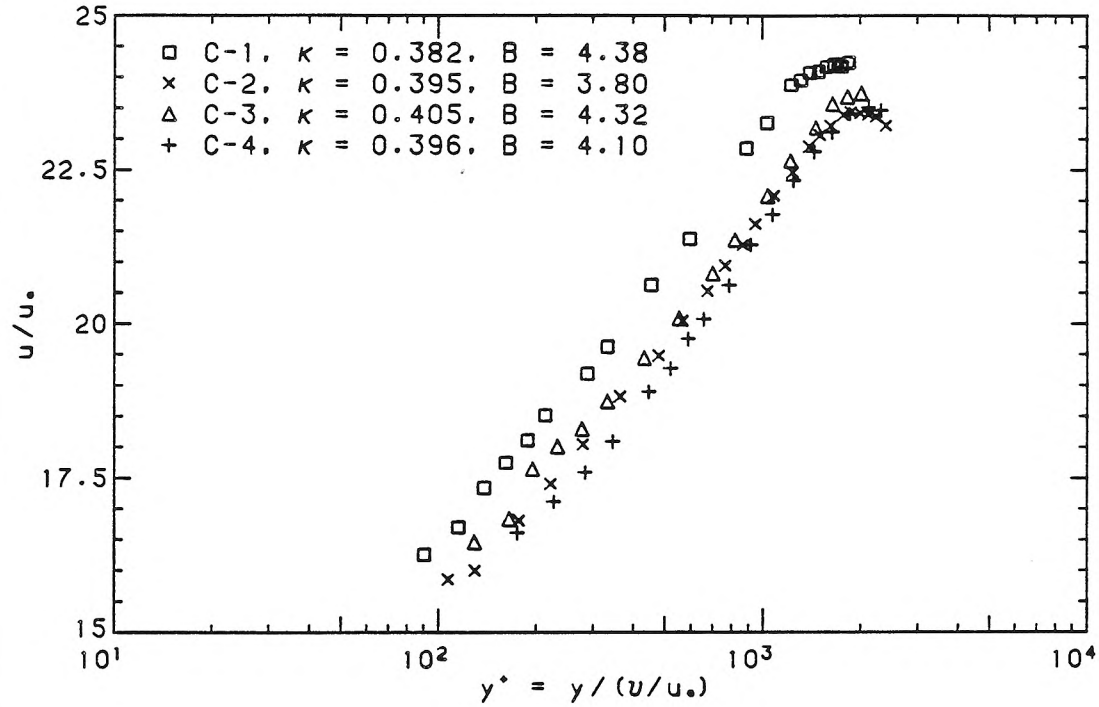

Velocity-defect profiles, more suitable for the outer region, $\eta = O(1)$, in both linear and logarithmic forms are given in Fig. 5.1.4. The collapse of the data is perhaps marginally adequate. Besides the ever-present error due to errors in u_*, two related effects largely explain the scatter, namely, the difference in the aspect ratios and the different values of η at which the maximum velocity, $u_{\max}$, is attained. If cases of constant b/h are plotted, as in Fig. 5.1.5, then the scatter is noticeably reduced.

Because $u_{\max}$ occurs at $\eta < 1$ (perhaps as low as $\eta \approx 0.75$), the fitting of the measured velocity defect to a universal profile is made more complicated. Since the wake-function model has recently gained some acceptance in the description of open-channel flows, we follow Coles (1956, 1971) and Coleman (1981) in fitting the region of flow only up to the point of maximum velocity, $y \equiv y_{\max}$, with the

Fig. 5.1.4 Velocity-defect profiles: a) linear-linear plot, b) linear-log plot

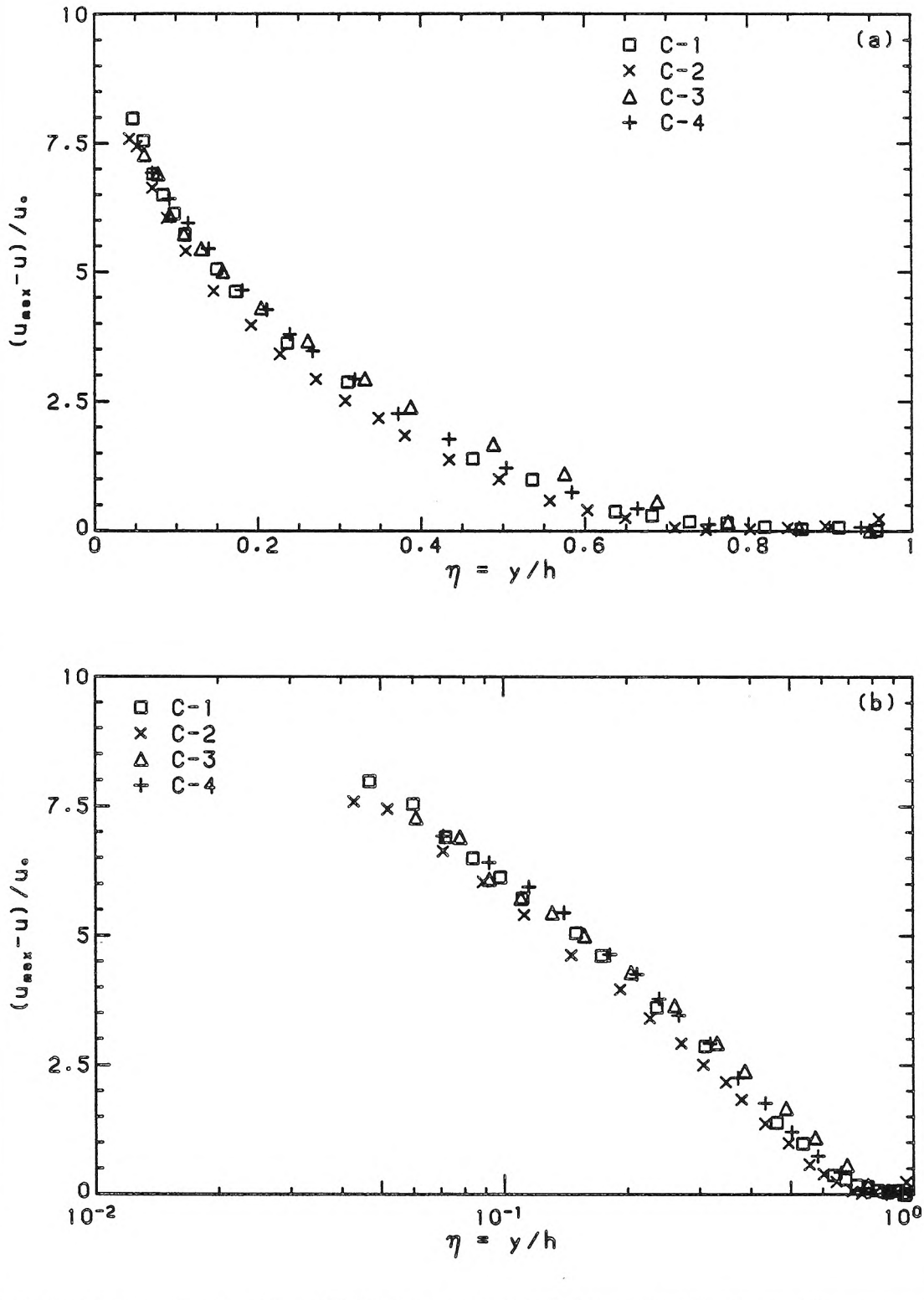

Fig. 5.1.5 Velocity-defect profiles, distinguished by aspect ratios:
a) $b/h = 4.0$, b) $b/h = 4.7$

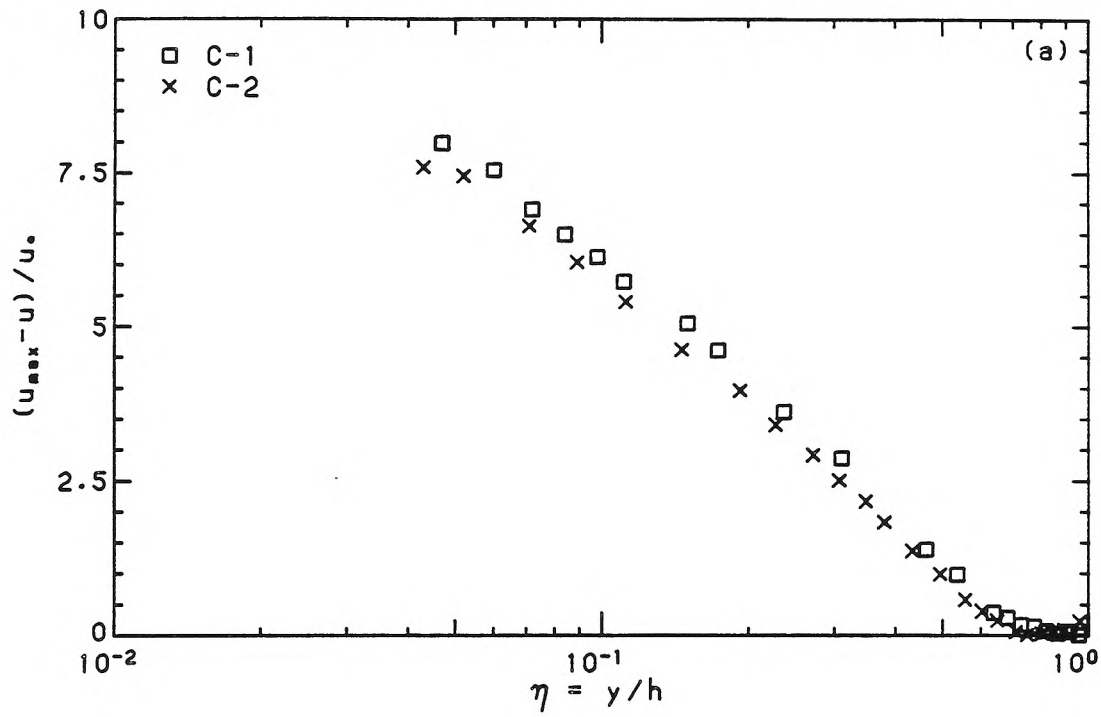

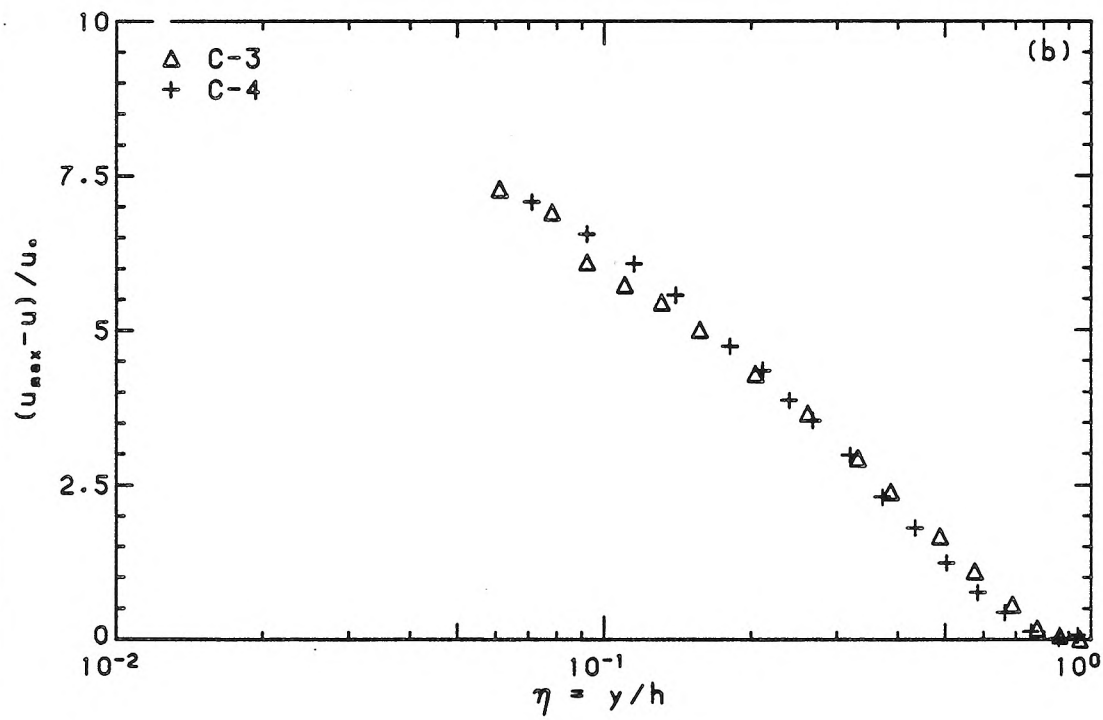

profile

$$\frac{u_{\max} - u}{u_*} = -\frac{1}{\kappa} \ln\left(\frac{y}{y_{\max}}\right) + \frac{2W_0}{\kappa} \cos^2\left(\frac{\pi}{2}\frac{y}{y_{\max}}\right). \qquad (5.1.3)$$

The fitting procedure used, however, differs in detail from either that of Coleman or of Coles. Coleman identifies $y_{\max}$ from the measurements, assumes u_* known, and uses κ and W_0 as fitting constants. Because the velocity profile is rather flat where it is a maximum, and with the measurement error in mind, the identification of $y_{\max}$ from the data is often not definitive. The maximum velocity, $u_{\max}$, may, however, be confidently identified. Coles (1971), therefore, treats $y_{\max}$ as a fitting parameter (assuming κ known) and fits the profile only over the central portion of the velocity profile, where measurements are more likely to be accurate *and* Eqn. 5.1.3 more likely to be valid. In the treatment of clear-water data, this approach is followed except that, where Coles uses u_* as the other fitting parameter, the wake-coefficient, W_0, is used here, since u_* is estimated from Reynolds' stress measurements. The fitting region was taken uniformly to be $0.1 \leq \eta \leq 0.65$ and typically included 8–12 data points. The sum of squares of the relative error was minimized in the fitting. A rather crude, multi-level search algorithm with grid refinement and range reduction (which, therefore, assumes a unimodal behavior) was used for the non-linear fitting.

The fitted profiles and the associated constants are shown in Fig. 5.1.6. The agreement is seen to be reasonable. The values obtained for the wake coefficient do vary by a factor of 2, although they are within the range quoted by other workers. Since the "wake" effect in open channel flows is small compared to that found in boundary-layer flow, accurate estimates of wake coefficients are rather prone to variance due to experimental scatter and errors in estimating u_*. The values of $y_{\max}$ obtained from the fitting tend to be somewhat smaller than would

Fig. 5.1.6 Comparison of velocity-defect profiles with fitted wake-type profiles

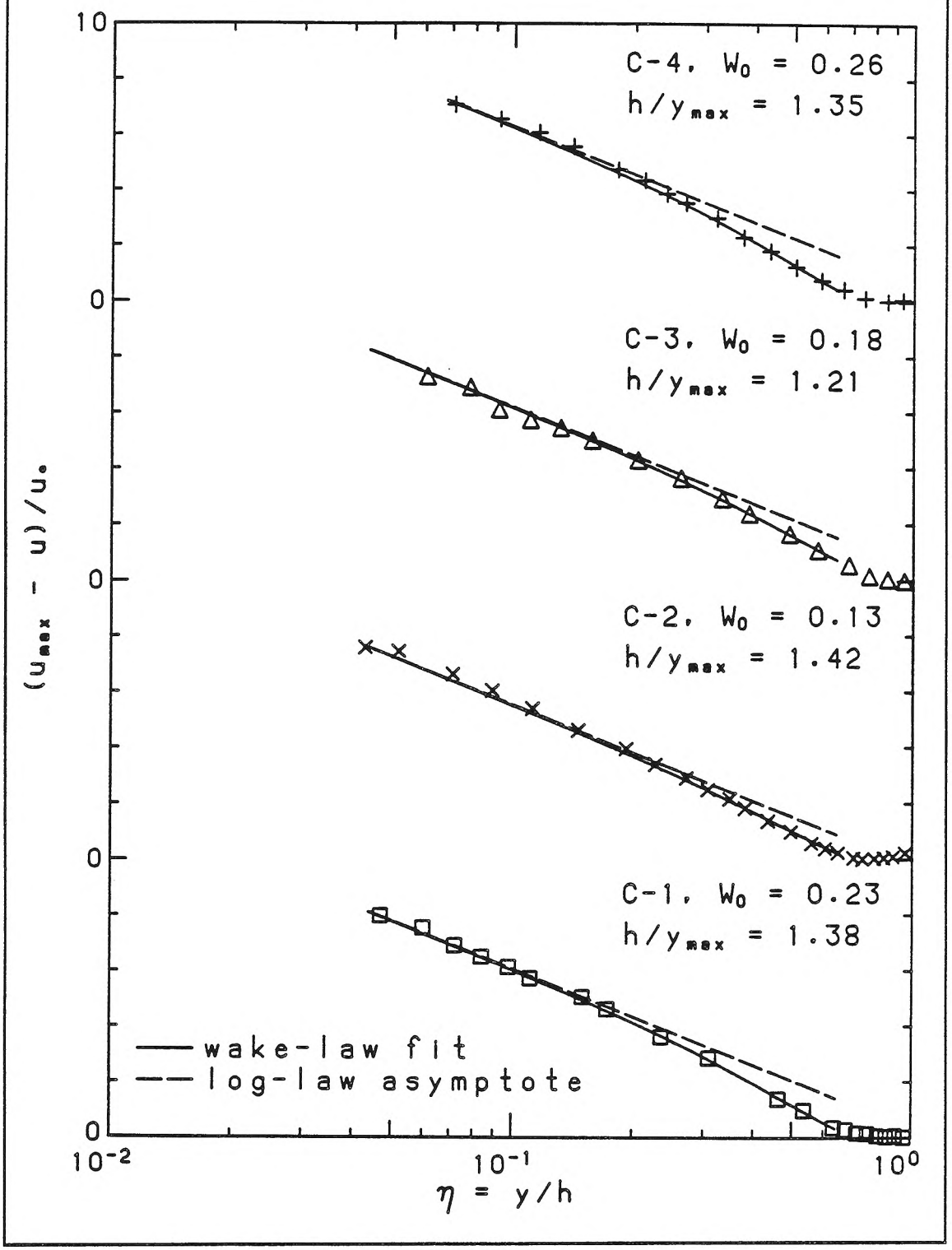

be expected from an inspection of the data points. Neither W_0 nor y_{max} seems to vary consistently with the aspect ratio. This last conclusion may, however, be an artifact of the use of the particular wake profile used or the specific fitting procedure.

In the idealized uniform flow, the mean vertical velocity $v = 0$. Fig. 5.1.7 plots the measured v relative to the local mean velocity, u, and also relative to the estimated u_*, against η. In most cases, $|v|$ was measured as less than 0.5cm/s, with a maximum of 1.3 cm/s. Relative to the local mean velocity, u, this is satisfactory, being typically less than 1%. If the more stringent criterion that $|v| << u_*$ is used, the situation is less satisfactory. This non-zero mean vertical velocity is attributed in large part to errors in the optical alignment of the LDV system per se, as well as in the alignment of the measuring volume with respect to the mean direction of flow, to which the measurement of v is extremely sensitive. There does seem to be a fairly consistent increase in v as the bottom is approached, as well as, in some cases, a change in sign from negative to positive. This may reflect a real downward velocity in the upper part of the flow caused by secondary currents. For example, if the alignment errors would result in only a positive vertical velocity in the absence of secondary currents, then a vertical velocity due to secondary currents which become weaker as the bottom is approached would produce the observed results. If secondary currents were the sole source of the non-zero measured v of this magnitude, it would be unlikely that the results for the wall shear estimates from the Reynolds stress profile would be as reliable as has been shown. Moreover, as will be seen, the effect of such a non-zero measured v on computed higher-order statistics does not seem to be important. Rather than trying to calibrate such

Fig. 5.1.7 Mean vertical velocity profiles: a) relative to the local mean horizontal velocity, u, b) relative to the shear velocity, u_*

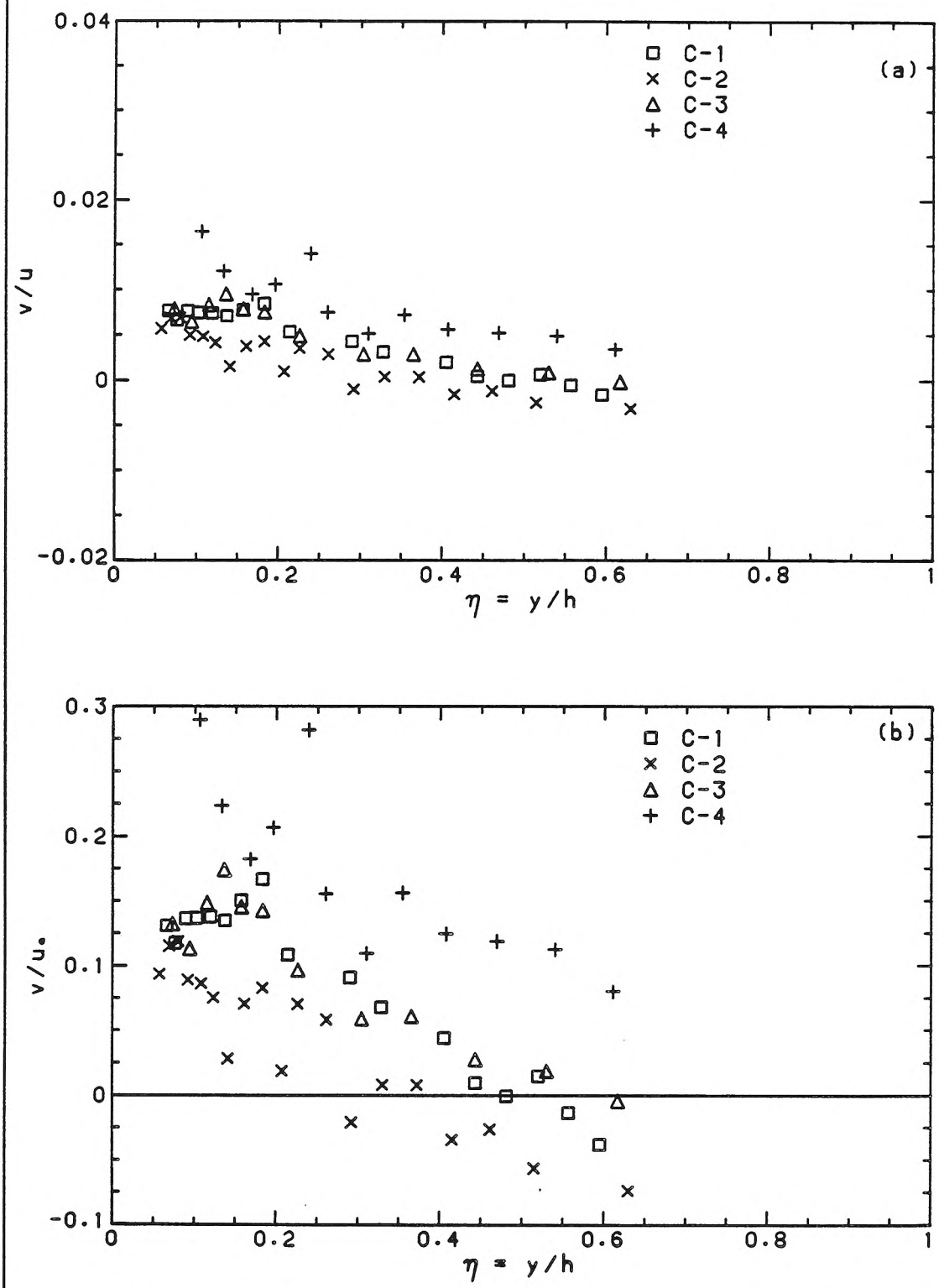

non-zero v away then, it is viewed as an indication of the magnitude of the errors in the measurement.

5.1.3 Summary: Mean quantities

The performance of the present LDV system is seen to be good for the measurement of the mean horizontal velocity profile, with close agreement between one- and two-component measurements as well as with Pitot-tube measurements. The measurement of the Reynolds-stress profile is somewhat less satisfactory, with a larger scatter but is considered adequate. The constants obtained from fitting the data to standard profiles also agree with values found in the literature, so that the fitting procedures developed from the clear-water experiments are seen to be consistently applicable. The effect of the decrease in the aspect ratio from ≈ 4.7 to ≈ 4 is seen to be noticeable, if slight, in the upper region of flow, $\eta \geq 0.5$, in both the mean velocity profile and the stress profile. A summary of the computed flow parameters is given in Table 5.1.2.

5.2 Higher-order statistics

5.2.1 Stability of statistics and averaging times

An example of the time record of both horizontal and vertical velocities (obtained in experiment C-2, $\eta \approx 0.4$) is given in Fig. 5.2.1. The variation of the computed statistics with the averaging time, T_{avg}, for this record was investigated by considering a subset of partial records. The total length of record was $\approx 200s$ and was divided into 10 successively longer records, including the complete record. A statistic, E_∞, computed using the complete record, was taken as the "true" statistic, and a relative deviation was defined as

$$\Delta E \equiv \frac{E(T_{\text{avg}}) - E_\infty}{E_\infty}, \tag{5.2.1}$$

Table 5.1.2 Computed flow parameters for clear-water flows

Experiment	C-1	C-2	C-3	C-4
maximum velocity, $u_{\max}$ (cm/s)	75.3	87.5	85.7	101.9
bulk velocity, $\langle\langle u\rangle\rangle \equiv Q/bh$ (cm/s)	62.1	72.7	70.2	83.4
depth-averaged velocity, $\langle u\rangle$ (cm/s)	65.80	77.21	73.38	86.79
shear velocity, u_* (cm/s)	3.11	3.73	3.61	4.33
$f_D \equiv 8(u_*/\langle u\rangle)^2$	0.0170	0.0179	0.0182	0.0186
$\langle\langle f_D\rangle\rangle \equiv 8gr_hS/\langle\langle u\rangle\rangle^2$	0.0175	0.0184	0.0189	0.0181
von Kàrman constant, κ	0.385	0.395	0.405	0.396
additive constant, B	4.38	3.95	4.32	4.10
wake coefficient, W_0	0.23	0.13	0.18	0.26
$Fr \equiv \langle u\rangle/\sqrt{gh}$	0.82	0.97	0.97	1.16
$Re \equiv 4r_h\langle u\rangle/\nu$ $(\times 10^5)$	1.11	1.39	1.20	1.39
$Re_* \equiv u_*h/\nu$ $(\times 10^3)$	1.96	2.50	2.12	2.47

where $\Delta E \rightarrow 0$ as $T_{\text{avg}} \rightarrow \infty$. This relative deviation is plotted in Fig. 5.2.2 against an averaging time, scaled by outer variables, $T_{\text{avg}}\langle u\rangle/h$. In general, it is seen that higher-order statistics, as expected, require a longer averaging time in order to reach a stable value. For the u- (and v-) statistics, the total record length used is seen to be sufficient for a sampling error within $\pm 5\%$ error. The Reynolds-stress statistics, on the other hand, are seen to be much more ill-behaved, and even the mean stress requires a long time for approximate stability to be attained.

5.2.2 Higher-order u- and v-statistics

The root-mean-square (rms) of the fluctuating u-velocity, $\sqrt{u'^2}$, scaled by u_*, for the four clear-water experiments is plotted in Fig. 5.2.3a. The results are quite consistent and collapse well in outer coordinates, as was noted by Perry

Fig. 5.2.1 Example of a time series of velocity measurements (from C-2 at $\eta = 0.38$)

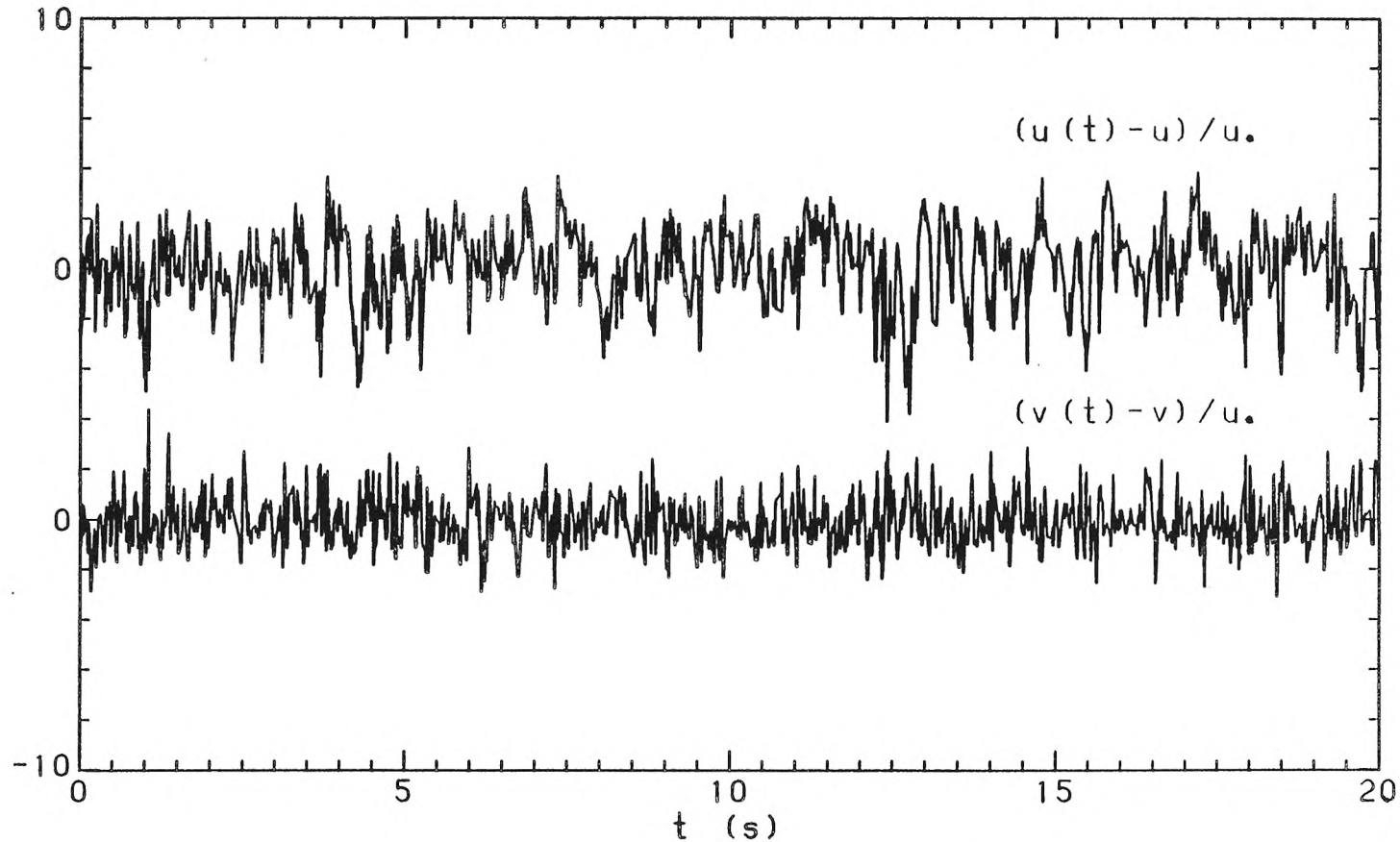

Fig. 5.2.2 Variation of statistics with averaging time, T_{avg}:
a) $u'v'$-statistics, b) u-statistics

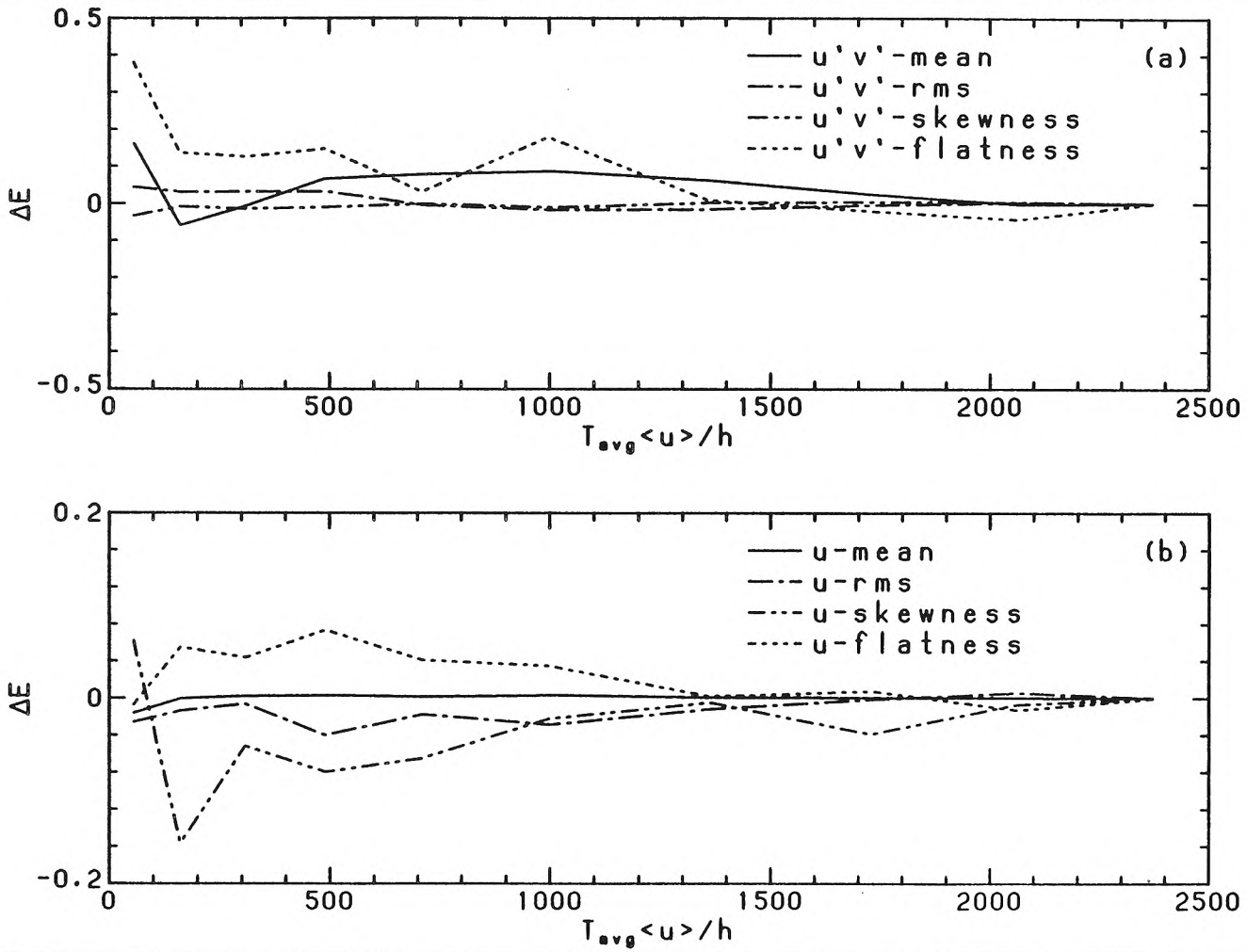

and Abell (1975). A slight but noticeable and consistent difference for $\eta \geq 0.5$ between experiments of different aspect ratios may be noted and is emphasized in Fig. 5.2.3b, where a distinction has been made only between experiments of different aspect ratios. Best-fit lines that will be used for comparison with previously published results are also given. The higher aspect ratio tends to be associated with a larger $\sqrt{u'^2}/u_*$ near the free-surface. Later, in Chap. 7, when the results for sediment-laden flows will be compared with results for clear-water flows, the latter will be represented by envelope curves (the term, envelope, being used somewhat loosely) rather than by the actual points. These curves, which will typically depend on the aspect ratio, are shown in Fig. 5.2.4, together with the data points.

A comparison with previously published data for $\sqrt{u'^2}/u_*$, is given in Fig. 5.2.5a. The agreement is quite good, the worst difference being with the data of Grass, which was obtained from visual observation of hydrogen bubbles, and so may be subject to a larger error. There seems to be a tendency towards lower values for $\eta \leq 0.1$, but the comparison does not yield a definite conclusion. An alternative presentation uses the local mean velocity, u, to non-dimensionalize $\sqrt{u'^2}$ and so avoids the estimate of u_*. Fig. 5.2.5b shows the present results in this form. A comparison in these coordinates with the result of other investigators shows rather more scatter than before, but the present results are clearly in the midst of the scatter.

The rms of the vertical velocity fluctuations, $\sqrt{v'^2}$, scaled by u_*, is also seen to collapse well in outer variables, as seen in Fig. 5.2.6a, although a slight effect of the aspect ratio may again be noted for $\eta \geq 0.5$. These results are compared

Fig. 5.2.3 Horizontal turbulence intensities, $\sqrt{u'^2}/u_*$, distinguished by a) experiments, and by b) aspect ratios

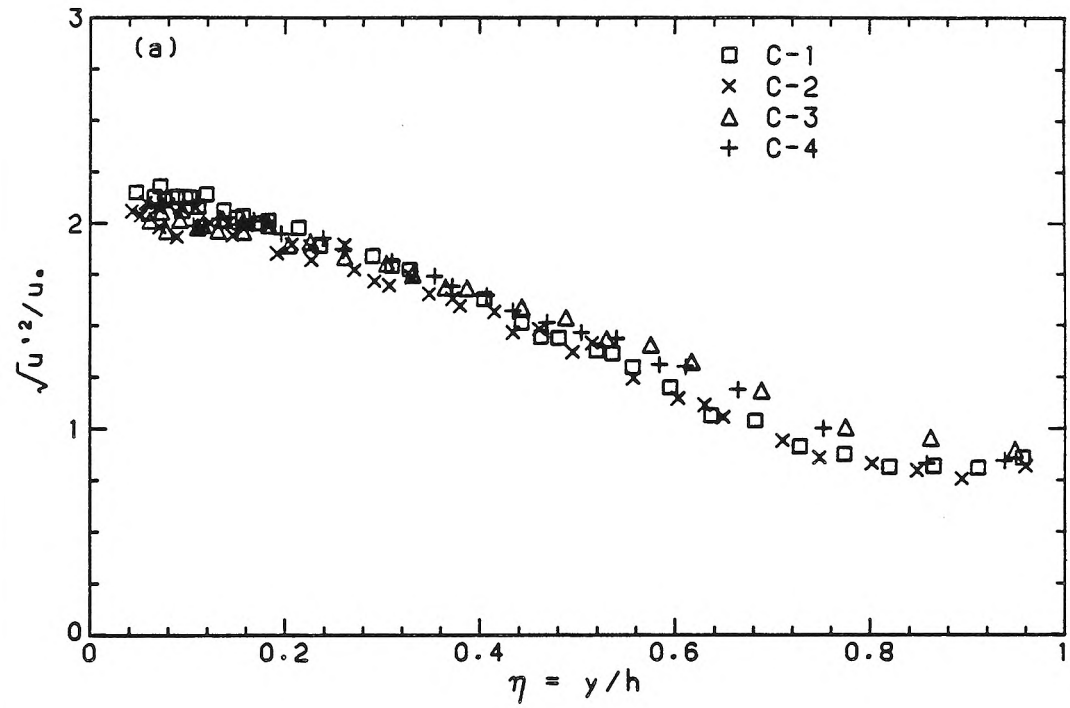

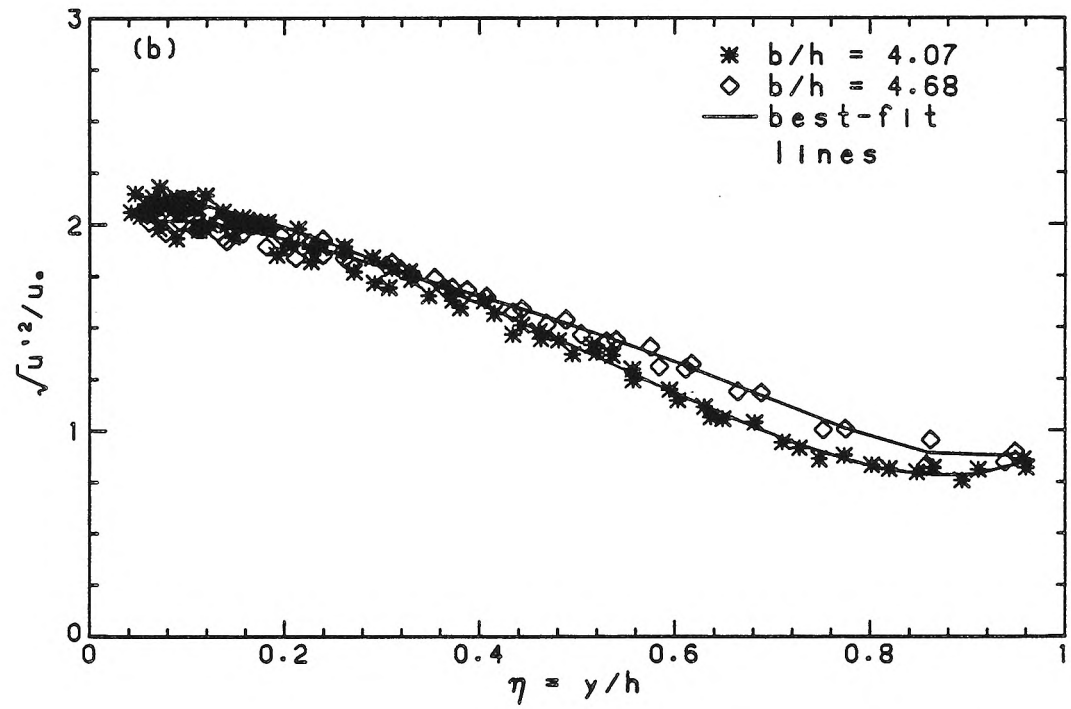

Fig. 5.2.4 Envelope of results for horizontal intensities, distinguished by aspect ratios: a) $b/h = 4.0$, b) $b/h = 4.7$

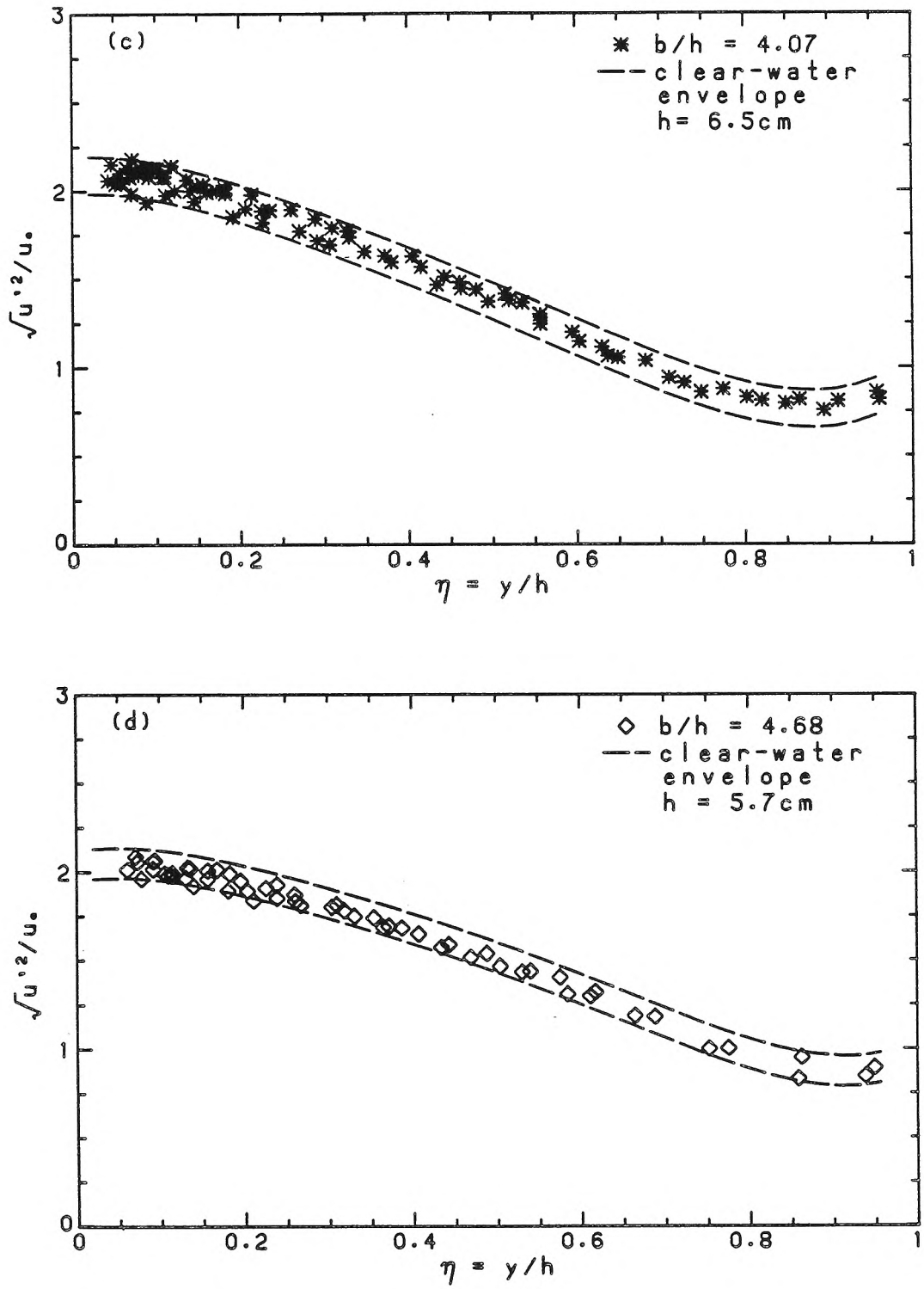

Fig. 5.2.5 Comparison of present results with previous results
a) $\sqrt{u'^2}/u_*$, b) $\sqrt{u'^2}/u$

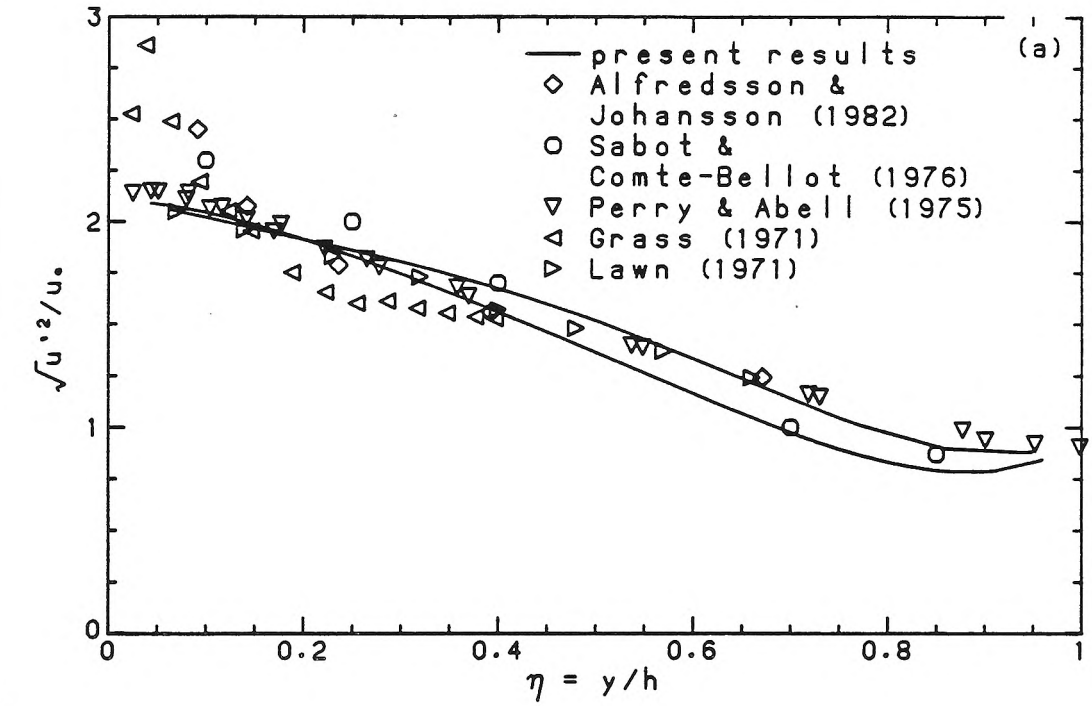

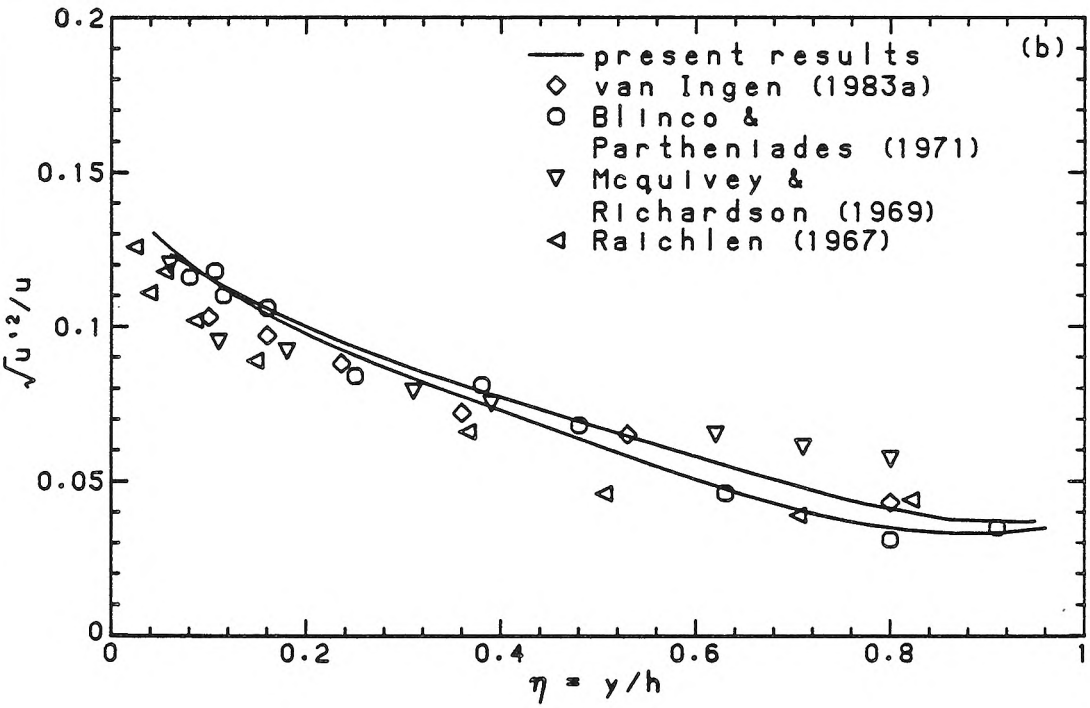

Fig. 5.2.6 a) Vertical turbulence intensities
b) Comparison of present results, $\sqrt{v'^2}/u_*$

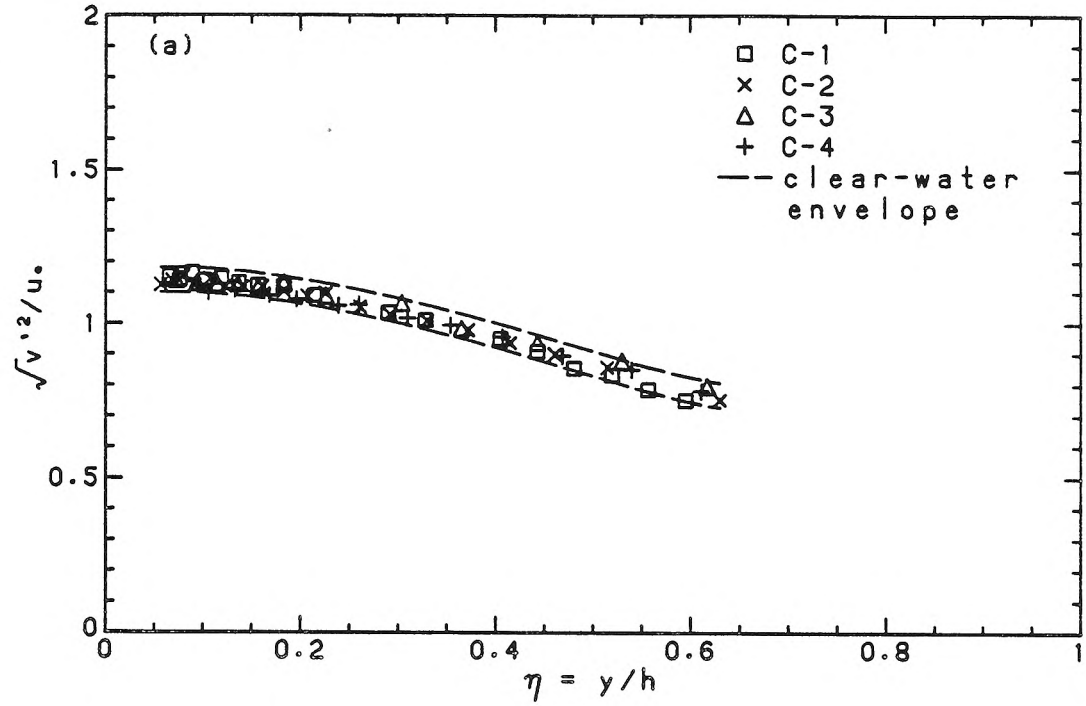

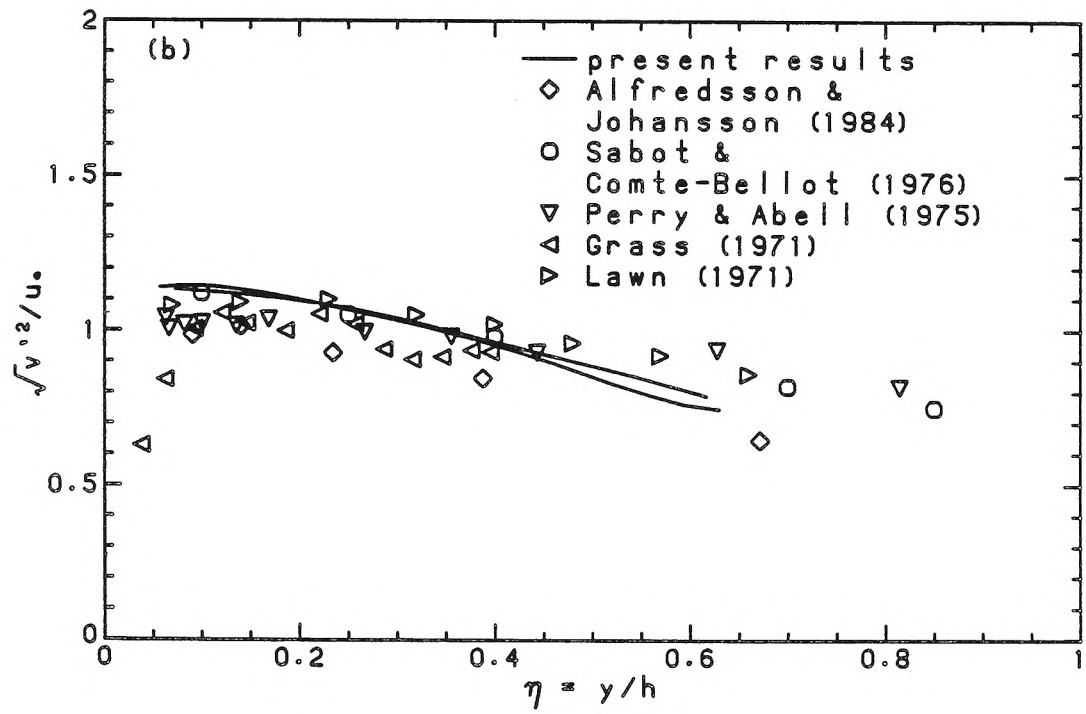

as before with the results of others in Fig. 5.2.6b and a satisfactory agreement is found.

The determination of spectra from time series obtained from single-scattering-particle LDV systems is not straightforward, even if the problem of bias is ignored. The simplest and computationally most attractive procedure is a linear interpolation of the raw, irregularly sampled series so as to generate a regularly sampled series with sampling rate lower than the original mean-sampling rate. Standard FFT algorithms can then be used to estimate the power spectrum. It was found, however, that, at the mean data rates obtained, the mean squares of the fluctuating quantities computed from the derived signal were reduced, particularly in the case of the vertical component. Alternative approaches were considered, including direct periodogram estimates from time integrals as suggested by Dimotakis (1976) and the old-fashioned estimation via the autocorrelation. Besides being computationally laborious, these methods gave very erratic results, e.g., negative spectral density estimates, even when block averaging was performed for smoothing purposes.

It was decided then to return to the interpolation approach, because these estimates, in their normalized form, were found to agree qualitatively with the result of others. In Table 5.2.1, the characteristics of the original and interpolated records, the latter denoted by the subscript I, are given. Because one-component measurements were associated with significantly higher data rates than the two-component measurements, particularly in sediment-laden flow experiments, only the former were used in determining the spectra of horizontal fluctuations. Spectra were computed at only a single elevation, $\eta \approx 0.4$. This compromise usually

Table 5.2.1 Characteristics of original and interpolated records: clear-water experiments

Experiment	C-1	C-2	C-3	C-4
u spectral computation				
$\eta = y/h$	0.46	0.38	0.39	0.37
mean sampling time, Δt (ms)	4.45	15.46	11.70	11.06
standard deviation, $\sigma_{\Delta t}$ (ms)	0.32	0.53	0.44	0.55
interp. sampling time, $(\Delta t)_I$ (ms)	10.00	16.67	12.50	12.50
$(u'^2)_I/u'^2$	0.94	0.84	0.86	0.88
v spectral computation				
$\eta = y/h$	0.41	0.37	0.37	0.41
mean sampling time, Δt (ms)	5.41	15.02	13.17	19.86
standard deviation, $\sigma_{\Delta t}$ (ms)	0.32	0.68	0.63	0.87
interp. sampling time, $(\Delta t)_I$ (ms)	13.33	20.00	15.63	25.00
$(v'^2)_I/v'^2$	0.81	0.66	0.70	0.69

provided an adequate data rate, and possible sidewall effects might be considered negligible.

The normalized spectral estimates for the fluctuating horizontal velocity are shown in Fig. 5.2.7. The sampling time, $(\Delta t)_I$, for the interpolation of the raw data was chosen to be the mean data rate, Δt, plus at least two standard deviations. Block averaging, using blocks of length 10 s, was used to smooth the estimates. A large scatter remains because of the inherent variability of spectral estimates, but the qualitative behavior — decay following an approximate -5/3 power-law beyond frequencies of $\approx$ 10Hz — seems well captured. For purposes of comparison with previously published data, best-fit lines to the spectra were also determined. It was verified that these lines integrated for all practical purposes to

Fig. 5.2.7 a) Normalized power spectra of horizontal velocity fluctuations
b) Comparison with previous results

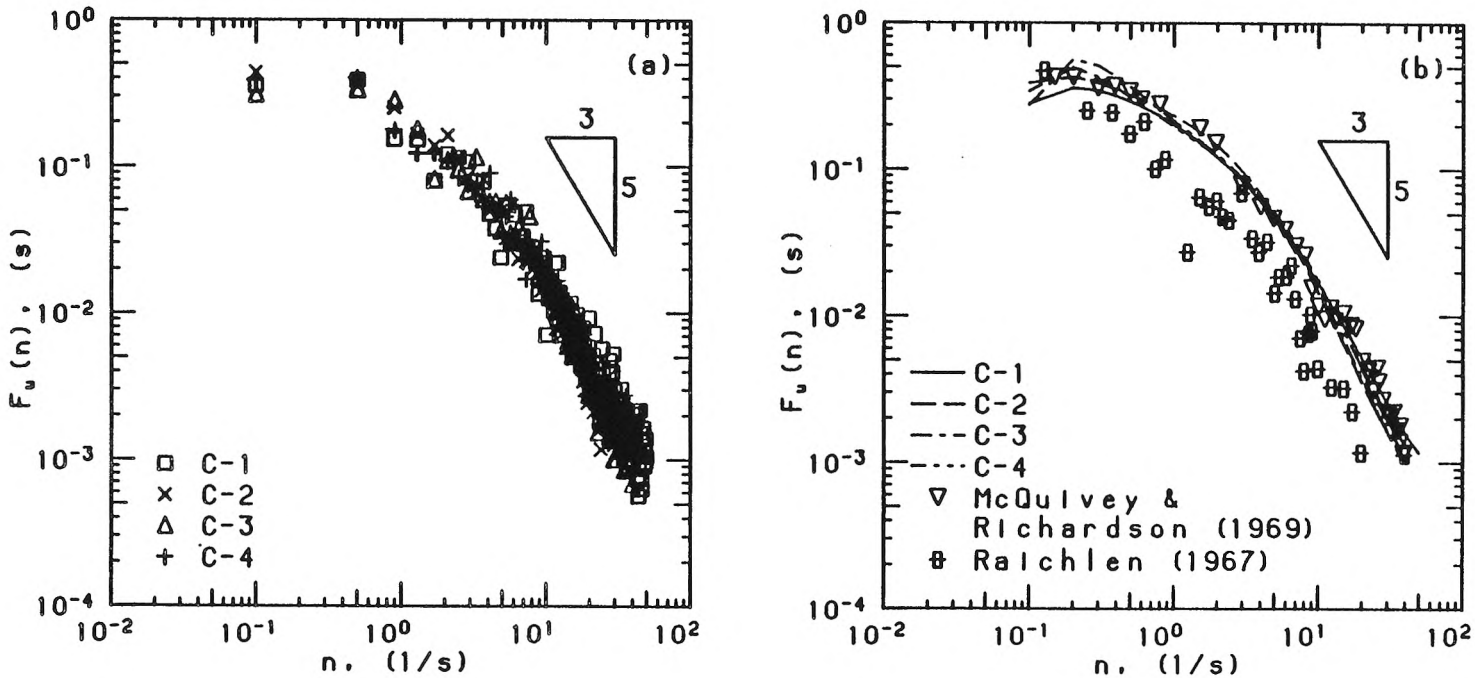

unity, so that the the curve-fitting could be considered as an additional smoothing operation.

The comparison with previous results is given in Fig. 5.2.7b and shows reasonable agreement. Since the shape of the power spectrum remains qualitatively accurate, it is conjectured that the use of the interpolation approach reduces energy over a wide bandwidth and not only, as might be expected, in the high-frequency range. In the case of experiment C-1, where a high mean data rate ($\approx$ 185Hz) was available, an investigation of the effect of different interpolation frequencies, ranging from 50Hz–150Hz, was undertaken. Except for an aliasing effect at lower interpolation frequencies, no significant change in the normalized spectra could be noticed. Differences between spectra computed from one-component and from two-component measurements were also investigated and found to be negligible where the two should be comparable.

The power spectra of the vertical velocity fluctuations are plotted in Fig. 5.2.8 in the wavenumber plane (in order to compare results with Lawn (1971)). Conversion from the frequency plane to the wavenumber plane was accomplished using Taylor's hypothesis, while retaining the normalization. Thus, $F_v(hk_1) = F_v(n)u/2\pi h$ and $hk_1 = 2\pi nh/u$. The oscillations seen in the smoothed spectra at small wavenumbers may be attributed to the curve-fitting operation. Much the same could be said of the v-spectra as was previously remarked of the u-spectra. The results of Lawn indicate a somewhat smaller energy in the small wavenumber range but agree well with the present results at higher wave numbers.

Skewness and flatness factors for u- and v- fluctuations are shown and compared with the results of others in Figs. 5.2.9-10. These higher moments exhibit

Fig. 5.2.8 a) Normalized power spectra of vertical velocity fluctuations
b) Comparison with Lawn's (1971) results

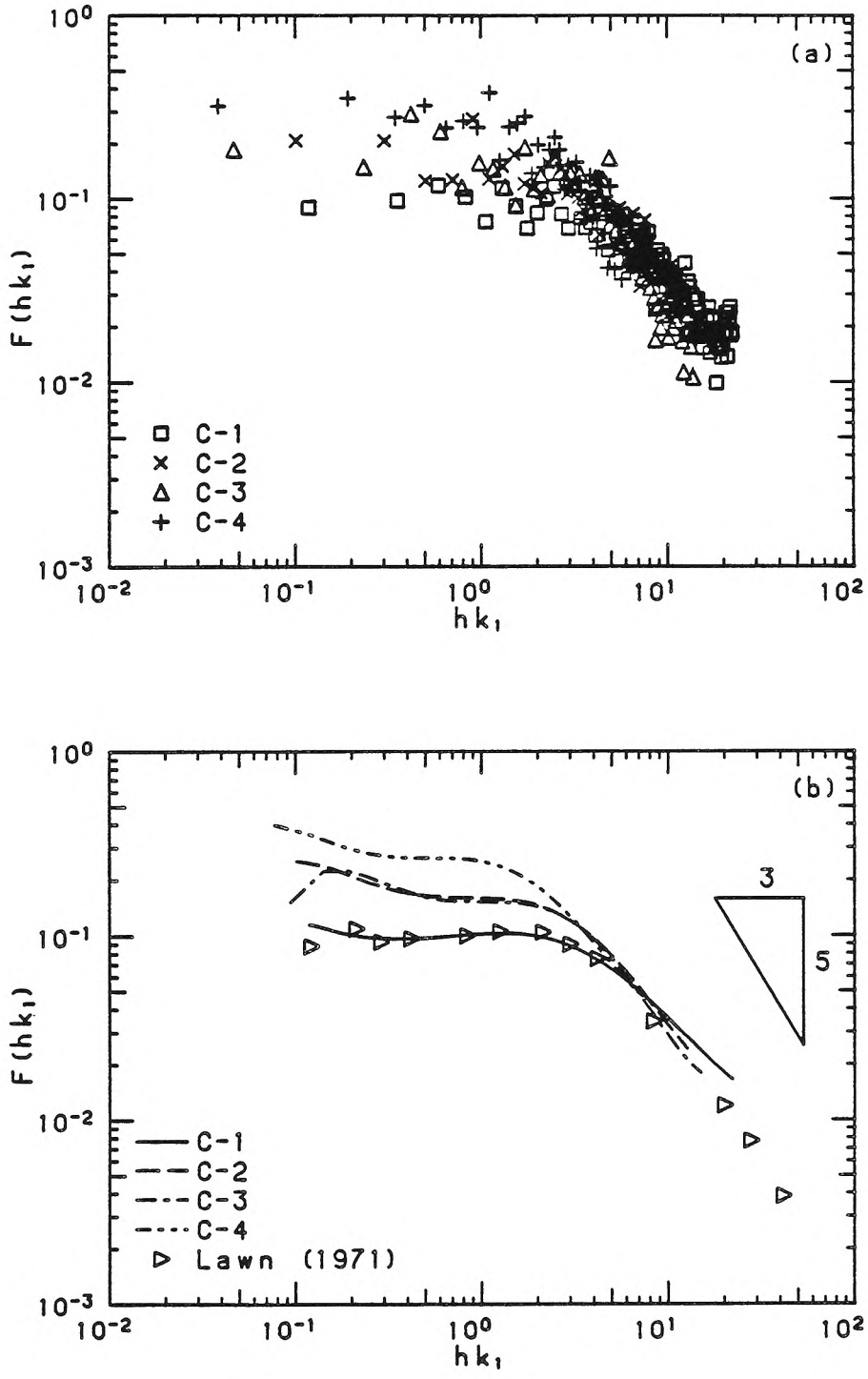

Fig. 5.2.9 Skewness of a) horizontal, and b) vertical velocity fluctuations

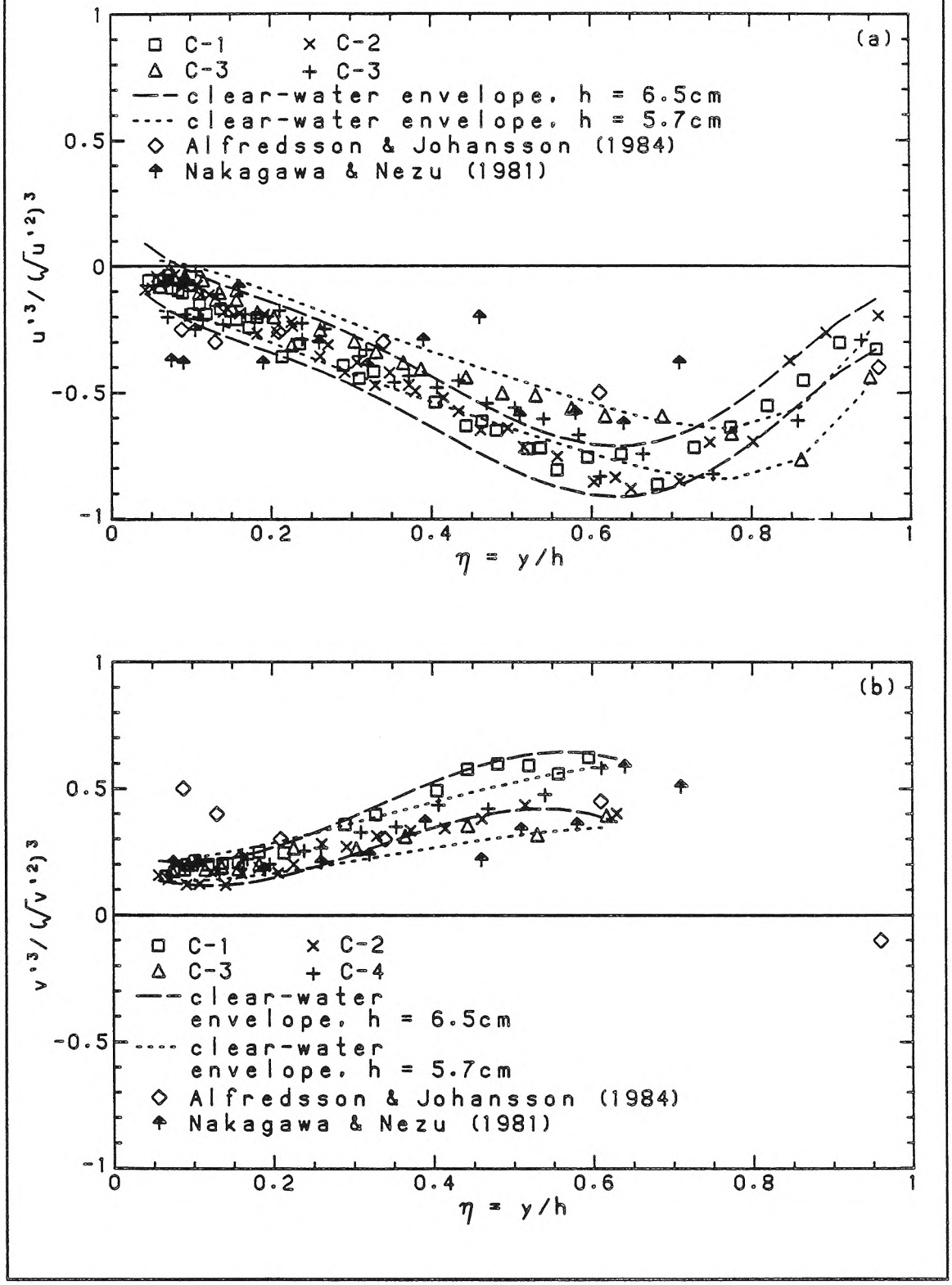

Fig. 5.2.10 Flatness of a) horizontal, and b) vertical velocity fluctuations

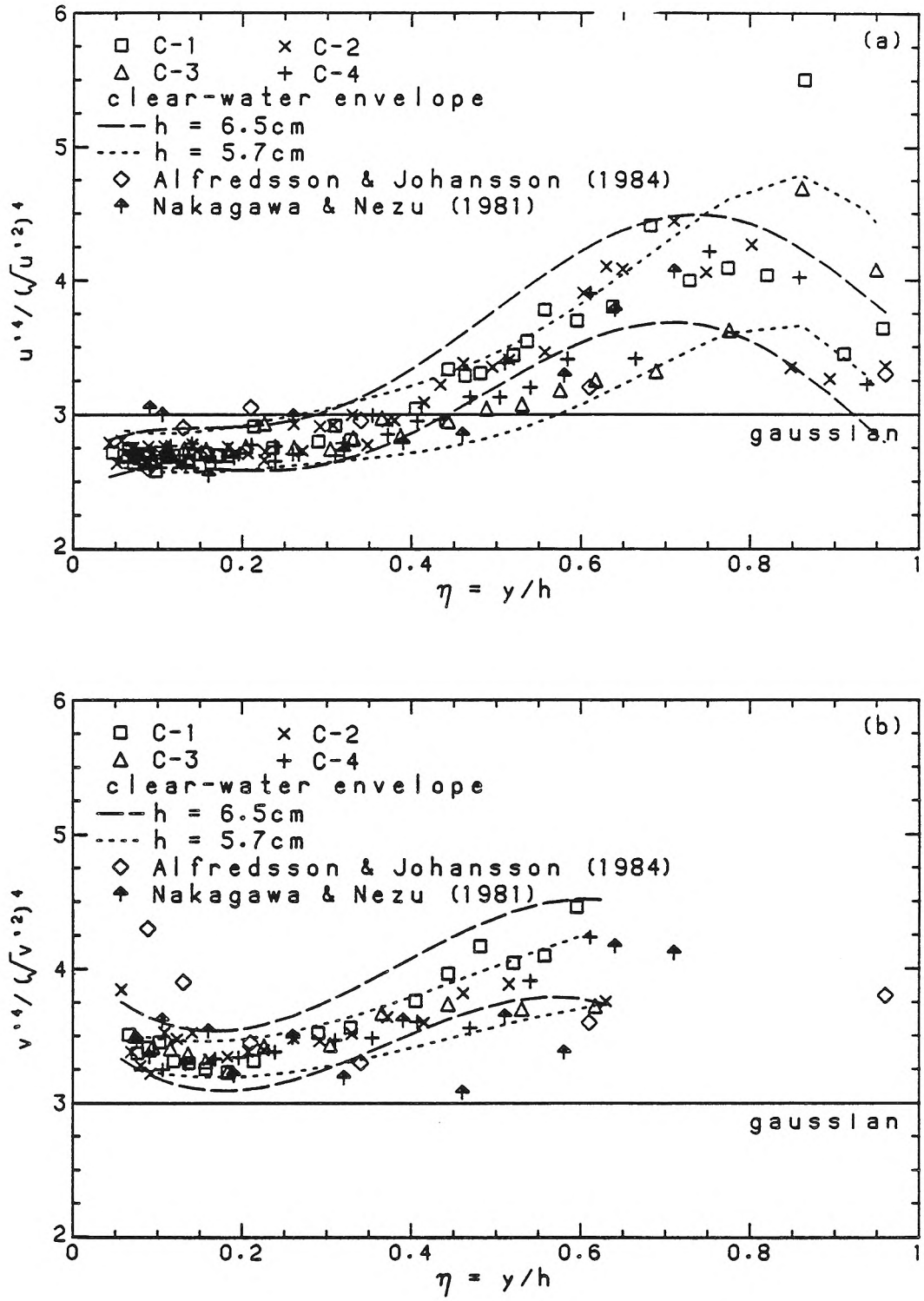

rather larger scatter, which is to be expected. The present results are, nevertheless, quite consistent, and agreement with previous results is adequate.

5.2.3 Higher-order Reynolds-stress statistics

Correlation coefficients are shown in Fig. 5.2.11a. These are somewhat smaller than expected, being typically 0.37–0.38, although there is significant scatter. Other results for higher-order statistics of the Reynolds stress are shown in Fig. 5.2.11-12. While these results are in qualitative agreement with the very few results in the literature, a qantitative difference is noted. Larger $\sqrt{(-u'v')'^2}$, less negative skewness, and slightly larger flatness, particularly as the bottom is approached, are noted. To some extent, this may be due to the susceptibility of the LDV system to noise. This may be seen in the results of experiment C-1, where somewhat lower threshold levels were set in order to obtain a high data rate, and which, therefore, should be more open to spurious results due to noise. This is borne out in the higher-order stress statistics, where the results for C-1 tend to give the extreme values of skewness and flatness. The larger $\sqrt{(-u'v')'^2}$ may also, in part, reflect an error in the estimation of u_*^2. The envelope curves, drawn in Figs. 5.2.11b-5.2.12, were determined by excluding the results for C-1, since these were thought to be less reliable.

5.2.4 Summary: Higher-order statistics

The present LDV system, as judged by a comparison of the present clear-water results and previous results, is seen to be reliable for obtaining higher-order $u-$ and $v-$statistics. Vertical intensities are slightly higher, and correlation coefficients are slightly smaller, than those found by others. The method of spectral estimation, using an interpolated signal, is difficult to justify on fundamental grounds at the

Fig. 5.2.11 a) Correlation coefficients, b) Intensities of Reynolds' stresses

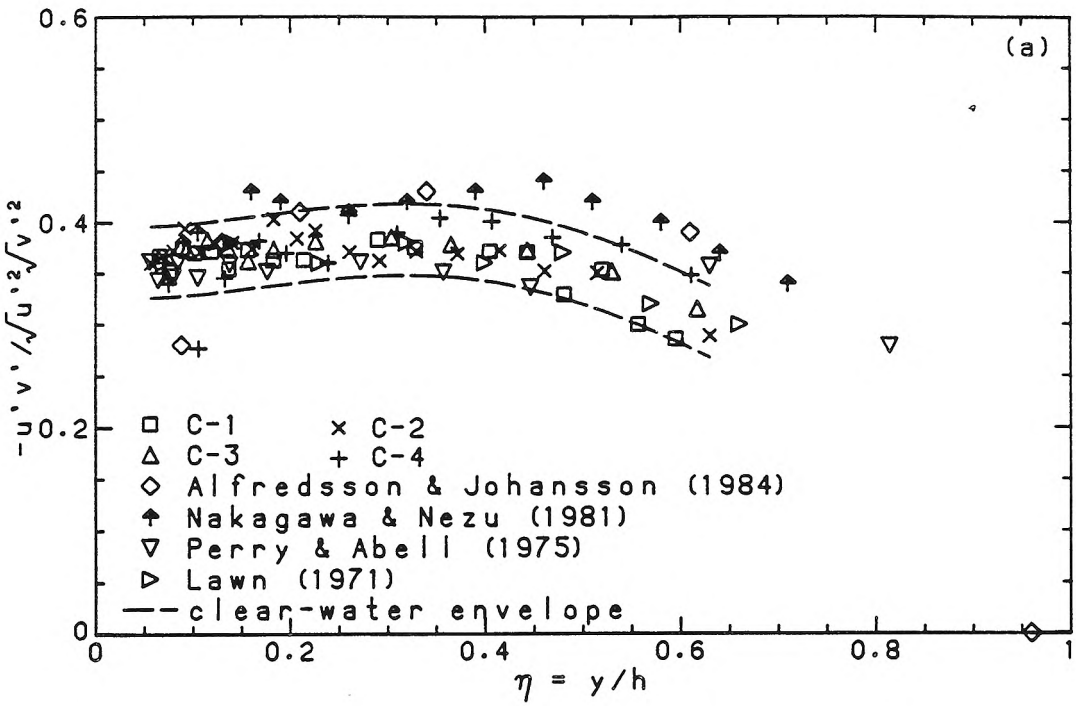

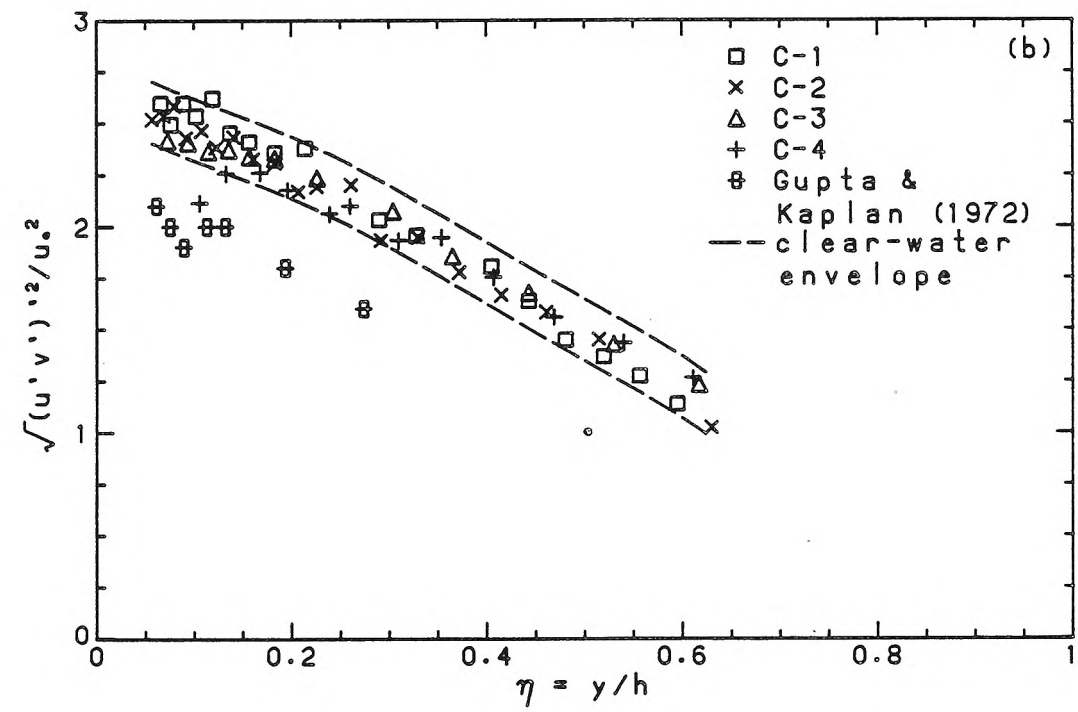

Fig. 5.2.12 a) Skewness and b) Flatness of Reynolds stresses

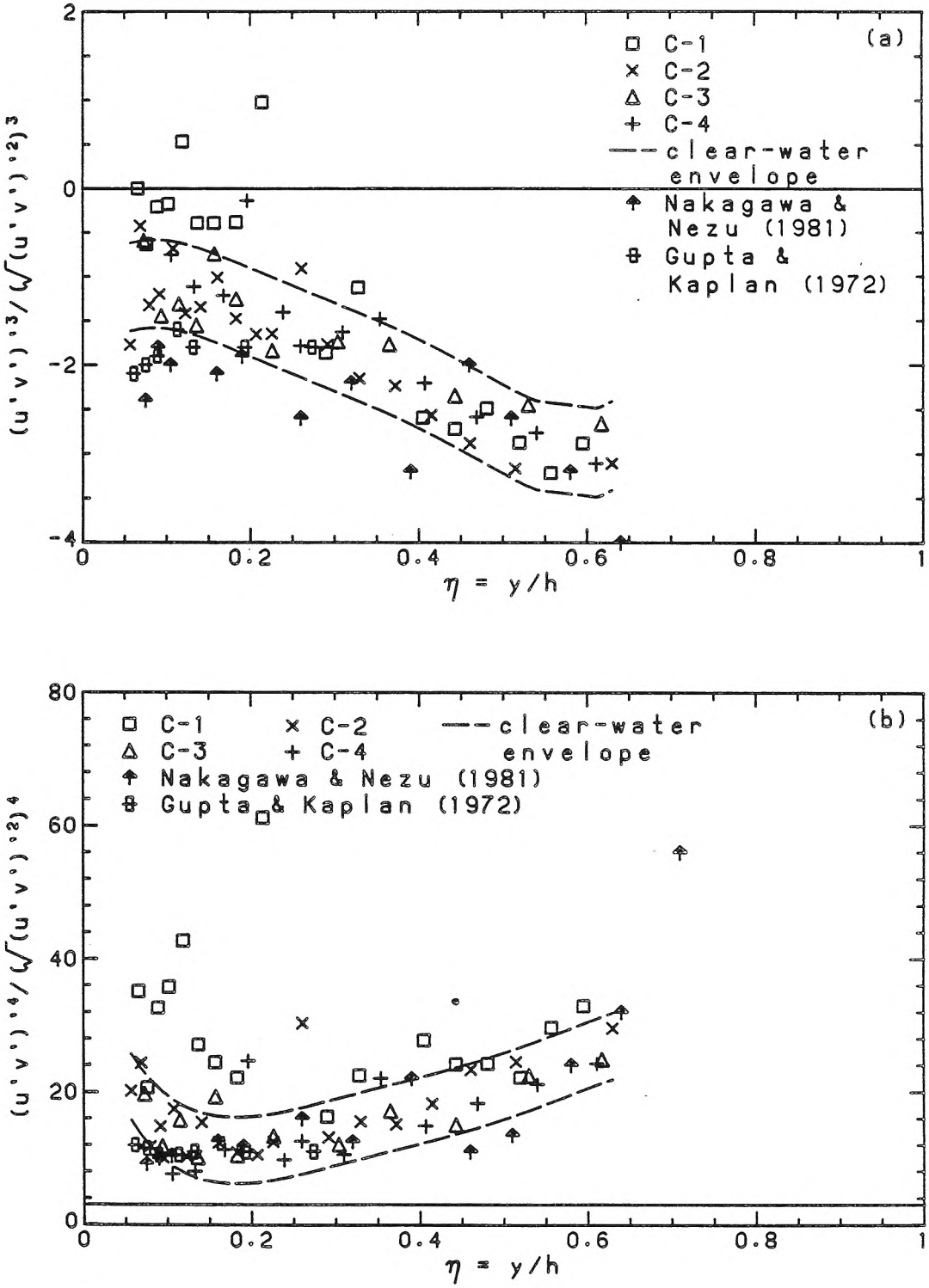

data rates achieved in view of the significant overall reduction in absolute energy. Normalized spectra, however, seem to agree with the results of others, and retain qualitative information such as the slope of the spectrum, and, therefore, may be used with some caution. While there is larger scatter, skewness and flatness of $u-$ and $v-$fluctuations in adequate agreement with others have also been obtained.

The reliability of Reynolds-stress statistics is more problematic. The higher-order stress statistics show large rms, negative skewness and large flatness factors in qualitative agreement with the few published results available. Quantitative comparison, however, reveal significant differences, e.g., intensitites larger by 30% than at least one other set of results. Because so few investigations have examined these higher-order stress statistics, the question of reliability cannot be answered conclusively.

The effect of the aspect ratio, although slight, remains noticeable in higher-order statistics, particularly in the turbulence intensities, and, to a lesser extent, in the skewness and flatness statistics, where the larger scatter tends to mask any slight effects.

6. Sediment-laden flow experiments: Mean profiles

6.0 Introduction

In this chapter, the experimental results for the mean stress, velocity, and concentration fields for both equilibrium-bed and starved-bed conditions are presented. (Gross flow characteristics for all experiments are tabulated in Appendix A.2.) The results are discussed in terms of previous approaches, as well as the similarity approach proposed in Chap. 3. Previous experimental results by others are also re-examined. A discussion of results on flow resistance is given.

6.1 Equilibrium-bed experiments

The conditions for the equilibrium-bed experiments are listed in Table 6.1.1. The labelling of the experiments is mnemonic, indicating the nominal grain size, the depth, and the presence of an equilibrium bed. Fig. 6.1.1 shows typical variations in bed elevations measured at the end of an experimental run. The idealized flat bed is never achieved. The standard deviation from a mean level is $\approx$ 0.6 mm ($\approx$ 3–4 grain diameters) or less for all experiments. For comparison,

Fig. 6.1.1 Variations in bed elevations for equilibrium-bed experiments

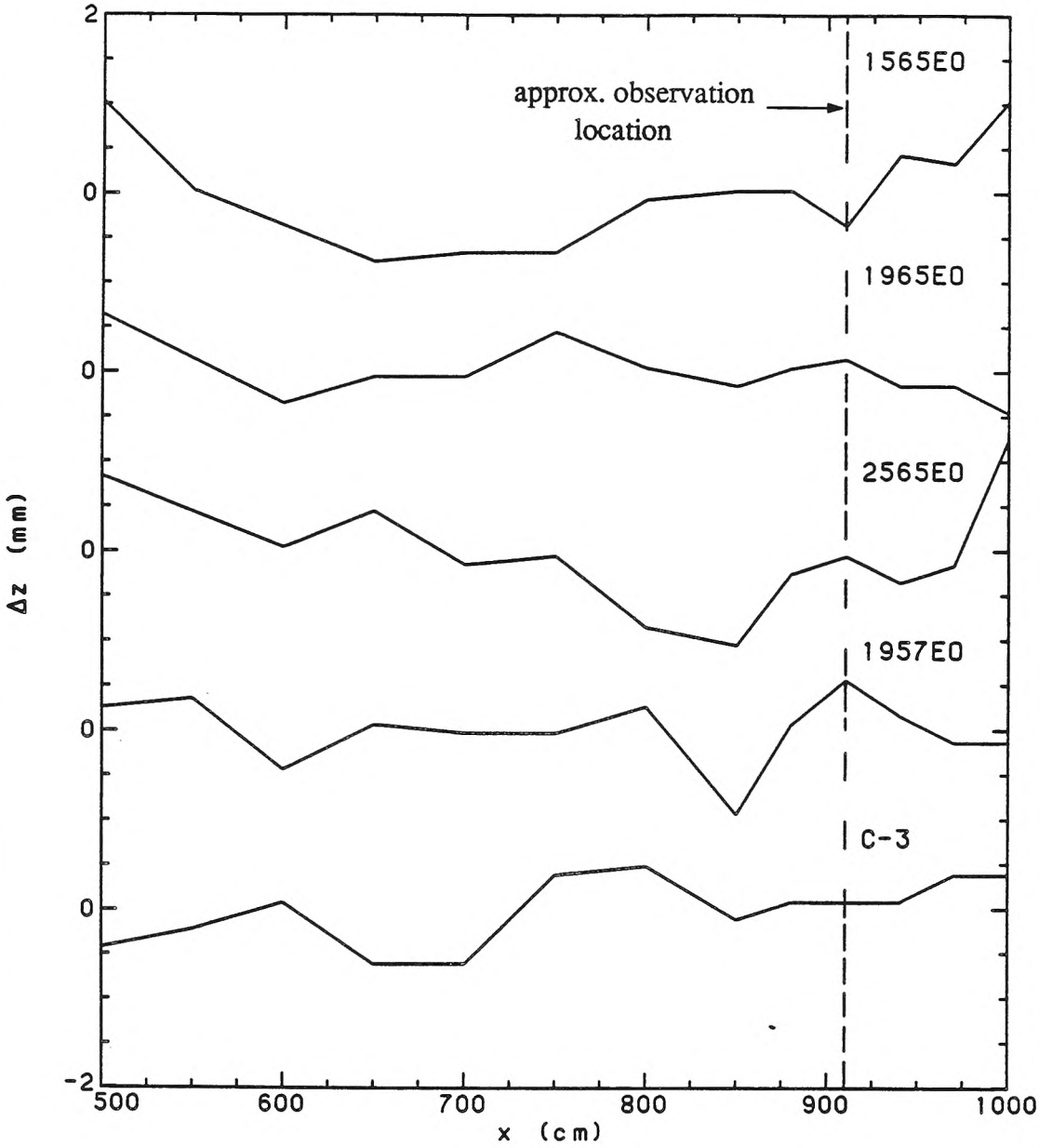

a profile of the bare flume, taken after a clear-water run, is also shown. *It*, also, cannot be said to be perfectly flat, although the standard deviation from the mean-bed level is smaller, being $\approx$ 0.3 mm, but, perhaps more important, the non-uniformities are immobile. Because the equilibrium bed is deformable and mobile,

the definition of the point of zero elevation is not well defined; the conventional definition as the mean level of the bed after the flow has been stopped is used.

Table 6.1.1 Conditions for equilibrium-bed experiments

Experiment	1565EQ	1965EQ	2565EQ	1957EQ
depth, h (cm)	6.45	6.51	6.54	5.72
hydraulic radius, r_h (cm)	4.35	4.38	4.39	4.00
aspect ratio, b/h	4.14	4.10	4.08	4.66
slope, S ($\times 10^{-3}$)	2.44	2.51	2.96	2.95
grain diameter, d_{50} (mm)	0.15	0.19	0.24	0.19
bulk discharge, Q (l/s)	10.80	11.05	12.07	9.85
temperature, T ($^{\circ}C$)	20.7	21.1	21.3	20.9

6.1.1 Stress profiles

Reynolds-stress estimates of u_* are based on fluid velocity fluctuations. In sediment-laden flows, some amount of momentum transfer is performed by the solid phase; this contribution is likely to be significant only in the very-near-bed region. Reynolds-stress measurements were typically limited to the region, $\eta > 0.1$, in which the suspension is dilute. The approximation that the Reynolds stress is equal to the total local stress should still be applicable in this region. The further approximation of a linear stress profile (§2.1.2) justifies the procedure, used previously for treating clear-water flow, of estimating wall shear.

Because reliable two-component measurements were obtained for only three of the four experiments (all except 1565EQ), the determination of the Reynolds-stress profiles was restricted to these three. The dimensional stresses are presented

Fig. 6.1.2 Reynolds-stress profiles: a) dimensional, b) normalized by u_*^2

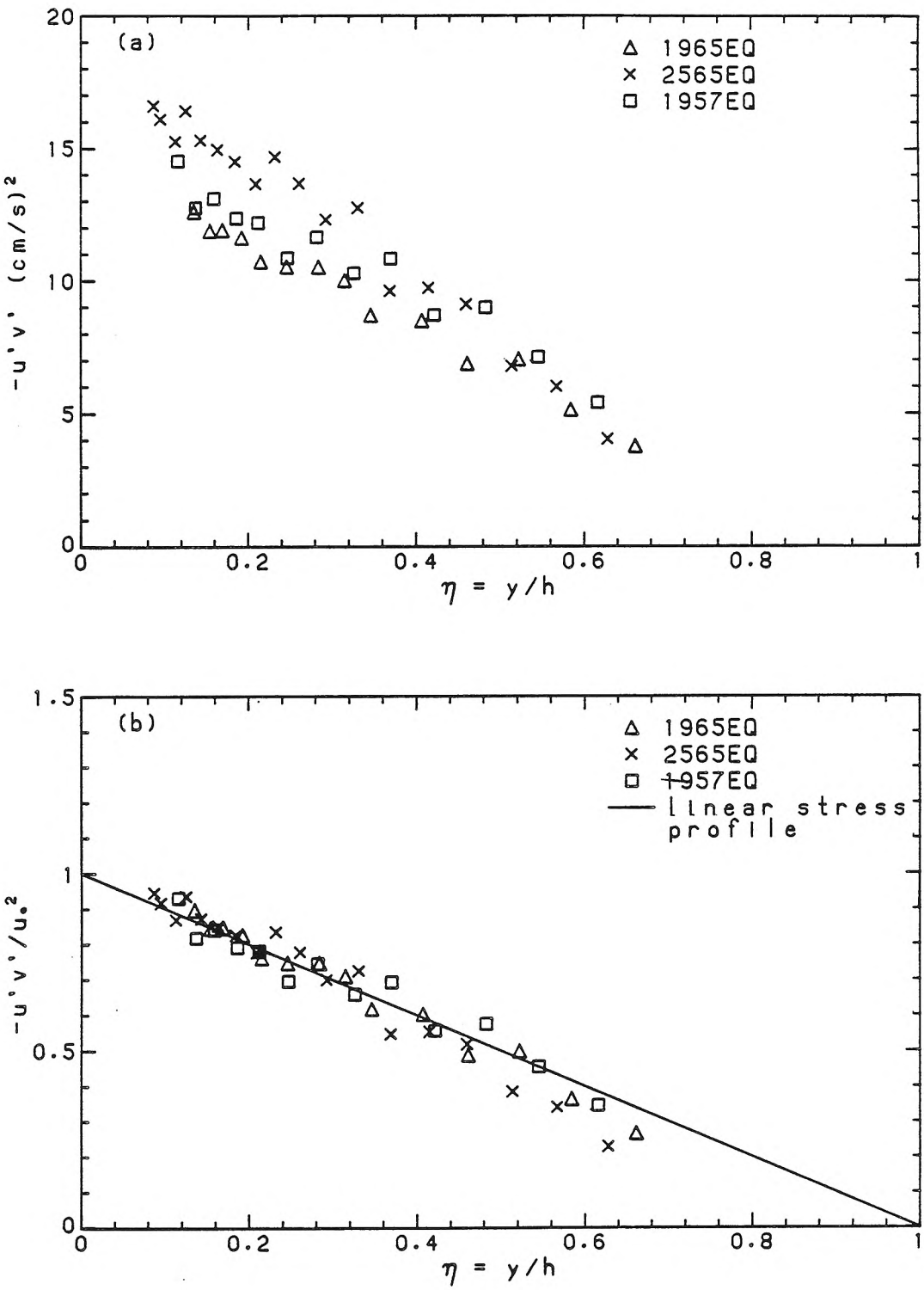

in Fig. 6.1.2a, while the normalized stresses are shown in Fig. 6.1.2b. The results are similar to those obtained in the clear-water experiments, with a decay near the free surface somewhat faster than the ideal linear profile. The estimates of u_* for each experiment are compared with other estimates in Table 6.1.2. In the case of 1565EQ, where Reynolds-stress measurements were not available, a crude estimate of u_* was obtained from noting a decreasing trend in $u_*/\sqrt{ghS}$ with decreasing grain diameter in cases where a Reynolds-stress estimate of u_* was available. This is attributed to decreasing bed roughness, which would reduce the relative contribution of the bed to the shear. This was crudely extrapolated, so that it was assumed that $u_*/\sqrt{ghS} = 0.91$ for 1565EQ. As such, this estimate is perhaps debatable, although it is believed that it remains reliable to within 5%.

Table 6.1.2 Comparison of estimates of u_* (cm/s)

Experiment	1565EQ	1965EQ	2565EQ	1957EQ
present estimate	3.58†	3.75	4.25	3.95
$\sqrt{ghS}$	3.93	4.00	4.36	4.07
$\sqrt{gr_hS}$	3.23	3.28	3.57	3.40
$u_*/\sqrt{ghS}$	0.91	0.94	0.96	0.97
$u_*/\sqrt{gr_hS}$	1.11	1.14	1.17	1.16

† not estimated from Reynolds-stress measurements

6.1.2 Velocity profiles

Dimensional velocity profiles from the direct one-component measurements are presented in Fig. 6.1.3, and a comparison between these and two-component results is given in Fig. 6.1.4. The agreement is perhaps marginally worse than

Fig. 6.1.3 Dimensional velocity profiles
a) 1957EQ, 2565EQ, b) 1565EQ, 1965EQ

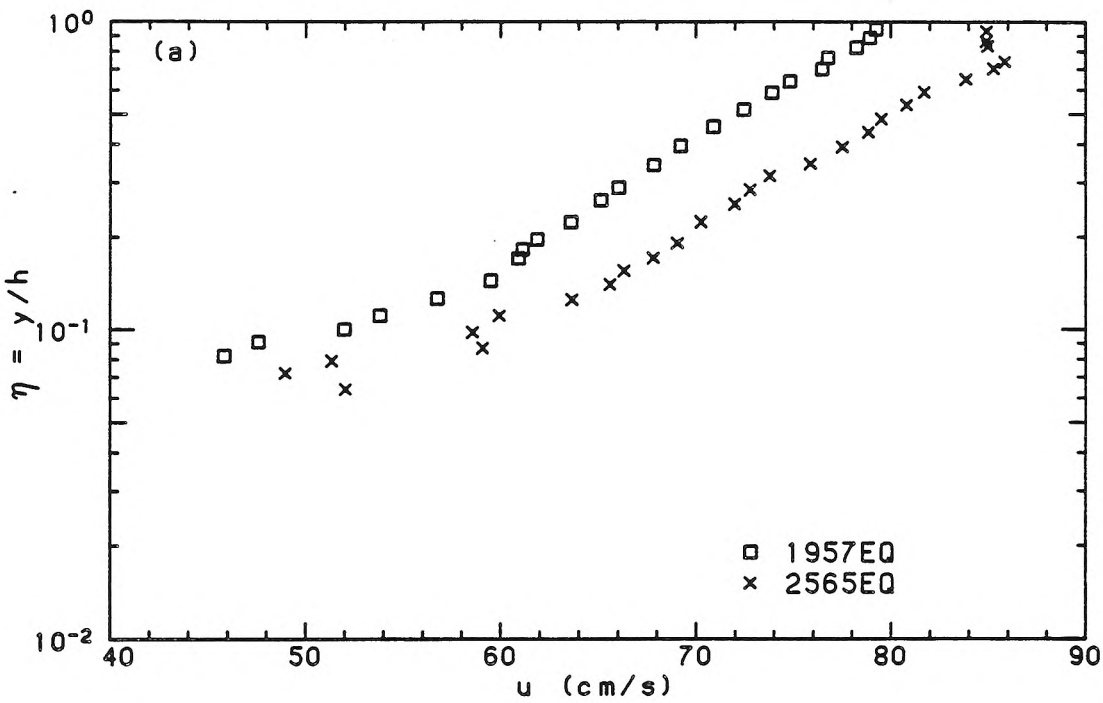

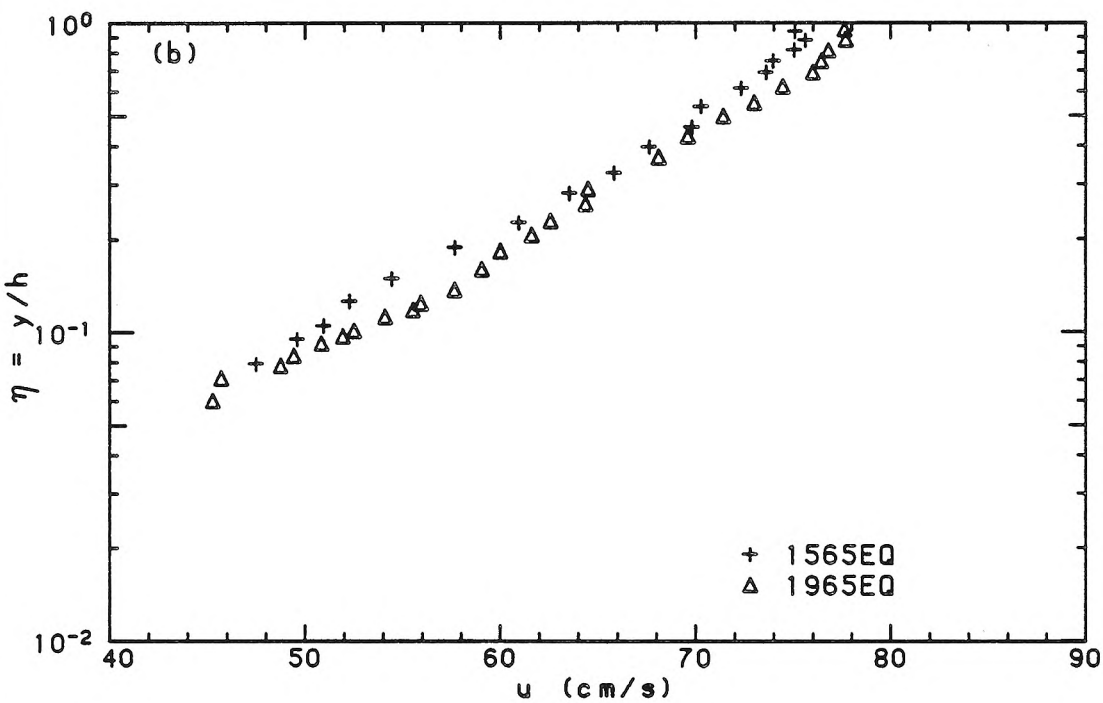

that observed in the clear-water experiments, but is considered adequate and so serves as a check on the reproducibility of experimental conditions as well as on the instrumentation. Fig. 6.1.5a shows the velocity profiles plotted in viscous coordinates, with a clear-water profile for purposes of comparison. If these coordinates were appropriate and differences could be attributed to variations in the additive constant, then the velocity profiles for sediment-laden flows, for small y^+, would simply be shifted parallel to the clear-water result. A wide scatter is, in fact, observed. The same remarks also apply to the use of the grain diameter as the inner length scale, as shown in Fig. 6.1.5b.

Fig. 6.1.4 Comparison of velocity profiles obtained by 1-component and 2-component measurements

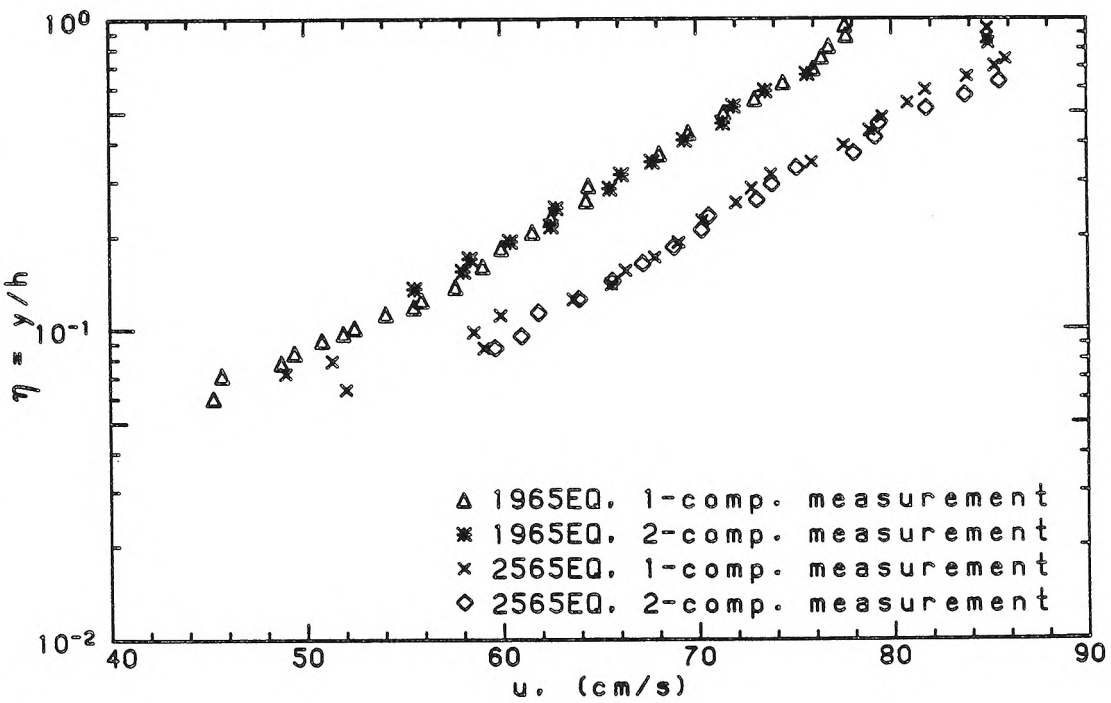

Velocity-defect profiles are compared with the traditional log-law fit in Fig. 6.1.6, where the log law has been fitted to the entire flow region, with κ_s as

Fig. 6.1.5 Velocity profiles in inner coordinates
a) l_ν, b) d_{50} as inner-length scales

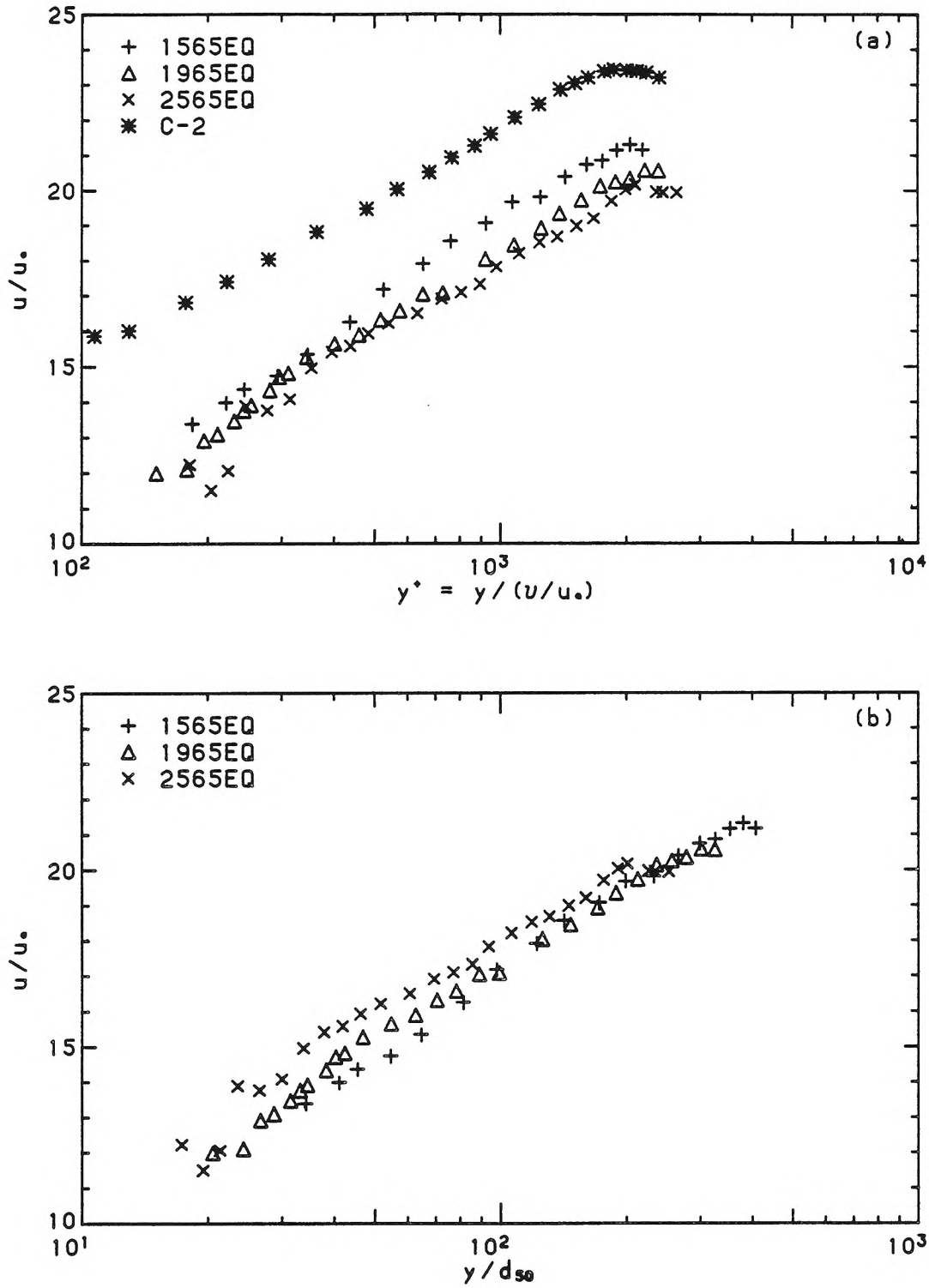

an adjustable parameter. The goodness-of-fit may be considered acceptable for engineering purposes. The value of κ_s found from the fit is seen to be significantly smaller than 0.4. Moreover, if 1957EQ is not considered, a trend to smaller values of κ_s for smaller grain sizes (and hence, larger concentrations) and constant depth may be deduced. This trend is consistent with the predictions of the Einstein-Chien (1955) correlation.

A wake-law fit, obtained using the same procedure as was applied to clear-water results, is compared with the experimental data in Fig. 6.1.7. The fit is noticeably worse than the log-law fit, with marked deviations for small η. The values of the wake coefficient, W_0, obtained from this fit do not differ significantly from those found in clear-water results, although this may be attributed in part to the specific fitting procedure used, which tends to give more weight to a better fit in the upper region.

On the basis of the empirical fit, the traditional approach with a varying κ_s would seem more appropriate, at least for the present range of experimental conditions. Nevertheless, this would conflict with the notion that, even for clear-water flows, a definite wake component can be identified. A possible reconciliation of the two approaches would incorporate a wake component that would not be significantly affected by the presence of sediment and a varying κ_s in order to account for the effects of the suspended sediment. The discussion of §3.1 suggests, however, that this can be justified only if a dimensionless parameter is found to be relevant in both the inner and the outer flow regions.

To clarify this issue, the fits for a single experiment, 1965EQ, are re-examined in Fig. 6.1.8. Examined more closely, the log-law fit is seen to track the observations on average, but does not follow the data in detail. The wake-law fit performs

Fig. 6.1.6 Comparison of velocity-defect profiles with fitted logarithmic profiles (κ_s as a fitting parameter, $W_0 = 0$)

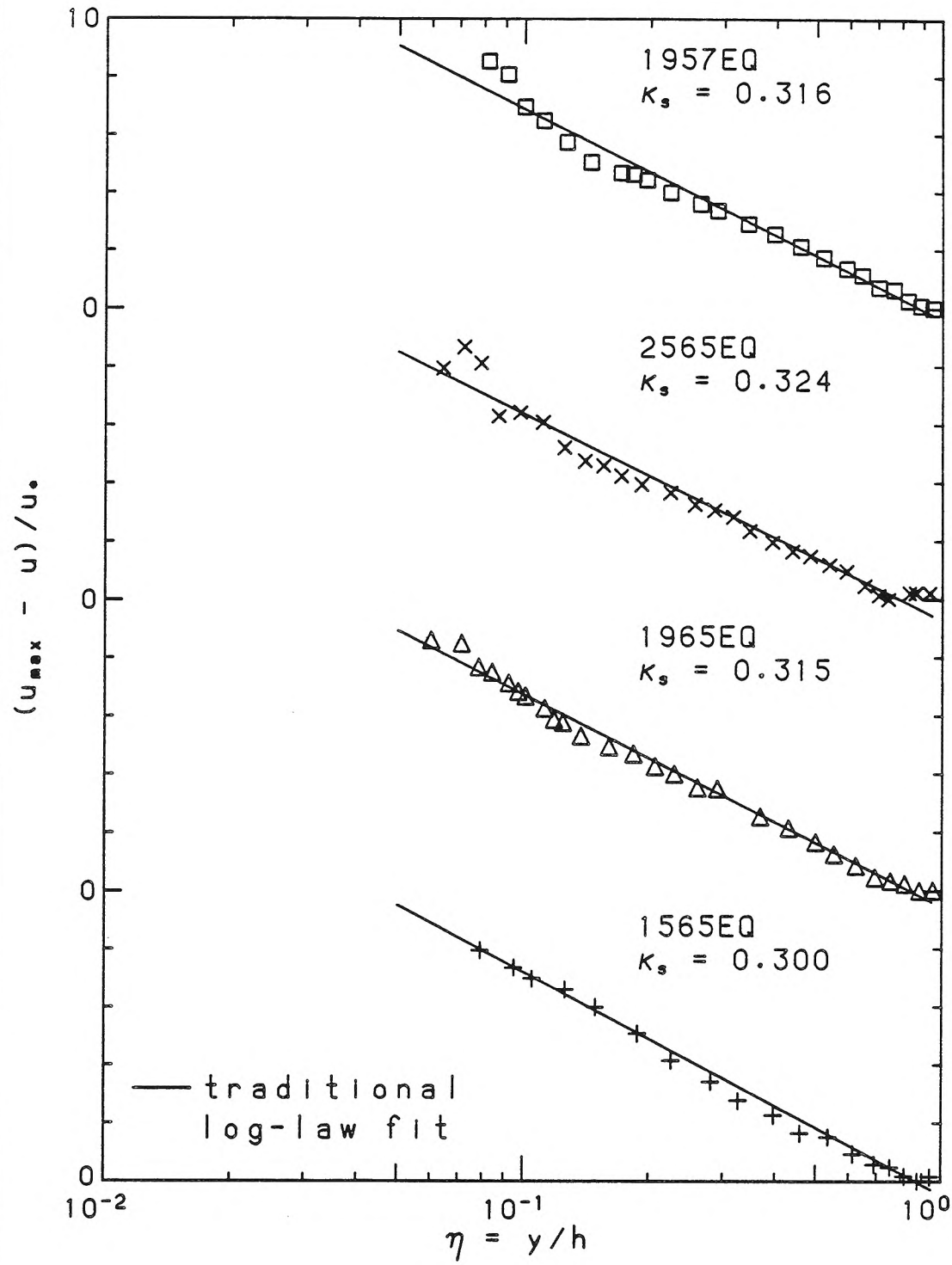

Fig. 6.1.7 Comparison of velocity-defect profiles with fitted wake-type profiles (W_0 as fitting parameter, $\kappa_s = \kappa$)

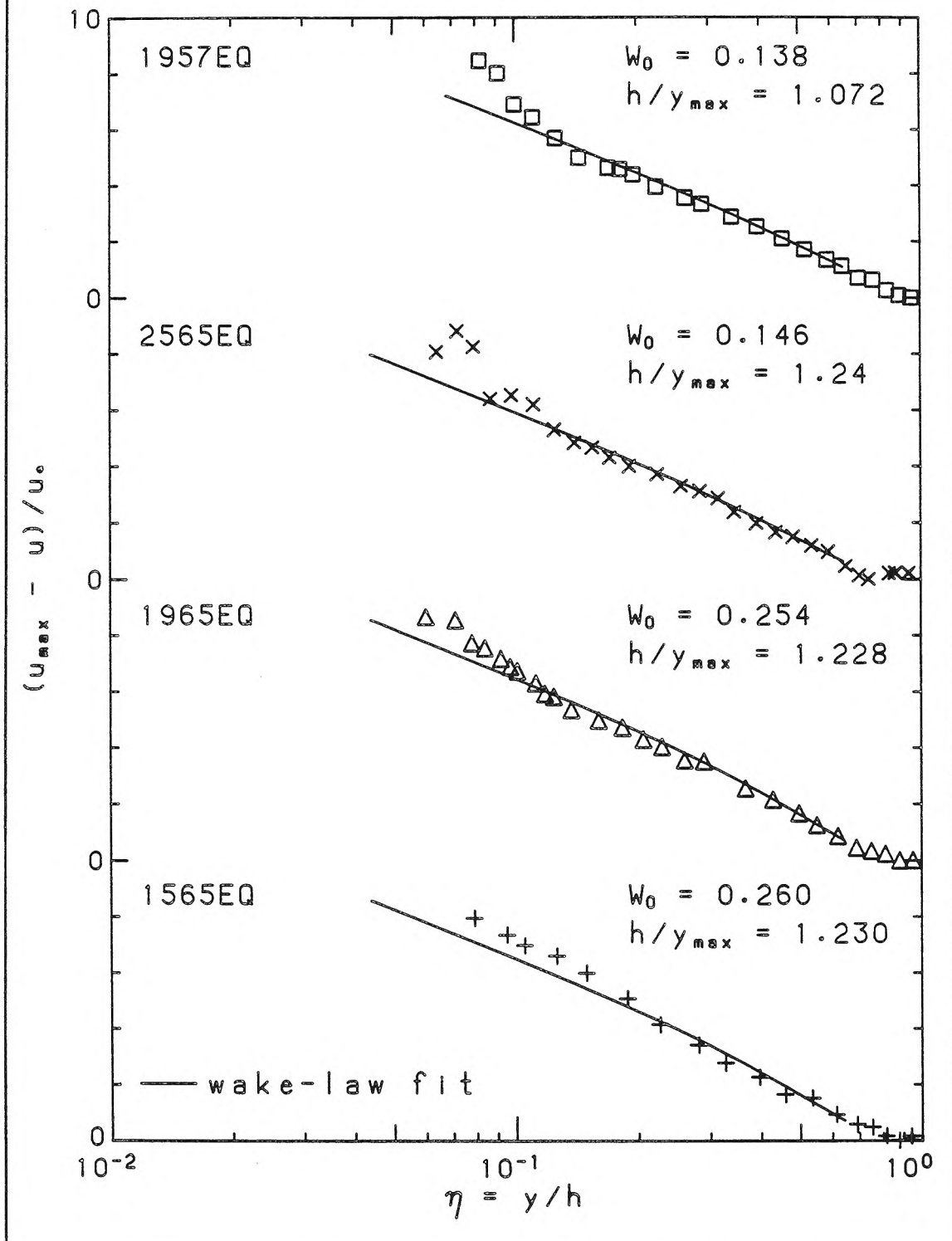

Fig. 6.1.8 A closer examination of a velocity-defect (1965EQ) profile

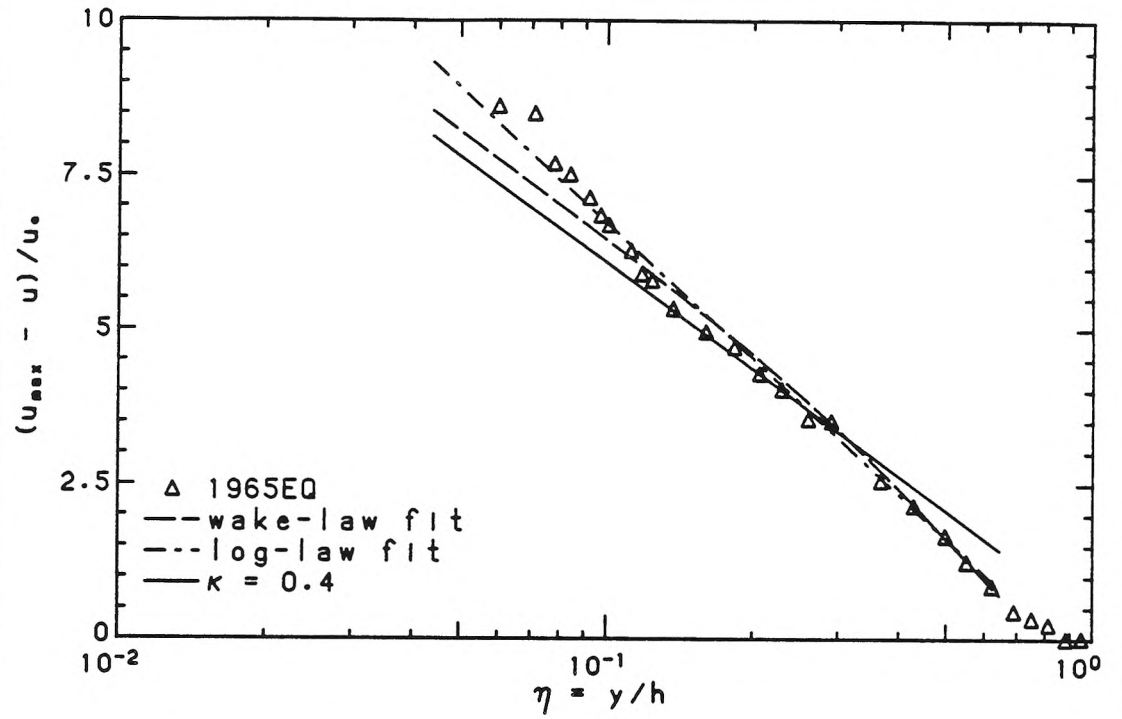

poorly for small η, because there seems to be a region, e.g., $\eta \geq 0.2$, for which it is indeed appropriate. This is emphasized in Fig. 6.1.8 by a solid line associated with $\kappa = 0.4$. This suggests that there exists a region of flow, more restricted than in clear-water flow, in which the velocity profile remains or approaches an approximately logarithmic profile with the traditionally accepted value of $\kappa = 0.4$. Below this region, however, the velocity profile deviates significantly from a logarithmic profile with a velocity gradient, which is at least initially larger than that associated with the log profile. Above this region, a wake component with a velocity gradient also larger than that of a log profile may be identified. The importance of the wake component itself seems, however, little changed from that observed in clear-water flows.

Velocity-defect profiles for all four experiments are plotted in Fig. 6.1.9a. The problem of $u_{\max}$ occurring at different points below $\eta = 1$ introduces some scatter

Fig. 6.1.9 Velocity-defect profiles
a) all experiments, b) only 1565EQ and 1965EQ

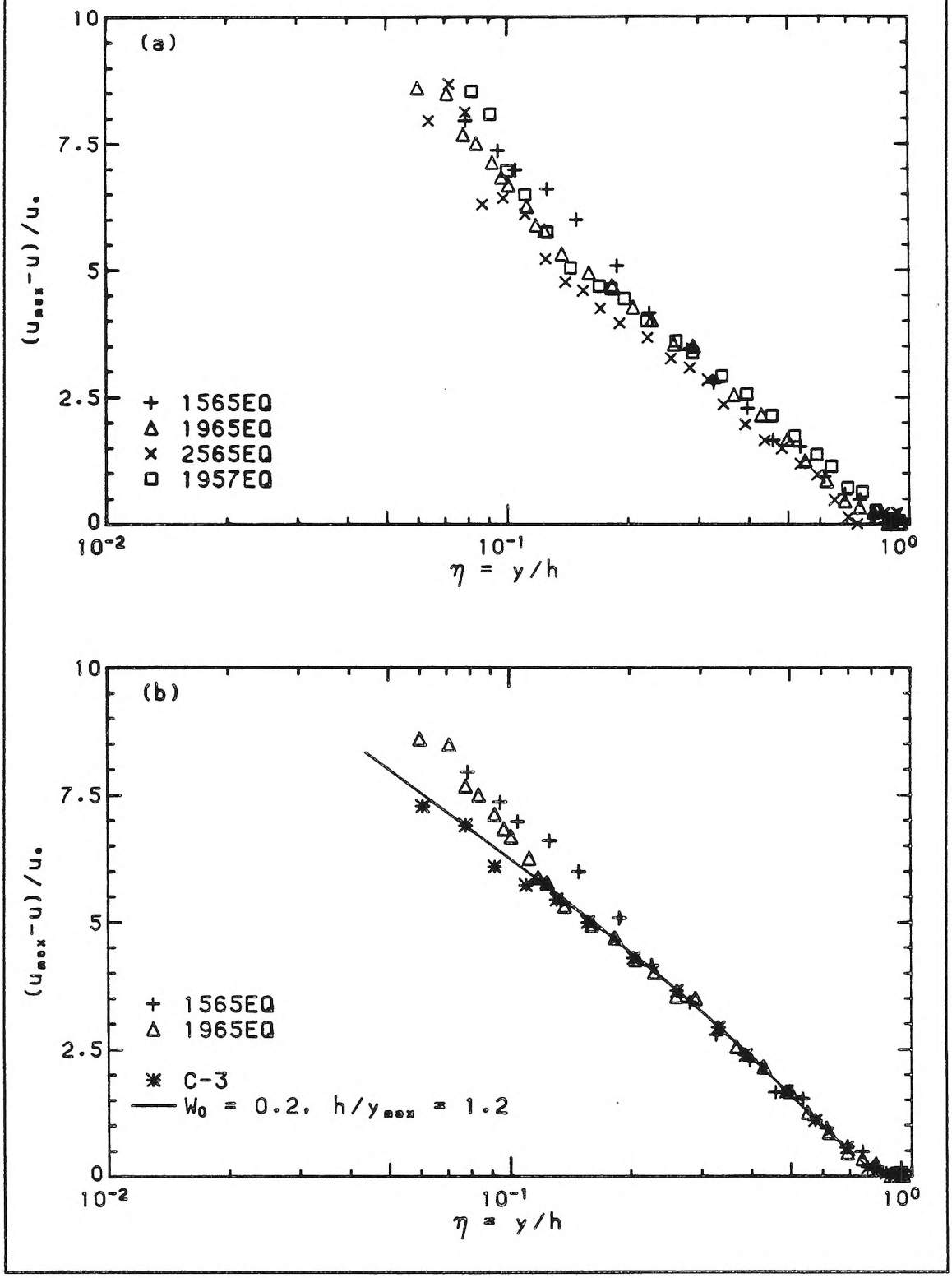

in the upper flow region, but the bulk of the scatter is seen to occur for small η, indicating the localized nature of the effect of the suspended sediment. A clearer picture emerges from a comparison in Fig. 6.1.9b of only two of the equilibrium-bed velocity-defect profiles, an actual clear-water profile, and a profile computed from a specific log-wake law, Eqn. 5.1.3, with $W_0 = 0.2$. The clear-water results (from C-3) were chosen, even though they were obtained in a flow with a smaller depth, because the maximum velocity occurred at approximately the same η as in the equilibrium-bed flows. A comparison between 1965EQ and C-3 reveals that while there is a significant difference below $\eta = 0.1$, no difference is seen above $\eta = 0.2$. A similar conclusion is reached in a comparison between 1565EQ and C-3. Further, while a region in 1965EQ may be discerned where an approximately logarithmic profile with $\kappa = 0.4$ is approached, such a region is less evident in 1565EQ. Because of this, the traditional approach of fitting a log law throughout the flow is able to give a better fit in the case of 1565EQ, as seen in Fig. 6.1.6. A growth in the extent of the region where the profile is affected by the presence of sediment is observed in the progression from C-3 to 1965EQ to 1565EQ.

6.1.3 The concentration profiles

The large (orders of magnitude) variation in local volume concentration can be seen in Fig. 6.1.10, where the concentration profiles are plotted in the traditional Rouse coordinate, $(1 - \eta)/\eta \equiv (h - y)/y$. The straight-line variation on log-log scales is not generally observed. In the upper flow, i.e., for small $(1 - \eta)/\eta$, a higher concentration is found than would be predicted by a straight-line (in log-log scales) fit to, say, the lower half of the flow. It is recalled that the van Rijn (1984) model tends to predict higher concentrations in the upper half of the flow

Fig. 6.1.10 Concentration profiles in Rouse coordinates

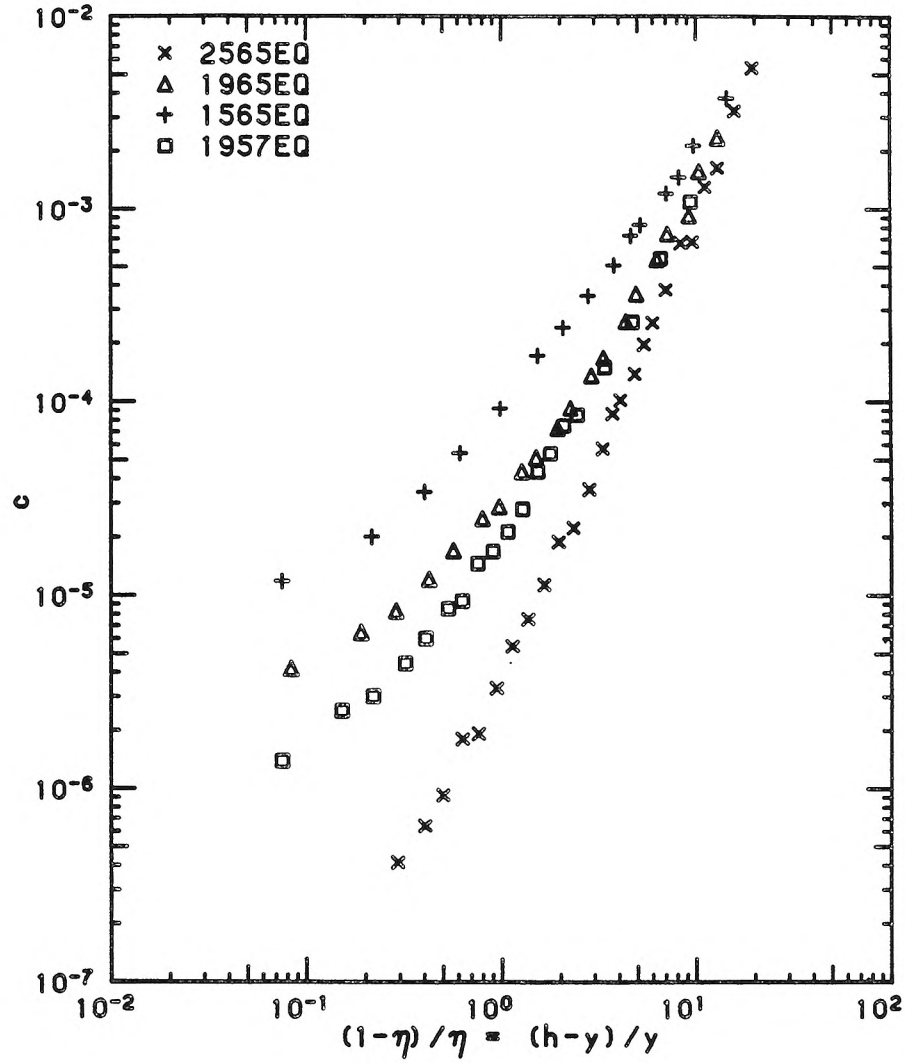

traditional model. These experimental results support the motivation for a model which can predict a higher concentration in the upper flow than the classic Rouse equation, Eqn 2.1.12, at least for this range of conditions. The model proposed in §3.4.2 has this flexibility since the exponent of the outer-flow correction term, Z_h, is not constrained to be unity; other recent models, e.g., that proposed by van Rijn (1984), also predict a higher concentration in the upper flow.

Fig. 6.1.11 Fits of concentration profiles
a) 1565EQ, b) 1965EQ, c) 2565EQ, d) 1957EQ

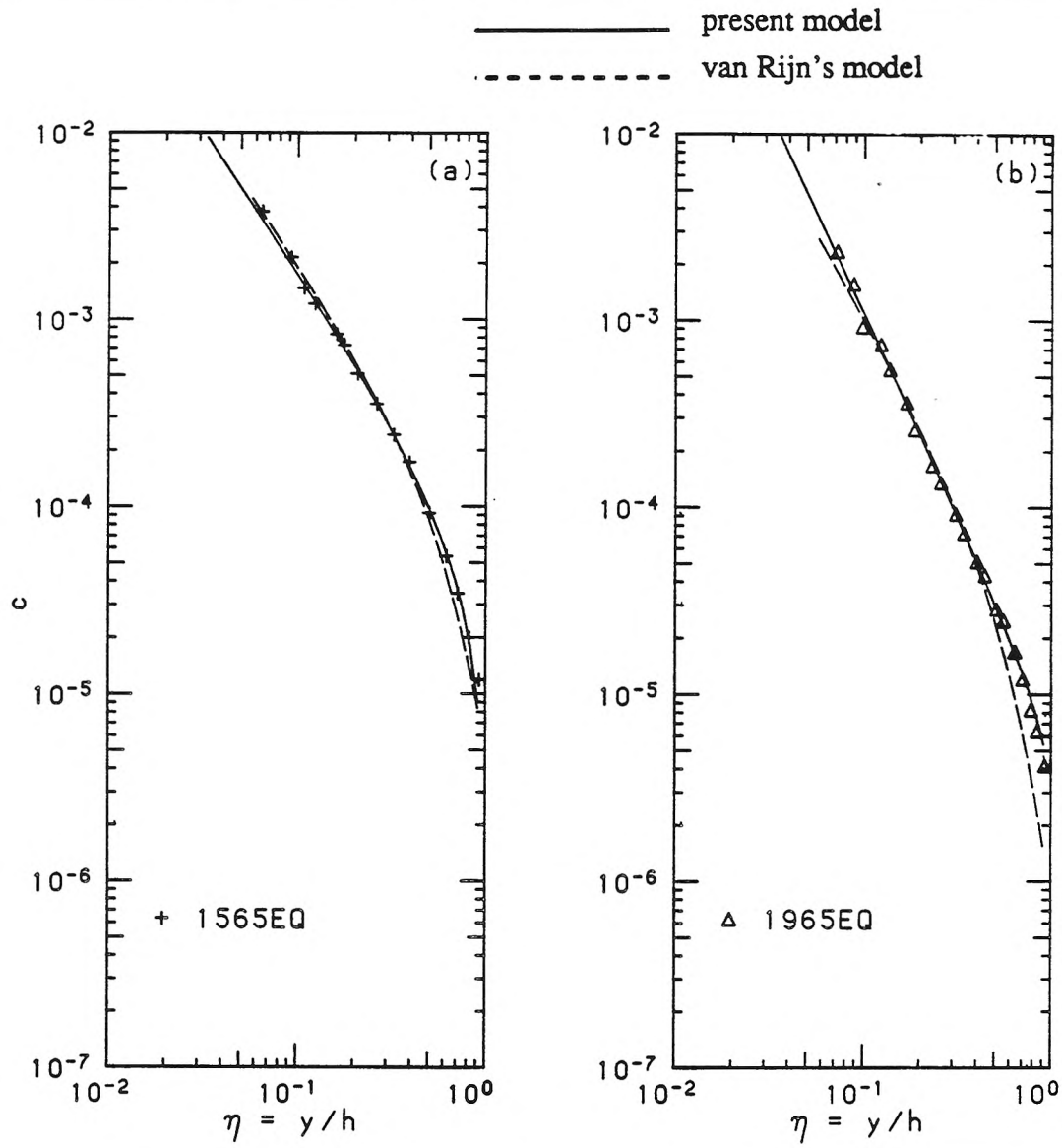

The results for the individual experiments are replotted in Fig. 6.1.11 with η rather than $(1-\eta)/\eta$ as the abscissa. The power-law variation for small η is perhaps more evident, as is also the deviation from the power-law as $\eta \to 1$. Two fits are compared in Fig. 6.1.11, one based on the model of van Rijn (1984), and the other based on the profile suggested in Chap. 3 with $W_{c0} = 1 - \eta$. The van Rijn profiles were obtained using a reference level of $a/h = 0.1$. This was

Fig. 6.1.11 c), d)

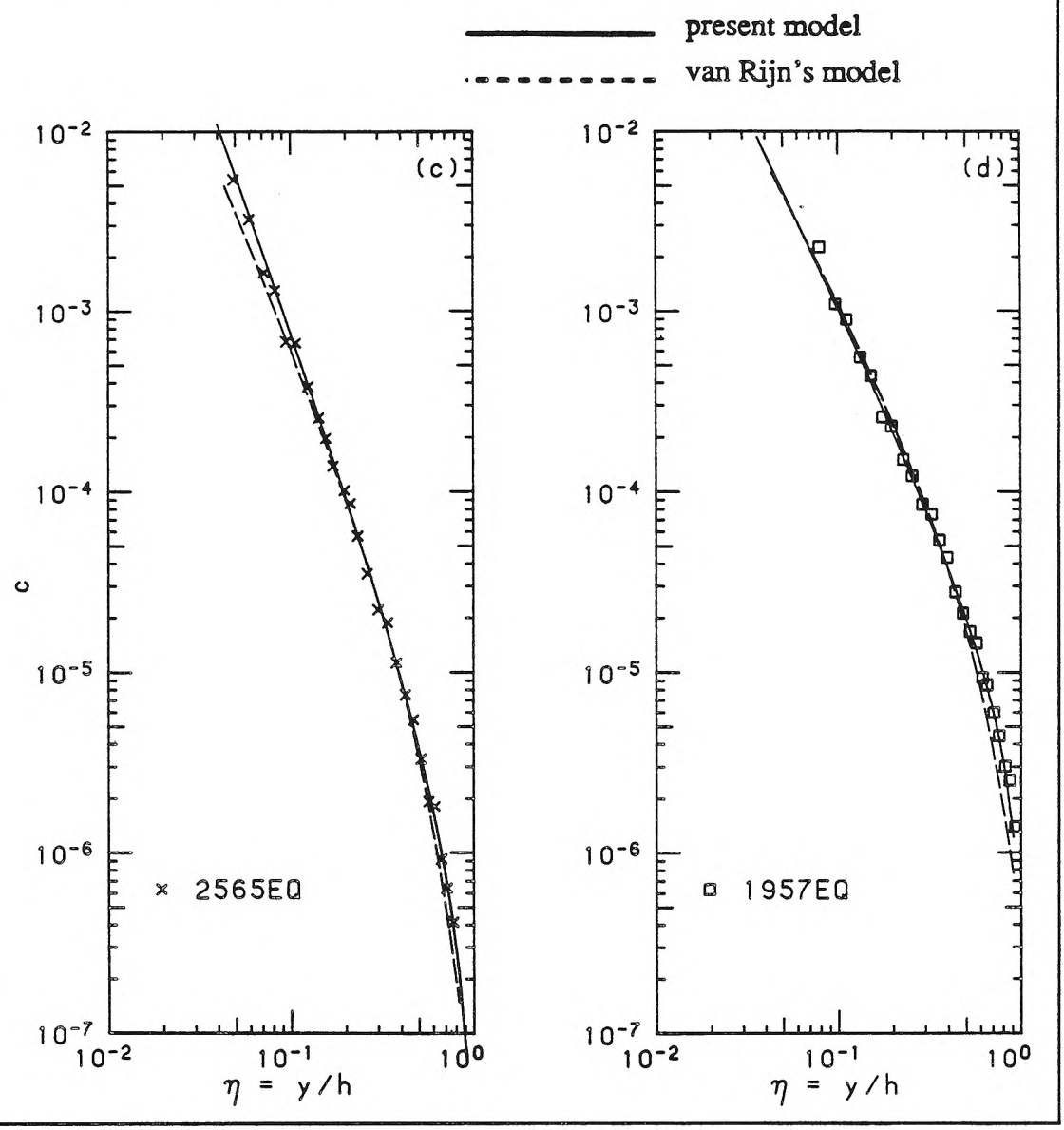

chosen since no measurements were made below $\eta = 0.06$, and it was deemed that interpolation to obtain $c(a/h = 0.1)$ was less prone to error than extrapolation to obtain $c(a/h = 0.05)$. The traditional suspended-load equation (Eqn. 2.1.10) was then fitted to the data for $\eta \leq 0.5$, to obtain Z_R, which then determined the profile in the upper half of the flow. A reasonable fit seems to be obtained for $\eta \leq 0.5$, deteriorating, however, in the upper half of the flow, sometimes quite

significantly, as for 1965EQ. Thus, even with a constant eddy diffusivity chosen as the maximum value of the traditional eddy diffusivity, the van Rijn fit still underestimates the concentration in the upper half of the flow, although in this regard, it does improve on the original unmodified Rouse profile.

The fit, proposed in Chap.3, was obtained following a procedure to be discussed in §6.3 that determines Z and Z_h. The values of Z so determined tend to be slightly larger, typically 10%, than those found from the van Rijn fit. It is remarked that there is little evidence of any significant deviation from the estimated power law in the near-bed region, which would parallel the deviation from the log law observed in the velocity profile. A better goodness-of-fit, particularly in the outer flow, is possible since it has an additional fitting parameter, Z_h.

6.1.4 Previous experimental results

Is there any evidence of similar behavior of the mean fields, particularly in the velocity field, in previous investigations? Experimental results for flat equilibrium-bed flows are few and of rather variable quality. Although the data of Brooks (1954) may be criticized for the small aspect ratios ($b/h = 3 - 4$), one of his experiments (BRK7) was run under conditions quite similar to those obtaining in 1565EQ, and so served as a check on the consistency of results. The other flat-bed results of Brooks are of interest because of the relatively small values of the ratio, $w_{s0}/u_* < 0.3$. In some regards, the best data are those reported by Barton and Lin (1955), who made a relatively large number of observations in the vertical, usually 12-15, measured point concentrations as well as point velocities, used a uniform sand ($\sigma_g = 1.3$), and had relatively large aspect ratios ($b/h > 5$). Some questions about the full development of the flow were raised by the investigators themselves,

Table 6.1.3 Conditions for some previous equilibrium-bed experiments

run id.	u_* (cm/s)	h (cm)	S ($\times 10^{-3}$)	d_{50} (mm)	w_{s0} (cm/s)	w_{s0}/u_*
Brooks (1954)						
BRK7	3.4	7.4	2.10	0.15	1.7	0.50
BRK21	3.5	7.2	2.25	0.09	0.8	0.23
BRK29	3.3	8.5	1.85	0.09	0.8	0.24
Barton and Lin (1955)						
BL36	5.6	16.2	2.10	0.18	2.0	0.36
BL35	5.0	17.1	1.60	0.18	2.0	0.40
BL31	3.8	12.7	1.23	0.18	2.0	0.52
BL29	4.5	18.3	1.21	0.18	2.0	0.44
BL26	4.8	21.0	1.25	0.18	2.0	0.42
Guy et al (1966)						
GUY46	5.9	22.6	1.67	0.27	3.7	0.63
GUY26	7.1	14.0	3.66	0.45	6.7	0.93
GUY25	6.4	20.4	1.99	0.28	3.7	0.58
GUY15	5.0	24.1	1.12	0.19	2.4	0.48

who moved the measurement position farther downstream during the course of the experiments. Only the flat-bed results for the later runs are therefore considered (run 26 or later). Unfortunately, there is little overlap between the range of flow conditions of our experiments and those of Barton and Lin, so that the consistency of the data could not be checked. The data compiled by Guy et al. (1966) prove rather less useful because of fewer observations in the vertical and the lack of point-concentration measurements. The sands used were also more graded in character ($\sigma_g \approx 1.6$, except for the 0.19 mm sand, for which $\sigma_g = 1.3$).

The important experimental parameters for these data are summarized in Table 6.1.3, with the run numbers being prefixed by a mnemonic indicating the source of the data. The values of u_* and w_{s0} do not necessarily correspond exactly to those reported by the original investigators. The results of Barton and Lin (1955) and those compiled by Guy et al. (1966) used the estimate, $u_* = \sqrt{ghS}$, which tends to overestimate u_*. In any case, the values of these parameters used in the present study differ typically less than 5% from those used by the original investigators. All of these previous results were obtained using standard Pitot-tube and suction-sampling techniques. As such, the results for the velocity profile also provide a test that the structure found in the present results is not due to the peculiarities of the LDV technique.

The results of Brooks (1954), who used the same flume as was used for our own results, are plotted in Fig. 6.1.12, together with those obtained for 1565EQ. (For clarity, only a line representing the clear-water results will hereafter be drawn for purposes of comparison with sediment-laden flow results; this line will be computed from the specific log-wake law, Eqn. 5.1.3, and a value of 0.2 will typically be used for the clear-water wake coefficient.) The velocity-defect profiles of BRK7 and 1565EQ are seen to agree quite well, and, to a lesser extent, this is also true of the concentration profiles. Differences in the concentration profile in the upper part of the flow may be consistently attributed to the differences in flow conditions as well as to possible three-dimensional effects because of the smaller aspect ratio in the experiment of Brooks. The results for the smaller sand (and larger concentrations) show an increased deviation from what may be taken as a clear-water profile. This accords with traditional and more recent thinking in that the effects of the suspension increase with concentration. The data are also

Fig. 6.1.12 Results of Brooks (1954)

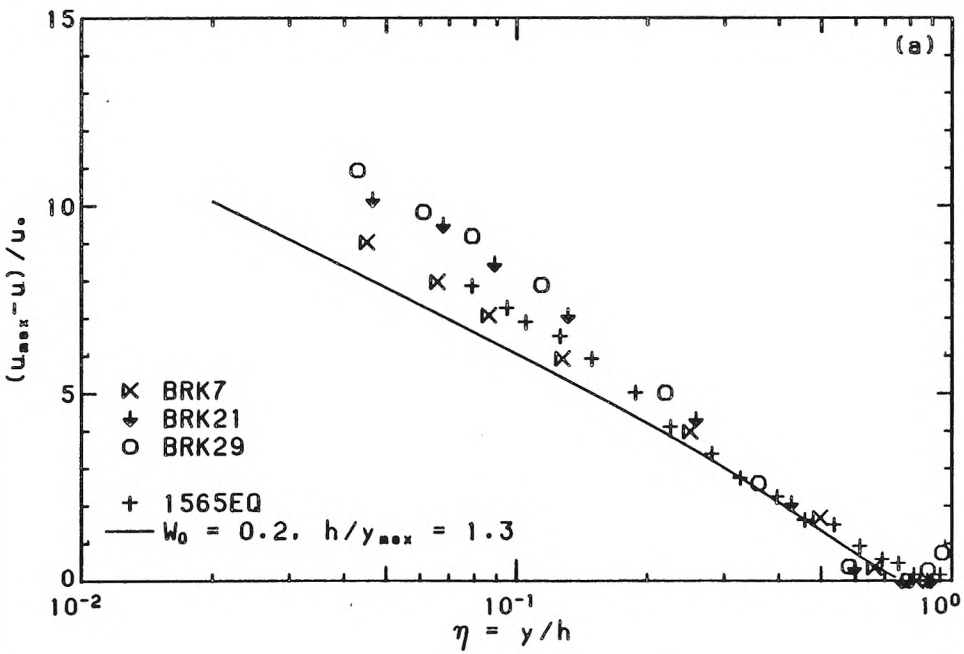

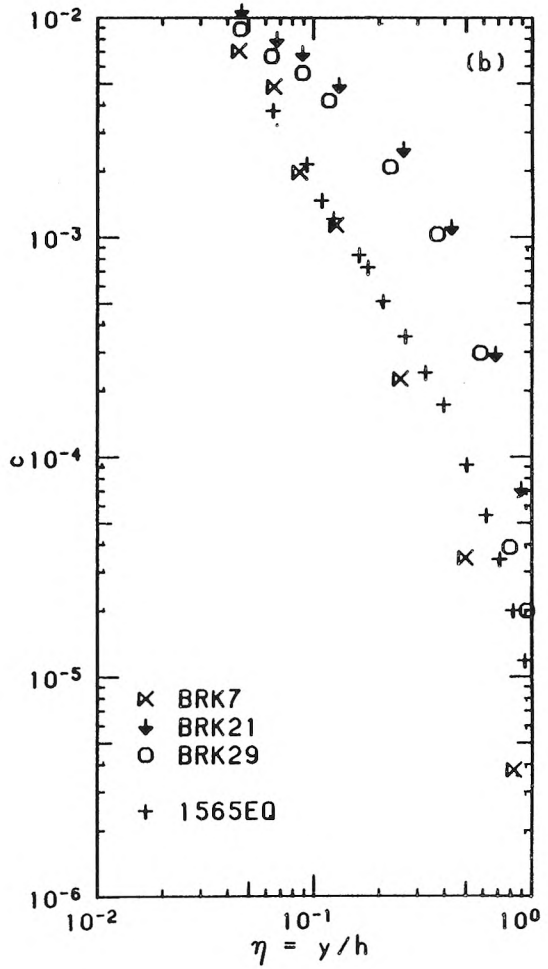

consistent with the previously noted trend, which saw a growth with decreasing sand size or increasing concentration in the extent of the region affected by the presence of sediment.

This trend is not, however, observed in the results of Barton and Lin (1955). The velocity-defect profiles of Fig. 6.1.13a indicate a distinct decrease in the extent of the effects of the suspension with decreasing w_{s0}/u_*, judged on the basis of the deviation from the clear-water profile. Fig. 6.1.14a clearly shows a general increase in concentration with decreasing w_{s0}/u_*, as expected. Nevertheless, in all except BL31, it is found that the effects of sediment are confined to a limited region near the bed. In Fig. 6.1.13b, the results for BL35, at a still smaller $w_{s0}/u*$, show no deviation from the clear-water profile. The measurement at the lowest point, $\eta = 0.018$, should, however, be regarded with caution since it is taken at $y \approx 3$mm from the bed, where probe-bed interaction may be operative. The next point at a more credible $\eta = 0.063$ ($y \approx 1$cm) still shows little departure from the clear-water reference.

The structure observed in the corresponding concentration profiles of BL29, BL26, and BL35 in Fig. 6.1.14a, with points of inflection at $\eta \approx 0.1$ (corresponding to $y \approx 2$cm), is totally unexpected in the traditional conceptual framework. The reliability of these results may be questioned. Our own results gave slight, if any, evidence of such structure. Further, the velocity and the concentration results for BL35 seem inconsistent, the former showing no deviation at all from the clear-water reference and the latter showing a marked deviation from a power-law profile. Nevertheless, for BL29 and BL26, such a structure would parallel that observed in the velocity profile. Deviation from a log-law velocity profile would then be associated with deviation from a power-law concentration profile. *If* this parallel

Fig. 6.1.13 Velocity results of Barton and Lin (1955)
a) BL31, BL29, BL26, b) BL35, BL36

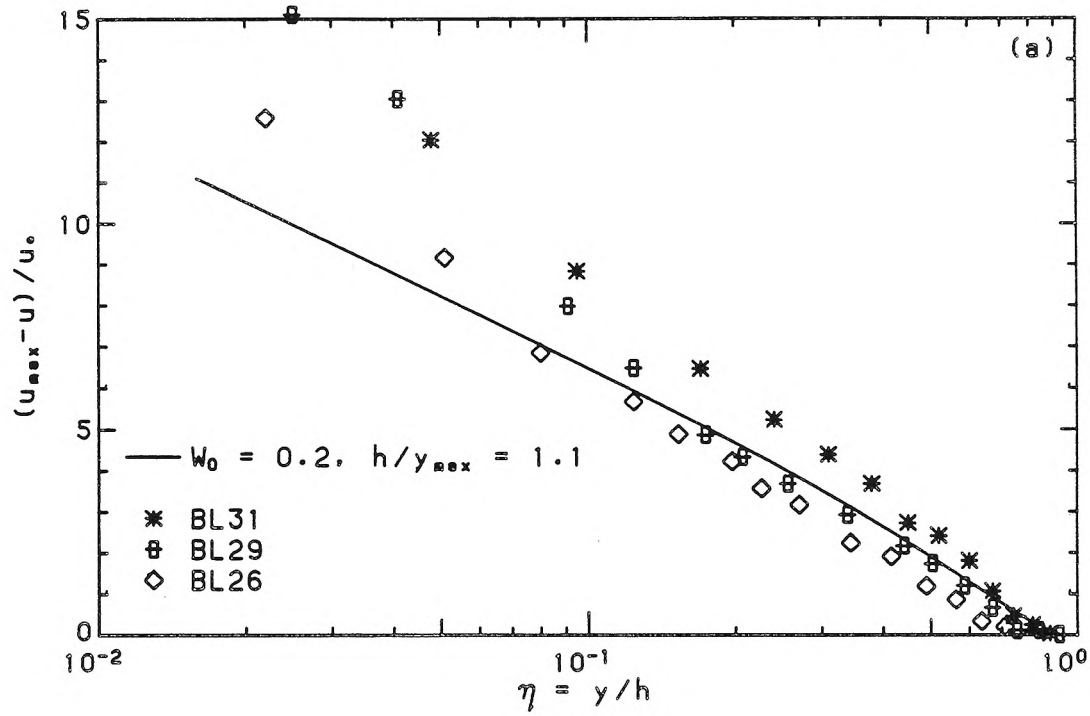

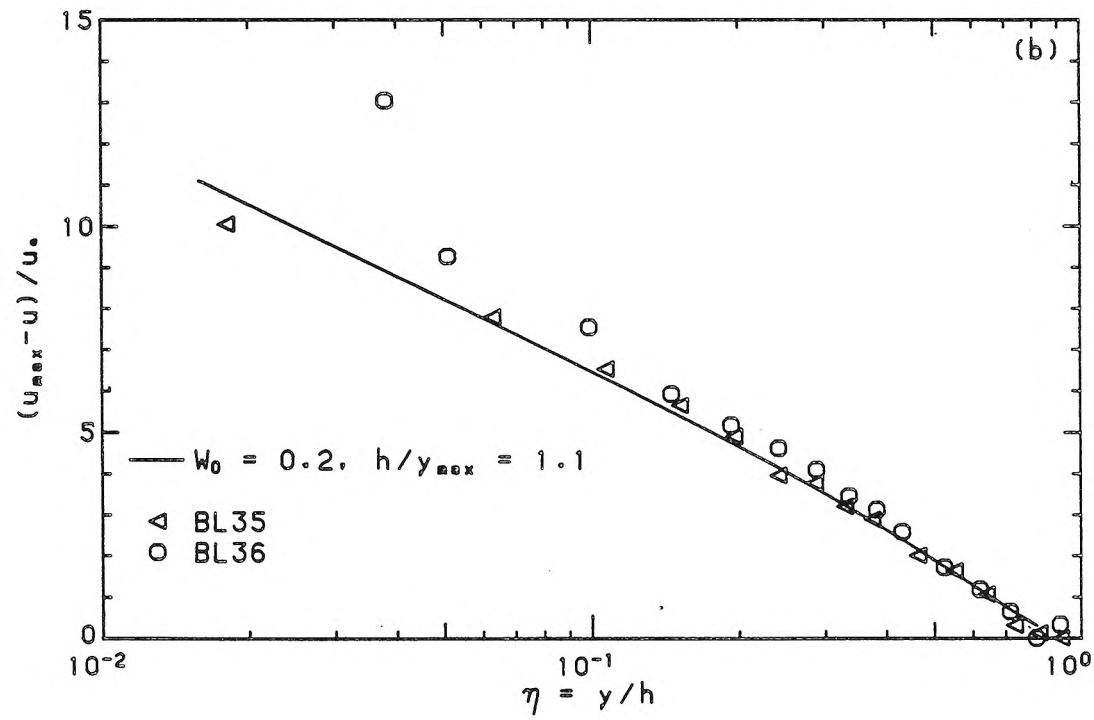

Fig. 6.1.14 Concentration results of Barton and Lin (1955)
a) all experiments examined, b) comparison with traditional fits

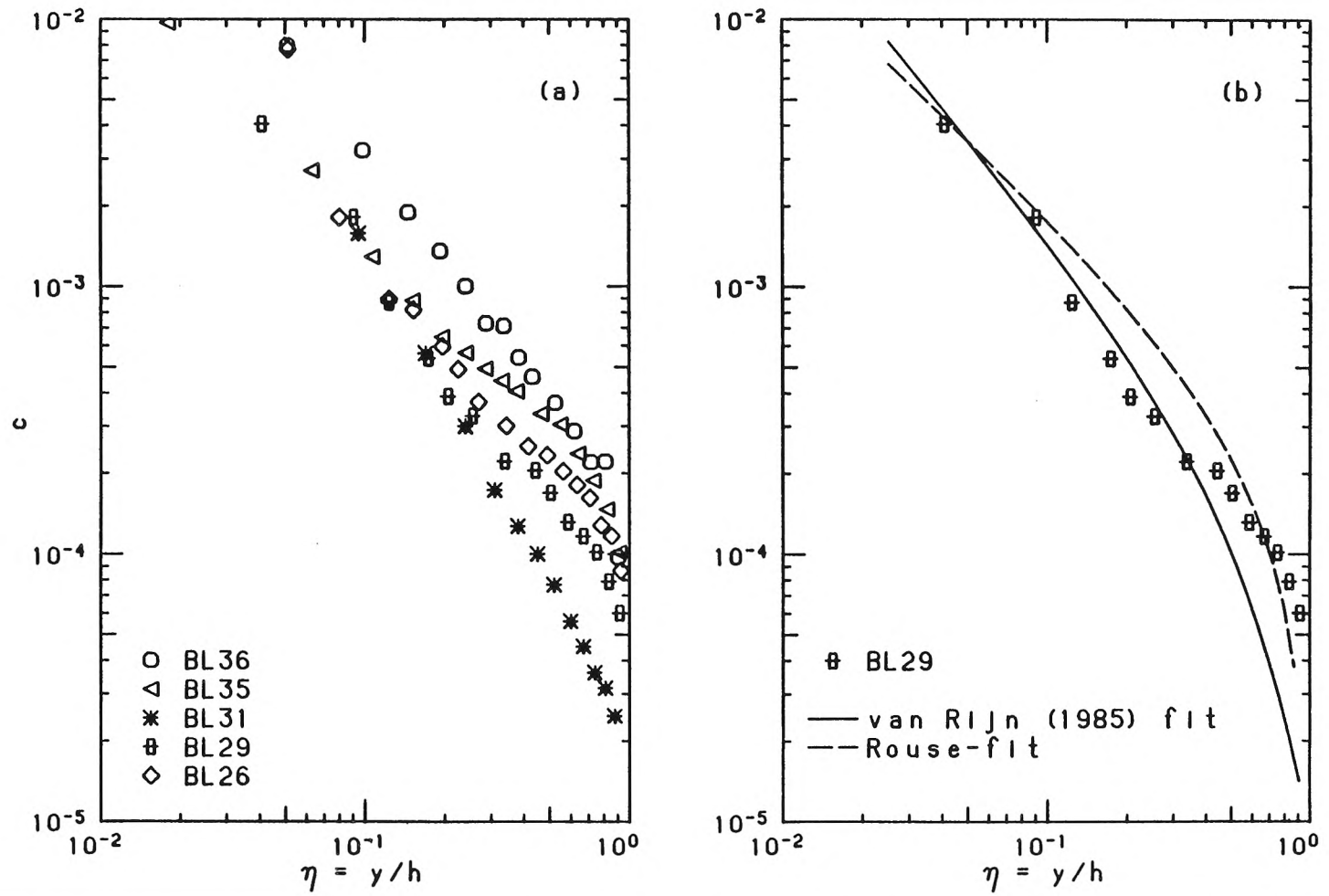

is genuine, then the inadequacy of the traditional model would be brought out in Fig. 6.1.14b, where both the modified suspended-load profile proposed by van Rijn (1984) and the traditional Rouse (1937) profile, using a reference level at $\eta = 0.05$, are compared to the results of BL29, and are seen to be erroneous.

The final data set to be considered, that of Guy et al. (1966), is plotted in Fig. 6.1.15. In GUY26, there is again evidence of a distinct inner region, although some caution in interpretation is necessary, since the lowest measurement was made very close to the bed. The large value of $w_{s0}/u_* = 0.93$ for GUY26 implies that there is little sediment in suspension, which may explain the extremely limited extent of this affected region. In GUY15 and GUY46, the effects of sediment are seen to be much more extreme. On the other hand, GUY25, like BL35, gives no indication of any effect of the suspension on the velocity-defect profile. The marked difference in the results for GUY46 and GUY25, which were performed under very similar conditions, should be noted. Unfortunately, no point concentration measurements were made, so that it cannot be ascertained whether analogous features in the concentration profiles could be found.

6.1.5 Discussion: Mean profiles in equilibrium-bed experiments

The velocity profile in equilibrium-bed flows has been seen to exhibit significant deviations from clear-water profiles both in our own results obtained with an LDV system, and in previous work obtained with the Pitot tube. Near the bed, velocity defects and velocity gradients were found to be larger than in clear-water flows. The extent of the region where significant deviations were observed varied widely. In the range of laboratory conditions investigated, the extent of the affected region is small relative to the depth of flow. Beyond this region, the shape of the velocity-defect profile is largely unaffected by the presence of sediment.

Fig. 6.1.15 Velocity results from Guy et al. (1966)
a) GUY26, GUY15, b) GUY46, GUY25

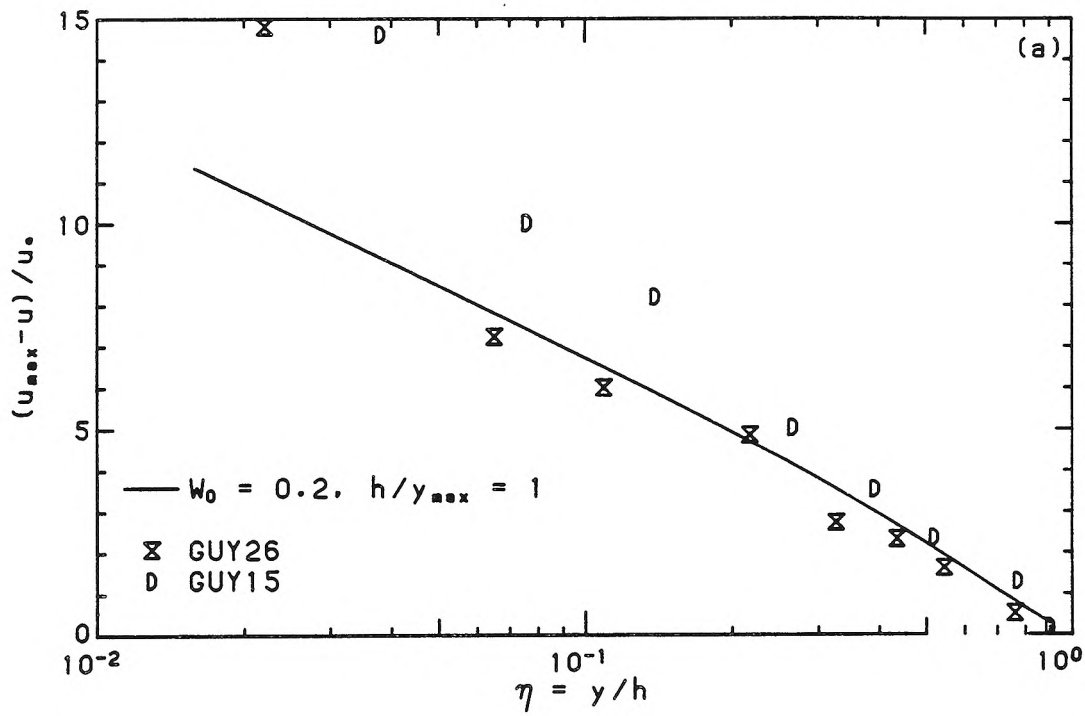

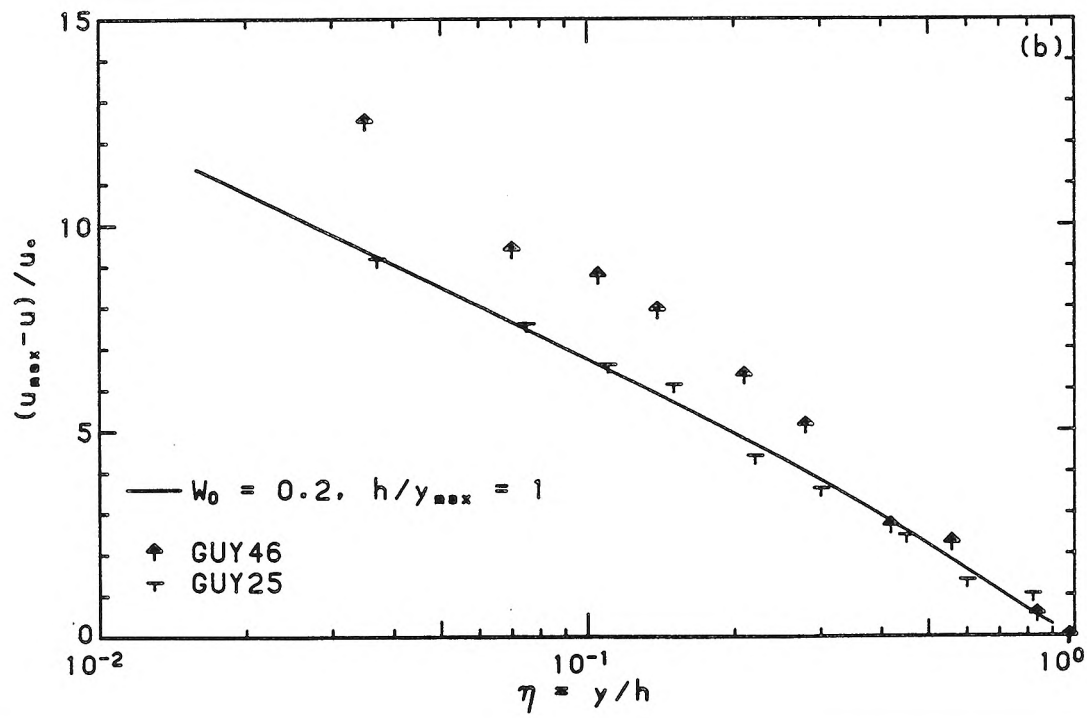

The lack of a natural reference to which concentration profiles can be compared, such as is afforded by the clear-water reference in the case of the velocity profile, leads to less definite conclusions about the concentration field. A power-law variation near the bed with an exponent that varies with hydraulic and grain parameters seems a plausible description. A deviation from this power-law in the upper flow is evident. The evidence of a deviation from the power-law in the near-bed region is mixed, with only a single data set supporting such a deviation.

The experimental evidence in the case of the velocity field does not support the views of previous models. According to the traditional model, the effects of sediment are felt throughout the flow, and the velocity profile is described by a log law with a reduced von Kàrman constant, κ_s. This does not apply to the majority of the experimental results examined, particularly our own. The smaller value of κ_s (compared to κ) reflects averaging not only over the larger velocity gradients in the wake component, as Coleman (1981) pointed out, but also over the larger velocity gradients in a region near the bed. Some cases *have* been observed where the effects of sediment are felt throughout the flow. Whether the traditional model without modification can be justified for such cases is open to question. It may be argued that a wake component reflecting the effect of the free surface should still be observed. Whether a variable κ_s may be usefully combined with a wake component to describe flows in which the effects of sediment are "global" remains an open question.

The more recent models (Itakura and Kishi, 1980; Coleman, 1981) fare no better. Not only is the greatest effect not seen in the upper flow, the velocity gradient in the near-bed region where measurements could be made was found to

be larger than in clear-water flows. The implicit assumption of a simple Monin-Oboukhov model that the effects of stratification are weak at the bed and gain in relative importance with distance from the bed is seen to be invalid for general sediment-laden flows in open channels. Under special conditions when the local buoyancy flux everywhere decays as or more slowly than the local production of turbulent kinetic energy; i.e.,

$$\frac{d}{dy}\left[\frac{g(s-1)w_s c}{u_*^2(1-y/h)du/dy}\right] \geq 0 \tag{6.3.1}$$

(which is an adaptation of the Barenblatt (1979) criterion for the existence of self-similar solutions), such an assumption may be more appropriate. Even then, other independent restrictions, e.g., on relative grain size, may apply.

If the behavior of the outer flow is not explained by simple stratified-flow models, can the marked effects that *were* observed in the mean-velocity profile in the near-bed region still be explained by buoyancy effects? In the near-bed region, the local "buoyancy flux", $g(s-1)w_s c$, may be quite significant relative to the rate of turbulent kinetic energy production. If issues such as the importance of non-diluteness and non-Boussinesq effects are ignored, then a possible model may posit an inner layer that is moderately stable and an outer layer that is neutrally stable. How such a modified stratified-flow analogy could be consistent with the experimental results on mean-velocity profiles in the outer flow is difficult to see. The stable inner layer would act to inhibit vertical transport in the region of the wall, which is the dominant source of turbulence production. The outer flow, which benefits from this large-scale transport in the absence of stratification, must then adjust to the reduced transport, e.g., by increasing the velocity gradient. It seems unlikely that the outer flow would be unaffected. The large buoyancy flux

may then be illusory in that it implicitly assumes a continuum model which, in turn, depends on other parameters such as the grain size.

On the other hand, some of the hypotheses made in the basic similarity model of Chap. 3 are seen to be physically sound. An inner region to which the effects of sediment are largely confined was found. The extent of this region does not scale with d_{50}. This is seen, e.g., in Fig. 6.1.9, where the extent of the affected region is noticeably larger in 1565EQ than in 1965EQ, although d_{50} is smaller. The results of Barton and Lin (1955), all obtained with a single sand-size, also show that a large variety of profiles may be obtained for the same d_{50}. That the extent does not scale with l_ν is less clearly seen. The large scatter near the bed in the velocity profiles, plotted in viscous coordinates (Fig. 6.1.5a), may be cited, as well as the large values of $y^+ \equiv y/l_\nu$ (ranging from 200–900) at which an effect due to sediment may be observed. That an approximate log-law with $\kappa \approx 0.4$ is possible, not in the near-bed region as suggested by the simple stratified-flow analogies but in an intermediate region, has also been seen. It was also found that the wake component may remain unaffected, even though the near-bed region is significantly affected. These qualitative results are all consistent with the similarity hypotheses of Chap. 3. As a more general model, the similarity approach further allows the possibility that the extent of the inner region may grow such that the affected region encompasses practically the entire flow region.

In some respects, both the proposed similarity model and the previous models agree qualitatively about the concentration profile. All are consistent with a power-law variation near the bed. While they differ in detail, all implicitly or explicitly recognize a wake component in the concentration profile. The proposed model is somewhat more flexible in having an additional fitting parameter, which

leads to noticeably better fits in the upper flow. Unlike previous models, it would be expected, from the similarity model, that a deviation from the power law in the near-bed region would parallel the observed deviation from the log law in the velocity profile. As remarked above, the experimental evidence in this regard is mixed.

6.2 Starved-bed experiments

Table 6.2.1 Conditions† for starved-bed experiments

Expt.	h (cm)	u_* (cm/s)	S $(\times 10^{-3})$	$c(\eta = 0.1)$ $(\times 10^{-3})$
1965ST	6.58	3.57	2.49	1.28
1957ST-1:A	5.69	3.74	2.99	0.57
1957ST-1:B	5.68	3.69	2.98	0.25
1957ST-2:A	5.84	4.25	4.00	2.08
1957ST-2:B	5.77	4.31	3.95	0.79
1957ST-2:C	5.75	4.28	4.00	0.47
1957ST-2:D	5.74	4.34	4.00	0.31

† see Appendix A.2 for additional information

The conditions in the starved-bed experiments are listed in Table 6.2.1. The experiments were done in two series (three, if 1965ST alone is considered a series) in which all conditions were kept constant, except for the local concentration, which was changed by the addition of sediment to the flow. All but one of the experiments were performed at the smaller aspect-ratio. The alphabetic suffix to the label indicates the relative saturation, with the concentration decreasing in

alphabetical order, e.g., 1957ST-2:A has the largest suspended load of the series, 1957ST-2.

All experiments were performed with the 0.19 mm sand, and, where an equilibrium-bed experiment had been previously performed, the conditions for starved-bed experiments were chosen to approximate the equilibrium-bed conditions. Care should be taken, however, in associating the actual equilibrium-bed experiment performed with that which would have resulted from a saturation of the starved-bed experiments. Because the appropriate scaling is unknown, small differences in experimental conditions, particularly in the shear velocity, make precise comparisons difficult. In the lower-transport series, 1965ST and 1957ST-1, small ripples, oblique to and extending $\leq$ 5cm into the flow, were formed at the sides of the flume, similar to those that were observed in the equilibrium-bed experiments although somewhat more random. No sign of permanent deposition was, however, observed on the centerline in the vicinity of the working area. In the high-transport series, 1957ST-2, no such ripples were apparent along the length of the flume. The temperature during all runs was $21.3 \pm 0.3°C$.

6.2.1 Mean profiles in starved-bed experiments

The normalized stress measurements for the starved-bed experiments are shown in Fig. 6.2.1. Although some scatter is again evident, there is little difference from the results for clear-water or for equilibrium-bed experiments.

Velocity-defect profiles are compared to the clear-water reference in Fig. 6.2.2, and, where available, to equilibrium-bed results. Deviations from the clear-water reference are seen to be most pronounced near the bed, while the outer-flow region seems largely unaffected. This latter point is dramatically seen in Fig. 6.2.2b, where the profiles are practically identical from the free surface to below $\eta = 0.2$

Fig. 6.2.1 Normalized Reynolds-stress profiles:
a) series 1965ST and 1957ST-1, b) 1957ST-2

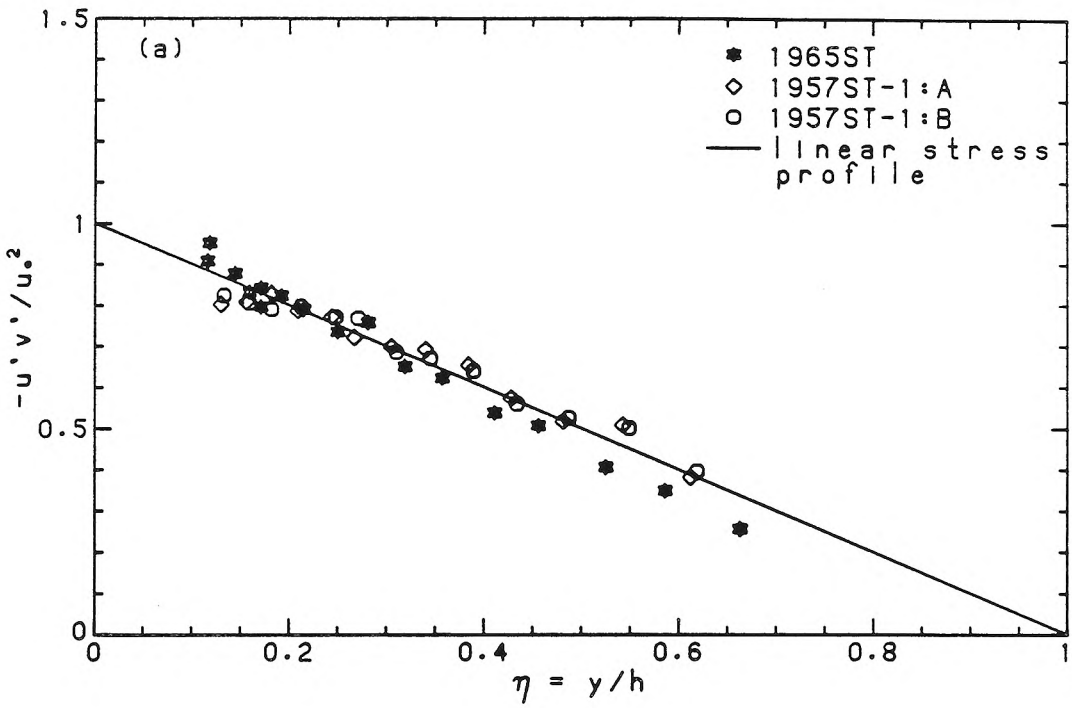

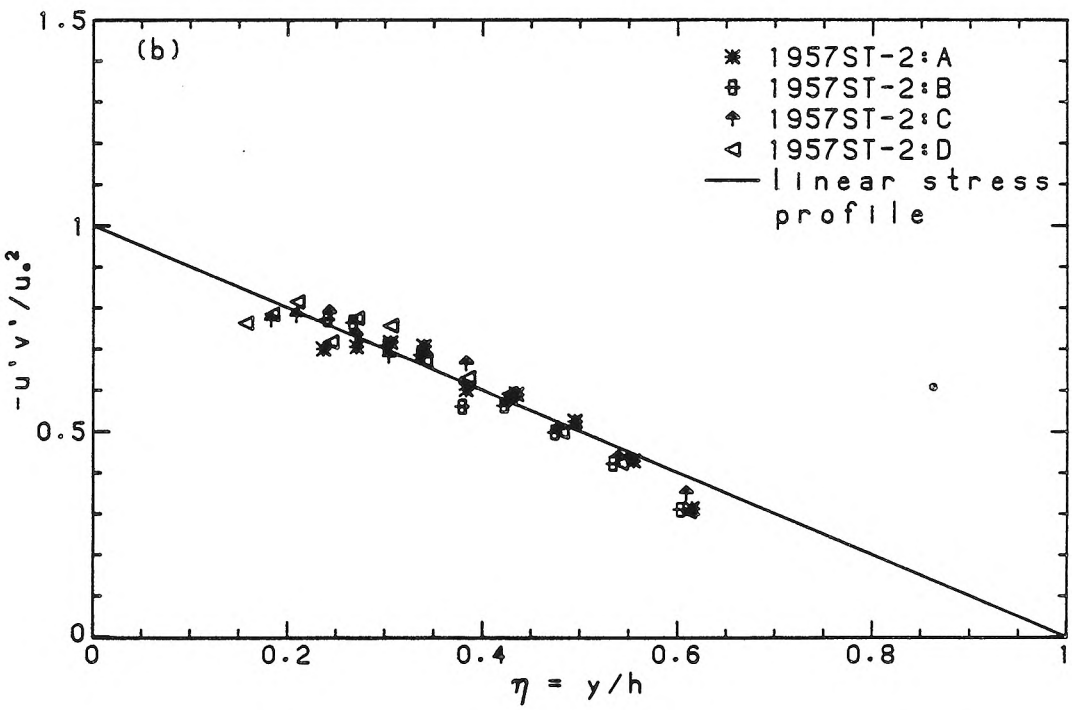

Fig. 6.2.2 Velocity-defect profiles for series:
a) 1965ST, b) 1957ST-1, c) 1957ST-2

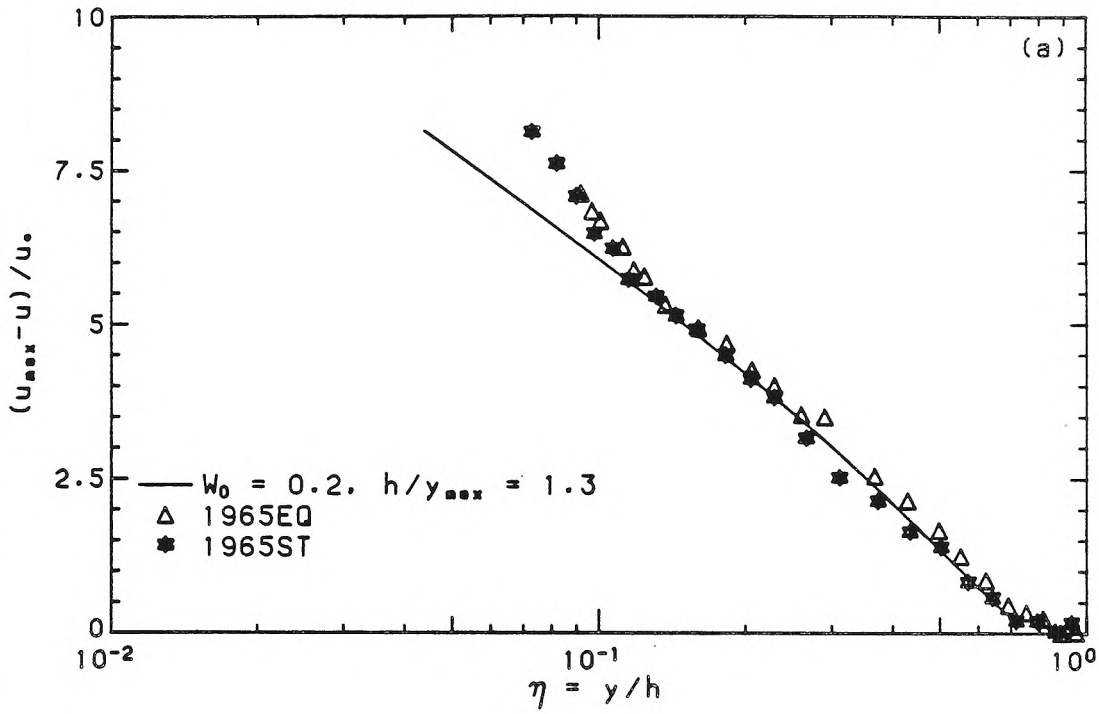

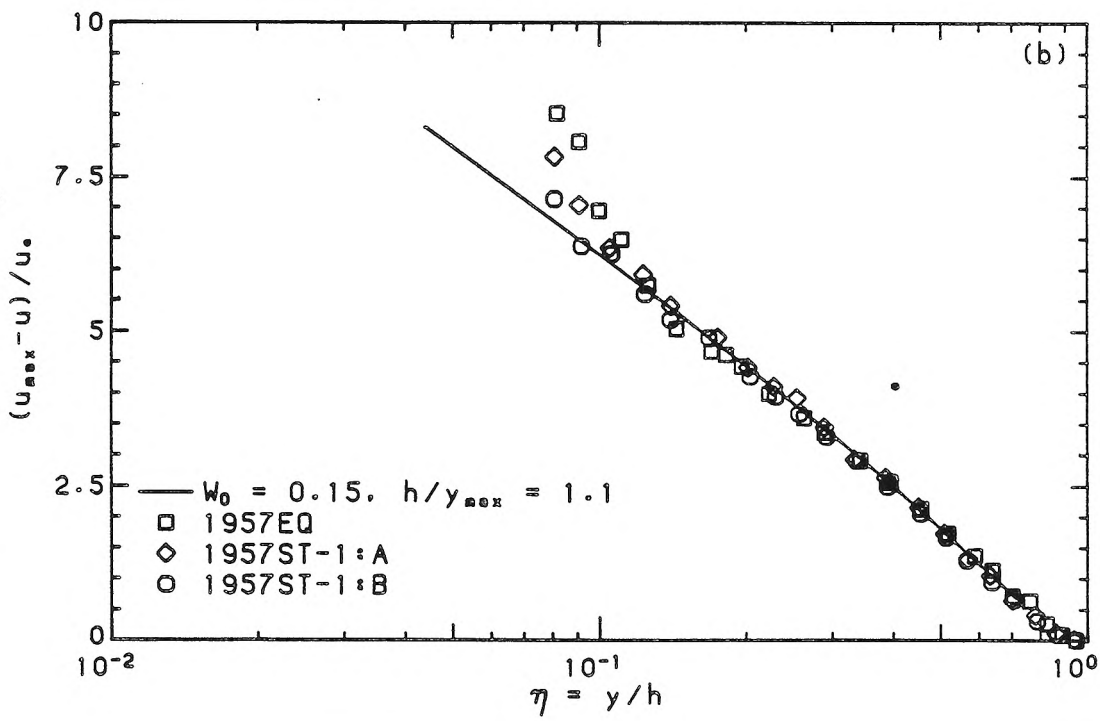

for the starved-bed as well as for the equilibrium-bed experiments and the clear-water reference. An intermediate, approximately log region with $\kappa = 0.4$ may also be discerned. As the local concentration is increased, two related effects may be distinguished; i) the extent of the affected region and ii) the magnitude of the deviation grow. In the affected region, the starved-bed results are bounded below by the clear-water reference and above by the "associated" equilibrium-bed results. A trend is noted from the clear-water to the equilibrium-bed results with increasing sediment concentration.

Fig. 6.2.2c

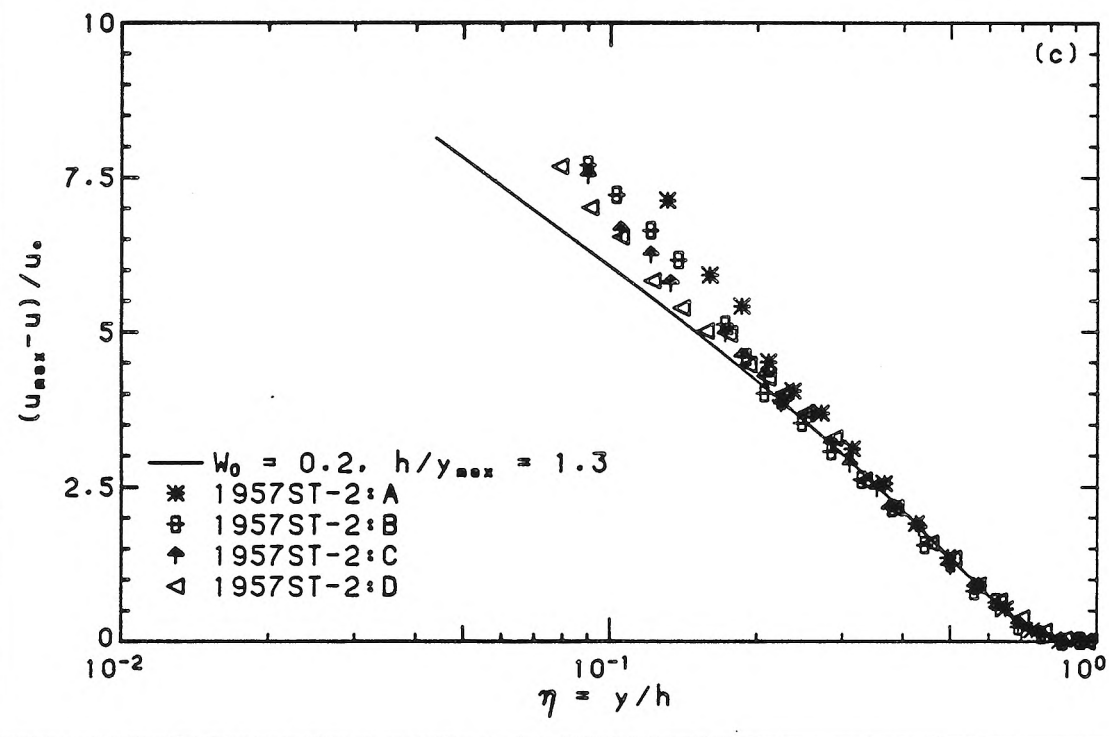

The corresponding concentration profiles are given in Fig. 6.2.3. The discussion of concentration profiles is complicated because, unlike the case of the

Fig. 6.2.3 Concentration profiles for starved-bed experiments

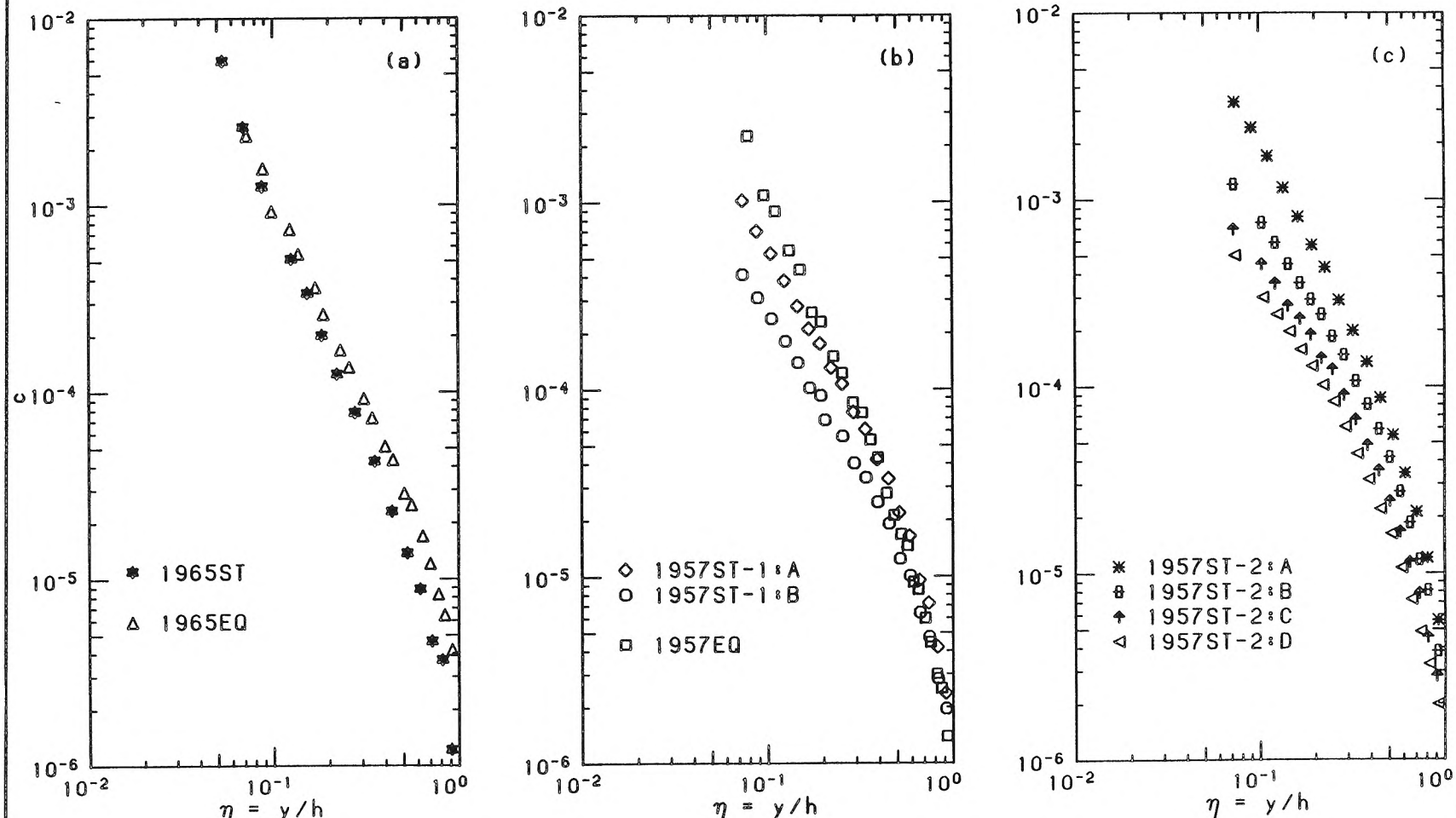

velocity field where the appropriate scaling, u_*, is known, the scaling of the concentration is not known. Thus, different experiments under different conditions are not directly comparable. The effect of slight differences, 5-10%, in u_* between starved-bed and equilibrium-bed experiments, which would result in 10-20% difference in shear, should be kept in mind.

The concentration in the near-bed region for 1965ST differs little from 1965EQ (even though the latter is characterized by a slightly higher u_*) and indicates a near-equilibrium state. This is also supported by the velocity-defect result which show a near-coincidence of starved-bed and equilibrium-bed profiles. In the upper region, however, there remain significant differences in the concentration profiles, which may be attributed, at least in part, to the slight difference in u_*. The profiles of the series, 1957ST-1, exhibit no obvious trend regarding the shape of the profile. A comparison with 1957EQ (the u_* of which is estimated to be $\approx 7\%$ larger) indicates a *smaller* concentration in the upper region of the equilibrium-bed experiment. In the lower region, however, concentrations for 1957EQ are larger than for the starved-bed cases, as expected. Even if a significant effect due to the larger u_* in 1957EQ is hypothesized, this would be expected to lead to concentrations uniformly larger than those found in starved-bed cases. The results of the most extensive series, 1957ST-2, exhibit a trend opposite to that observed for 1965ST. A distinct steepening of the profile in the near-bed region is seen to occur in going from 1957ST-2:B to 1957ST-2:A. On the other hand, in the transition from 1957ST-2:D to 1957ST-2:B, little change, if any, is observed in the shape of the near-bed profiles.

Some of the results of Vanoni (1946), whose experiments were conducted under starved-bed conditions, were re-examined. The experiments to be considered

Fig. 6.2.4 Results of Vanoni (1946)

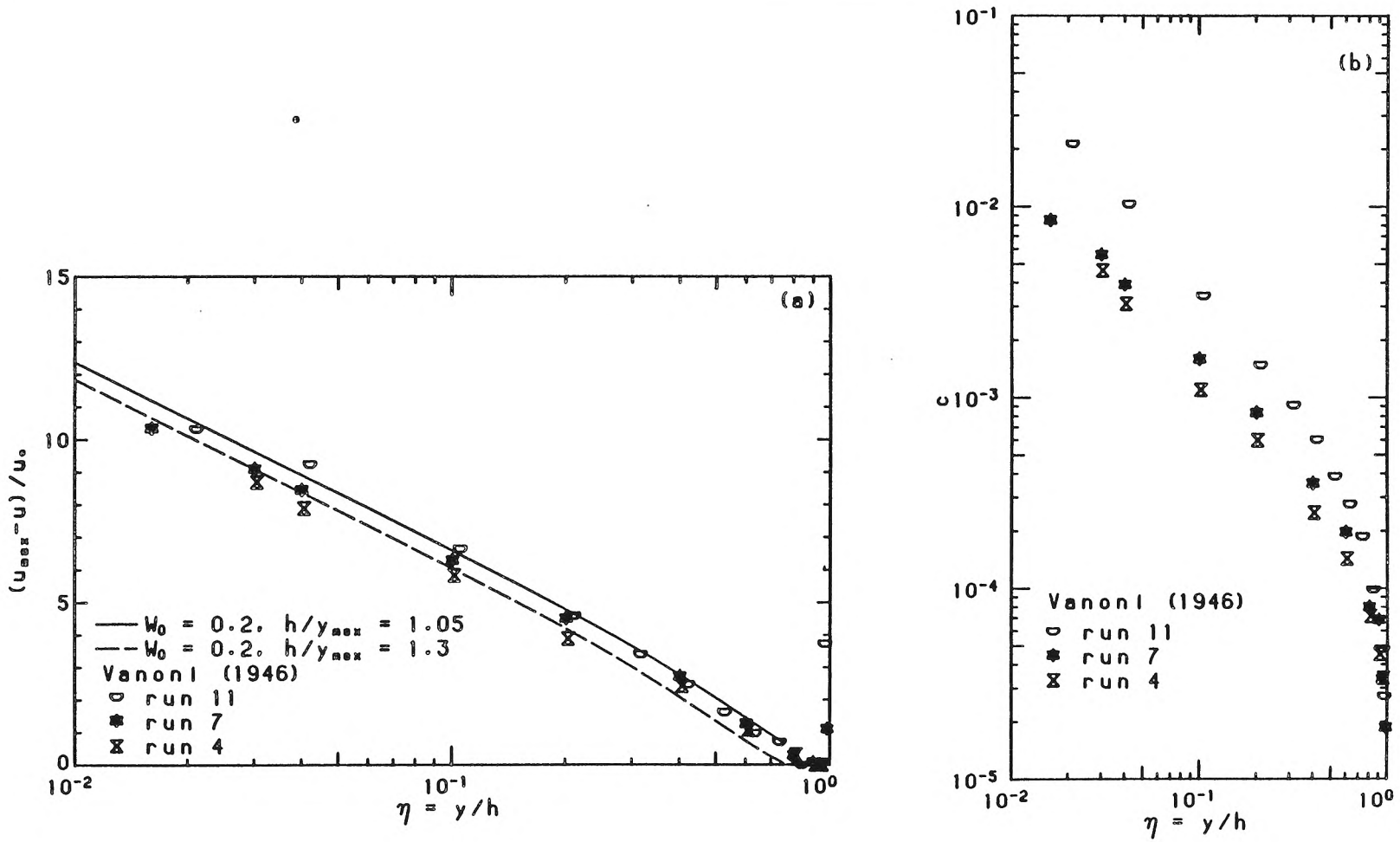

were performed keeping all parameters nearly constant: $h \approx 15$ cm, $S = 0.0025$, $u_* \approx 5.5$ cm/s, and $d_{50} = 0.15$ mm, except for the concentration, which increases from run 4 to run 7 to run 11. An aspect ratio greater than 5 was obtained. The flume bed was artificially roughened with an epoxied layer of ≈ 0.8 mm sand. These runs, then, constitute a series like those of our own experiments. Vanoni was not entirely satisfied with the experimental conditions of these runs because of a disturbed inlet condition. Unfortunately, the later experiments in which this was corrected did not offer any series in which all conditions were kept constant except for the concentration.

Velocity-defect and concentration profiles are shown in Fig. 6.2.4. There is little evidence of any effect on the velocity-defect profile compared to the more dramatic results of our own experiments, even though the local concentrations in the experiments of Vanoni are larger. This behavior is reminiscent of some of the equilibrium-bed results, e.g., BL35, GUY25, discussed previously. The behavior of the concentration profile in going to equilibrium is, again, seen to be complicated. The increase in concentration from run 4 to run 7 leads to a somewhat shallower near-bed profile, while the increase from run 7 to run 11 leads to a steeper profile.

6.2.2 Discussion: Mean profiles in starved-bed experiments

The qualitative effects of the presence of sediment, discussed previously in the examination of equilibrium-bed results, are also found in starved-bed experiments. The remarks concerning the applicability of previous models and the consistency of the similarity model made in the previous discussion remain generally justified for starved-bed flows. The effect of slight departures from the idealized flat-bed condition is seen from the results of the series, 1957ST-2. In that series, no permanent deposition was observed along the length of the flume, which may be considered

as flat as in clear-water experiments. Yet, the measured velocity profiles exhibit the same characteristics found in equilibrium-bed results. These slight departures do not account for the observed effects on the velocity profiles. The approach to equilibrium in the velocity profile proceeds monotonically, as might be expected, from an almost clear-water profile at the lowest concentration to the equilibrium profile. A re-examination of some starved-bed data from Vanoni (1946) showed little effect of sediment, and so resembles some of the equilibrium-bed results from Barton and Lin (1955) and Guy et al. (1966).

At a general level, the concentration profiles in starved-bed experiments exhibit characteristics similar to those in equilibrium-bed flows. Unlike the velocity profile, however, no simple trend was found in the approach to equilibrium, the rate of approach seemingly non-uniform over the depth and probably depending on the distance from equilibrium. With respect then to the concentration field, starved-bed flows seem to present more difficulties in interpretation than equilibrium-bed flows.

6.3 A more specific model

The above discussions of experimental results have been concerned with the qualitative difference between clear-water and sediment-laden flows. Even at this general level, previous models were found inadequate, at least for describing the velocity profile. In contrast, the qualitative evidence is consistent with the basic similarity hypotheses. The more specific physical assumptions make statements concerning length and concentration scales and their correlation with the given physical parameters and are investigated in this section.

6.3.1 Similarity of velocity profiles

As pointed out in §3.4.3, the length scale, l_s, which characterizes the extent of the region affected by the presence of sediment, must be operationally defined in order to determine its relation to given physical parameters. If a distinct inner layer exists, and the corresponding asymptotic log layer can be distinguished, then, by an appropriate choice of a reference velocity, u_s, and l_s, the velocity profiles in the logarithmic layer should collapse onto a line defined by

$$\frac{u_s - u}{u_*} = -\frac{1}{\kappa} \ln \xi_s, \tag{6.3.1}$$

where $\xi_s \equiv y/l_s$.

Table 6.3.1 Parameter values used in collapsing velocity profiles

run id.	l_s (cm)	l_s/h	l_s/d_{50}	l_s/l_ν	u_s (cm/s)
1565EQ	1.3	0.20	87	468	60
1965EQ	0.6	0.092	32	225	54
2565EQ	0.5	0.081	22	223	59
1957EQ	0.6	0.11	33	249	57
BL36	1.4	0.088	79	795	93
BL29	2.2	0.12	122	986	63
BL26	1.8	0.085	99	859	63
GUY26	0.8	0.057	18	568	85

By an admittedly crude trial-and-error procedure, the parameters, l_s and u_s, were determined so as to obtain a somewhat subjective good collapse of the data. The values of u_s and l_s obtained, as well as some dimensionless ratios involving l_s,

Fig. 6.3.1 Velocity profiles of equilibrium-bed experiments, (l_s as length scale): a) present results, b) previous results

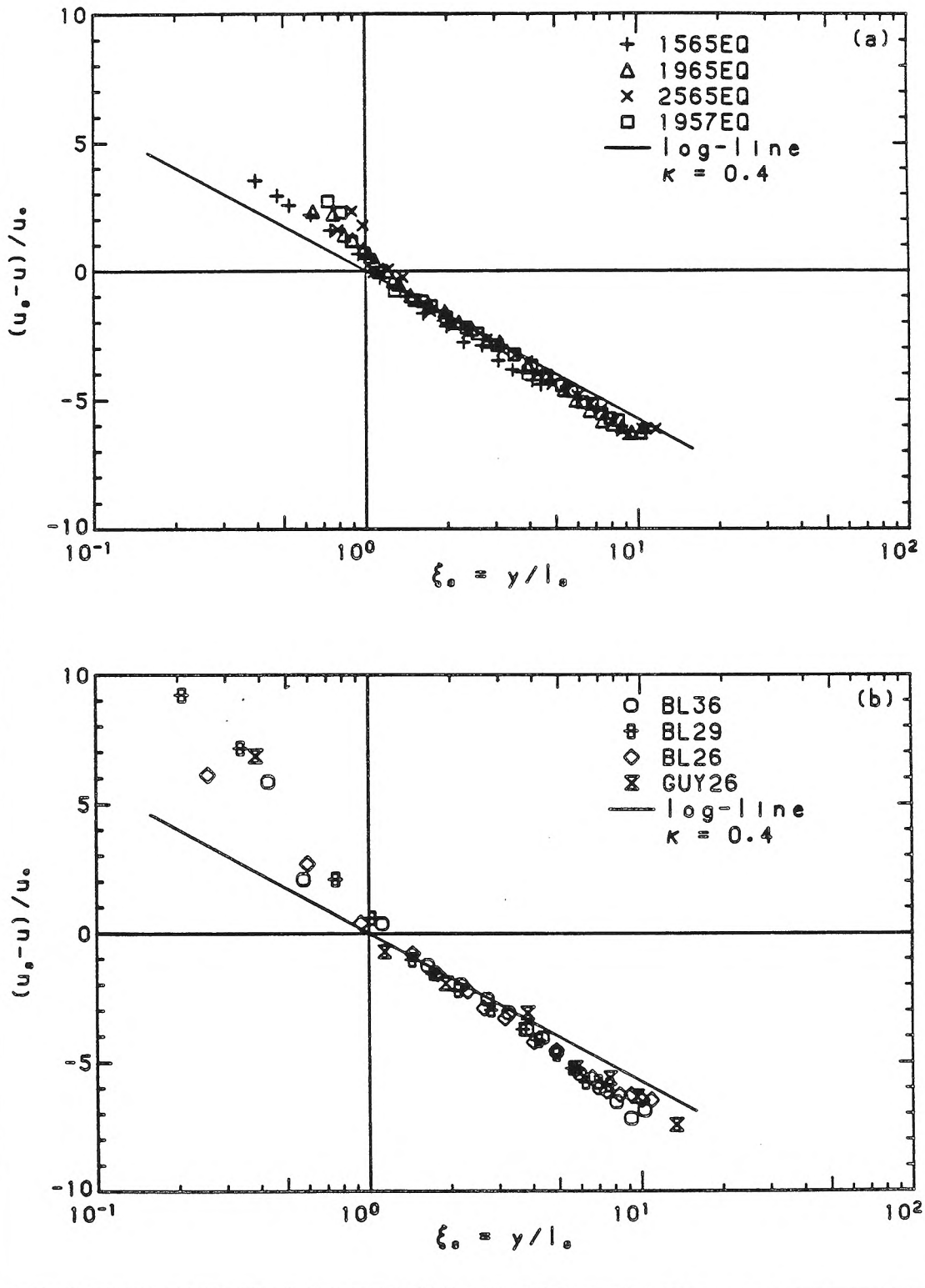

are given in Table 6.3.1. The results of this procedure for those equilibrium-bed results which exhibit a distinct inner layer, are shown in Fig. 6.3.1. The deviation from the logarithmic line for $\xi_s < 1$ is clear in both our data as well as in those of others. Similarly, the deviation as $\xi_s > 1$, $\eta \to 1$, due to the wake component, is also clearly seen.

Fig. 6.3.2 Velocity-defect profiles in which no inner layer was discerned

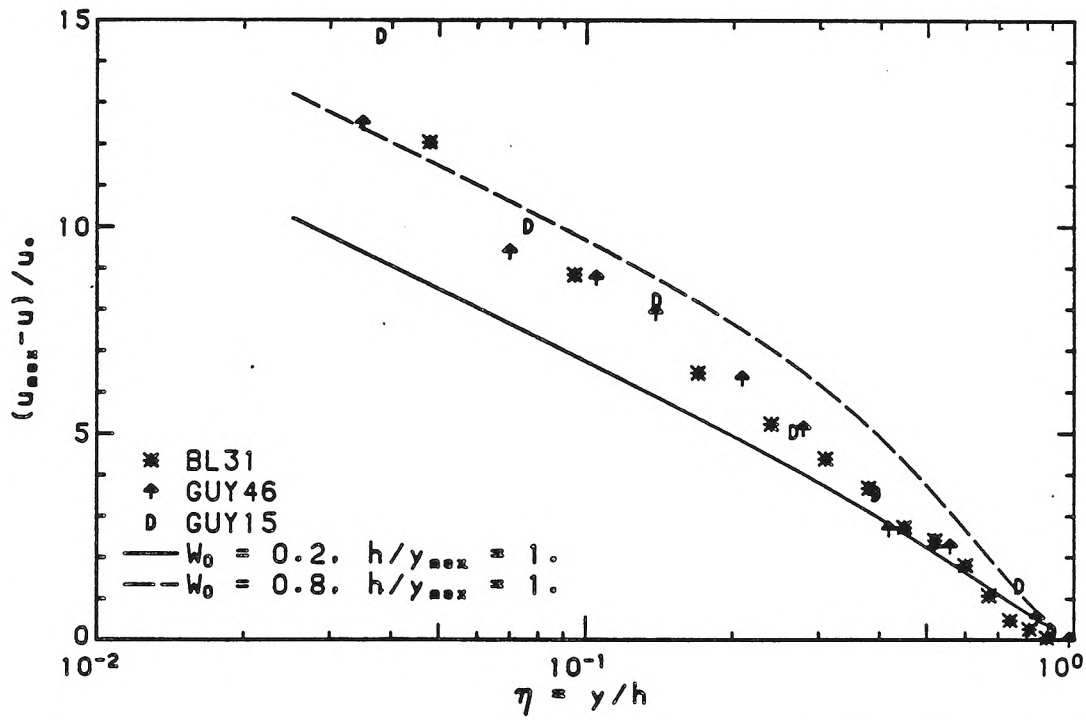

The velocity-defect profiles of those experiments in which the inner scale, l_s, is interpreted to have grown so large as to merge with the outer scale are plotted in Fig. 6.3.2. The good collapse of the data, particularly in the range, $\eta \geq 0.1$, suggests that an asymptotic similarity might also obtain in such cases where the sediment-laden flow profiles deviates *maximally* from the clear-water profile. Such a similarity may be explained in that it is physically unreasonable to expect that

the deviations from the clear-water profile should increase without bound. This was also suggested implicitly by Coleman (1981) in his wake-law approach, in which the wake coefficient was found to approach a maximum value of ≈ 0.8 (compared to the clear-water value of ≈ 0.2). In these cases where $l_s \sim h$ and the effects of the suspension are observed in the outer flow, it might be argued that the wake-function approach would be more appropriate. Wake-law profiles based on the wake function of Coles with $W_0 = 0.2$ and 0.8 (using $\kappa = 0.4$) are also plotted and seem an inadequate description of the profile. Although not shown, a better fit may be obtained by using a variable κ_s (≈ 0.25) and a wake component with $W_0 = 0.2$.

The inner scale, l_s, for each experiment, which resulted in Fig. 6.3.1, in its non-dimensional form, $\Delta_s \equiv [g(s-1)l_s]/u_*^2$, is plotted against w_{s0}/u_*, in Fig. 6.3.3. A point corresponding to the starved-bed experiment, 1957ST-2:A, is also plotted. It should be emphasized that the estimates of l_s, so crudely obtained, may be in error by 10%-20%. Keeping this and the limited data available in mind, we find a promising correlation between Δ_s and w_{s0}/u_*. Δ_s is seen to be very sensitive to changes in w_{s0}/u_*, changing by an order of magnitude from $w_{s0}/u_* = 0.93$ to $w_{s0}/u_* = 0.45$. Although Δ_s decreases as w_{s0}/u_* increases for $w_{s0}/u_* > 0.5$, as might be intuitively expected, the results of Barton and Lin (1955) suggest that, below $w_{s0}/u_* = 0.5$, Δ_s may actually increase as w_{s0}/u_* increases. Such behavior may, perhaps, be rationalized on the grounds that, for smaller w_{s0}/u_*, the suspended sediment may be less efficient at affecting large scale motions. Thus, at large values of w_{s0}/u_*, there is little sediment in suspension and the effect on the velocity profile is negligible. For small w_{s0}/u_*, the sand grains essentially follow the large-scale motions without slip and therefore do not

influence these motions. It may be speculated that an optimum value of w_{s0}/u_* (perhaps $\approx 0.4 - 0.5$ if the peak in Fig. 6.3.1 is significant) may exist in the sense of maximizing the effect on the velocity profile. It is intriguing to note that this "peak" occurs where $w_{s0}/\kappa u_* \approx 1$, which is the Barenblatt (1979) criterion for self-similar solutions based on a stratified-flow analogy. Nevertheless, since the only direct evidence of this "peak" is to be found in a single data set, it should be viewed with some caution.

To the extent that Δ_s is well correlated with w_{s0}/u_* alone, the effect of the grain diameter seems negligible. This may be explained by the relatively large magnitude of l_s/d_{50}, which is greater than 20 in all cases except for GUY26, where it is ≈ 12. The magnitude of l_s as determined from this procedure should not be interpreted in a manner analogous to the viscous sublayer. The latter is typically considered taken, in homogeneous flows, to be $y < 5l_\nu$, even though the effects of viscosity are noticeable (in the deviation from the log law) up to $y \approx 60l_\nu$. If an analogy to scales in homogeneous flows is to be made, the region bounded by l_s may be considered as analogous to the buffer layer between the viscous sublayer and the log layer.

A useful correlation should give some indication of regions in which it is inapplicable. The correlation given in Fig. 6.3.3 is mainly concerned with those cases where a distinct inner layer can be found. Does it say anything of those cases where such an inner layer is not seen, either because the effect of sediment is felt throughout the layer or because there is no evident effect? In the experiments, BL31 and GUY15, with similar values of w_{s0}/u_* (0.52 and 0.48), the velocity-defect profiles were noticeably affected throughout the flow. These would still be consistent with the correlation in Fig. 6.3.3, which show a peak at $w_{s0}/u_* \approx 0.5$.

Fig. 6.3.3 Correlation of Δ_s with w_{s0}/u_*

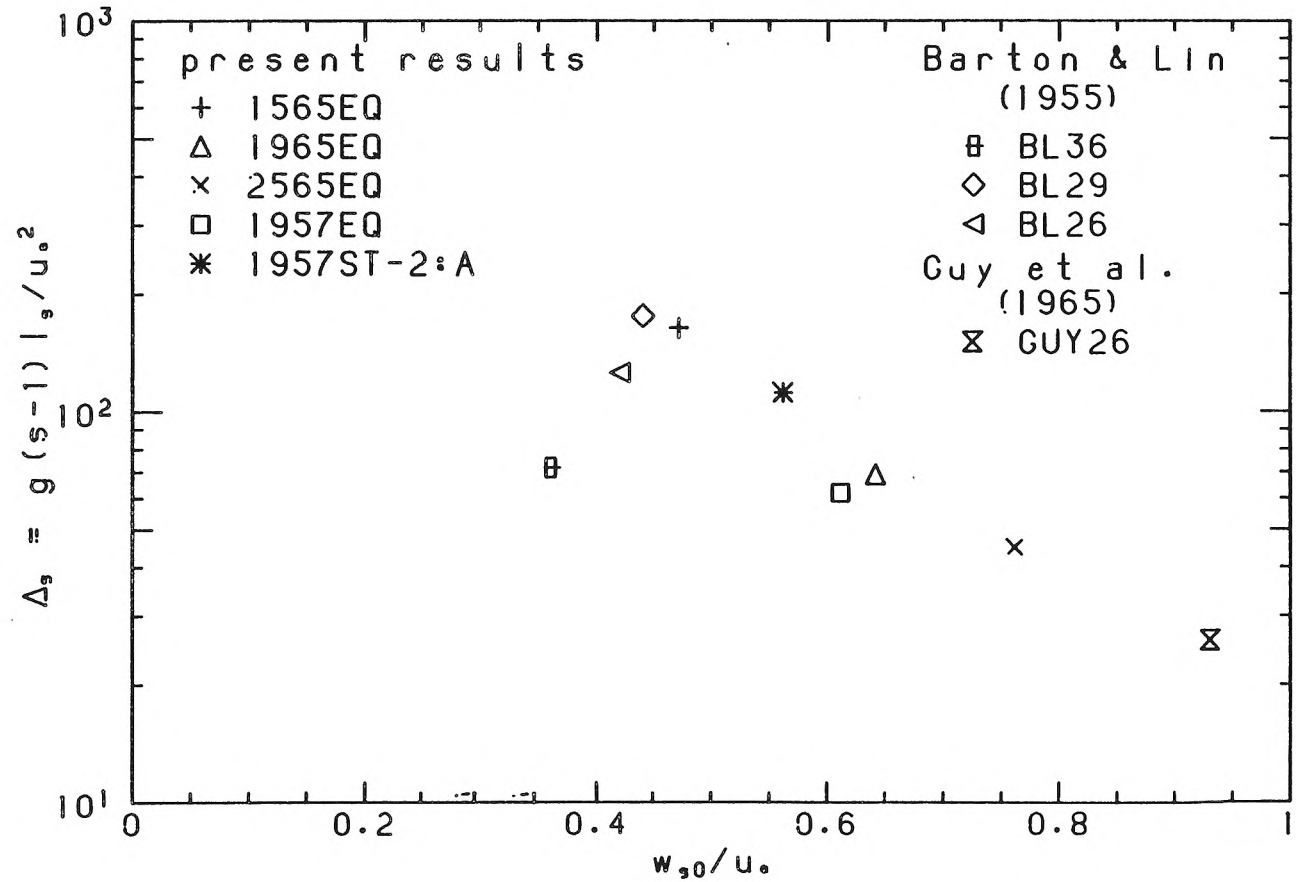

On the other hand, the case of GUY46 ($w_{s0}/u_* = 0.63$), which also was similarly affected, does not fit neatly into this scheme. Those cases, in which no effect of the suspension is evident, namely, BL35 and GUY25, also do not fit into this scheme. While it may be argued that the results for BL35 may be in error, as has been previously discussed (§6.1.4) it is not clear why the results of GUY25 should be discounted. What is puzzling is the similarity of experimental conditions in GUY46 and GUY25 and the remarkable dissimilarity in the velocity-defect profiles. Whether these anomalies may all be attributed to the influence of the omitted dimensionless parameter, $g(s-1)d_{50}/w_{s0}^2$, is debatable. In the case of BL35, for example, this parameter is the same as in all the other experiments of Barton and Lin (1955) since only a single sand size was used. This also applies to GUY46 and GUY25; the sand used in GUY46 was obtained from the sand used in GUY25 by excluding the largest size fraction (thereby also reducing the σ_g). The scarcity of data precludes, however, a more definite conclusion regarding the possible importance of $g(s-1)d_{50}/w_{s0}^2$.

Another area, subject to speculation, is the behavior of the correlation for still smaller values of w_{s0}/u_*, e.g., $w_{s0}/u_* \leq 0.3$. The results of Brooks (1954) (BRK21 and BRK29), with $w_{s0}/u_* \approx 0.25$, suggest that Δ_s becomes large at lower values. In contrast, the starved-bed experiment of Vanoni (1946) closest to saturation, run 11 ($w_{s0}/u_* = 0.31$ and concentrations comparable to Brooks') showed little effect in the velocity-defect profiles. These results of Vanoni would be consistent with the trend of decreasing Δ_s for decreasing w_{s0}/u_* observed in the results of Barton and Lin (1955). The results of Brooks would then suggest that, at still smaller w_{s0}/u_*, this trend may be reversed.

In order to predict the absolute velocity profile rather than just the shape, it would be necessary to obtain a correlation for u_s or u_s/u_*. This will depend, as in the case of homogeneous flows, on a Reynolds number, a roughness parameter, as well as on w_{s0}/u_*. As such, a much larger data set would be required to give any useful result, and so no attempt was made to determine such a correlation.

6.3.2 A generalized similarity of concentration profiles

A simple two-parameter rescaling, such as that used to collapse the data on velocity-defect profiles, is inadequate for analysing concentration profiles. Concentration profiles differ from each other, not only in scale but also in shape. To what extent would a three-parameter transformation be useful in collapsing data on concentration profiles? In Chap. 3, the parameter, $Z = Z(w_{s0}/u_*)$, was introduced, in addition to a length scale, l_s, and a concentration scale, c_s. The similarity model hypothesized that the length scale, previously found to be important in the description of the velocity profile, is also important for the concentration profile. With l_s determined from analysis of the velocity profile, the treatment of the concentration profile is considerably simplified. In this regard, Z may be thought of as an analogue of u_* in its role of scaling not the concentration but the logarithm of the concentration, as the form of Eqn. 3.4.19 was meant to suggest. Because l_s largely determines c_s, in that $c(y = l_s) \approx c_s$, only the parameter, Z, remains to be specified. This was done following a procedure similar to that which was previously used for the velocity profiles. The concentration profiles for $\xi_s \gg 1$, $\eta \ll 1$ (interpreted here rather loosely) was required to collapse to a line defined by

$$\frac{\log c - \log c_s}{Z} = -\log \xi_s. \tag{6.3.2}$$

The results of this procedure for our data and those of Barton and Lin (1955) are shown in Fig. 6.3.4. The deviation from the -1 power line as the free surface is approached is clear and reminiscent of the wake component of the velocity profile. From our own data, the behavior of what might be called the log-concentration excess is ambiguous for $\xi_s < 1$. Except for 1957ST-2:A, the magnitudes tend to be slightly larger than those that would be predicted by the -1 power line. It should be recalled, though, that 1957ST-2:A is not strictly an equilibrium-bed case. Nevertheless, the deviations from the -1 power-law line for $\xi_s < 1$ are not striking in our data. The situation is, however, significantly different in the data of Barton and Lin. There, the deviations below $\xi_s = 1$ are more dramatic and indicate a larger log-concentration excess than predicted by the -1 power line. This evidence also gives some support to the hypothesis that l_s, as determined from the velocity profile, is also important for the concentration profile. Since this is the only data set that shows such marked deviation, these results should be regarded with some caution.

In the asymptotic case when l_s is independent of d_{50}, then the concentration scale, c_s, should depend solely on w_{s0}/u_*. It has been argued that Δ_s, where it is well-defined, correlates well with w_{s0}/u_* for the range of experimental conditions investigated and does not seem as sensitive to variations in d_{50}. A plot of c_s against w_{s0}/u_* is shown in Fig. 6.3.5. Keeping in mind the limited data and the crudeness of the estimates of l_s, we find a fair correlation between c_s and w_{s0}/u_* that is largely a reflection of the correlation for Δ_s. Thus, the dip at $w_{s0}/u_* = 0.5$ stems from the peak found there in the correlation for Δ_s.

The correlation for Z with w_{s0}/u_*, shown in Fig. 6.3.6, is more problematic. For the most part, Z is seen to decrease with decreasing w_{s0}/u_*, as intuitively

Fig. 6.3.4 Similarity plot of concentration profiles
a) present results, b) results of Barton and Lin (1955)

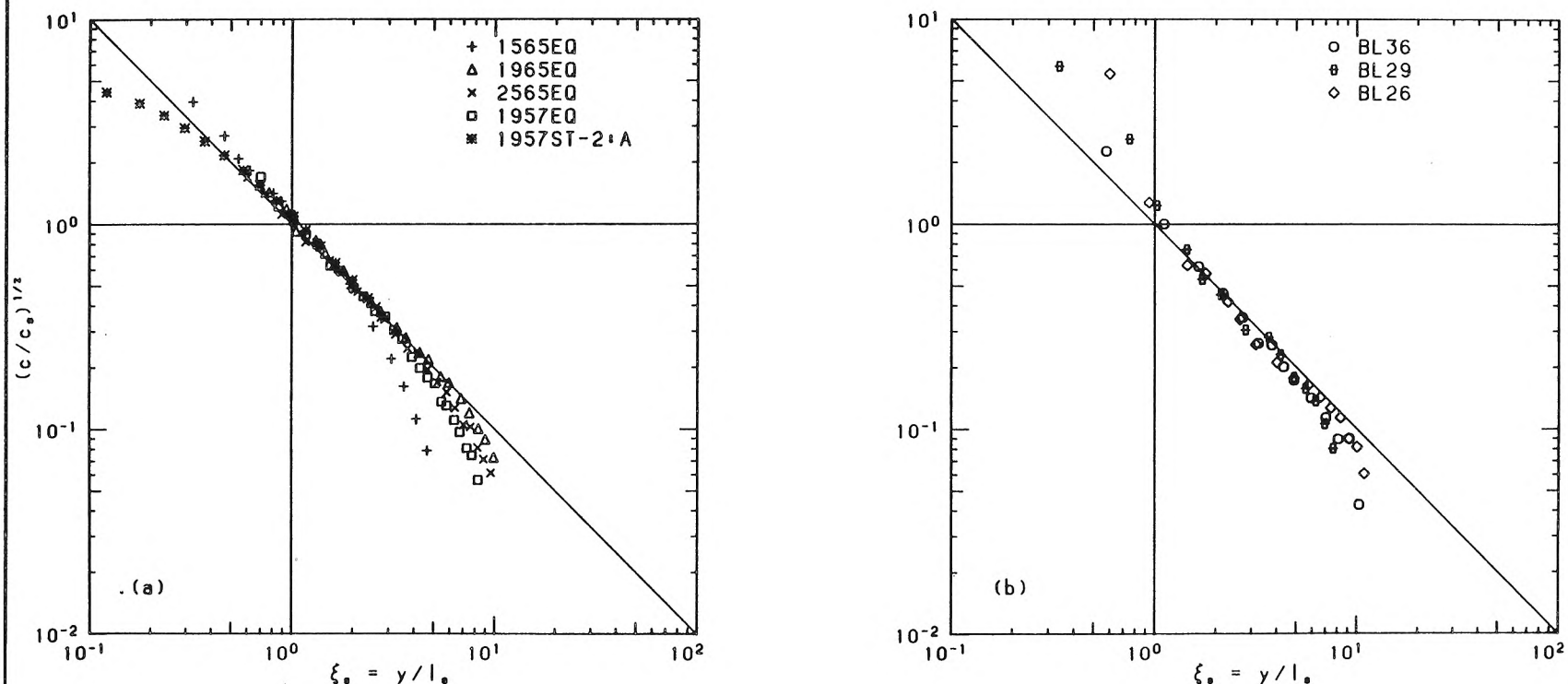

Fig. 6.3.5 Correlation of c_s with w_{s0}/u_*

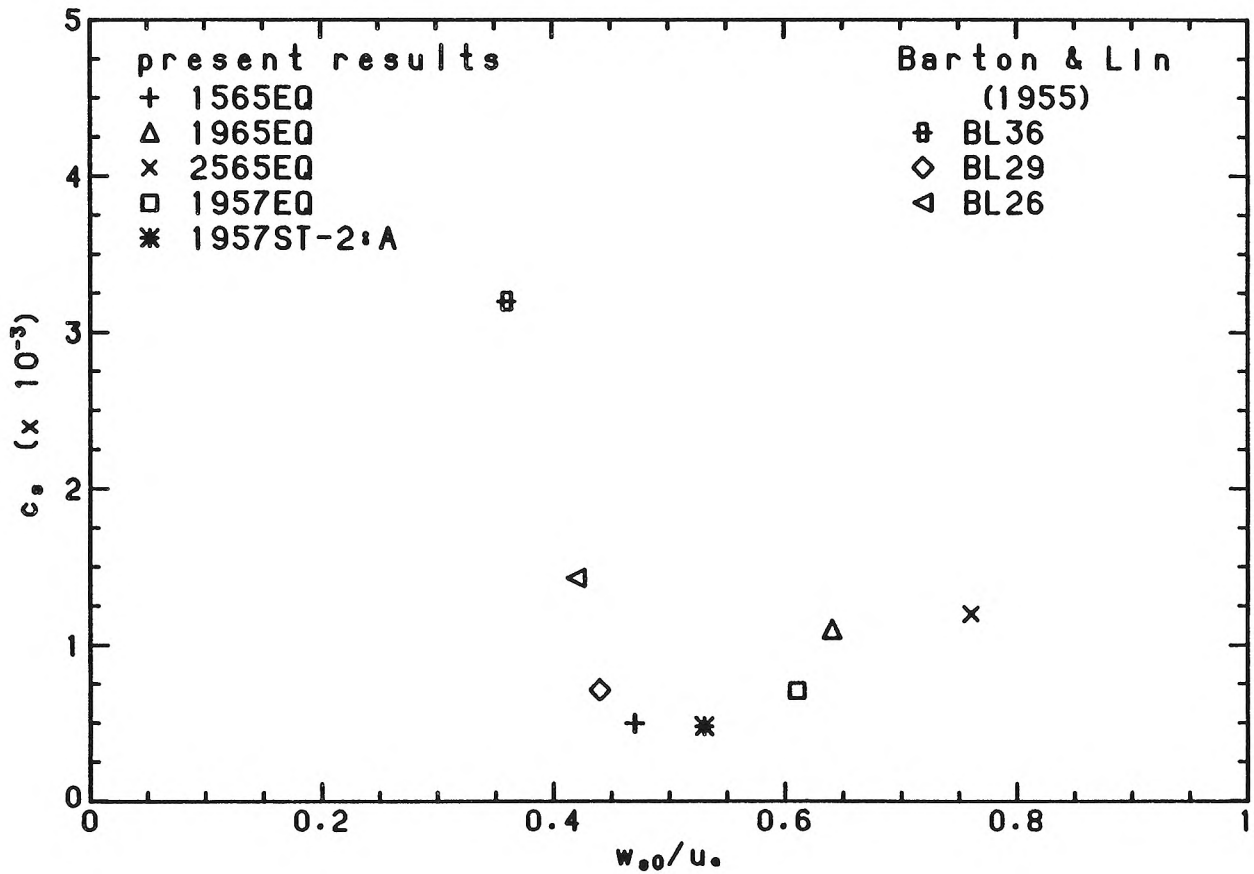

Fig. 6.3.6 Correlation of Z with w_{s0}/u_*

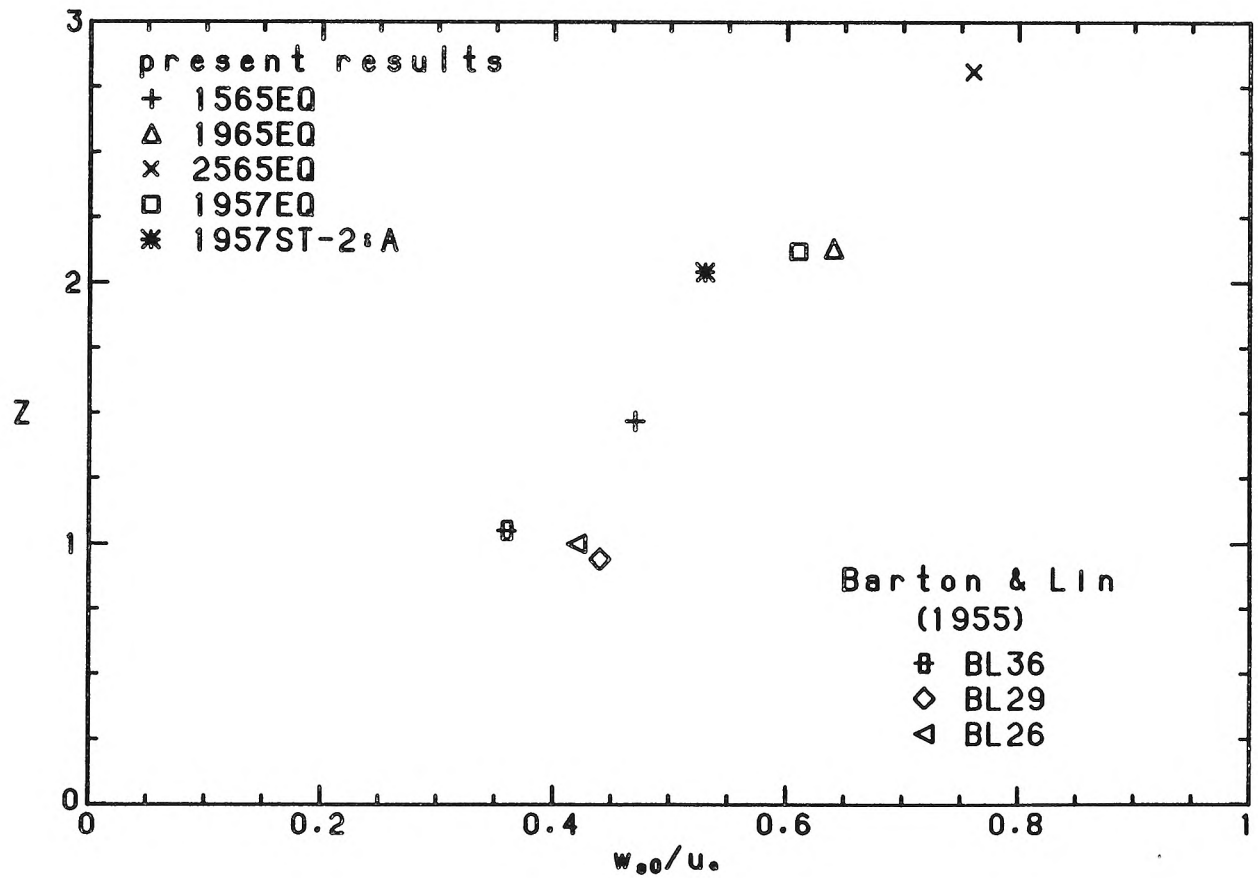

expected. The results deduced from the data of Barton and Lin (1955), however, indicate the possibility of a region, $0.3 < w_{s0}/u_* < 0.45$, where Z may increase with decreasing w_{s0}/u_*. In this region, it was previously seen from the same data set that Δ_s decreased with decreasing w_{s0}/u_*. From the simplest mixing-length model, in which $\beta_s \kappa_s$ = constant, a linear relation between Z and w_{s0}/u_*, with $Z \rightarrow 0$ as $w_{s0}/u_* \rightarrow 0$, would be expected. If a region were to exist where Z increases with decreasing w_{s0}/u_*, then the mixing-length model is clearly inadequate. If the data of Barton and Lin are ignored, then a plausible linear relation may be inferred from the results; however, this linear relation would not satisfy the condition, $Z \rightarrow 0$ as $w_{s0}/u_* \rightarrow 0$.

A log-concentration wake function, of the form suggested in Chap. 3, was also investigated. With Z and c_s determined from the above procedure, only the exponent of the outer-flow correction or "wake" component, Z_h, needs to be found. The resulting fit to our equilibrium-bed data has already been seen in Fig. 6.1.11. The ratio, Z_h/Z, is plotted against w_{s0}/u_* in Fig. 6.3.7. A large scatter is seen which tends to suggest that Z_h/Z is independent of w_{s0}/u_*, with a mean value of ≈ 0.3. This is unlikely to remain true for smaller w_{s0}/u_*, since the free surface should then exert a greater effect. The large scatter also recalls the scatter found in the wake coefficient of the velocity profile, even for clear-water flows. Factors which may explain the scatter include three-dimensional effects in the upper flow due to the sidewalls, vertical sorting of sediment because of the slight nonuniformity in size distribution, as well as errors in measuring small concentrations. Nevertheless, the value of ≈ 0.3 for Z_h/Z is significantly different from that predicted by the traditional suspended-load equation in which $Z_h/Z \equiv 1$. That $Z_h/Z < 1$ implies

Fig. 6.3.7 Correlation of Z_h/Z with w_{s0}/u_*

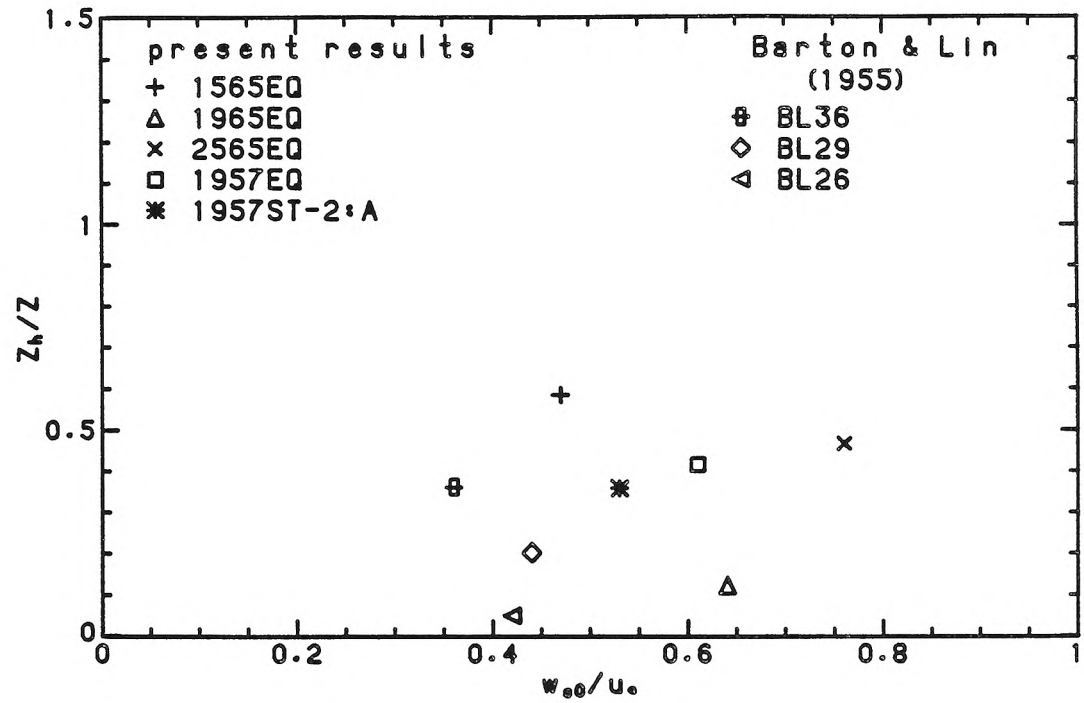

that the eddy diffusivity associated with the suggested profile is larger than that used by the traditional model.

As in the similarity treatment of the velocity profile, the appropriate analysis for those cases in which a distinct inner layer is not discernible is not clear. The power-law wake function profile may still be applied as a purely empirical fit. It may be speculated whether,in those cases where $l_s \sim h$, another inner length scale may be defined which could be used to justify such a profile. Because of the lack of data for such cases, this was not pursued.

6.4 Results on flow resistance

6.4.1 Comparison of friction factors

An important quantity in practice is the flow resistance defined by the Darcy-

Weisbach friction factor, $f_D \equiv 8(u_*/\langle u \rangle)^2$. The velocity profile in turbulent open-channel flow suffers substantial changes in the presence of suspended sediment, with consequent changes in flow resistance. In Fig. 6.4.1, f_D, determined from a numerical integration of the velocity profiles and the estimated u_*, is plotted against $(f_D)_{\rm cw}$, the friction factor for the corresponding clear-water flow with the same overall Reynolds number, $Re \equiv 4\langle u \rangle r_h/\nu$, and a roughness height equal to the grain diameter. The latter friction factor was determined from curves, based on the data of Nikuradse, given by Brownlie (1981). A tabulation of various estimates of the friction factor is given in Appendix A.2.

The clear-water results obtained in the present study essentially agree with the established results, as should be expected. All of the equilibrium-bed experiments, with the exception of BRK29, exhibit an increase in f_D over $(f_D)_{\rm cw}$. Even with a 10% error in f_D to account for errors in the estimation of $\langle u \rangle$ and u_*, the large majority of flows would still be judged to exhibit an increase. Indeed, increases of 30%–50% are often seen. It may be added that the use of an entirely empirical friction-factor correlation for sediment-laden flows due to Brownlie (1981) resulted in estimates of f_D, which were typically 25% larger again than the f_D obtained here (Appendix A.2). These point to the conclusion that flow resistance in nominally flat equilibrium-bed sediment-laden flows is typically increased over that found in clear-water flows.

To what extent this is due directly or indirectly to the suspension of particles is a more difficult question. It has been noted previously that nominally flat sand-beds are not ideally flat and may have mobile small-amplitude distortions particularly at corners, which will act to increase the flow resistance. In previous

Fig. 6.4.1 Comparison of flow resistance

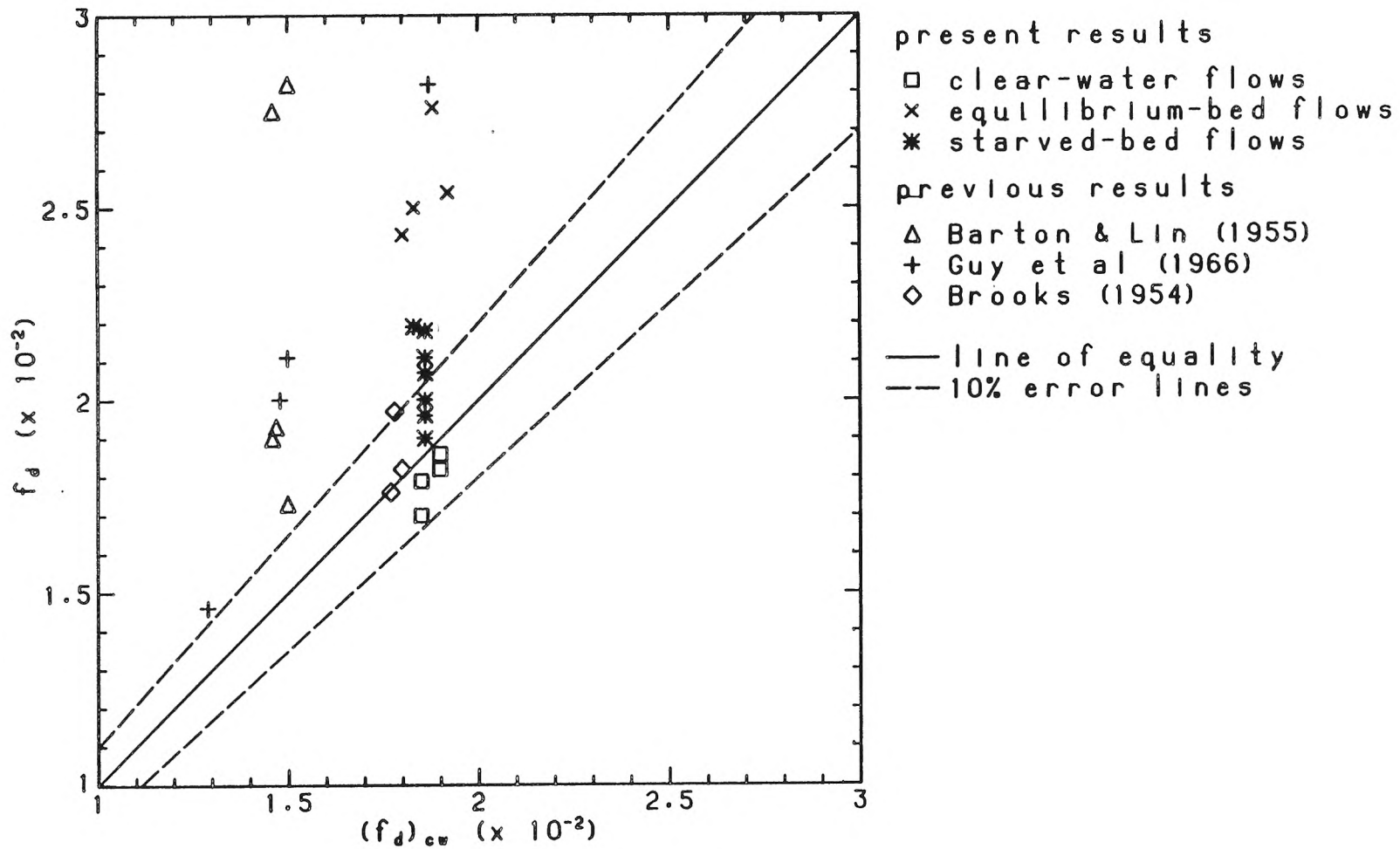

work, where u_* is estimated from the slope and the depth (or the hydraulic radius), the u_* so obtained is a spatial average over the area of the working section. In the present work, u_* is estimated from Reynolds-stress measurements on the centerline and therefore is not directly liable to spatial averaging. It is, however, based on temporal averaging and some effective spatial averaging is incurred. The equilibrium-bed results alone, then, are not the strongest evidence in favor of the conclusion that flow resistance is generally increased in sediment-laden flows. The starved-bed results, however, also tend to indicate that f_D is increased. In the high-transport series, 1957ST-2, where no permanent deposition of sand occurred along the length of the flume, the friction factor still increased with increasing concentration from a value approximately that of a clear-water flow to a value $\approx$ 15% larger (appendix A.2). Because of the problem of small-amplitude bed distortions, the *magnitude* of the increase (in extreme cases, $\approx$ 50%) in friction factor observed in the present equilibrium-bed experiments may be debated.

6.4.2 Friction and the velocity profile

It is paradoxical that, even though the friction factor has been found to be increased in a sediment-laden flow, the velocity profile exhibits regions where the velocity gradients are larger than those found in clear-water flows. *If*, for given u_*, the velocity gradient in a sediment-laden flow is nowhere less, and in some region larger, than that in a clear-water flow, then f_D must decrease. Thus, in the traditional view in which $du/dy = u_*/\kappa_s y$ everywhere and $\kappa_s < \kappa$, it is concluded that flow resistance is reduced (Vanoni, 1946, 1953). Even from the more recent viewpoint of the wake-function approach, it has been argued that flow resistance is decreased because of the larger gradients associated with the larger wake-coefficients (Lau, 1983). The stratified-flow analogy implies, in

general, a decreased friction factor because of the increased velocity gradients associated with stratification effects. That flow resistance may increase in some cases indicates again the failure of such an analogy.

In Fig. 6.4.2a, the results of the starved-bed series, 1957ST-2, are compared to those of the clear-water experiment, C-4, which, in terms of u_* and h, as well as bed flatness, is almost identical to the starved-bed series. The larger gradient near the bed of 1957ST-2:A compared to C-4 is evident. Nevertheless, the velocities associated with C-4 are noticeably larger. In order to resolve this, it must be concluded that, nearer the bed where all velocities must approach zero, there must exist a region where the velocity gradient in 1957ST-2:A is smaller than that in C-4. Since no measurements are available in this bed region, direct analysis of this region is not possible. From the results of the series, however, it is seen that, with decreasing concentration, the velocity profiles in the sediment-laden flows change in, at least, two significant ways. As has been emphasized before, the extent of the logarithmic region increases downward. More important with regard to the friction factor is the upward shift of the entire profile.

From these results, it seems clear that the smaller velocity gradients in the very-near-bed region increase to their clear-water values with decreasing concentration. The downward displacement of the velocity profile and the consequent increased friction factor result therefore from the presence of sediment in the flow. Since the displacement is due to processes occurring in the very-near-bed region, it is debatable whether it should be attributed to the sediment in suspension rather than to the saltating bed-load. This downward displacement as well as the localized nature of the effects of sediment, both rather reminescent of roughness effects,

Fig. 6.4.2 Velocity profiles for sediment-laden flows exhibiting a downward displacement relative to the clear-water results a) series 1957ST-2, b) some previous results

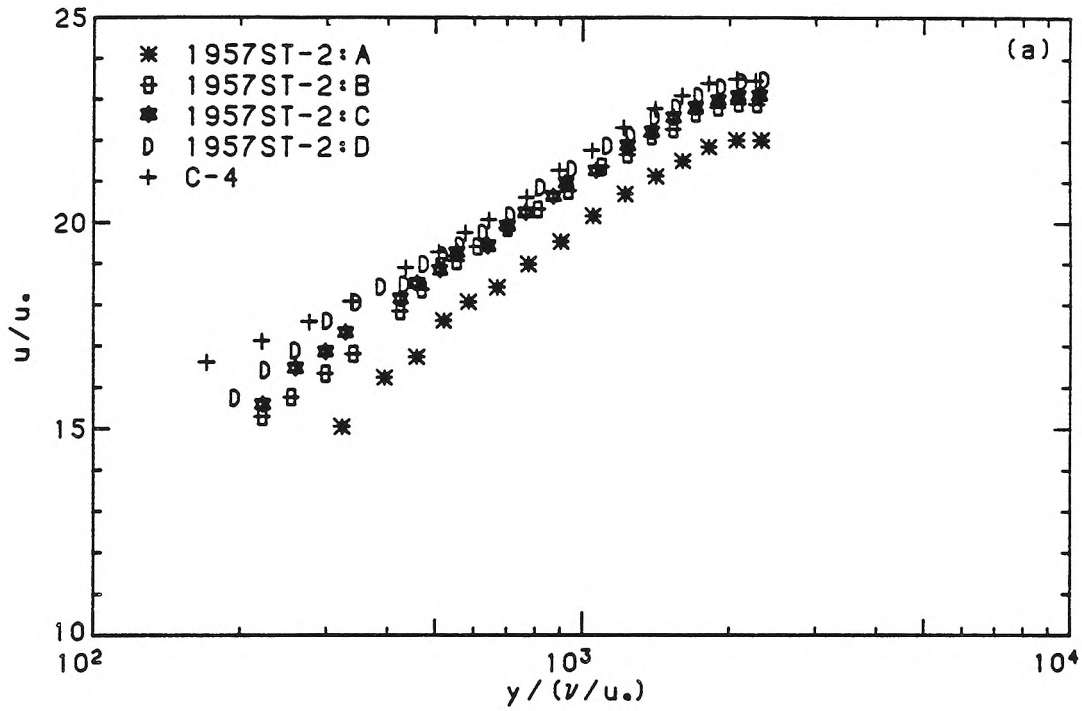

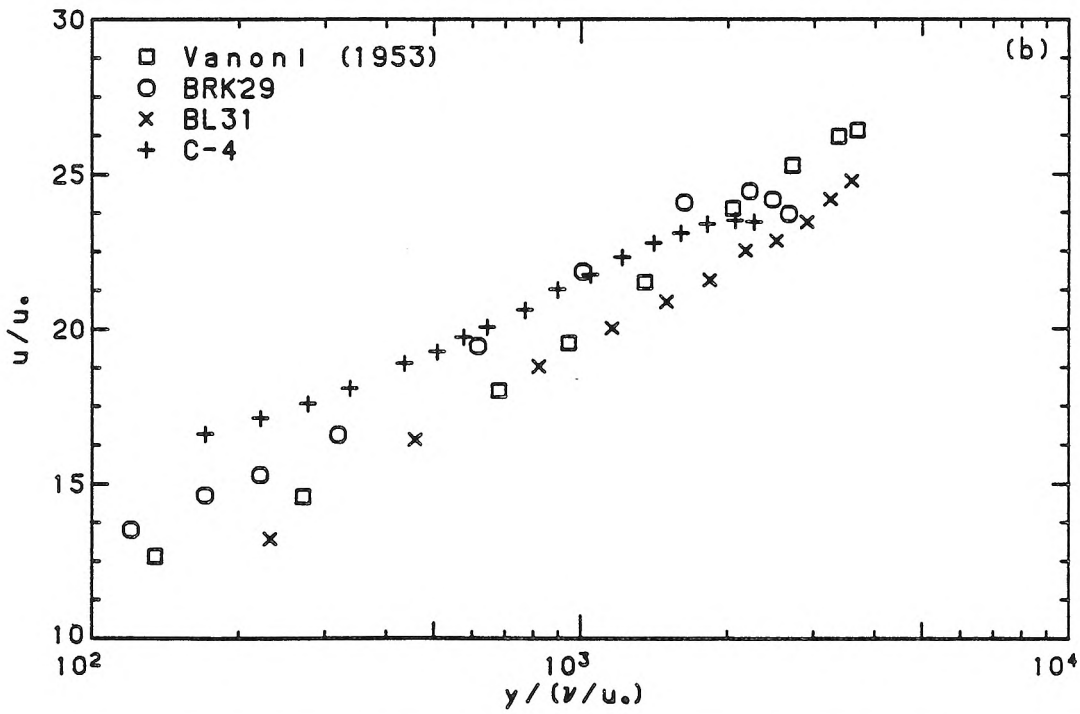

gives rise to the speculation that an interesting analogy with rough-surface flows may be made.

That a downward displacement of the velocity profile results from the presence of sediment does not necessarily preclude the possibility of a decrease in friction factor in sediment-laden flows, although the likelihood of such a decrease is reduced. In Fig. 6.4.2b, the clear-water profile is compared to sediment-laden profiles which exhibit regions with velocities greater than clear-water velocities. Both the data of Vanoni (1953) and Brooks (1954) were obtained with fine sand (d_{50} = 0.09mm), such that the bed roughnesses should be comparable to the clear-water experiment. It is seen that the regions of larger velocity gradients in sediment-laden flows may be of sufficient extent that velocities, even if they are initially smaller than clear-water velocities, become larger eventually. In this way, the depth-averaged velocity, $\langle u \rangle$, may become, for the same u_*, larger and may lead to a smaller f_D. For example, the friction factor associated with BRK29 was estimated to 0.0176 (Brooks reported it as 0.019), which, within the accuracy of the determination, is identical to that of a clear-water flow, estimated to be 0.0177.

6.4.3 Discussion: flow resistance in sediment-laden flows

The picture that emerges, regarding friction factors in sediment-laden flows, is more complicated than previously thought. The evidence does not support a categorical answer that f_D always increases or always decreases. What seems to be generally true is that, in the near-bed region, a downward displacement of the velocity profile in sediment-laden flows relative to clear-water profiles is found. In all of the data examined, this downward displacement dominates and results in an f_D equal to or, more often, greater than $(f_D)_{cw}$. It may be speculated that this downward shift is due to the high concentration ($O(0.1)$ perhaps) in the

very-near-bed region and the drag on saltating sand grains. Farther from the bed, where the concentration rapidly decreases, the velocity profile becomes steeper than that found in clear-water flows. The extent of this region has been defined here operationally as l_s. If this region is sufficiently small compared to h, it is succeeded by a log and then a wake region much like in clear-water flows. Since the downward displacement of the velocity profile is relatively dominant, this case will typically lead to an increased friction factor. If the region of larger velocity gradients is extensive, i.e., $l_s \sim h$, then, provided the initial downward shift is not too large, a small reduction in f_D may result.

6.5 Summary

Neither the traditional nor any of the more recent models explain the experimental results, our own as well as those of others. A distinct inner layer, the extent of which varied with hydraulic and grain parameters, was discerned. Since it was found using the standard Pitot tube as well as the LDV technique, it is doubtful that this observation is entirely a result of instrumentation bias. Similarly, because both equilibrium-bed and starved-bed experiments gave evidence of this layer, it cannot be entirely attributed to departures from an idealized bed condition or to the existence of a mobile bed layer. Since the extent of this layer scales neither with the viscous scale nor with the grain diameter, it does not accord with previous models.

On the other hand, the basic multiple-scales model developed in Chap. 3 seems sufficiently flexible as to be qualitatively consistent with the experimental evidence. What is perhaps less established is the validity of the correlations for the various scales and exponents. While, for the most part, a fair correlation is

found for the limited data available, and hence for the limited range of flow and grain parameters, some disturbing exceptions have been noted and are not easily explained. The validation of the correlations awaits, therefore, a systematic series of experiments under much wider ranges of conditions than could be obtained in the present study.

The results of the starved-bed experiments, besides amplifying and supporting the results of the equilibrium-bed experiments, confirmed expectations that such experiments present a more difficult problem of interpretation. The changes of shape in the concentration profiles and probably also in the velocity profiles in the region, $y < l_s$, suggest that the degree of saturation may not be parameterized by a single additional parameter such as the depth-averaged concentration.

It has also been seen that, under a wide variety of laboratory conditions, the friction factor in sediment-laden flows is more likely to exhibit an increase over that found in clear-water flows.

7. Sediment-laden flow experiments: Turbulence characteristics

7.0 Introduction

The similarity treatment of the mean fields eschews any detailed considerations of the dynamics of turbulent sediment-laden flows in order to obtain a useful model with a minimum of assumptions. This generality entails, however, a large reliance on empirical correlations. To ultimately reduce such reliance, a deeper understanding of the dynamics is necessary. As a first step in this direction, an investigation of the statistics of the fluctuating turbulent signal has traditionally been the path to take. In the following, these higher-order statistics are examined with the particular aim of illuminating the results for the mean fields, in general, and examining more closely some of the implications of the stratified-flow analogy, in particular.

Typical non-dimensional signals are shown in Fig. 7.0.1. The two examples are drawn from 1957EQ and differ in the relative elevation at which each was taken; one was measured in the middle of the flow at $\eta \approx 0.4$, the other at the lowest point obtainable, at $\eta \approx 0.12$. Comparison of the two shows the severe

Fig. 7.0.1 Examples of velocity time series (from 1957EQ): a) $\eta \approx 0.4$, b) $\eta \approx 0.1$

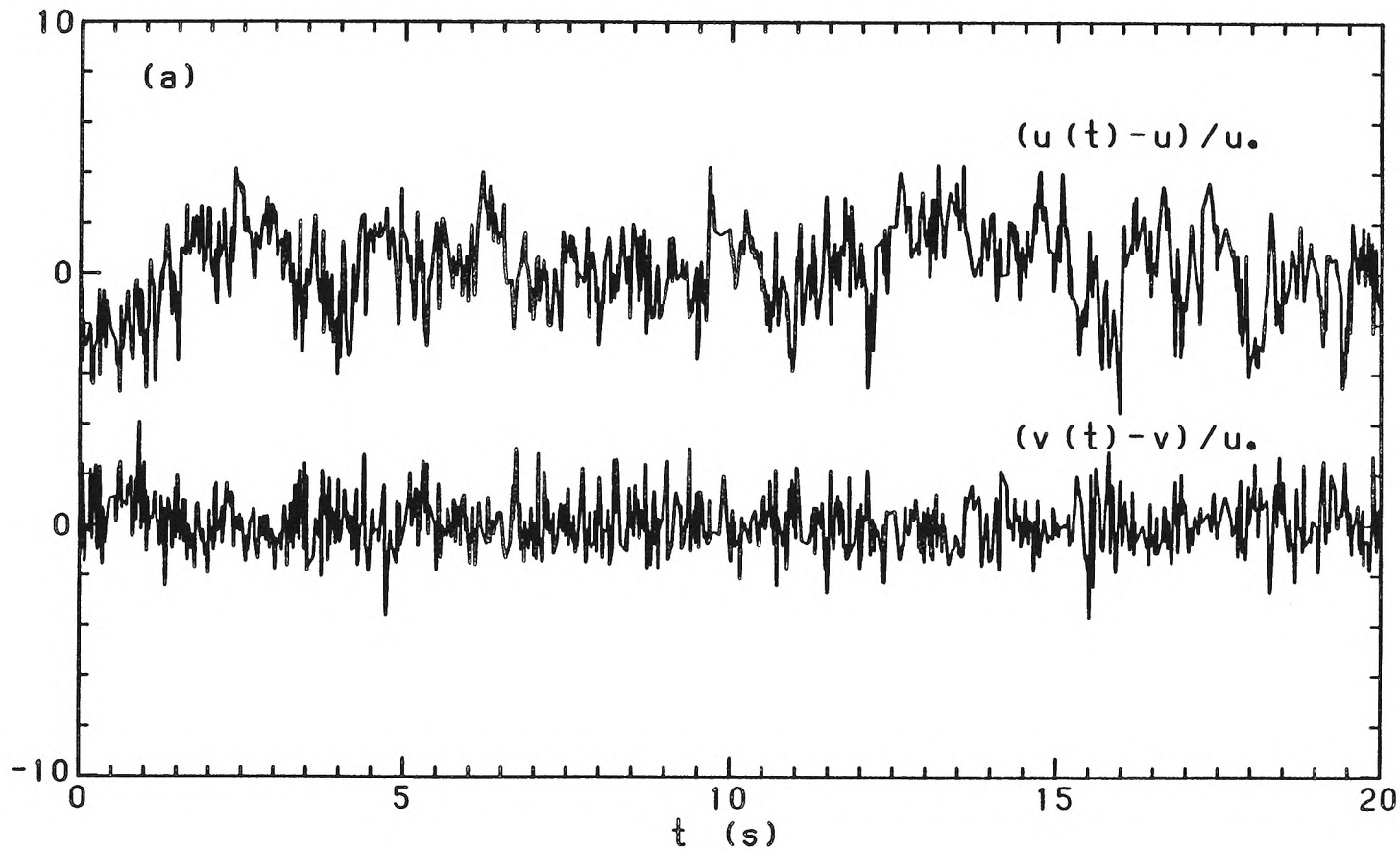

Fig. 7.0.1 b)

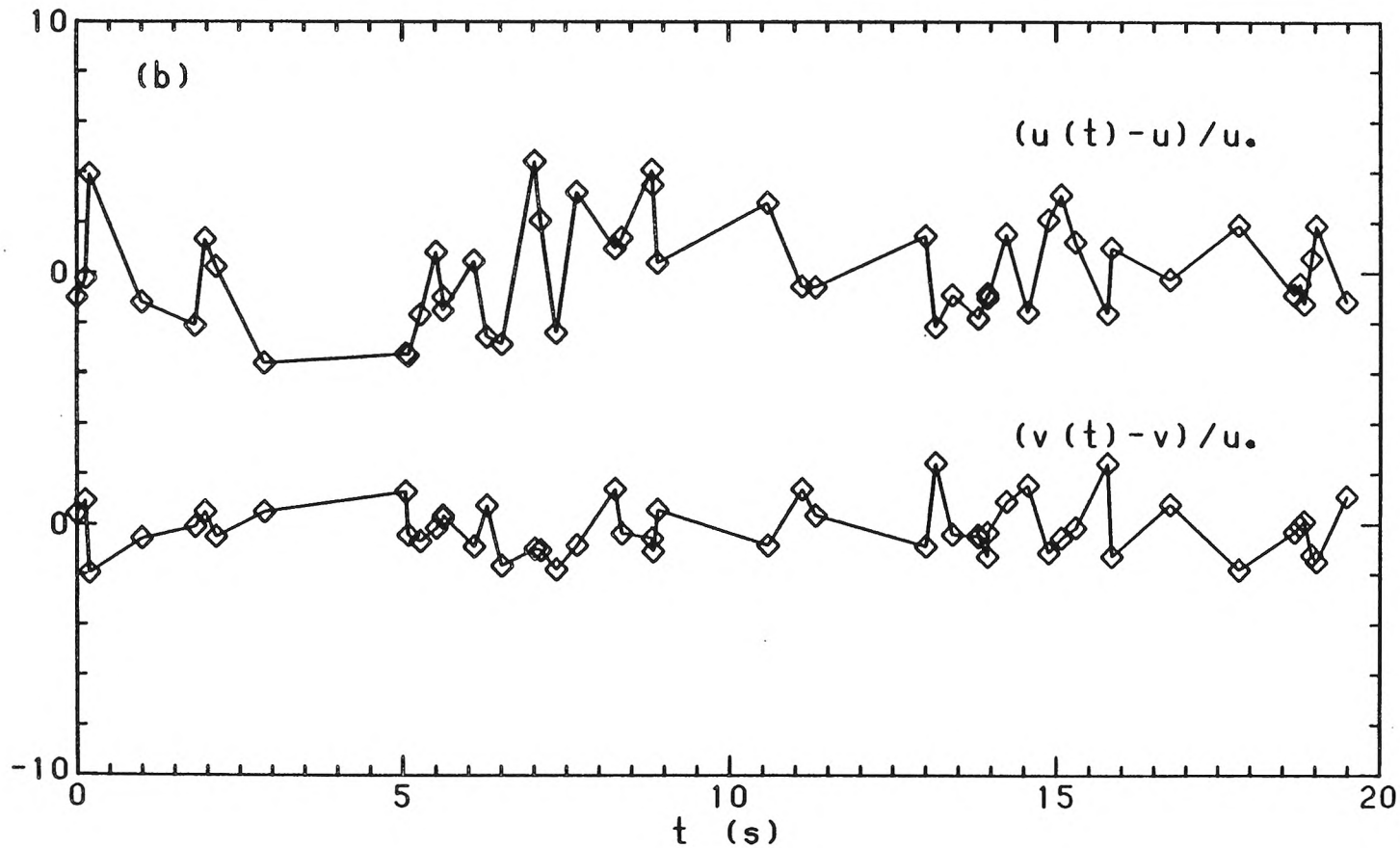

Fig. 7.0.2 Stability of statistics for time series (1957EQ, $\eta \approx 0.4$)
a) $u'v'$-statistics, b) u'-statistics

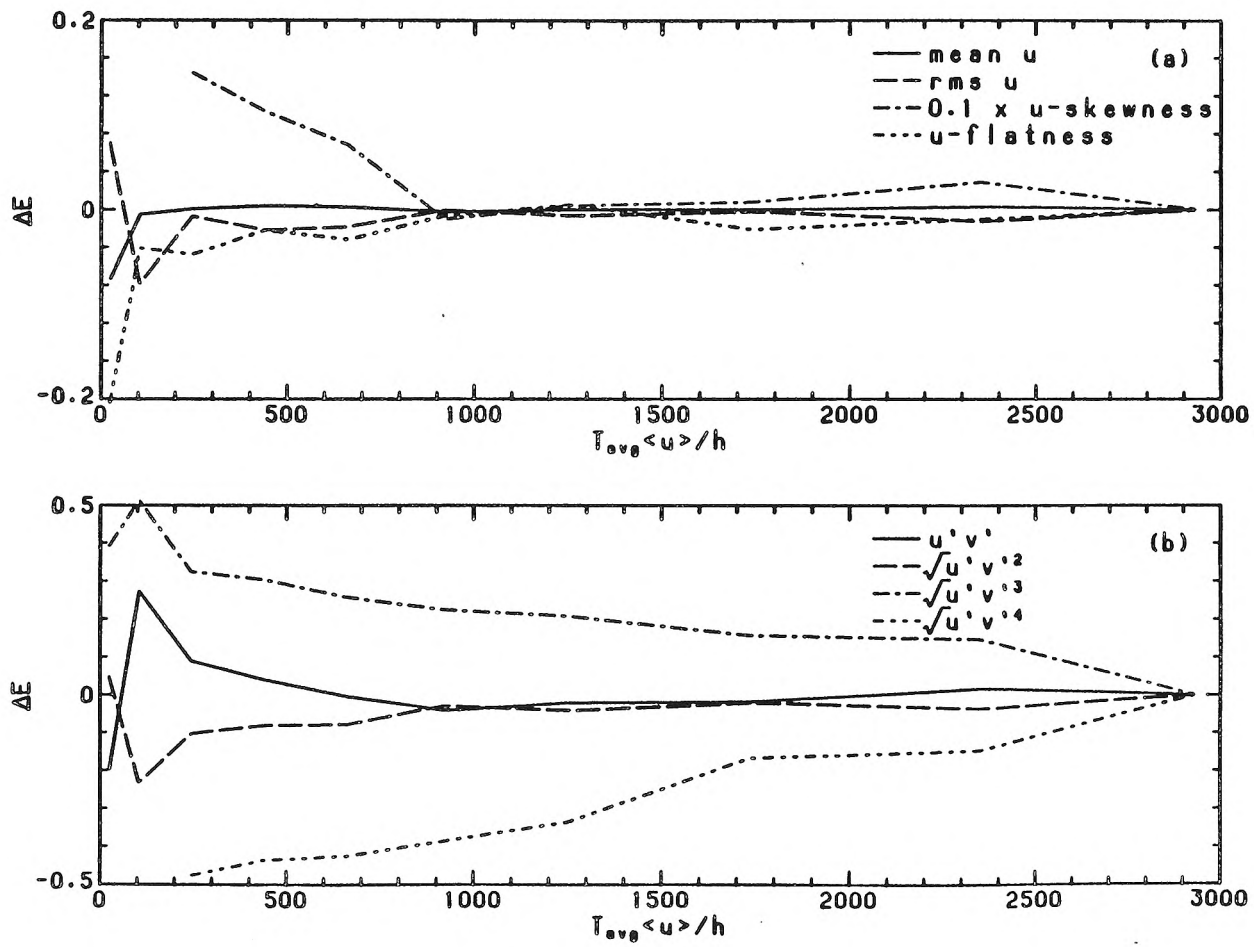

Fig. 7.0.3 Stability of statistics for time series (1957EQ, $\eta \approx 0.1$)
a) $u'v'$-statistics, b) u'-statistics

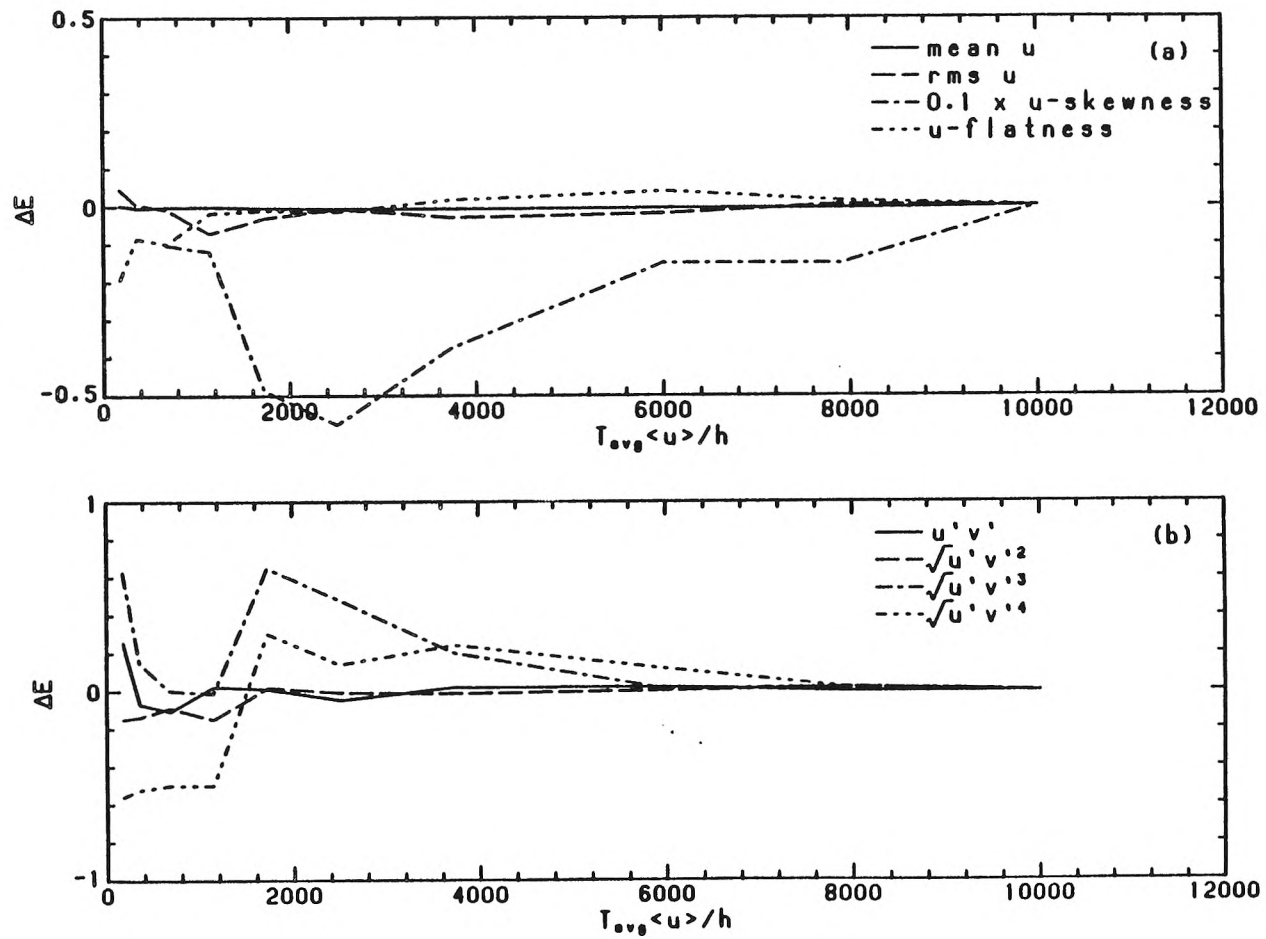

reduction, from $\approx$ 51Hz to $\approx$ 3Hz, in the mean data rate as the measurement point approaches regions of relatively high concentration of sediment. The low data rates as the bed is approached do not reflect the frequency response of the LDV, which is quite fast; they reflect the sporadic detection of validated signals. The variation of statistics of u' and $u'v'$ with averaging times for both of the above signals is shown in Fig. 7.0.2 and 7.0.3. Note that the averaging time for the point in mid-flow was $\approx$ 248s, while that for the lowest point was $\approx$ 846s, a total of 2675 data points being obtained for the latter. The statistics of u (and, by analogy, v) have attained stability in both of these measurements. Such a conclusion is somewhat more questionable with regard to the higher-order $u'v'$ statistics.

Second-order statistics receive the most discussion since they are closely related to the turbulent kinetic energy and more is known of them in homogeneous fluid flows. They are also the most reliable. Higher-order u- and v- statistics and Reynolds-stress statistics are then considered.

7.1 Second-order one-point statistics

7.1.1 Turbulence intensities

The implications of simple stratified-flow models (Itakura and Kishi, 1980; Coleman, 1981) were not supported by the experimental results for the range of conditions examined in this study. The possibility that the behavior in the near-bed region may still be attributed to buoyancy effects was raised and questioned in §6.1.5. One measurable indication of the validity of a stratified-flow analogy would be a decrease in vertical turbulence intensity with distance from the wall, over and above that found in clear-water flows. This would reflect the inhibition of vertical transport by the effect of stable stratification and has been observed,

for example, in the stably stratified, atmospheric surface layer (Panofsky, 1974). This view seems also implicit in the early suggestion by Vanoni (1946) that the presence of suspended sediment "damps" turbulence.

One of the main interests of the present work was, therefore, the search for any evidence of such damping of vertical turbulence intensities. The profiles of vertical intensities for the equilibrium bed experiments are shown in Fig. 7.1.1, together with the envelope of the results obtained for clear-water experiments. There is little evidence for any damping of the vertical turbulence intensities. In Fig. 7.1.2 are compared the profiles obtained from starved-bed and equilibrium-bed experiments, as well as the clear-water experiment closest in terms of experimental conditions to the respective series of starved-bed experiments. In none of these results is there any evidence of any difference between the vertical intensities found in sediment-laden and in clear-water flows.

The lack of any notable signature of the suspended sediment in the vertical turbulence intensity leads then to a consideration of the horizontal intensities. The results for the equilibrium-bed experiments are shown in Fig. 7.1.3. The distinction between results with different aspect ratios has been retained, with envelope curves being drawn for the two aspect ratios. The most noticeable difference between the equilibrium-bed results and the envelope of clear-water results is the slight tendency to an increase in the intensity in the region, $0.5 \leq \eta \leq 0.9$. The results for 2565EQ fall, however, within the clear-water envelope. Compared to the small scatter in clear-water results obtained in the present study, these slight differences found in the sediment-laden flows could be judged significant; compared to the larger scatter in clear-water results of other studies, the significance is more debatable. *If* these differences are considered significant, one might

Fig. 7.1.1 Vertical intensities in equilibrium-bed experiments

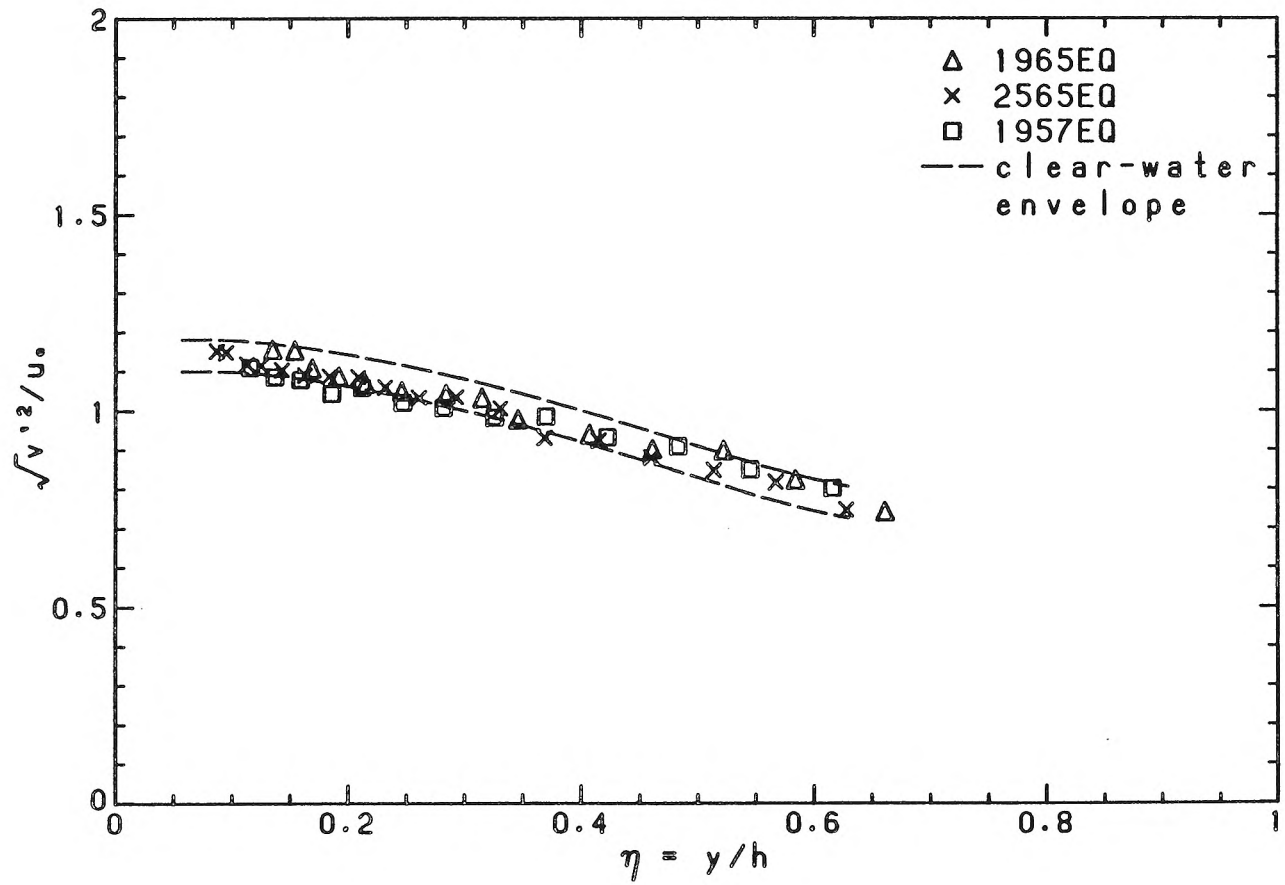

Fig. 7.1.2 Vertical turbulence intensities in starved-bed experiments
a) series 1965ST, b) series 1957ST-1, c) series 1957ST-2

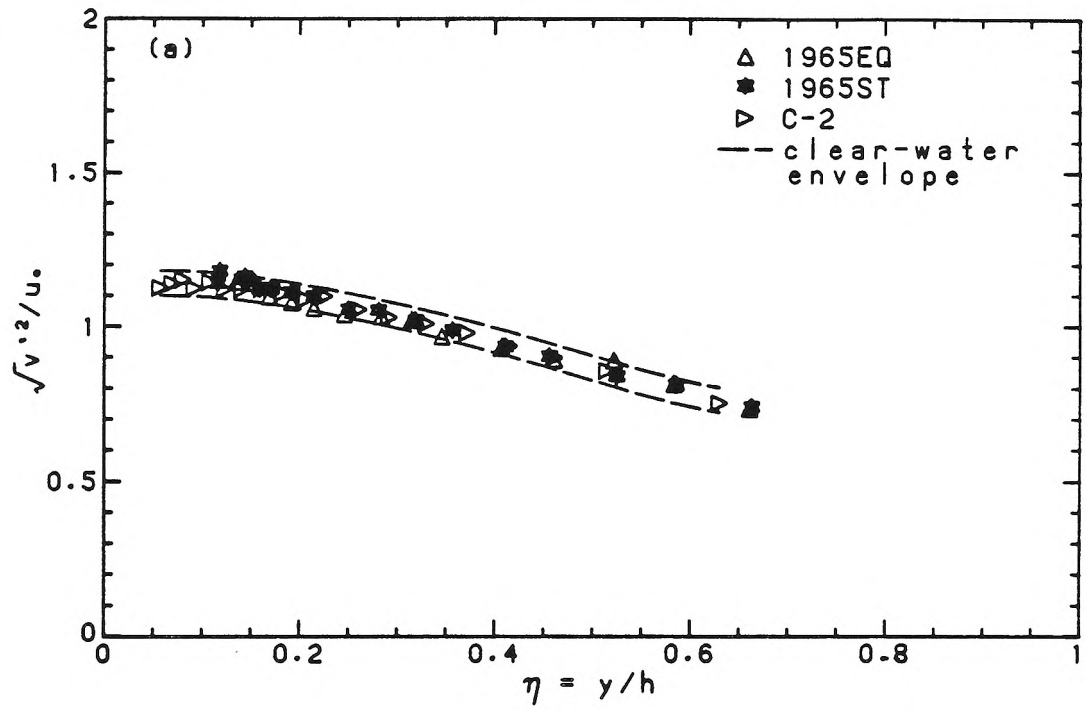

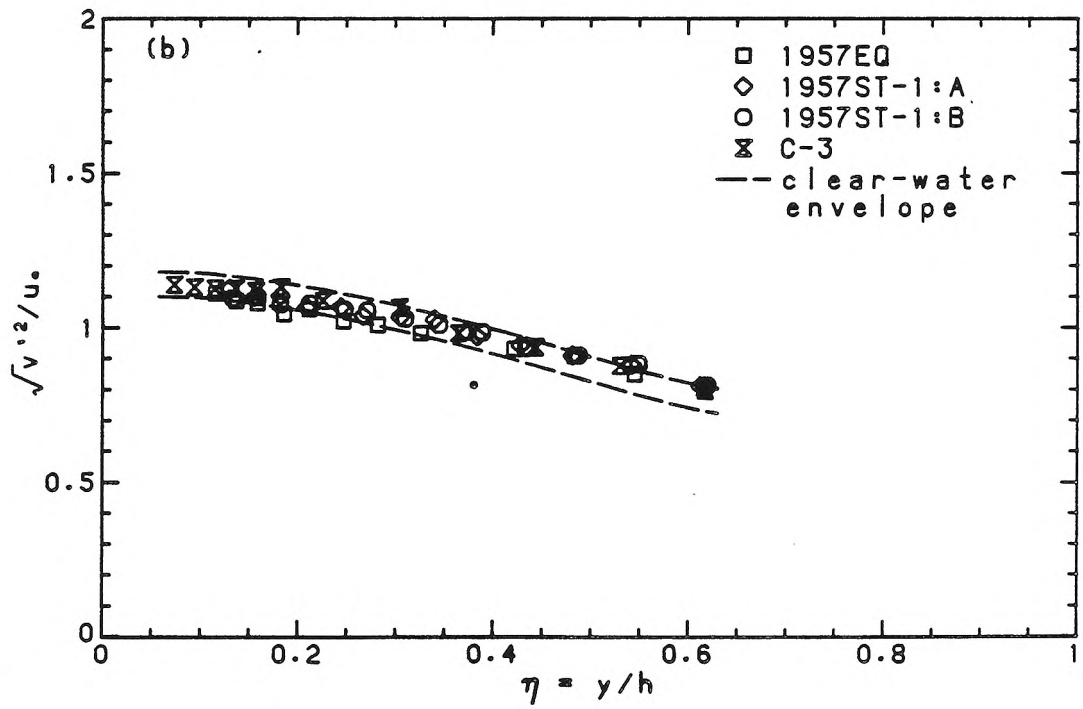

Fig. 7.1.2 c)

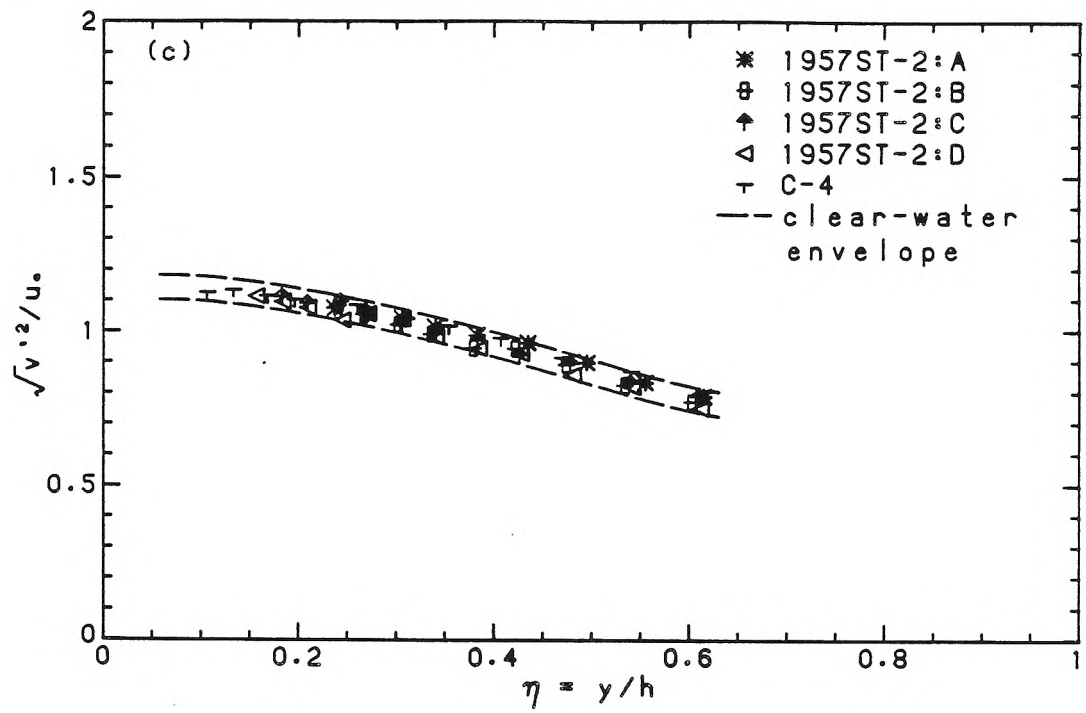

question whether they may be due to changes in roughness rather than due to the suspended sediment. The results for 2565EQ, which presumably would present the largest grain roughness, exhibit no difference at all. On the other hand, a more consistent picture is obtained if these differences are attributed to the suspended sediment, since 2565EQ had the least amount of suspended sediment.

The results of the starved-bed experiments are shown with the results of the equilibrium-bed and the clear-water experiment closest in terms of experimental conditions, as well as the appropriate envelope. The increase in intensity in the outer region is clearer in Fig. 7.1.4a and 7.1.4b in a direct comparison with a clear-water result. Moreover, the starved-bed results for the series, 1957ST-1 and 1965ST, also exhibit this tendency. A trend to a larger increase with the approach to equilibrium may also be discerned. These results recall the earlier work of Elata

Fig. 7.1.3 Horizontal turbulence intensities in equilibrium-bed experiments distinguished by aspect ratios, a) $b/h = 4.0$, b) $b/h = 4.7$

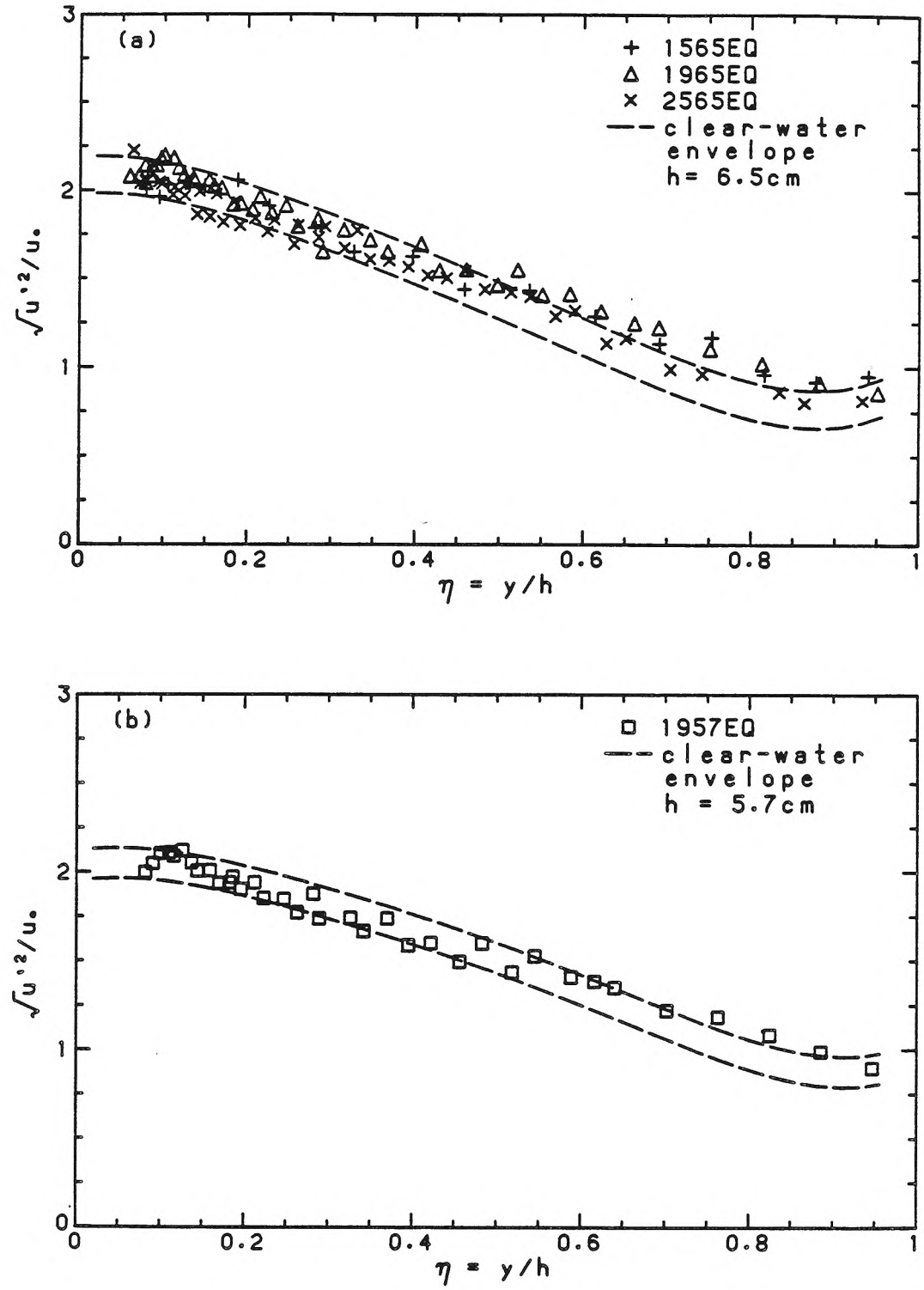

Fig. 7.1.4 Horizontal turbulence intensities in starved-bed experiments
a) series 1965ST, b) series 1957ST-1, c) series 1957ST-2

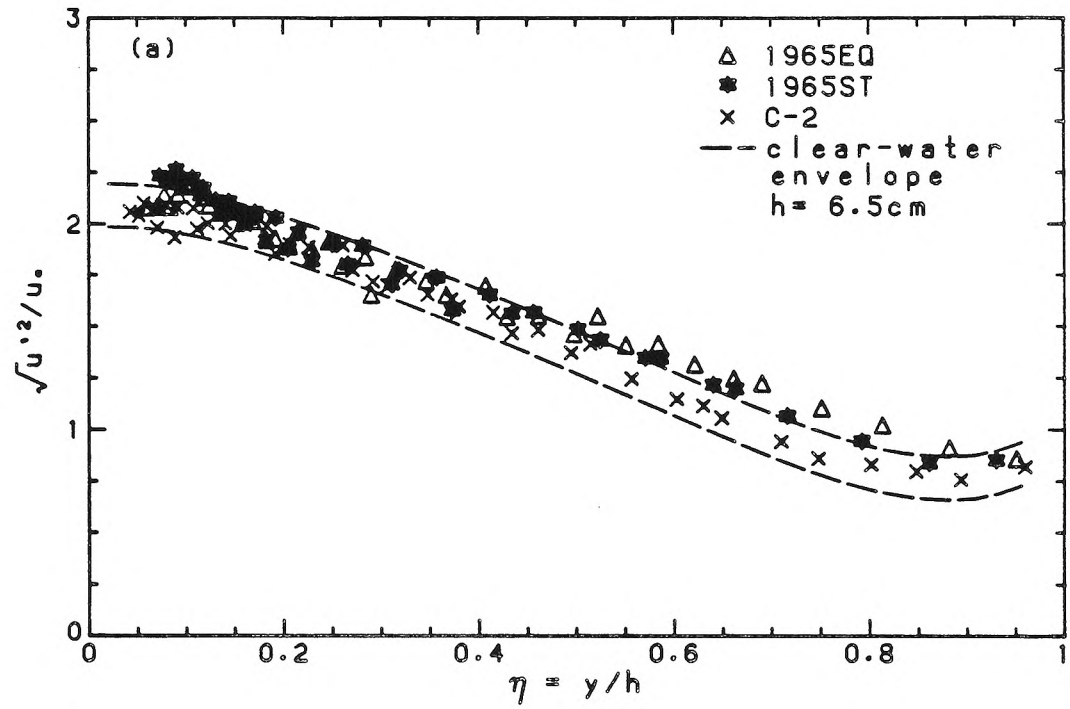

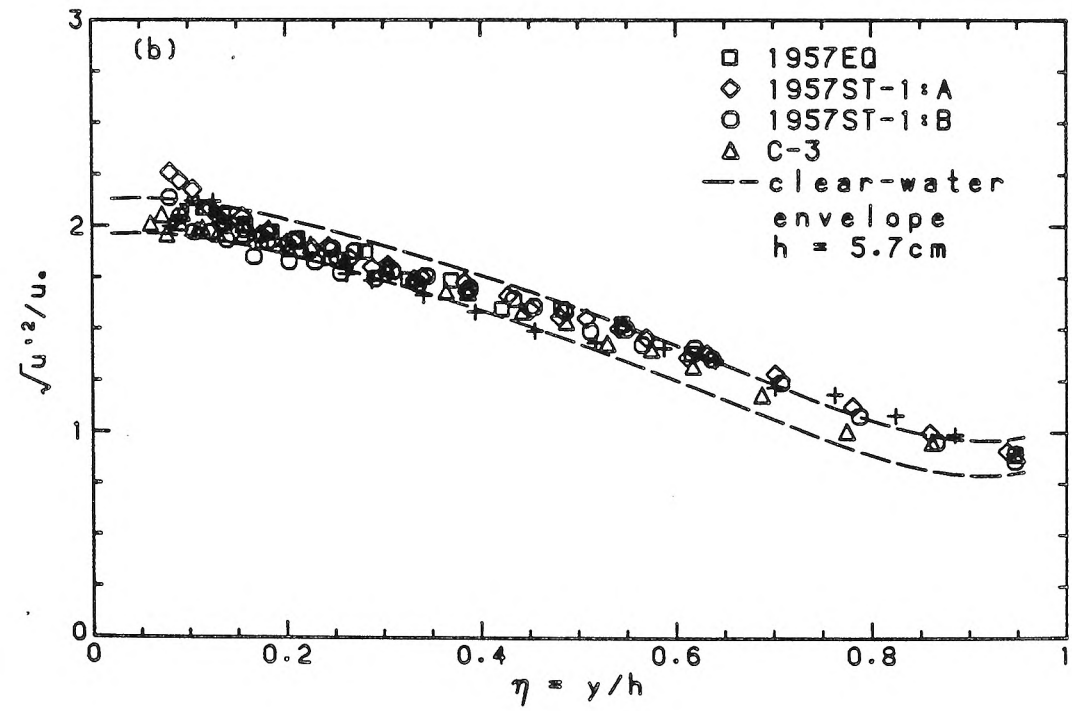

and Ippen (1961) and Bohlen (1969), whose reliability and applicability must be questioned, but who also found an increase in horizontal intensity with increasing concentration. van Ingen (1983a), who used the LDV technique, also reported a slight increase in horizontal intensity. In marked contrast to these results, however, are those for the starved-bed series, 1957ST-2, shown in Fig. 7.1.4c. No difference between sediment-laden and clear-water flows can be discerned in this particular series of experiments.

Fig. 7.1.4 c)

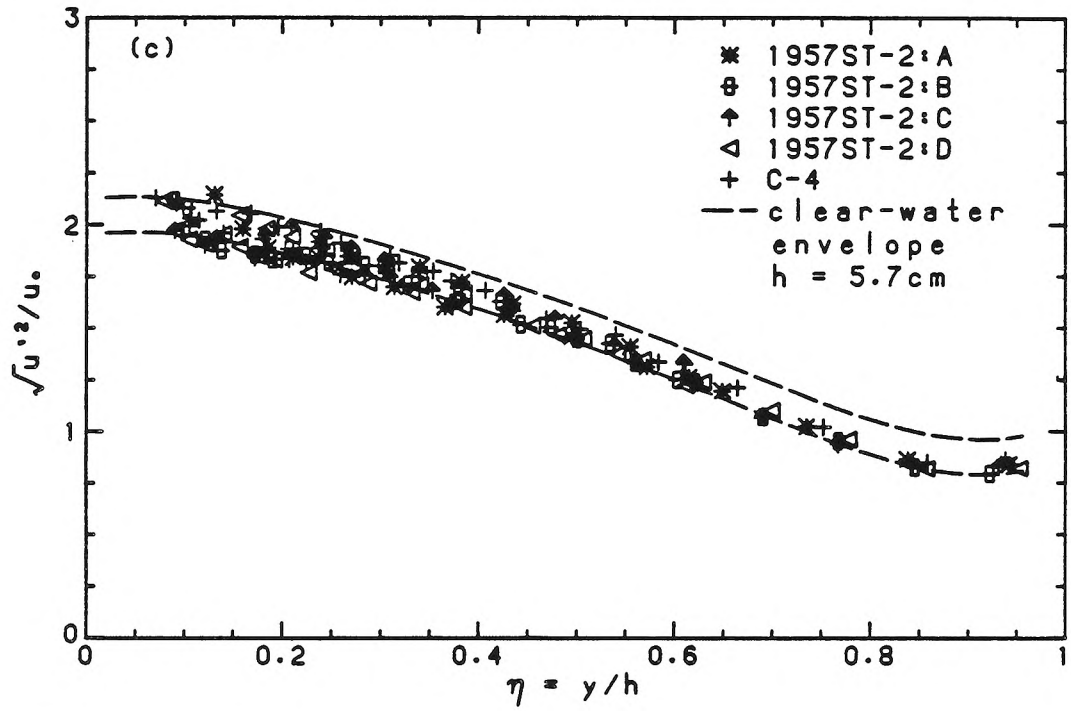

The increase in intensity observed in some of the cases examined is surprising in that it occurs in the outer flow where the presence of sediment seemed to have little effect on the mean-velocity profile. A significant effect would have been anticipated in the region near the bed where the effect of the presence of

sediment was found to be the greatest. Some such effect may be found, although again slight, in Figs. 7.1.3 and 7.1.4, where a few data points for the sediment-laden flows are seen to lie outside of the clear-water envelope in the region, $\eta < 0.2$. Unfortunately, problems posed by the high concentrations near the bed, particularly in equilibrium-bed experiments, may be masking such effects.

The starved-bed results are plotted in Fig. 7.1.5 in semi-log coordinates in order to emphasize the near-bed region. A trend to an increase in intensity with the approach to equilibrium can be seen in the near-bed region. The actual equilibrium-bed result in the inner region goes, however, counter to this trend, but it is not clear whether this is genuine or spurious. Since this increase in intensity begins at approximately where deviations from the clear-water mean-velocity profiles begin, a relation between these two results is suggested. Nevertheless, the scatter in results of both clear-water and sediment-laden flows in the near-bed region renders uncertain the importance of such a trend.

7.1.2 Power spectra of velocity fluctuations

The remarks concerning the determination of spectra for clear-water experiments should be kept in mind, as the results for the sediment-laden flows were obtained in a similar way. The relevant parameters of the spectral estimation are listed in Table 7.1.1. The smoothed power spectra of the vertical velocity fluctuations for the equilibrium-bed experiments are shown in Fig. 7.1.6. The collapse at higher frequencies indicates that small-scale motion in a saturated flow may be approximately independent of grain parameters. Variations may, however, be seen in the larger scales. A comparison with clear-water results is given in Fig. 7.1.6b. The differences are slight and their significance uncertain. If a tendency

Fig. 7.1.5 Horizontal turbulence intensities in starved-bed experiments in semi-log coordinates to emphasize the inner region
a) series 1965ST, b) series 1957ST-1, c) series 1957ST-2

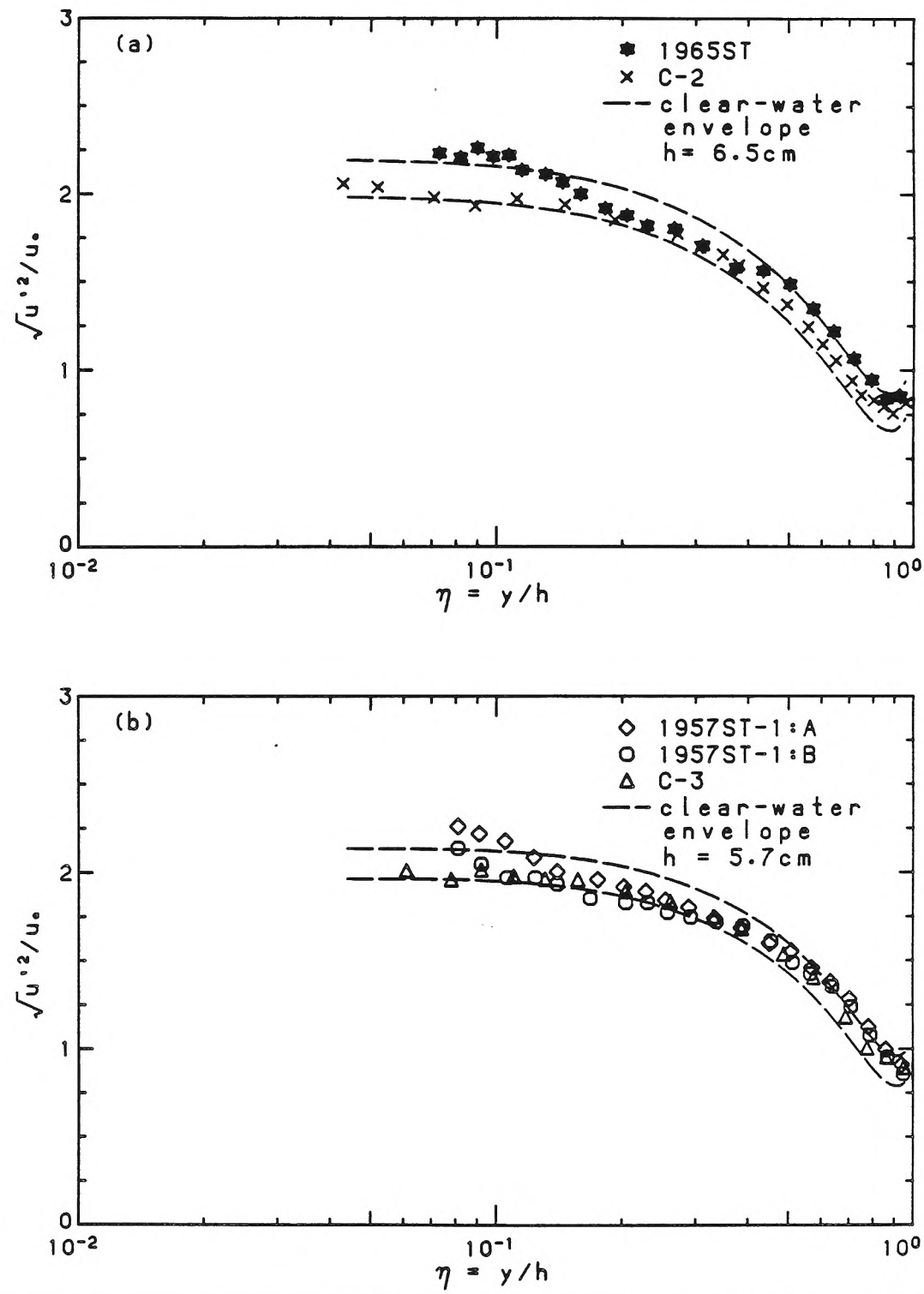

Fig. 7.1.5 c)

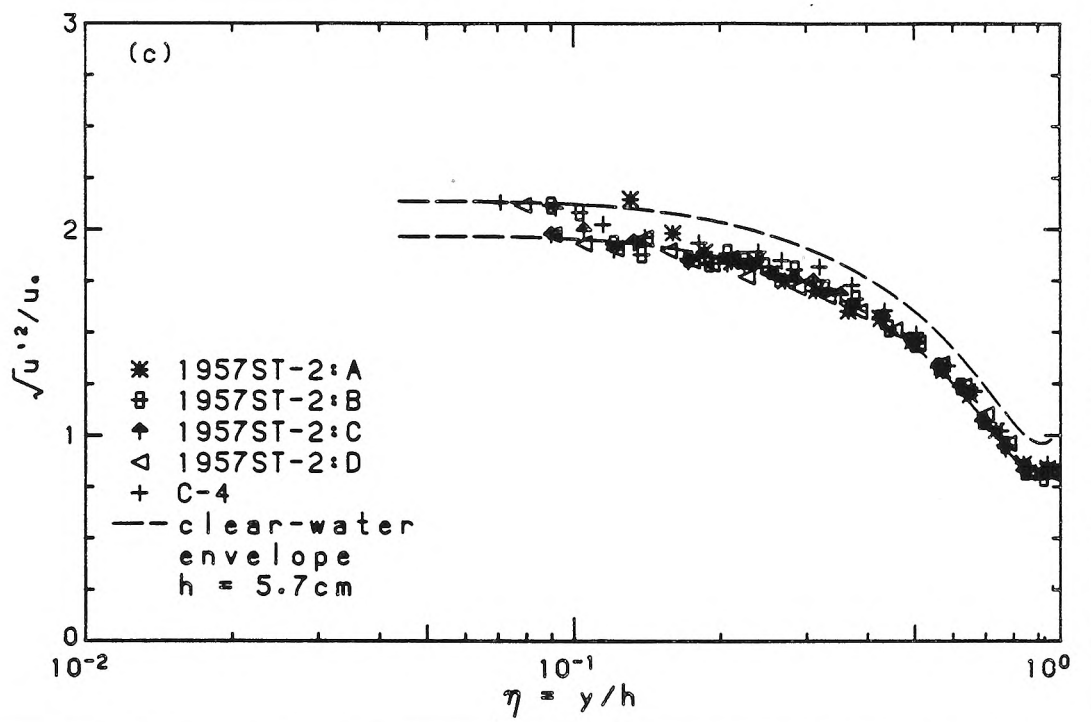

can be seen, it is the greater relative importance in sediment-laden flows, such as 1957EQ, of larger scales at the expense of smaller scales. To some extent, this tendency is also exhibited in the results for the starved-bed experiments, plotted in Fig. 7.1.7. The relative decline in the importance of small scales is found in the results for 1965ST (Fig. 7.1.7a) and for 1957ST-2:C (Fig. 7.1.7c). At the larger scales, the spectra for sediment-laden flows are found either above or near the upper extreme of the clear-water envelope.

The power spectra of the horizontal velocity fluctuations exhibit similar features. The equilibrium-bed results are shown in Fig. 7.1.7. Less variation is seen at the lower frequencies and more variation at the higher frequencies than was seen in the case of the vertical fluctuations. In the comparison with the clear-water envelope, it is again seen that larger scales gain in importance relative to

Table 7.1.1 Characteristics of original and interpolated records

	equilibrium-bed				starved-bed				
					1965ST	1957ST-1		1957ST-2	
Expt.	1565EQ	1965EQ	2565EQ	1957EQ		A	B	C	D
u spectral computation									
η	0.40	0.37	0.39	0.40	0.37	0.39	0.39	0.37	0.39
Δt, (ms)	11.6	10.9	8.8	10.9	10.2	17.2	16.1	8.9	17.5
$\sigma_{\Delta t}$, (ms)	0.40	0.44	0.38	0.38	0.44	0.57	0.59	0.40	0.64
$(\Delta t)_I$, (ms)	13.9	12.5	12.5	12.5	12.5	20.0	20.0	12.5	20.0
$(u'^2)_I/u'^2$	0.95	0.97	0.88	0.95	0.93	0.88	0.86	0.92	0.86
v spectral computation									
η		0.41	0.42	0.37	0.41	0.38	0.39	0.38	0.39
Δt, (ms)		15.7	13.0	19.4	10.8	16.9	15.8	25.0	20.2
$\sigma_{\Delta t}$, (ms)		0.62	0.58	0.74	0.62	0.69	0.65	0.97	0.83
$(\Delta t)_I$, (ms)		20.0	15.6	25.0	12.5	25.0	20.0	25.0	25.0
$(v'^2)_I/v'^2$		0.71	0.67	0.70	0.73	0.81	0.72	0.69	0.68

smaller scales in sediment-laden flows. The effect at smaller scales is seen to be quite pronounced in the case of 1565EQ and becomes even more so if the evident aliasing is taken into account. Interesting also is the result for 2565EQ, which is seen to be most like a clear-water result, particularly at smaller scales, even though some aliasing is also apparent. This was also seen previously in the case of the spectra of vertical fluctuations. There is also some indication that the spectra associated with starved-bed experiments approach those found in clear-water experiments with decreasing concentration, as should be expected. In this regard, the results of the series, 1957ST-2, are again anomalous. The higher concentration experiment, 1957ST-2:C, gives results more like clear-water results than the lower concentration experiment.

Fig. 7.1.6 Normalized power spectra of vertical velocity fluctuations
a) equilibrium-bed results
b) comparison with clear-water results

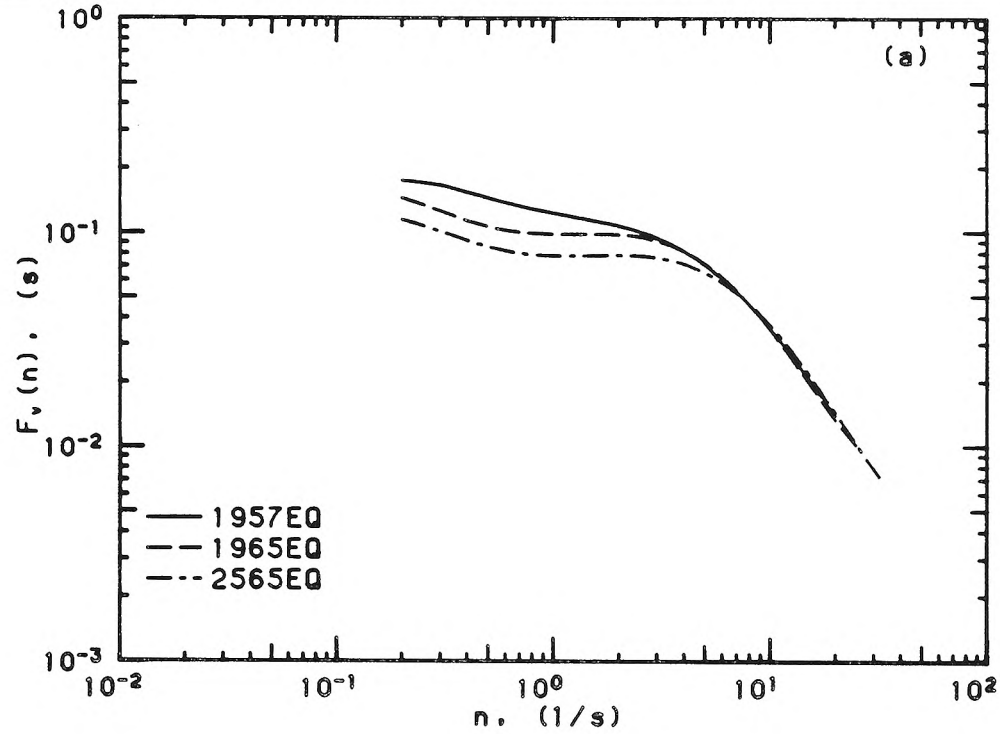

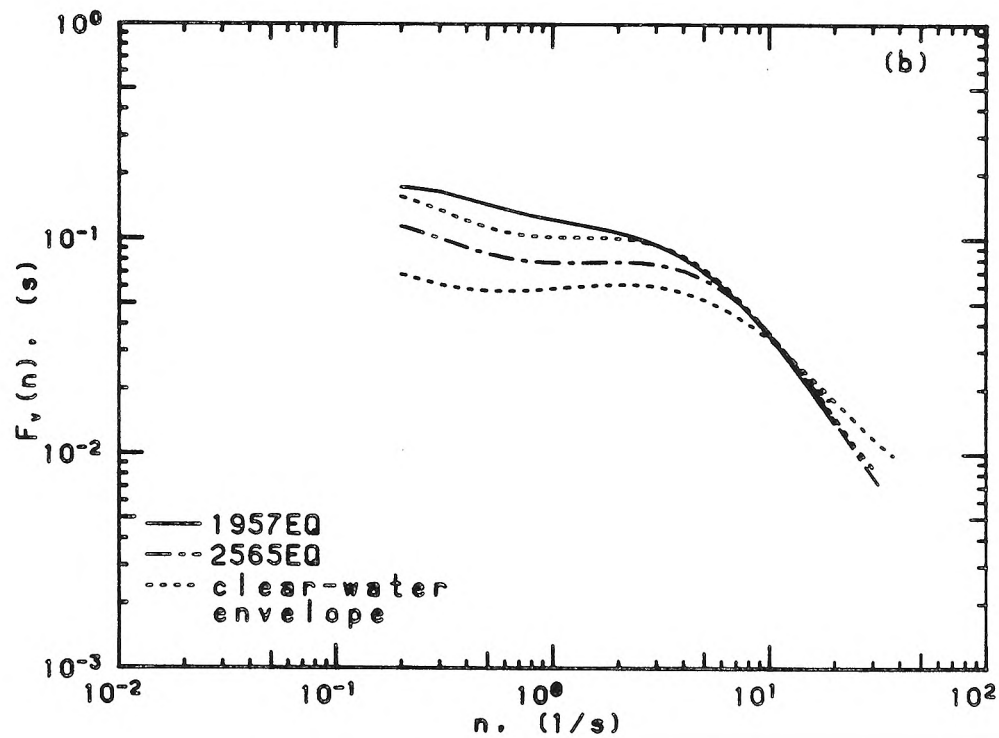

Fig. 7.1.7 Normalized power spectra of vertical velocity fluctuations for starved- and equilibrium-bed experiments
a) series 1965ST, b) series 1957ST-1, c) 1957ST-2

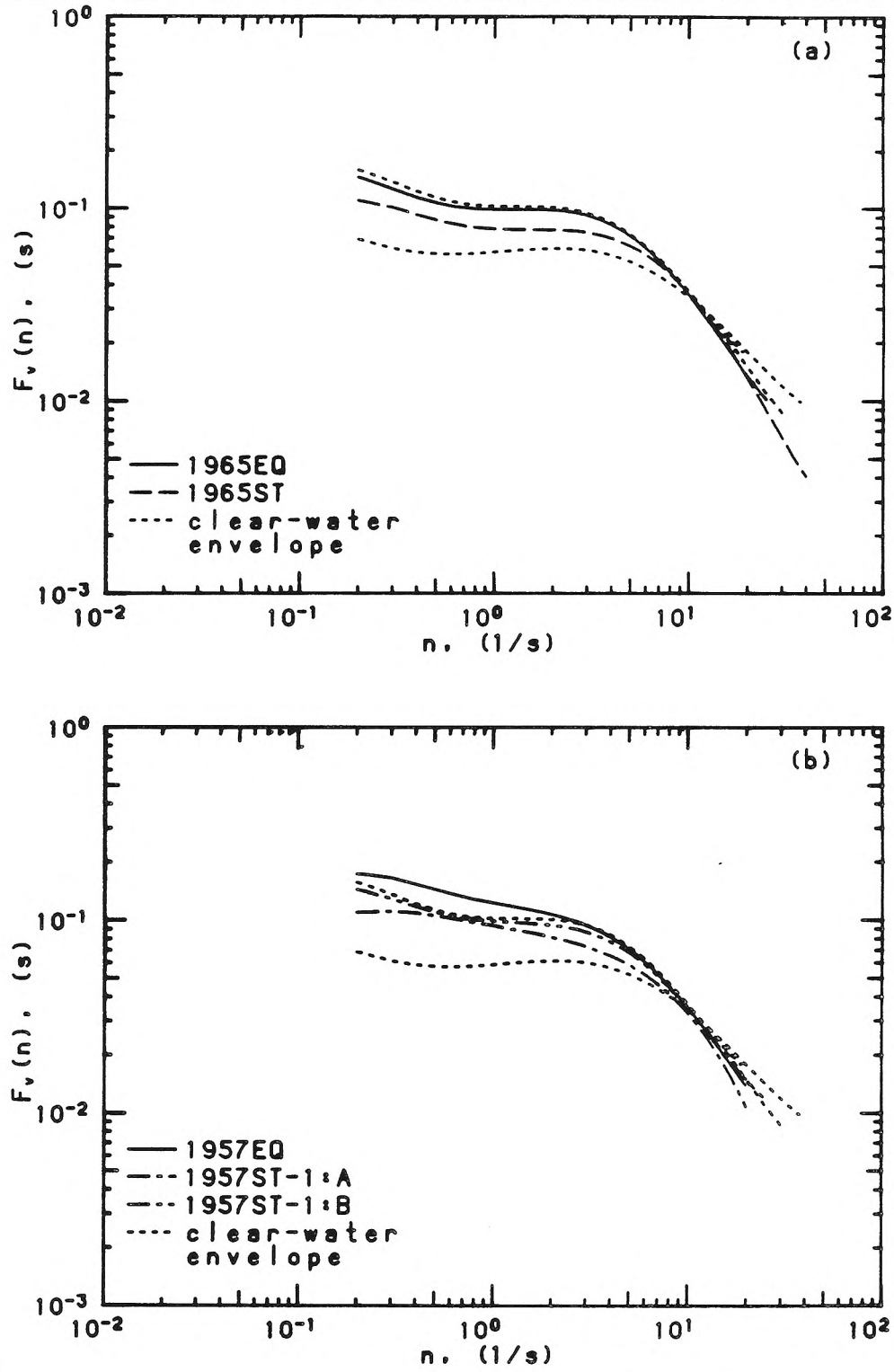

Fig. 7.1.7 c)

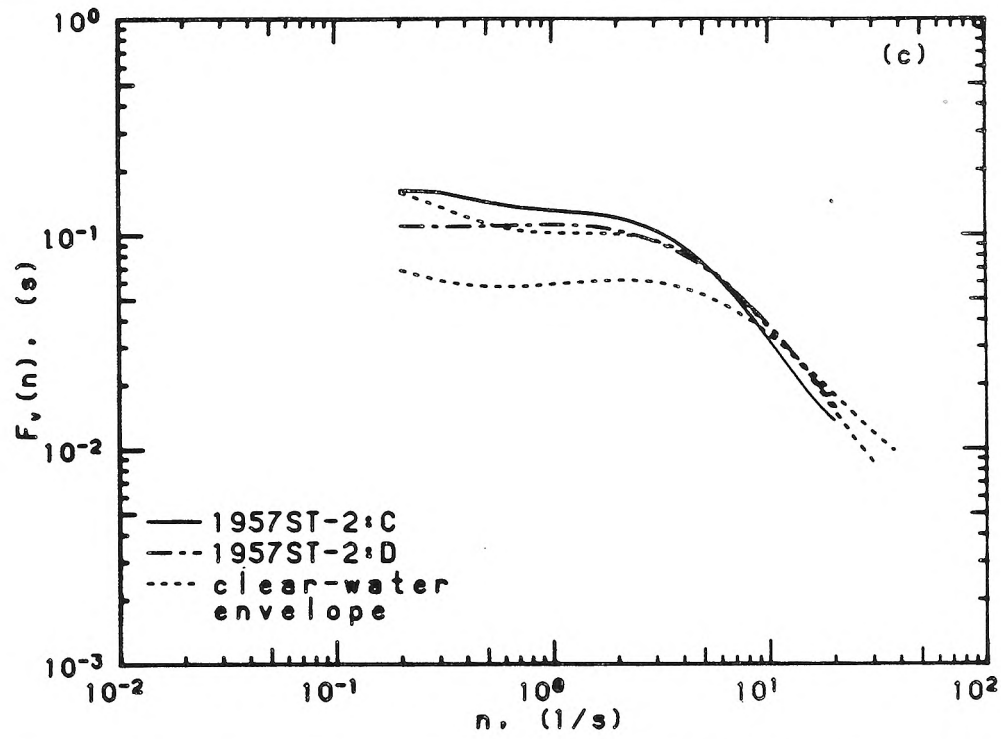

7.1.3 Discussion: Second-order one-point statistics

The overall impression that arises from the examination of 2^{nd}-order quantities is the little difference that the presence of suspended sediment makes. A strictly objective conclusion, taking into account experimental and statistical errors and the scatter found in the results of others, would insist that no significant effect of the suspension has been found. This was the cautious conclusion drawn previously by van Ingen (1983a) in a study of only the horizontal fluctuations. That this applies also to the vertical velocity fluctuations and applies under a wider range of experimental conditions than previously studied is surprising and hence, significant. Because the more reliable results on fluctuating quantities have been limited to a region, $\eta \geq 0.2$, these negative results tend to support one of the main contentions of this study that, under a wide range of laboratory conditions, the outer-flow region remains largely unaffected by the presence of sediment.

Fig. 7.1.8 Normalized power spectra of horizontal velocity fluctuations
a) equilibrium-bed results
b) comparison with clear-water results

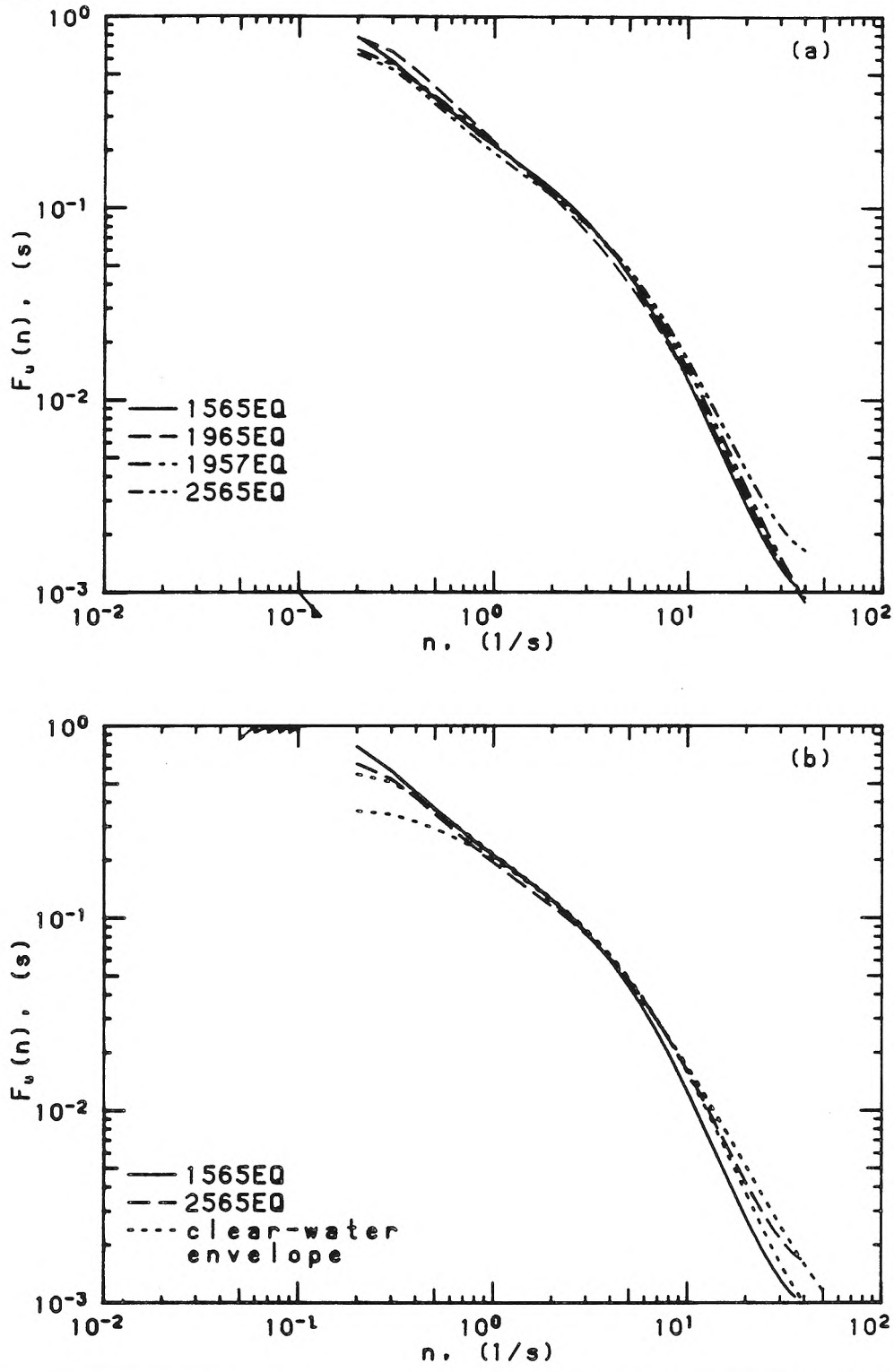

Fig. 7.1.9 Normalized power spectra of horizontal velocity fluctuations: starved-bed results
a) 1965ST, b) 1957ST-1, c) 1957ST-2

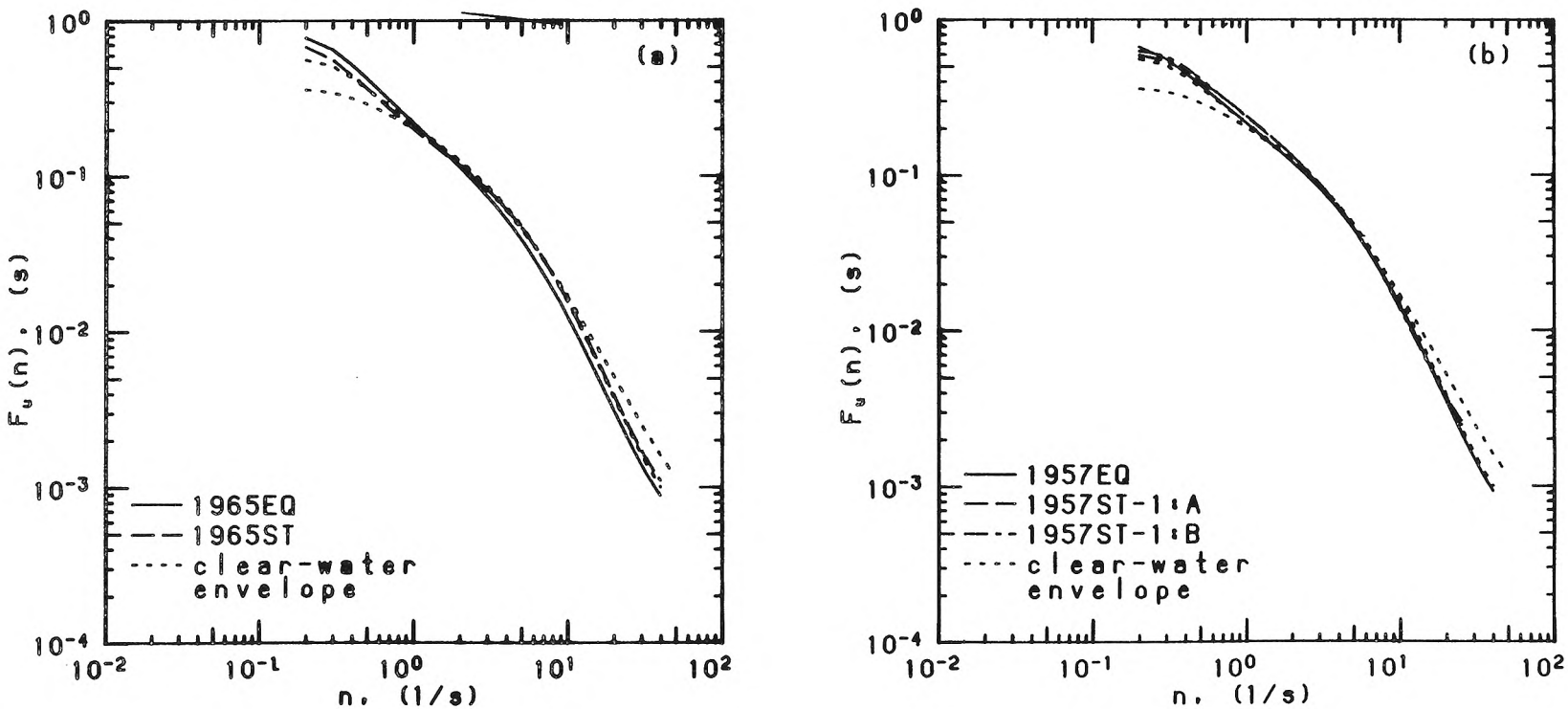

Fig. 7.1.9 c)

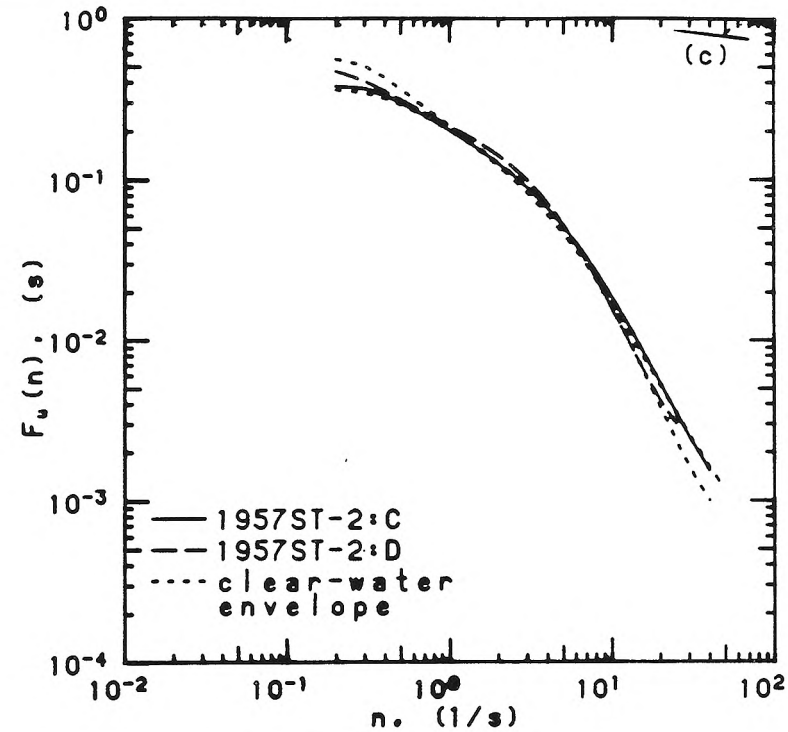

On the other hand, the results are also significant because they throw further into doubt explanations previously given of the effects observed in the mean-velocity profiles. If the "damping" of turbulence, hypothesized by the traditional view, is interpreted as implying a general decrease in vertical intensities, then it is seen that marked effects can be observed in the mean profile without such a decrease being found. The more specific implications of a simple analogy with weakly stable density-stratified flows are also not supported by the results on intensities or on power spectra. In the latter case, if *any* change is noticeable, it is the decline in importance of smaller scales relative to larger scales. This is opposite to what would be expected in the case of a stably stratified flow.

The question whether, for the range of experimental conditions studied, any effects of stratification should be observable must, however, be raised. Since there

is controversy about the occurrence, even, of such effects, agreement on a definitive criterion has yet to be reached. One possible criterion, that due to Barenblatt (1979) (or in its adapted form, Eqn. 6.3.1), is clearly not satisfied since $w_{s0}/\kappa u_* > 1$ (assuming that $w_s \approx w_{s0}$) in all the experiments for which vertical intensities could be reliably measured. It may be argued that such a criterion is too stringent since stratification effects need not dominate for them to be measurable.

The use of the Richardson number suggested by Coleman (1981) involves the bed concentration, which is practically impossible to estimate accurately in the presence of an equilibrium bed. The starved-bed experiments of Coleman were conducted with sands ranging from 0.1 mm – 0.4 mm in grain diameter and an almost constant $u_* \approx 4$ cm/s. If stratification effects were observable in *all* of these starved-bed experiments, then they should also be observable in equilibrium-bed experiments conducted under comparable conditions, since the bed concentration in the latter must be at least equal to or, more likely, greater than that of starved-bed experiments.

Another crude estimation considers the vertical momentum equation with the effect of stratification included:

$$\frac{d}{d\eta}\left(\frac{v'^2}{u_*^2}\right) = -\frac{1}{\rho_w u_*^2}\frac{\partial P}{\partial \eta} - \frac{g(s-1)c_h h}{u_*^2}\frac{c}{c_h}, \tag{7.1.1}$$

where a Boussinesq approximation has been made. If the bold assumption is made that changes in $\partial P/\partial y$ due to the presence of sediment are negligible compared to the effect of the term, $g(s-1)c_h h/u_*^2$, then the additional decrease in v'^2/u_*^2 with distance from the wall may be attributed entirely to the effect of the suspension. The integrated magnitude of this effect, then, may be estimated for the particular example of 1965EQ, in which $Z \approx 2$, as

$$\frac{g(s-1)c_h h}{u_*^2}\int_{0.05}^{0.5} \eta^{-Z}\, d\eta \approx 0.1. \tag{7.1.2}$$

An effect of magnitude, $\approx 5\%$, on $\sqrt{v'^2}/u_*$ may then be attributed to the suspension, which is, perhaps, at the limit of experimental determination. This estimate may be considered conservative in that i) the lower limit of the integral was taken to be 0.05 rather than the bed itself, and ii) it is assumed that the maximum vertical intensity is not decreased in sediment-laden flows. If the lower limit is taken as $\eta = 0.02$ ($y \approx 6d_{50}$), and it is assumed that $c \sim \eta^{-2}$ is still a good approximation, then the estimate is revised to 14%, which should be within the limits of experimental observation. If stratification effects are significant near the bed, then it may be argued that even the maximum vertical intensity, which occurs near the bed in the absence of any suspension, should be smaller than that of a clear-water flow.

The uncertainties involved in the above estimates and in the measurements are such that a definite conclusion regarding the importance of stratification effects cannot be drawn in general. The evidence on vertical turbulence intensities and power spectra both strongly suggest that these effects are weak, at least for the range of experimental conditions investigated. The weakness of such effects would then be consistent with the observation that the mean-velocity profile in the outer flow is largely unaffected by the presence of sediment. Whether such effects would be important under other conditions, e.g., a heavier suspended load, is not clear. An increased concentration due to a smaller w_{s0}/u_* would tend to be accompanied by a more uniform concentration profile and, hence, a milder effective stratification. A similar estimate as was done for 1965EQ in Eqn. 7.1.2 may be performed for the case of 2565EQ for which w_{s0}/u_* is 20% higher. A slightly larger effect is, in fact, predicted ($\approx 7\%$ using a lower limit of $\eta = 0.05$).

Although large differences between sediment-laden and clear-water flows were not found, a number of slight differences were sufficiently consistent to be suggestive, namely: i) an increase in $\sqrt{u'^2}/u_*$ in the inner region, $\eta < 0.2$, ii) a relative increase in importance of larger scales at the expense of smaller scales as implied by the power spectra, and iii) an increase in $\sqrt{u'^2}/u_*$ in the region, $0.5 < \eta < 0.9$.

The increase in $\sqrt{u'^2}/u_*$ in the inner region is perhaps most interesting because that region has been seen to exhibit significant deviations from the clear-water mean-velocity profile. In particular, the velocity gradients in parts of this region were found to be notably larger than those predicted by a log law with $\kappa \approx 0.4$. Are these larger gradients related to the observed increased intensities? It is commonly argued (Hinze, 1975; Tennekes and Lumley, 1980) that all of the turbulent kinetic energy produced by shear goes initially and entirely into the horizontal "component," u'^2, and is then distributed to the other components by way of pressure-velocity interactions. Although this argument may be faulted because it is based on time-averaged equations, it does provide an explanation for the observed anisotropy of intensities.

This argument may then be extended to sediment-laden shear flows. The larger velocity gradients, for given wall-shear stress, result in a greater total production of turbulent kinetic energy. If the efficiency of the mechanism inducing isotropy is relatively unchanged by the presence of sediment, then it is plausible that the larger gradients lead to an increased intensity in the inner layer. This relation between larger velocity gradients and increased intensities is familiar from wall-bounded flows of homogeneous fluids. In the upper part of the buffer layer between the viscous sublayer and the logarithmic inertial layer, velocity gradients are greater than in the inertial layer, and a corresponding increase in horizontal

intensity is observed. The analogy between the buffer layer in a homogeneous-fluid flow and the inner layer, characterized by l_s, in sediment-laden flows, noted previously in §6.3.1, is here reinforced.

Changes in power spectra in the presence of sediment may also be interpreted in a similar way. It has been remarked, e.g., by Tennekes and Lumley (1980), that the inertial subrange of the energy spectrum, to which the Kolmogorov - 5/3 law applies, is the spectral equivalent of the inertial sublayer in wall-bounded flows, to which the log-law applies. The results on the mean-velocity profiles were interpreted as indicating the existence of an inner layer, which could grow to such an extent as to preclude the possibility of a logarithmic inertial layer. The changes in the frequency domain may be interpreted as reflecting this process. The relative increase in the rate of dissipation in a given frequency interval (in the high-frequency range) indicates a growth in the scales of dissipation corresponding to the existence of an inner layer whose extent, l_s, is significantly larger than either l_ν or d_{50}. Because the spectra presented were normalized such that their integrals were unity, a relative increase in energy content of the larger scales accompanies the relative decrease in energy content of the smaller scales.

In the proposed explanations or speculations concerning the increase in horizontal intensities in the near-bed region and the changes in the power spectra, a potential analogy was raised between the observed results and the results that might have been observed if a layer analogous to a buffer layer extended much farther up into the flow. This would be consistent with the mean-velocity profiles since, in the upper part of the buffer layer, velocity gradients are larger than those in the logarithmic layer. The idea of rescaling, important in the similarity treatment of the mean fields, offers, perhaps, a tool for interpreting the second-

or even higher-order turbulence characteristics in sediment-laden flows. From this perspective, the increase in horizontal intensities in the outer region may, perhaps, be viewed as a displacement upward of intensities that would, in clear-water flows, be associated with a region closer to the wall.

The concern so far has been mainly with gross differences between clear-water and sediment-laden flows. If these differences are slight, the differences between the various sediment-laden flows are, in general, even slighter. Of note, however, is that the results for 2565EQ, of all the equilibrium-bed flows, most closely resembles the clear-water flows. Since this was the case in which the suspended load was least important, it may be speculated that, for larger ratios of w_{s0}/u_*, turbulence characteristics will approach those of clear-water flows. The consistently anomalous case of the starved-bed series, 1957ST-2, which exhibited marked effects in the mean-velocity profile and yet no effects at all in intensities or spectra, must also be noted. No adequate explanation for this anomaly has yet been found. One should, perhaps, be wary of expecting monotonic trends where the magnitude of changes increase with, say, increasing concentration.

These speculations have attempted to extend some ideas on 2^{nd}-order statistics, familiar in the context of wall-bounded flows of homogeneous fluids, to the case of sediment-laden flows. In spite of the suggestiveness of some of the observed results, the cautious remarks made earlier should be kept in mind, in view of the slight differences that stimulate these speculations.

7.2 Higher-order u- and v- statistics

Turbulence intensities and power spectra provide only limited information. Being non-Gaussian, the fluctuating u- and v-signals cannot be characterized entirely by their 2^{nd}-order statistics. Since they are as easily determined as the 2^{nd}-order statistics, the skewness and the flatness are natural candidates for further

examination. These will, however, be more prone to both statistical estimation as well as experimental errors than the lower-order statistics and should be viewed accordingly.

The results on the skewness of the vertical fluctuations for equilibrium-bed and starved-bed experiments are given in Figs. 7.2.1 and 7.2.2, and compared to clear-water envelopes. Although some differences from clear-water results can be seen, e.g., in 2565EQ and 1965ST, a lack of any evident consistency does not support their significance. This reinforces the tentative conclusion drawn earlier that vertical motion is little affected by the suspended sediment. In contrast, the corresponding results for the horizontal fluctuations (Figs. 7.2.3 and 7.2.4) do exhibit consistent differences from the clear-water results. Most notable again is the increase in the same outer region where an increase in horizontal intensities was observed. Remarkable also are the anomalous results for the series, 1957ST-2, which show no increase, and which were also anomalous with regard to the horizontal intensities.

Since these results seem to parallel those on intensities, it may be asked whether a parallel exists for the higher intensities in the region closer to the bed. On this point, interpretation becomes more hazardous. In the discussion on intensities, it has been cautioned that, particularly for the equilibrium-bed experiments, problems of measurement may give rise to spurious results. The significance of the results in the region, $\eta < 0.1$, showing a definite positive skewness (Fig. 7.2.3), is thus rather uncertain.

Flatness factors for the vertical fluctuations are shown in Figs. 7.2.5 and 7.2.6. That almost all of these fall within the relatively narrow envelope of clear-water

Fig. 7.2.1 Skewness of vertical velocity fluctuations in equilibrium-bed experiments distinguished by aspect ratios
a) $b/h = 4.0$, b) $b/h = 4.7$

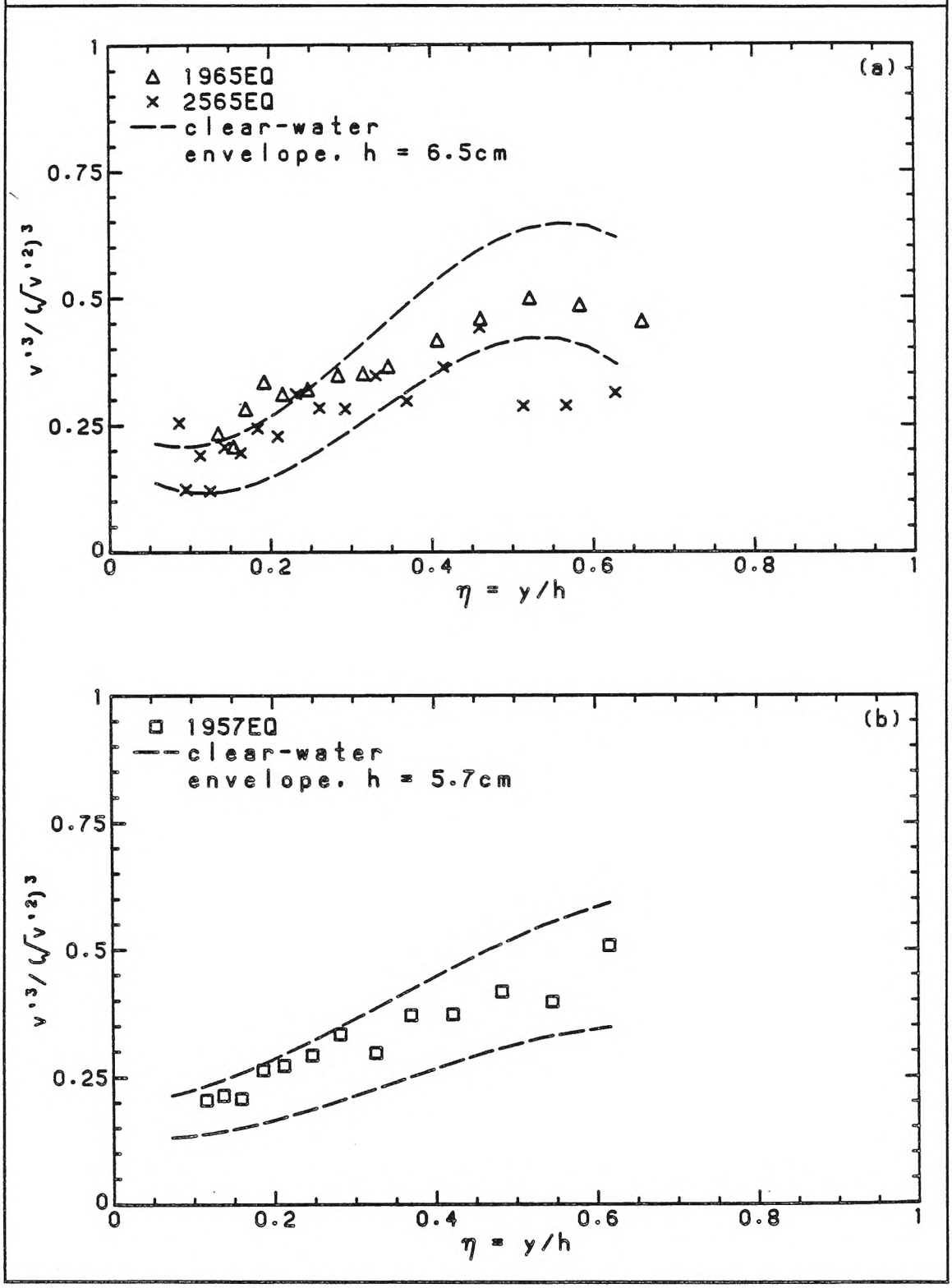

Fig. 7.2.2 Skewness of vertical velocity fluctuations in starved-bed experiments
a) series 1965ST, b) series 1957ST-1, c) series 1957ST-2

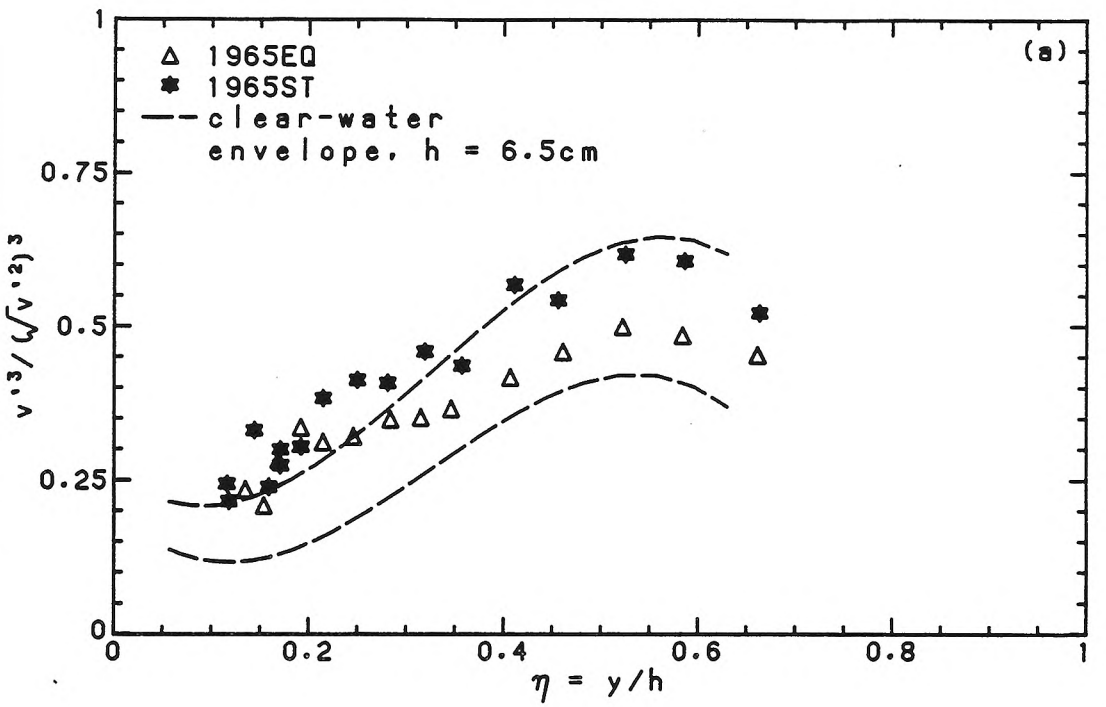

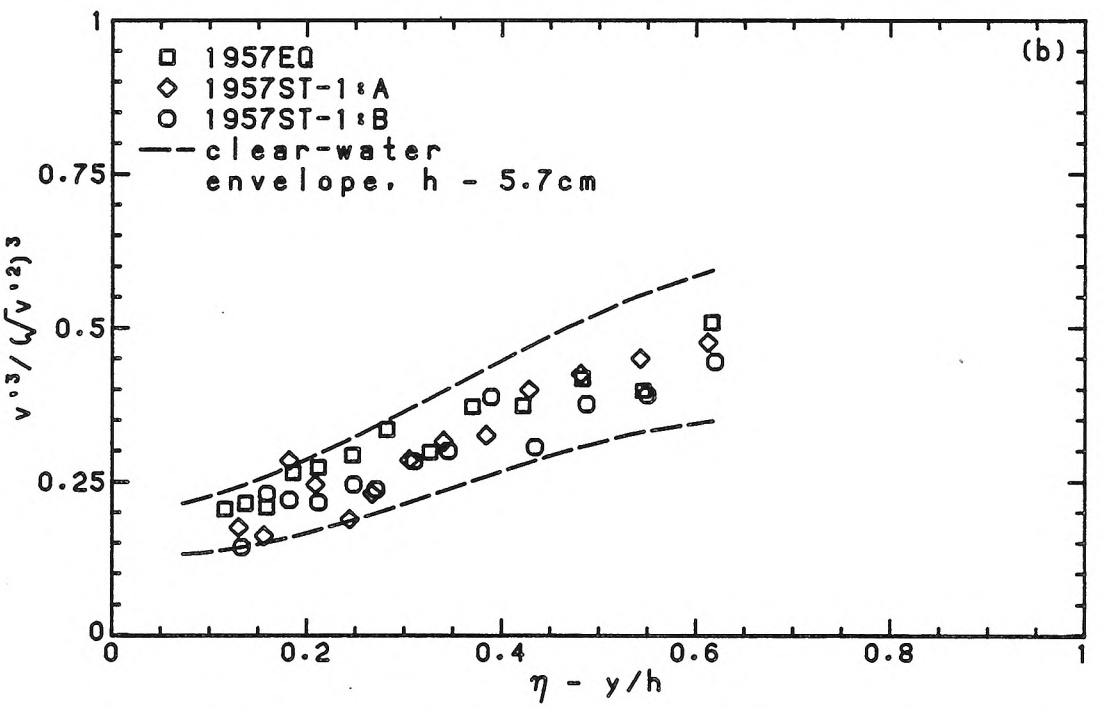

Fig. 7.2.2 c)

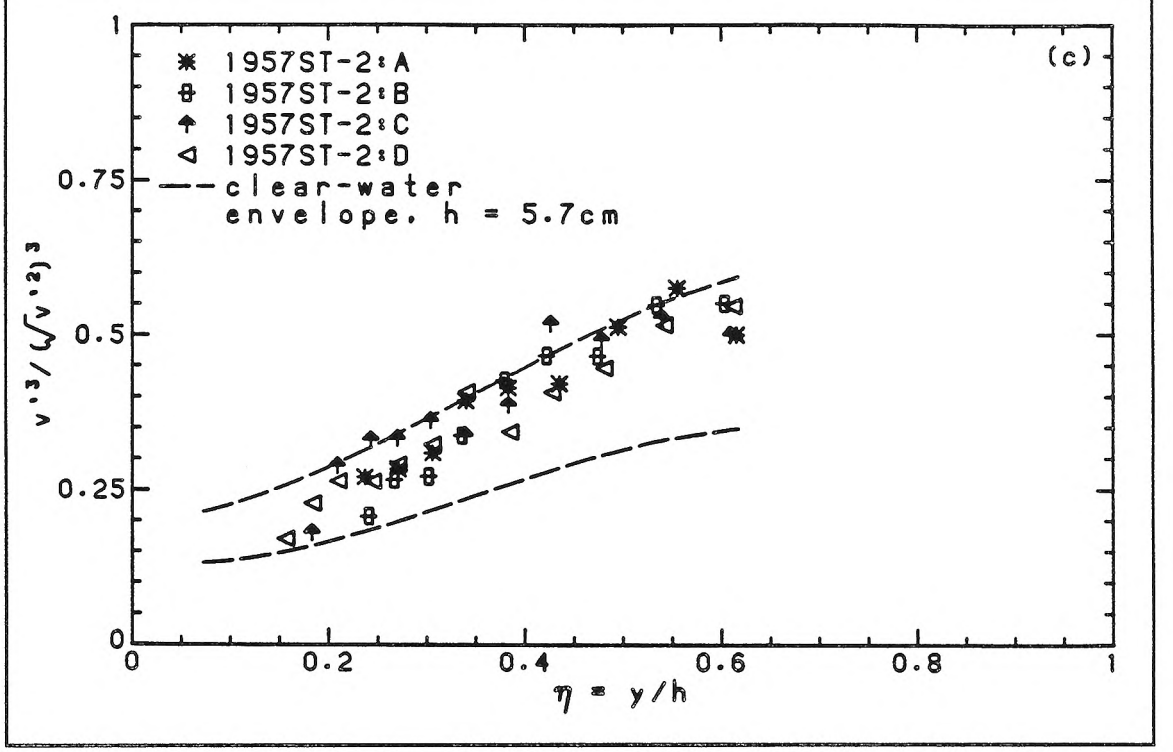

results, while remarkable, should no longer be surprising, in view of the earlier results on the lower-order statistics. On the other hand, the flatness factors for the horizontal fluctuations exhibit, in Figs. 7.2.7 and 7.2.8, the by now expected deviation from clear-water results in the outer region. The anomalous case of 1957ST-2 remains an anomaly. In the near-bed region, some tendency is seen for the flatness factors to decrease towards a value of 3.

The higher-order u- and v-statistics have been shown to be largely consistent with the results of the 2^{nd}-order statistics, both in where they deviate and do not deviate from clear-water results. No evidence has been found in the v-statistics to support the hypothesis that the suspended sediment affects primarily vertical motion. What evidence there is, in both the 2^{nd}- and higher-order statistics, points rather to slight changes in the probability distribution of u. These conclusions

Fig. 7.2.3 Skewness of horizontal velocity fluctuations in equilibrium-bed experiments distinguished by aspect ratios
a) $b/h = 4.0$, b) $b/h = 4.7$

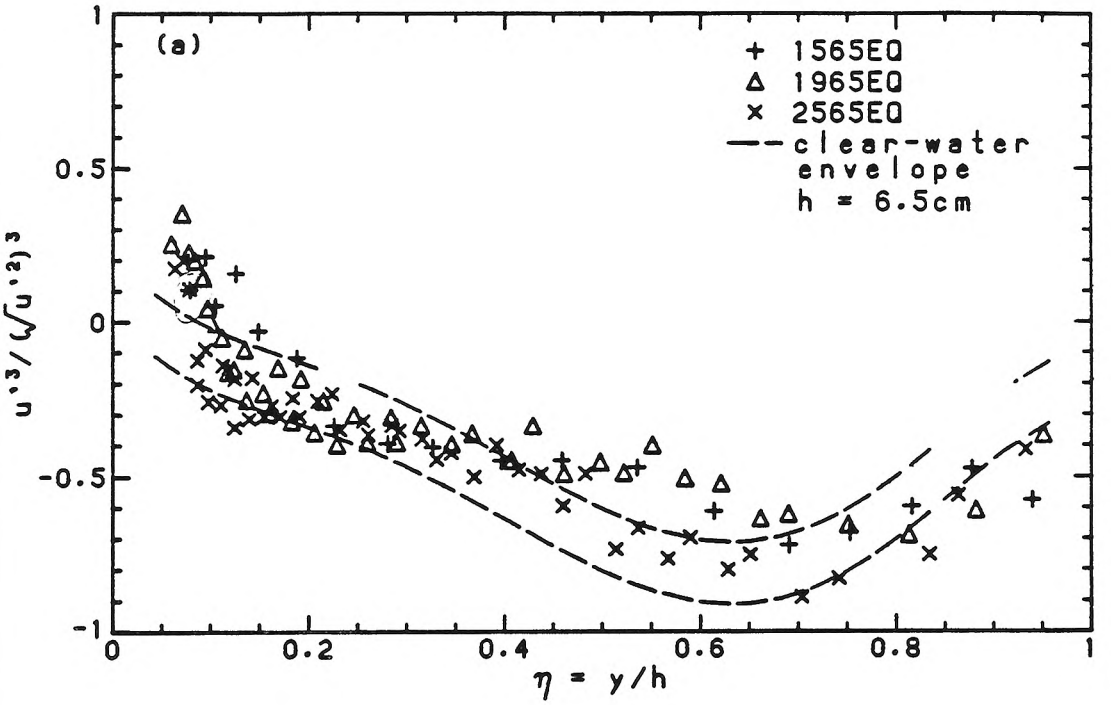

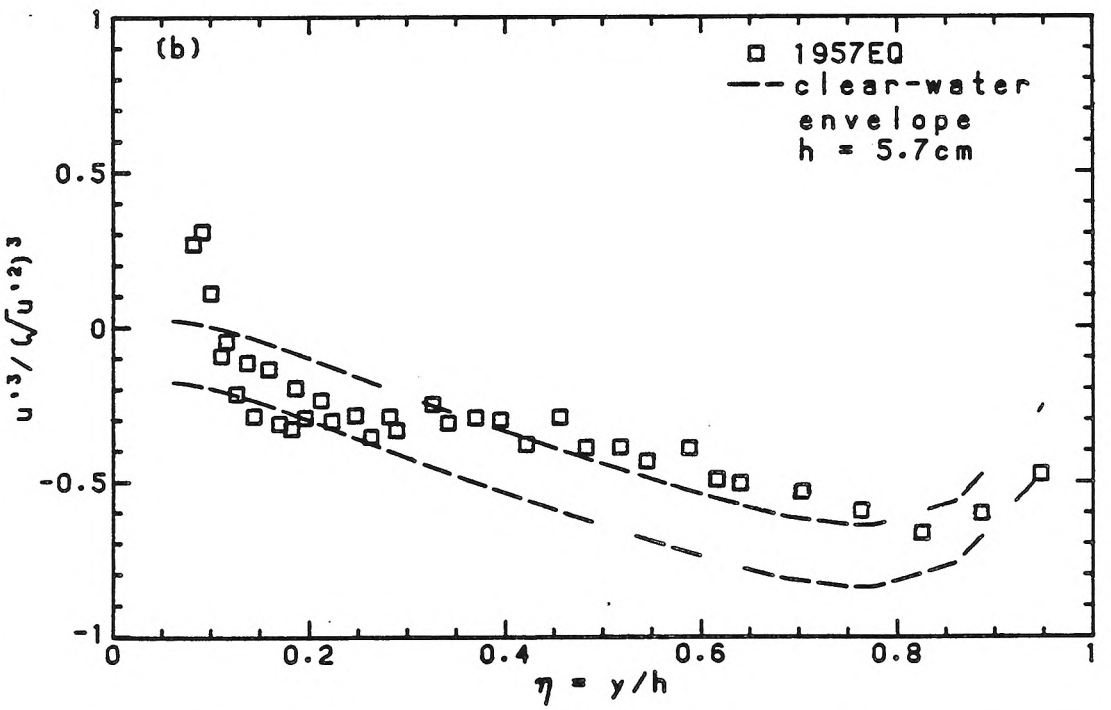

Fig. 7.2.4 Skewness of horizontal velocity fluctuations in starved-bed experiments
a) series 1965ST, b) series 1957ST-1, c) series 1957ST-2

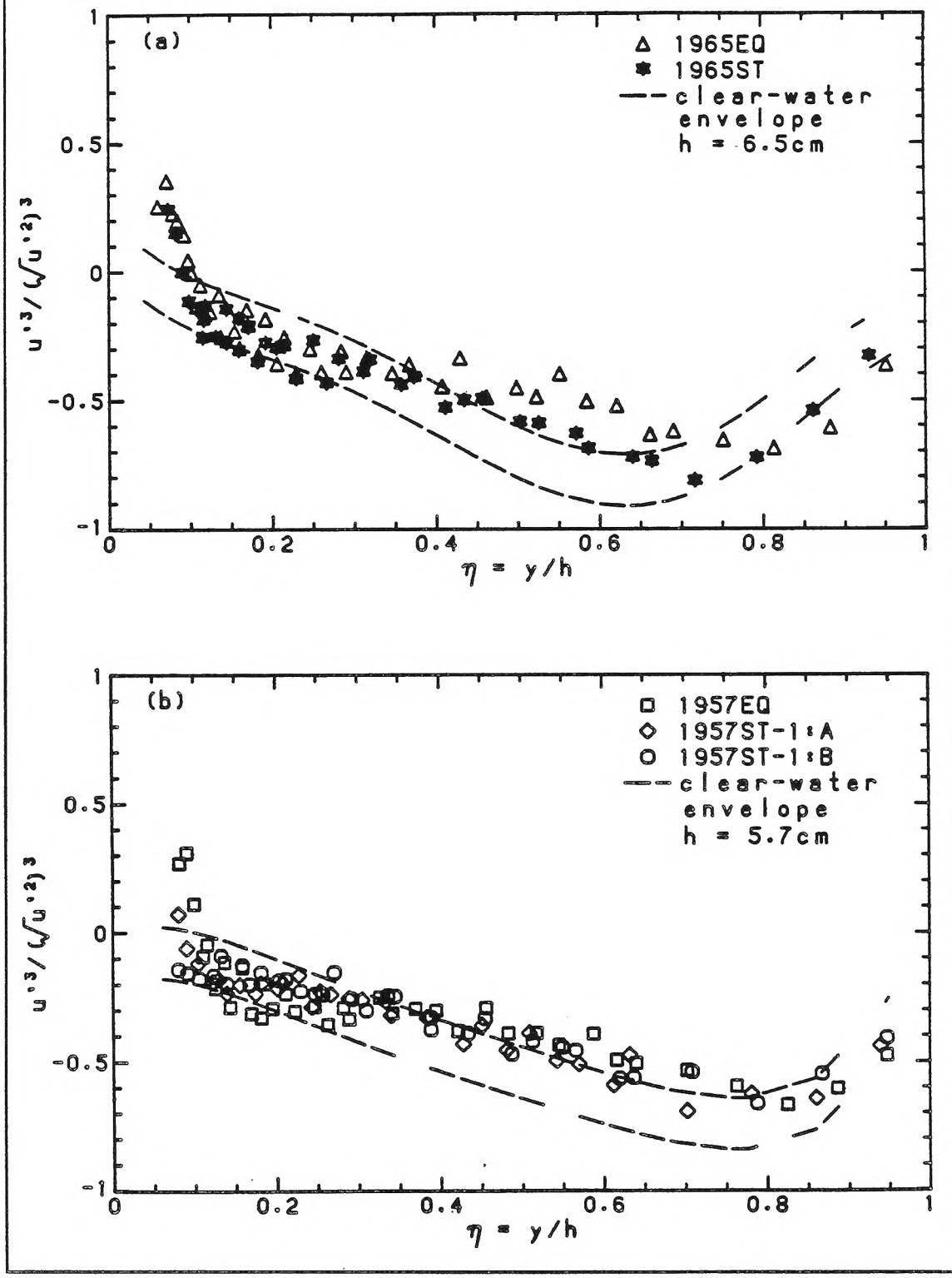

Fig. 7.2.4 c)

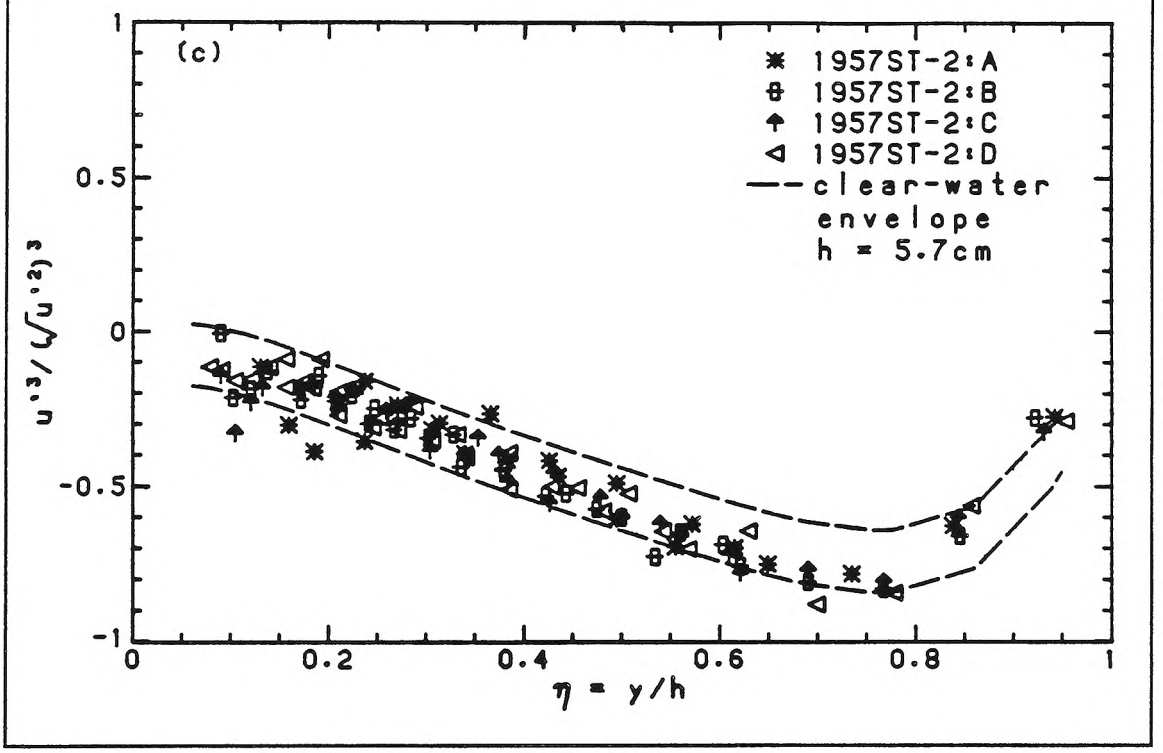

are meant to apply primarily to the flow in the outer region, because the LDV measurements are thought to be more reliable there; slight increases in the horizontal intensities observed in the near-bed regions of starved-bed experiments, while highly suggestive, are more speculative. Some evidence indicates that, with a small suspended load, e.g., in the starved-bed experiments and in 2565EQ, the slight changes observed vanish as they should.

Although the statistical implications of higher-order results (by comparison with the Gaussian standard) are clear, the physical implications are not. Some basis of interpretation may perhaps be found, again, in the idea of rescaling and the analogy with higher-order statistics in the buffer layer of homogeneous-fluid flow. The changes in skewness and flatness, as for the horizontal intensities, in the outer region are interpreted as an extension of the behavior of these statistics

Fig. 7.2.5 Flatness of vertical velocity fluctuations in equilibrium-bed experiments distinguished by aspect ratios
a) $b/h = 4.0$, b) $b/h = 4.7$

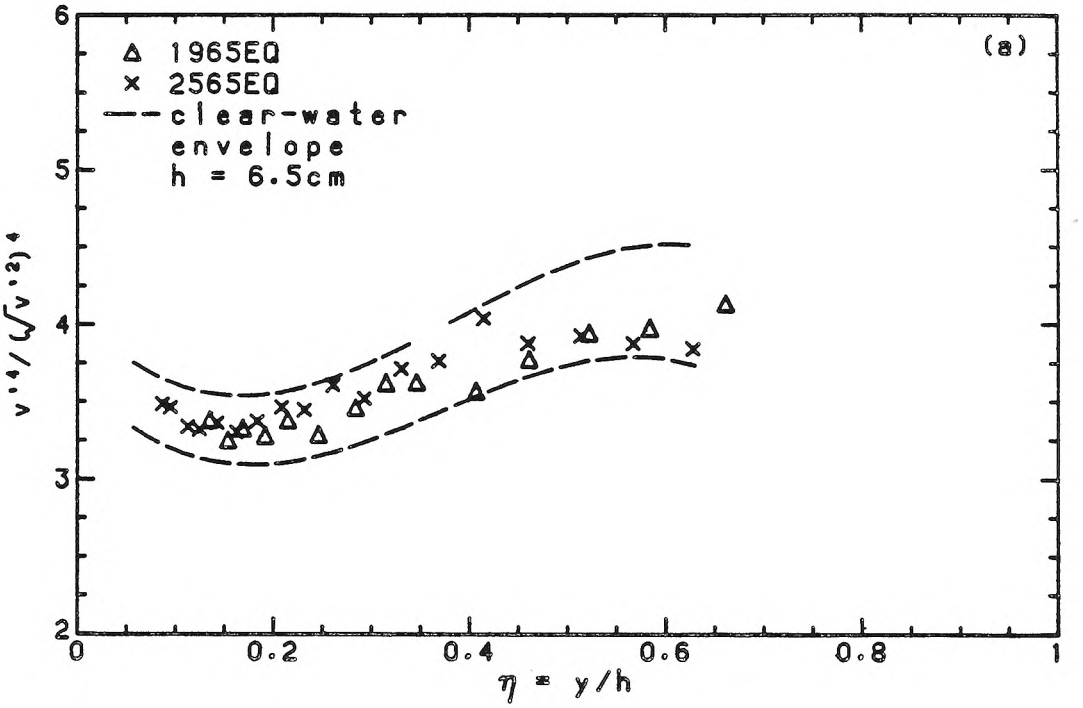

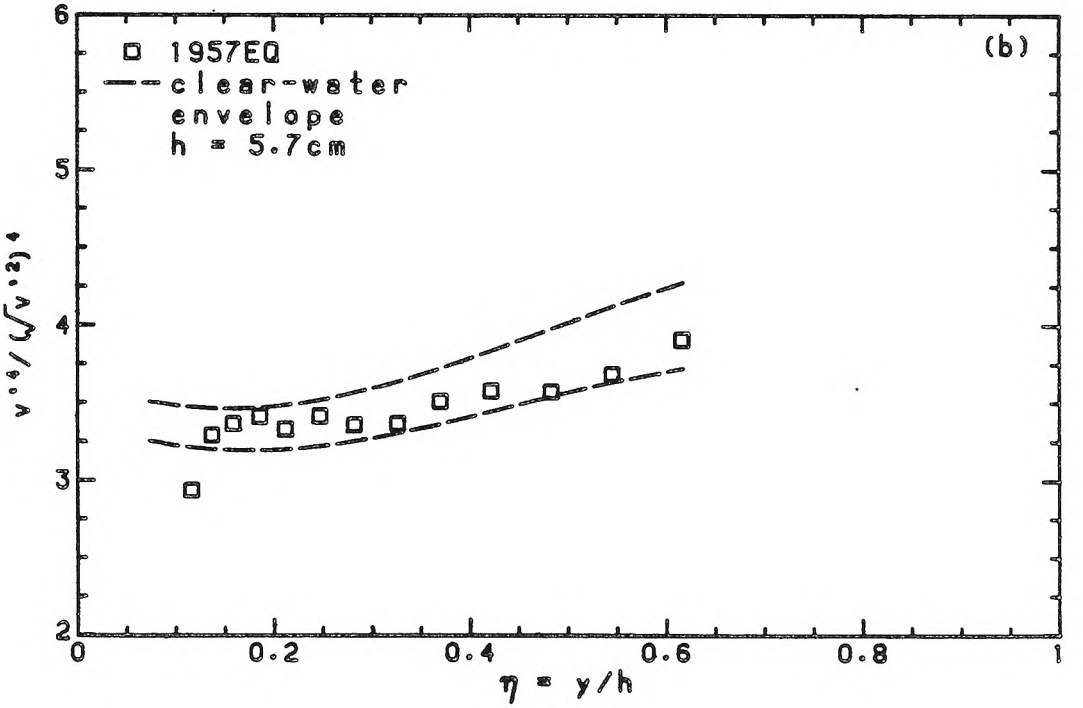

Fig. 7.2.6 Flatness of vertical velocity fluctuations in starved-bed experiments
a) series 1965ST, b) series 1957ST-1, c) series 1957ST-2

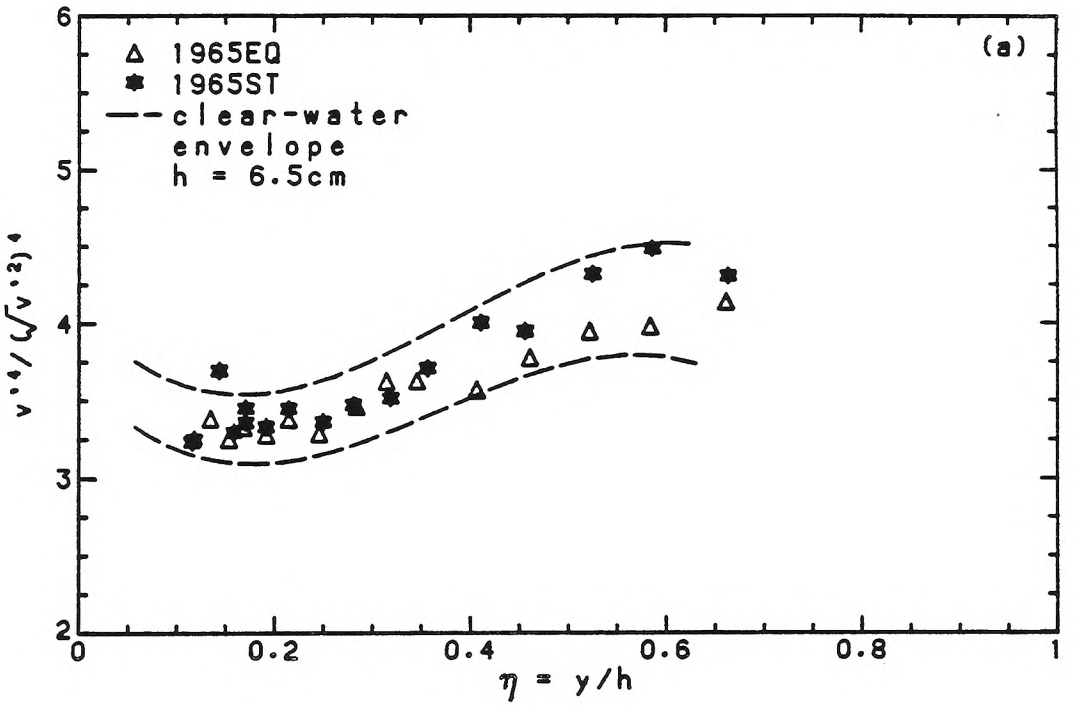

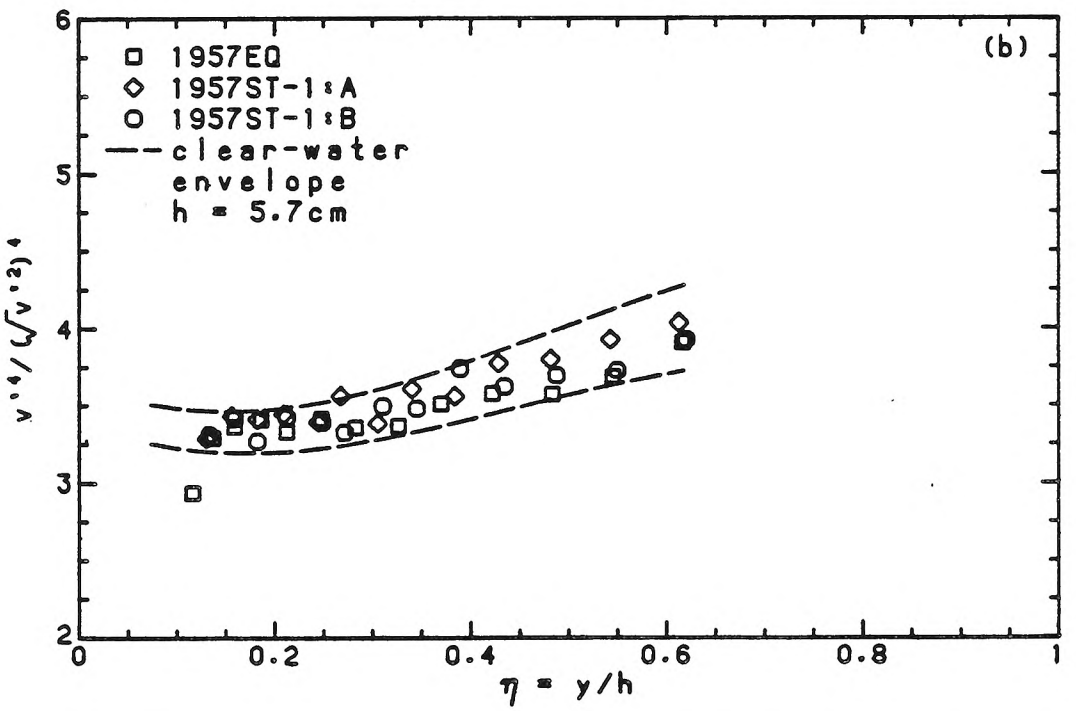

Fig. 7.2.6 c)

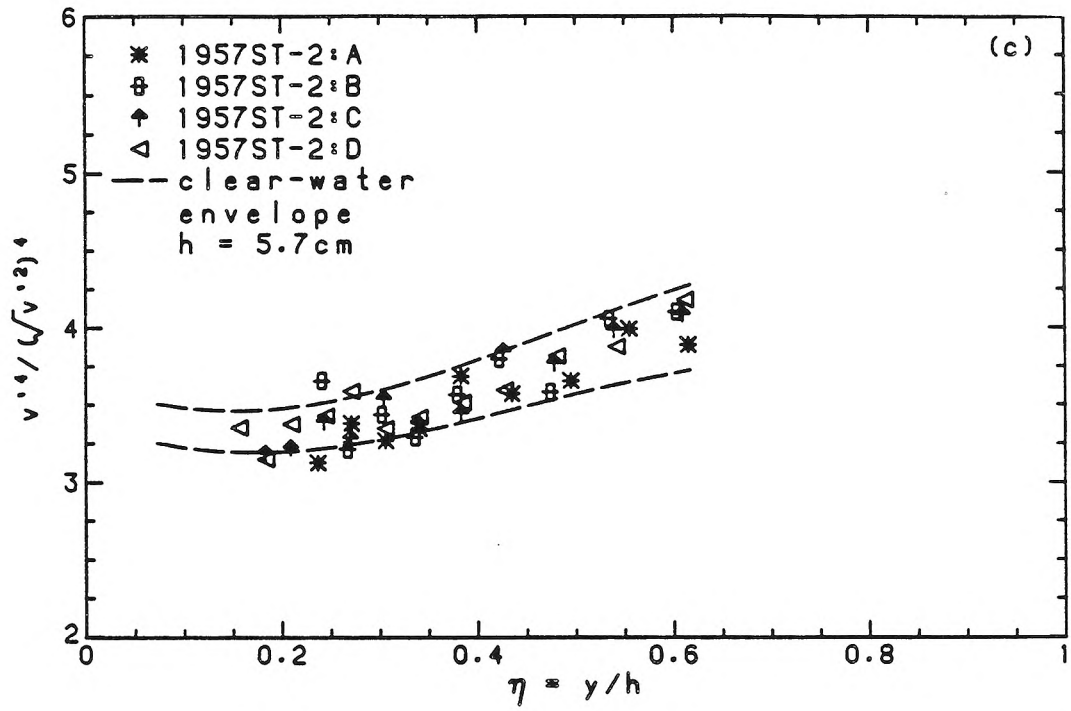

in a region closer to the bed. Thus, the positive skewness and the decrease in the flatness factor observed in sediment-laden flows at $\eta \approx 0.1$ have counterparts in the buffer layer.

7.3 Results on Reynolds-stress statistics

The statistics of Reynolds' stress are of interest because they bring out clearly the highly intermittent structure of turbulent transport. Whether the presence of sediment affects these statistics is, therefore, of interest.

In Figs. 7.3.1-7.3.4 are shown the results for the correlation coefficient and the central moments of the Reynolds stress. In none of these is there any definite evidence of any effect ascribable to the presence of sediment. To some extent, this reflects the substantial scatter already present in the results for the clear-water

Fig. 7.2.7 Flatness of horizontal velocity fluctuations in equilibrium-bed experiments distinguished by aspect ratios
a) $b/h = 4.0$, b) $b/h = 4.7$

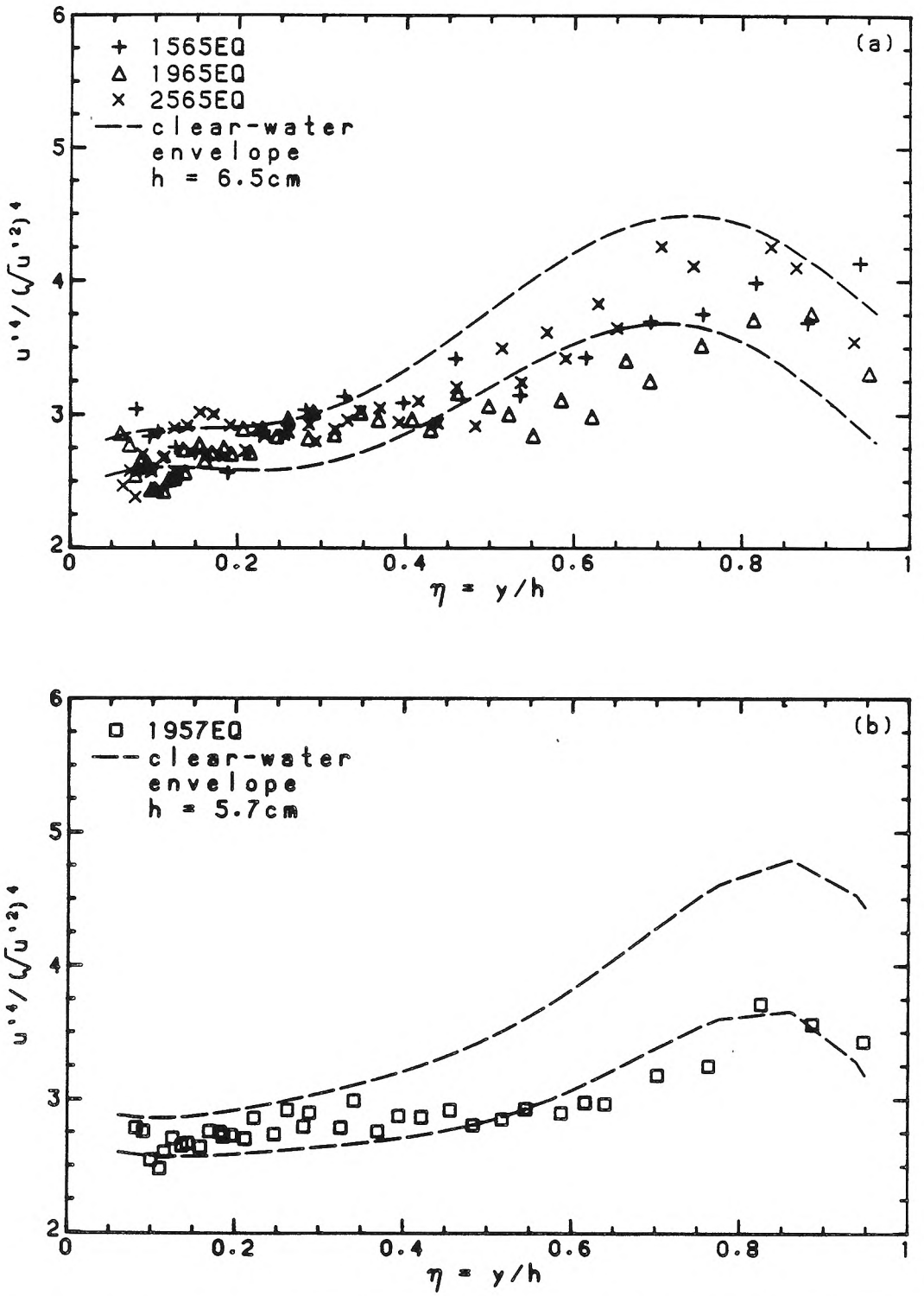

Fig. 7.2.8 Flatness of horizontal velocity fluctuations in starved-bed experiments
a) series 1965ST, b) series 1957ST-1, c) series 1957ST-2

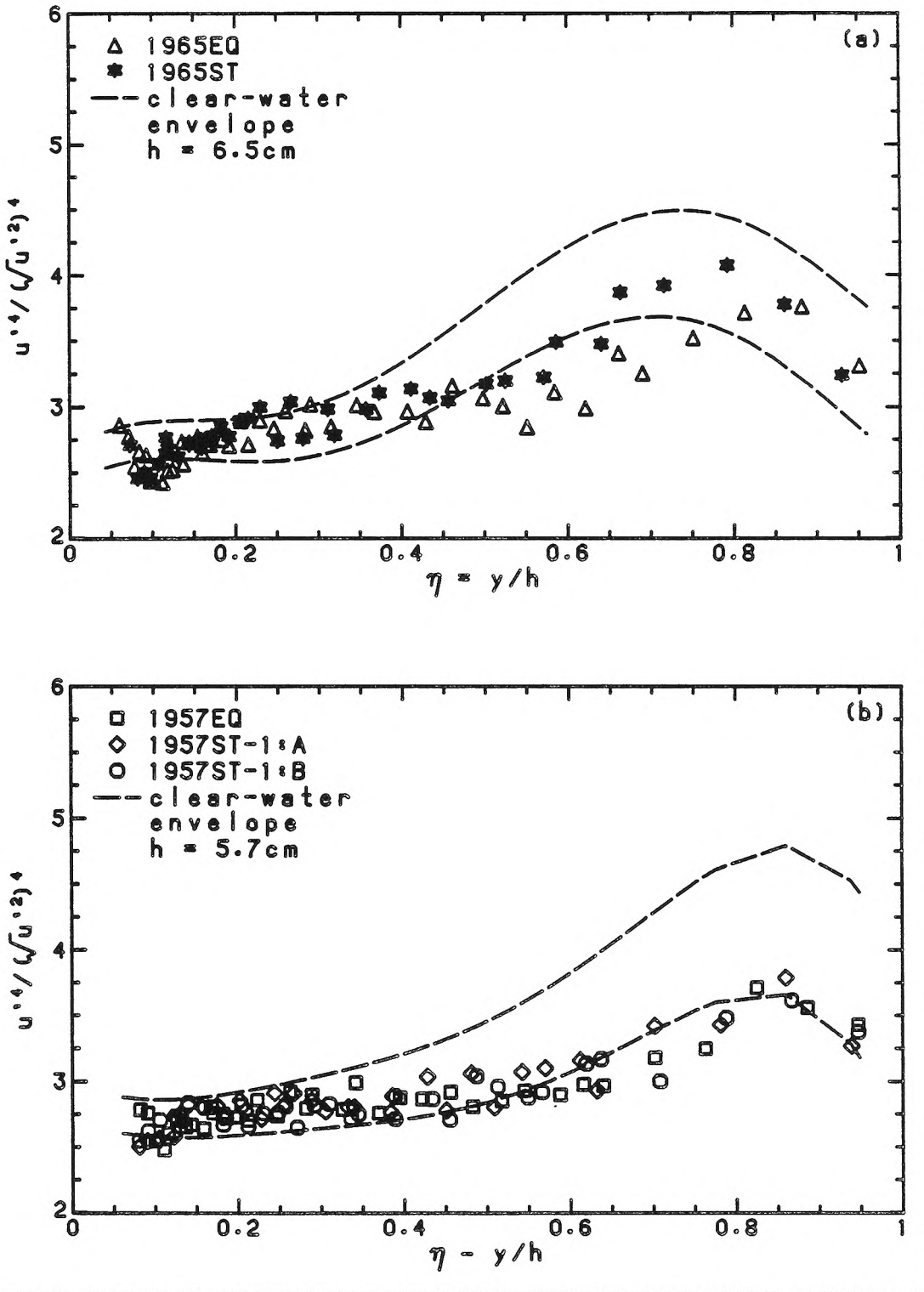

Fig. 7.2.8 c)

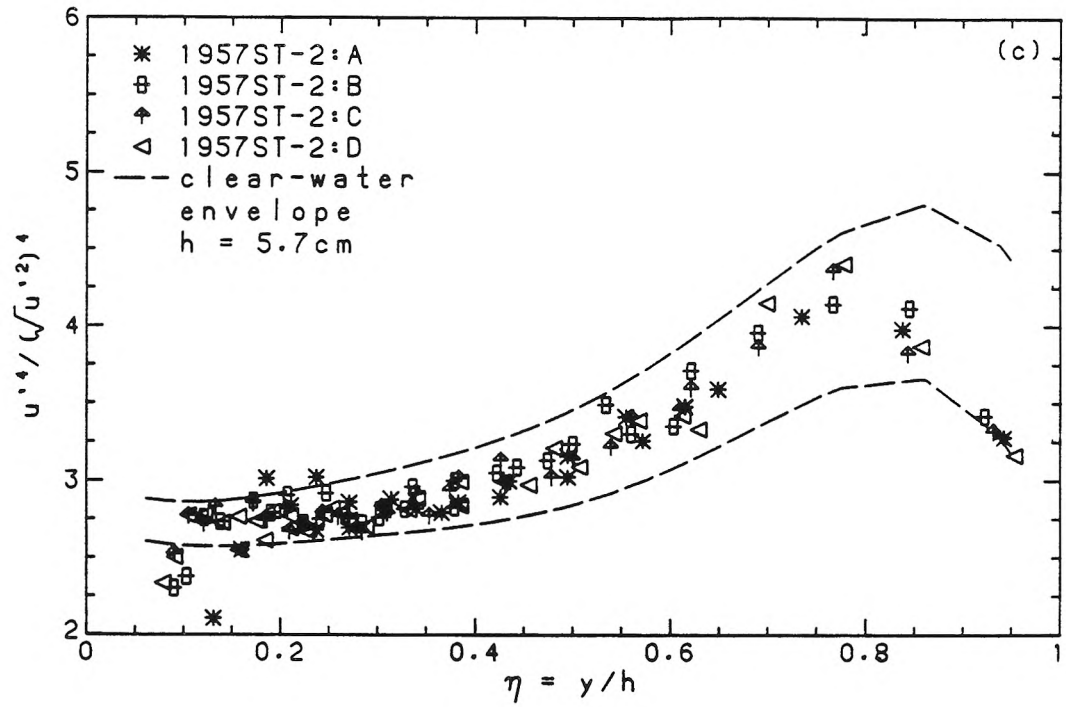

experiments, which were conducted under relatively "ideal" conditions. The slight effects found in the u-statistics would, for example, be submerged completely in the scatter. Further, like the v-statistics, reliable Reynolds-stress statistics are available only in a limited region, $0.2 \leq \eta \leq 0.6$. In spite of these qualifications, it is difficult to arrive at any conclusion other than that, in the range of experimental conditions studied, the presence of sediment does not significantly alter the statistics of the Reynolds stress. Although information about phase relationships are not contained in these time-averaged statistics, this might be tentatively taken to imply no significant alteration in the structure of turbulence. Additional evidence from an examination of the contribution to the total Reynolds stress from each quadrant of the u'-v' plane is presented in Appendix A.1.

Fig. 7.3.1 a) Correlation coefficients, b) Intensities of Reynolds-stresses in equilibrium-bed experiments

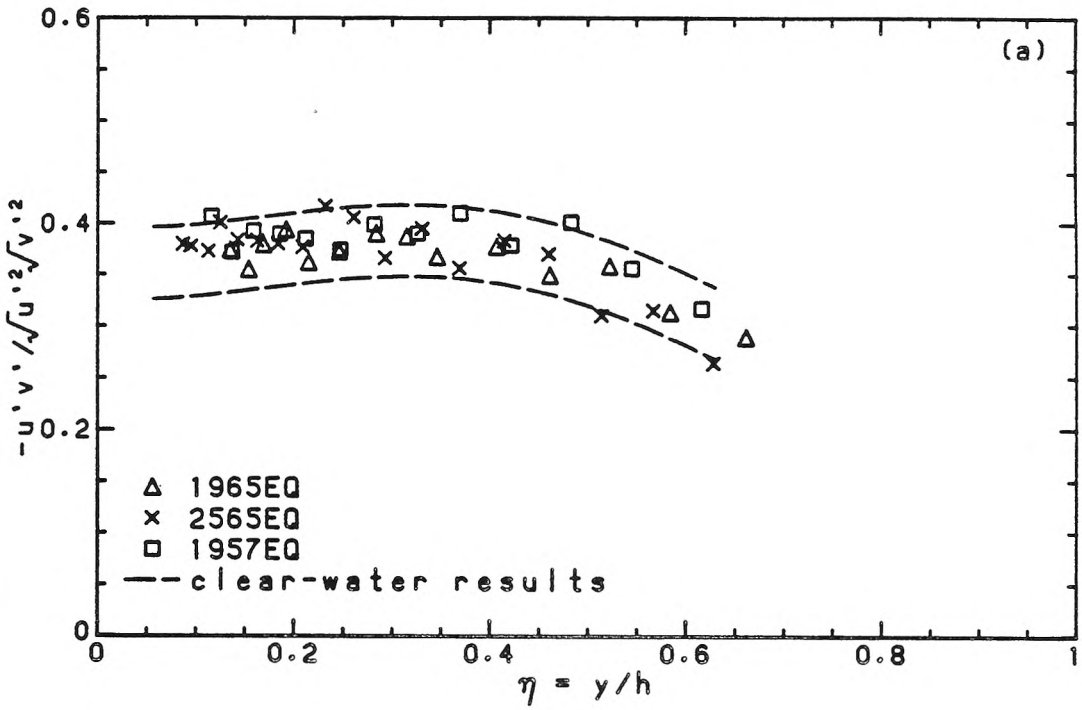

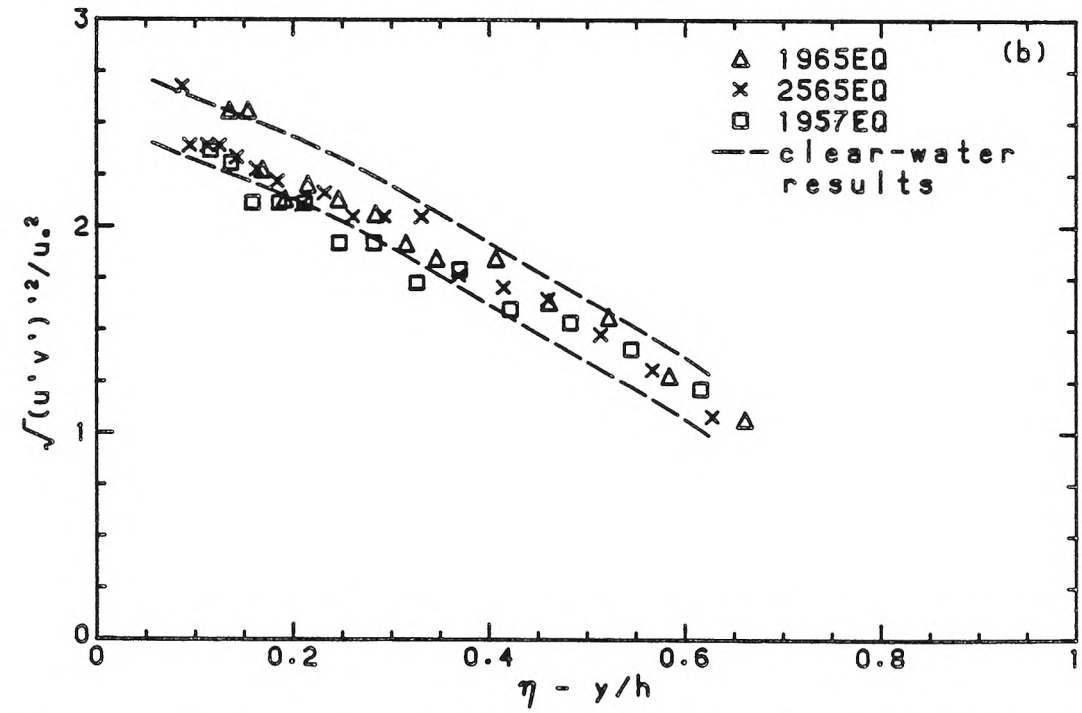

Fig. 7.3.2 a) Correlation coefficients, b) Intensities of Reynolds-stresses in starved-bed experiments

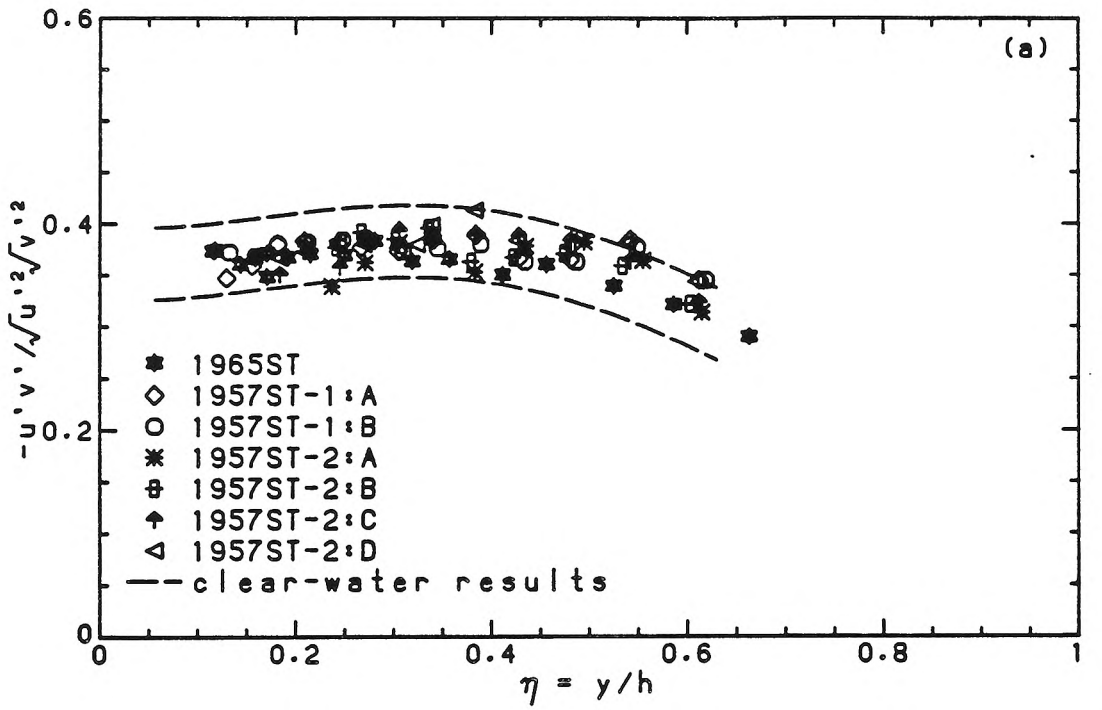

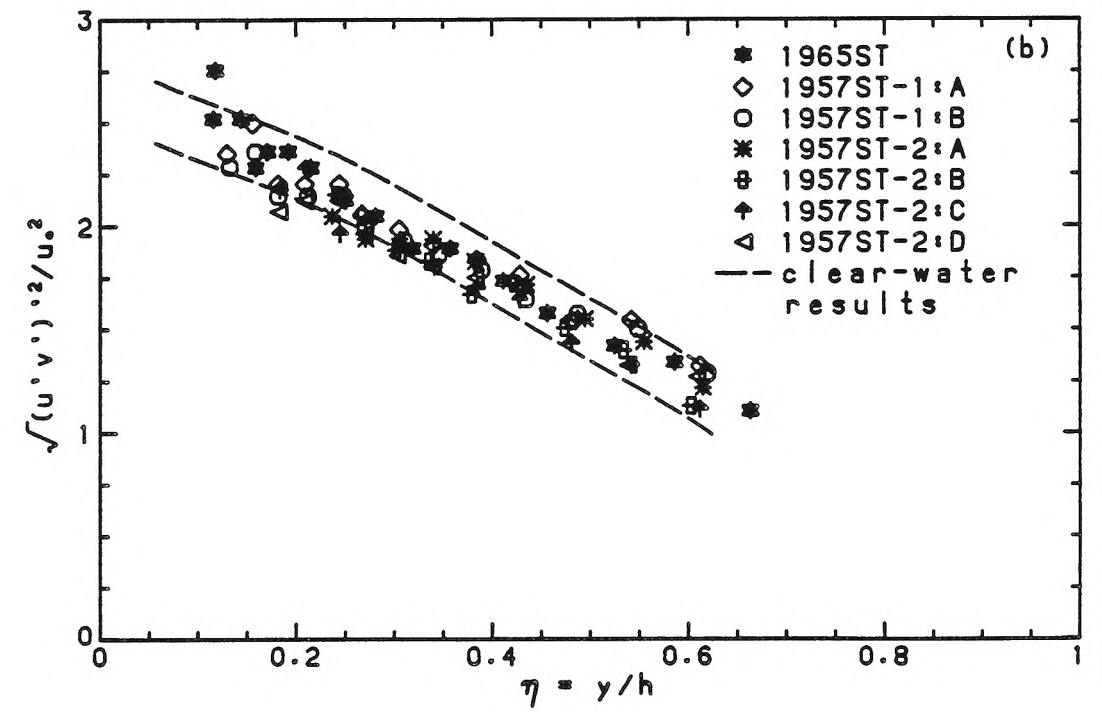

Fig. 7.3.3 a) Skewness, b) Flatness of Reynolds-stresses in equilibrium-bed experiments

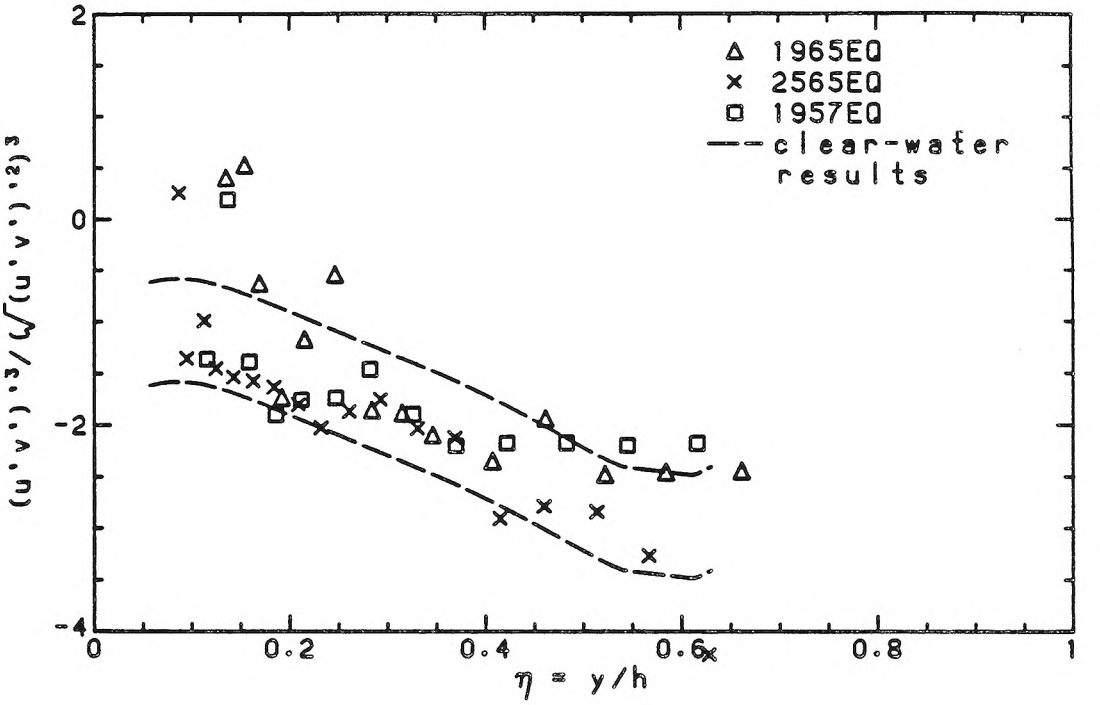

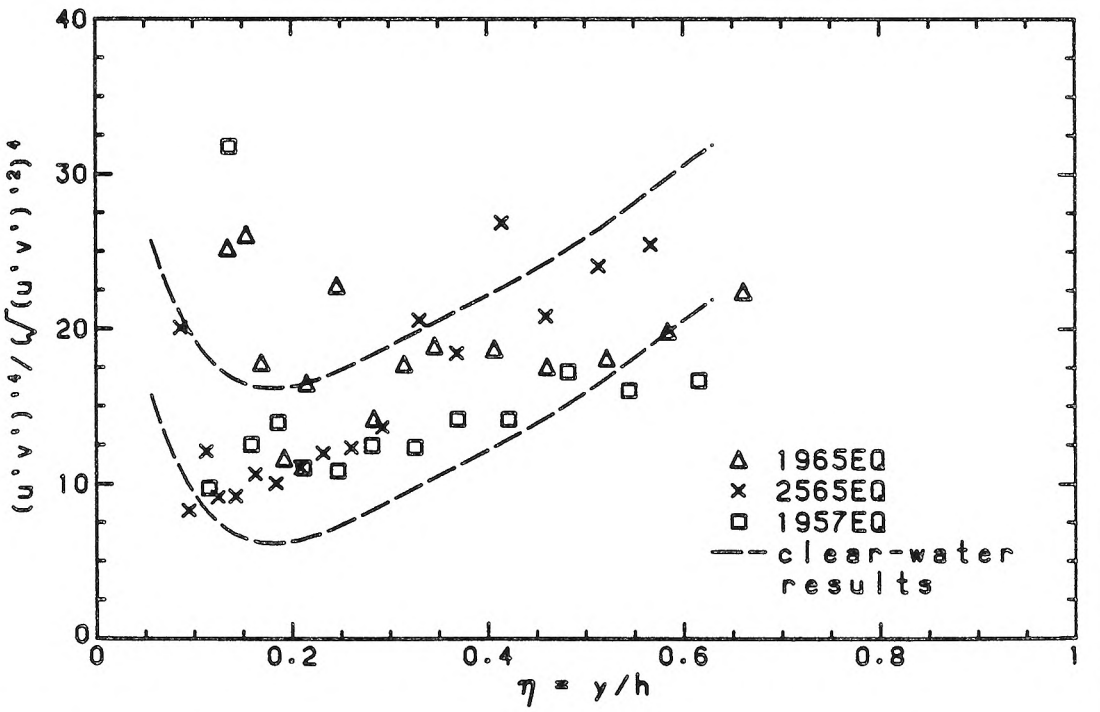

Fig. 7.3.4 a) Skewness, b) Flatness of Reynolds-stresses in starved-bed experiments (symbols as in Fig. 7.3.2)

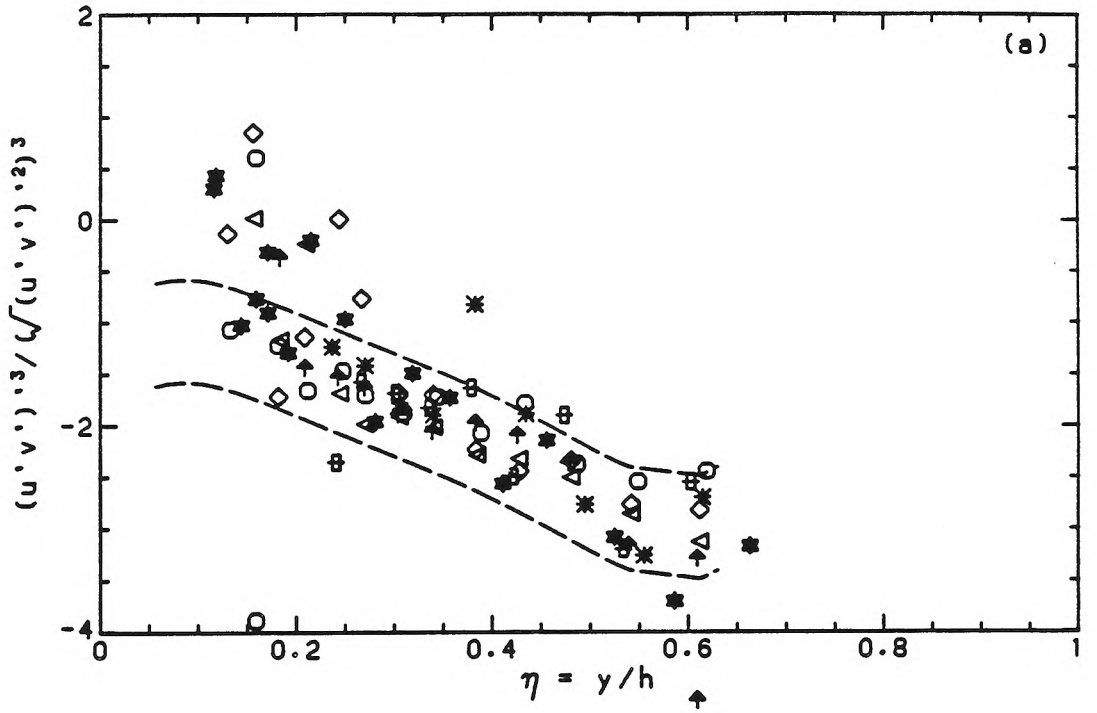

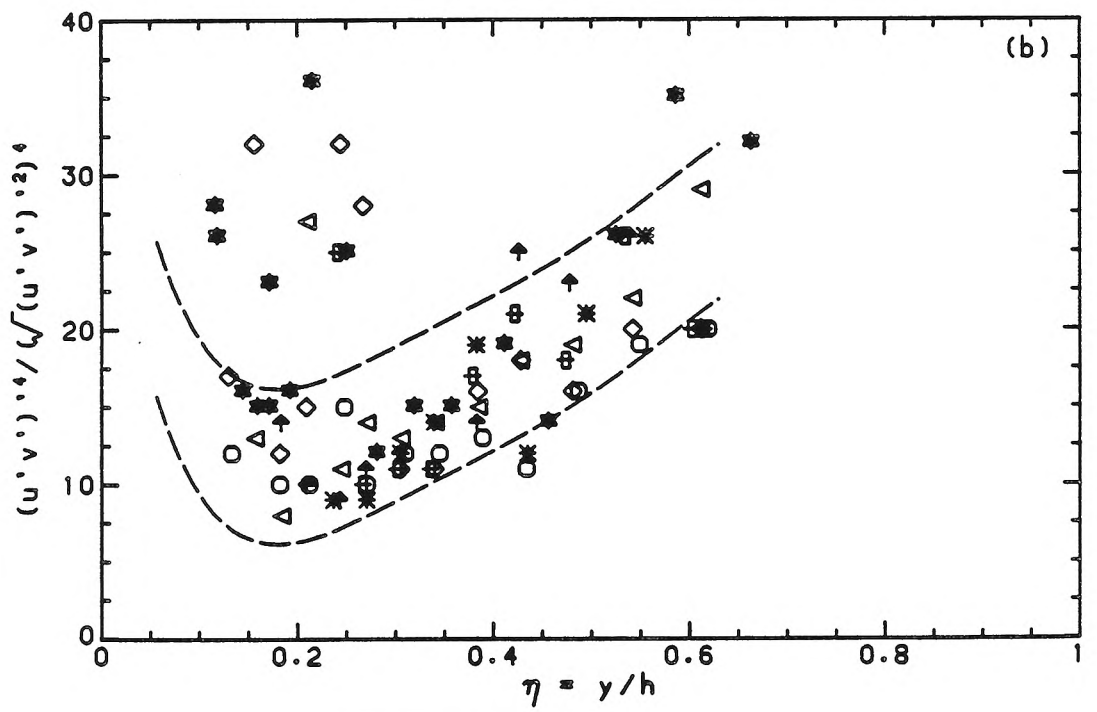

7.4 Summary

Examination of the statistics of the fluctuating field has yielded a negative result in the sense that no dramatic changes due to the presence of sediment could be definitely observed. Because measurements become more reliable with increasing distance from the bed, this negative result should be qualified as being more applicable to the outer flow region. It is, therefore, interpreted as supporting the claim that the effect of sediment is felt primarily in the region closer to the bed. The null results for the v-statistics are also significant because they indicate the inadequacy of any simple model of turbulence "damping". Indeed, if any evidence for changes in the fluctuating field have been found, these have been in the u-statistics. Thus, horizontal intensities were found to be increased in the outer region and, less certainly, in the near-bed region. Power spectra indicate that the scale of dissipation increases in the presence of sediment rather than that larger scales are inhibited. A basis for interpreting results in terms of rescaling and of an analogy with the turbulence characteristics of the buffer layer of an homogeneous-fluid flow is suggested.

8. Summary

8.1 Experimental results

Experiments in turbulent, sediment-laden, uniform open-channel flows over nominally flat beds, both saturated and unsaturated, were performed. Three sand sizes (d_{50} = 0.15 mm, 0.19 mm, 0.24 mm) were used, and ratios of w_{s0}/u_* = 0.46, 0.62, 0.76 were obtained. The experiments were conducted in a tiltable recirculating flume (26.7 cm wide, 13 m long). The laser-Doppler technique was used to obtain extensive one- and two-component velocity measurements. Detailed vertical profiles of local concentration were also made using the traditional suction-sampling technique.

The following observations were made regarding the mean-velocity profile:

i) The shape of the velocity-defect profiles was unchanged from that of clear-water flows *except* in a region of limited extent near the bed.

ii) The affected region exhibited larger velocity defects *and* larger velocity gradients than in clear-water flows.

iii) The extent of this region varies with hydraulic and grain parameters but does not scale with either the viscous scale or the grain diameter.

iv) Flow resistance was typically found to be greater than that of the corresponding clear-water flow of the same Reynolds number ($4ur_h/\nu$) and relative roughness ($d_{50}/4r_h$).

The following observations were made regarding the statistics of the fluctuating velocity field:

i) No consistent effect of sediment was found in the statistics of the vertical velocity fluctuations.

ii) Small but consistent effects in the outer region ($y/h > 0.5$) were found in the statistics of the horizontal velocity fluctuations; for example, $\sqrt{u'^2}/u_*$ showed consistent increases of 5%–10%. Evidence of smaller effects in the inner region ($y/h < 0.2$) was also found but may be more questionable.

iii) Normalized power spectra indicate relatively less energy content in the smaller scales and more in larger scales than those observed in clear-water flows, but the effects are small.

8.2 Interpretations of the experimental results

8.2.1 The traditional model

This traditional model characterizes the mean-velocity profile by a log-law throughout the flow with a reduced von Kàrman constant. While this model may be of use in engineering applications, it does not follow in detail the experimental results. It implies that the effect of suspended sediment is felt in the velocity profile throughout the flow. The present experiments show that this need not be so, and that marked effects may be observed in a region of only limited extent.

As has been noted by previous workers, the original Rouse equation describing the concentration profile was found to be an inadequate if applied to the entire

flow region. Fitted only to the lower half of the flow, it underestimated local concentrations in the upper half. Although a good fit may be obtained for the profile nearer the bed, a simpler power-law fit would perform as well.

8.2.2 Models based on a stratified-flow analogy

The implications for the velocity field of a stratified-flow analogy would be several:

i) the effects of sediment should be felt primarily in the upper flow;

ii) conversely, the near-bed region should be dominated by boundary-shear turbulence and essentially unaffected by an effective stratification due to the suspended sediment;

iii) The velocity gradient in the near-bed region should be the same as in clear-water flows (for given u_*), and elsewhere should be at least equal or greater, implying that flow resistance should decrease in sediment-laden flows;

iii) the effective stable stratification, in inhibiting vertical transport, should be reflected

   a) in a damping of vertical turbulence intensity, and

   b) in a reduced importance of larger scales to smaller scales.

Since none of the above implications is supported by the present experimental results, the stratified-flow analogy appears to have limited applicability in modelling dilute sediment-laden flows.

8.2.3 The proposed similarity model

The proposed similarity model is based on similarity hypotheses from which general results are deduced. Neither balance equations nor an eddy-diffusivity model is invoked. Specific scales are suggested in a more specific model. This

model applies strictly only to flows over flat beds in equilibrium with the suspension, but may have implications for more general flows.

The characteristics of the proposed basic model are:

i) the effects of sediment are confined to a limited region of extent, l_s (this is a hypothesis rather than a result);

ii) if $l_s/h \ll 1$, then

   a) a region exists where a logarithmic velocity profile, with the same value of κ as in clear-water flows, is approached;

   b) the wake or outer-flow component of the velocity profile is unaffected by the presence of sediment;

   c) the concentration profile in the region where the velocity profile is approximately logarithmic may be described by a power law with a possibly varying exponent;

   d) a wake or outer-flow component in the concentration profile exists;

   e) an inner component in the concentration profile exists in which the concentration profile deviates from the asymptotic power law in the affected region;

   f) for $y \gg l_s$, the standard velocity-defect profile for clear-water flows may be used, and a concentration profile of the form,

$$\frac{c}{c_h} = \left(\frac{y}{h}\right)^Z \left(1 - \frac{y}{h}\right)^{Z_h}, \tag{8.2.1}$$

   is suggested, where c_h, Z, and Z_h are related to physical parameters;

iii) if $l_s \sim h$, then the model does not give any definite result.

The proposed scales for the specific model are

$$\Delta_s \equiv \frac{g(s-1)l_s}{u_*^2} = \Xi\left(\frac{w_{s0}}{u_*}, \frac{g(s-1)d_{50}}{w_{s0}^2}\right), \tag{8.2.2}$$

$$Z = Z\left(\frac{w_{s0}}{u_*}\right), \tag{8.2.3a}$$

$$Z_h = Z_h\left(\frac{w_{s0}}{u_*}\right), \tag{8.2.3b}$$

$$c_s = \left[\frac{u_*^2}{g(s-1)l_s}\mathcal{E}_s\left(\frac{w_{s0}}{u_*}\right)\right]^Z, \tag{8.2.4a}$$

$$c_h = \left[\frac{u_*^2}{g(s-1)h}\mathcal{E}_h\left(\frac{w_{s0}}{u_*}\right)\right]^Z, \tag{8.2.4b}$$

where c_s and c_h are inner and outer concentration scales, and Z and Z_h are the exponents in the suggested concentration profile. With these scales, Eqn. 8.2.1 becomes

$$c = \left[\frac{u_*^2}{g(s-1)y}\mathcal{E}_h\left(\frac{w_{s0}}{u_*}\right)\right]^Z \left(1-\frac{y}{h}\right)^{Z_h}. \tag{8.2.5}$$

If $l_s/d_{50} \gg 1$, it is hypothesized that, in the region, $y/l_s \geq O(1)$, Eqn. 8.2.2 and 8.2.4a may be simplified to

$$\Delta_s = \Xi_\infty\left(\frac{w_{s0}}{u_*}\right), \tag{8.2.2'}$$

$$c_s = c_{s\infty}\left(\frac{w_{s0}}{u_*}\right). \tag{8.2.4a'}$$

Except for the implication (ii e), the experimental results are consistent with the similarity model at the qualitative level. Evidence for the implication (ii e) was found in only a single data set. The length scale, l_s, was operationally defined for the purposes of determining the correlation, Eqn. 8.2.2', as approximately where the velocity profile begins to deviate from the clear-water profile as y/h decreases. In cases where an inner layer can be distinguished and l_s is well defined ($0.05 \leq l_s/h \leq 0.2$), fair correlations between Z, Z_h, c_s, Δ_s and w_{s0}/u_* were found for nominally flat-bed equilibrium-bed flows.

8.3 Open questions

This study has, perhaps, raised more questions than it has answered. The following come to mind:

i) The traditional model and those based on the stratified-flow analogy were found inapplicable to the present range of experimental conditions; would either or both be more appropriate for *other* conditions, e.g., a heavier suspended load ($w_{s0}/\kappa u_* < 1$?)?

ii) If the proposed similarity model is to be more useful in engineering practice,

   a) what are the limits of validity of the suggested correlations, e.g., the neglect of the dimensionless grain diameter, $g(s-1)d_{50}/w_{s0}^2$, the behaviour for small w_{s0}/u_*?

   b) what can be done in cases where l_s is ill defined, e.g., when $l_s \sim h$?

iii) In spite of the havoc created by the presence of a high concentration of particles near the boundary, the turbulence characteristics in the outer-flow region display a remarkable stability; how can this be reconciled with recent views of wall turbulence in homogeneous fluids which focus on instabilities occurring just outside the viscous sublayer?

References

Alfredsson, P.H. and Johansson, A.V. (1982) "On the Structure of Turbulent Channel Flow," *Journal of Fluid Mechanics*, **122**, 295-314.

Alfredsson, P.H. and Johansson, A.V. (1984) "On the Detection of Turbulence-Generating Events," *Journal of Fluid Mechanics*, **139**, 325-345.

Barenblatt, G.I. (1953) "On the Motion of Suspended Particles in a Turbulent Flow," *Prikl. Mat. Mekh.* **16**, no. 1, 67-78.

Barenblatt, G.I. (1979) *Similarity, Self-Similarity, and Intermediate Asymptotics*, translated from the Russian, Consultants Bureau, New York.

Barenblatt, G.I. and Z'eldovich, Ya. B. (1972) "Self-Similar Solutions as Intermediate Asymptotics," *Annual Review of Fluid Mechanics*, **4**, 285-312.

Barton, J.R. and Lin, P-N. (1955) *A Study of the Sediment Transport in Alluvial Streams*, Civil Engineering Dept. , Colorado A & M College, Fort Collins, Colorado.

Batchelor, G.K. (1965) "The Motion of Small Particles in Turbulent Flow," *Proceedings of the* 2^{nd} *Australasian Conference on Hydraulics and Fluid Mechanics*, O19-O41.

Blinco, P.H. and Partheniades, E. (1971) "Turbulence Characteristics in Free Surface Flows over Smooth and Rough Boundaries," *Journal of Hydraulic Research*, **9**, No. 1, 43-68.

Bohlen, W.F. (1969) *Hot Wire Anemometer Study of Turbulence in Open-Channel Flows Transporting Neutrally Buoyant Particles*, Rept. 69-1, Experimental Sedimentology Lab., Dept. of Earth and Planetary Sciences, MIT, Cambridge, Mass.

Bradshaw, P. (1976) "Introduction," in *Turbulence*, ed. P. Bradshaw, Springer-Verlag, Berlin, 1-44.

Brooks, N.H. (1954) *Laboratory Studies of the Mechanics of Motion of Streams Flowing over a Movable-Bed of Fine Sand*, Ph.D thesis, California Institute of Technology, Pasadena.

Brownlie, W.R. (1981) *Prediction of Flow Depth and Sediment Discharge in Open Channels*, Rept. KH-R-43A, W.M.Keck Laboratory of Hydraulics and Water Resources, California Institute of Technology, Pasadena, Calif.

Buchhave, P., George, Jr., W.K., and Lumley, J.L. (1979) "The Measurement of Turbulence with the Laser-Doppler Anemometer," *Annual Review of Fluid Mechanics*, **11** 443-503.

Coleman, N.L. (1969) "A New Examination of Sediment Suspension in Open Channels," *Journal of Hydraulic Research*, **7**, No. 1, 1969, 61-82.

Coleman, N.L. (1981) "Velocity Profiles with Suspended Sediment," *Journal of Hydraulic Research*, **19**, no. 3, 211-229.

Coleman, N.L. (1985) "Effects of Suspended Sediment on Open Channel Velocity Distribution," *Euromech 192 on Transport of Suspended Solids in Open Channels*, June 11-15, 1985, Munich, Federal Republic of Germany, A2:1-14.

Coleman, N.L. and Alonso, C.V. (1983) "Two-Dimensional Channel Flows over Rough Surfaces," *Journal of Hydraulic Engineering*, **109**, No. 2, 175-188.

Coles, D. (1956) "The Law of the Wake in the Turbulent Boundary Layer," *Journal of Fluid Mechanics*, **1**, 191-226.

Coles, D. (1971) "The Young Person's Guide to the Data," *Proc. AFOSR-IFP Stanford Conference on Computation of Turbulent Boundary Layers*, eds. D. Coles and E. Hirst, vol. 2, 1968, Stanford University, Calif., 1-48.

Daily, J.W. and Harleman, D.R.F. (1966) *Fluid Dynamics*, Addison-Wesley, Reading, Mass.

Dimotakis, P.E. (1976) "Single-Scattering Particle Laser-Doppler Measurements of Turbulence," *AGARD Symposium on Non-Intrusive Instrumentation in Fluid-flow Research*, Saint Louis, France, Paper 10.

Drain, L.E. (1980) *The Laser-Doppler Technique*, Wiley-Interscience, New York.

Durst, F., Melling, A.H., and Whitelaw, J.H. (1981) *Principles and Practice of Laser-Doppler Anemometry*, 2nd ed., Academic Press, London.

Drew, D.A. (1975) "Turbulent Sediment Transport over a Flat Bottom using Momentum Balance," *Journal of Applied Mechanics, Transactions of the ASME*, March, 38-44.

Einstein, H.A. (1950) *The Bedload Function for Sediment Transportation in Open Channel Flows*, Technical Bulletin No. 1026, United States Dept. of Agriculture, Soil Conservation Service, Washington D.C.

Einstein, H.A. and Chien, N. (1955) *Effects of Heavy Sediment Concentration Near the Bed on Velocity and Sediment Distribution*, MRD series #8, University of California, Institute of Engineering Research and United

States Army Engineering Division, Missouri River, Corps of Engineers, Omaha, Nebraska.

Elata, C. and Ippen, A.T. (1961) *Dynamics of Open Channel Flow with Suspensions of Neutrally Buoyant Particles*, Technical Rept. no. 45, MIT Hydrodynamics Lab., Cambridge, Mass.

George, Jr., W.K. (1978) "Processing of Random Signals," *Proceedings of the Dynamic Flow Conference, 1978*, Skovlunde, Denmark, 757-793.

Grass, A.J. (1971) "Structural Features of Turbulent Flow over Smooth and Rough Boundaries," *Journal of Fluid Mechanics*, **50**, 233-255.

Gupta, A.K. and Kaplan, R.E. (1972) "Statistical Characteristics of Reynolds Stress in a Turbulent Boundary Layer," *Physics of Fluids*, **15**, no. 6, 981-985.

Guy, H.P., Simons, D.B., and Richardson, E.V. (1966) *Summary of Alluvial Channel Data from Flume Experiments, 1956-1961*, Geological Survey, Professional Paper 462-I, United States Government Printing Service, Washington D.C.

Hill, H.M., Srinivasan, V.S., and Unny, Jr., T.E. (1969) "Instability of Flat Bed in Alluvial Channels," *Journal of the Hydraulics Division, ASCE*, **95**, HY 5, Proc. paper 6770, 1545-1556.

Hino, M. (1963) "Turbulent Flow with Suspended Particles," *Journal of the Hydraulics Division, ASCE*, **89**, HY4, Proc. Paper 3579, 161-185.

Hinze, J.O. (1972) "Turbulent Fluid and Particle Interaction," in *Progress in Heat and Mass Transfer*, **6**, 433-452, Pergamon Press, New York.

Hinze, J.O. (1975) *Turbulence*, 2nd edition, McGraw-Hill, New York.

Itakura, T and Kishi, T. (1980) "Open Channel Flow with Suspended Sediments," *Journal of the Hydraulics Division, ASCE*, HY 8, 1325-1343.

Izakson, A. (1937) *Zh. Eksper. Teor. Fiz.*, **7**, No. 7.

Kevorkian, J. and Cole, J.D. (1981) *Perturbation Methods in Applied Mathematics*, Springer-Verlag, Berlin.

Knight, D.W., Demetriou, J.D., and Hamed, M.E. (1984) "Boundary Shear in Smooth Rectangular Channels," *Journal of Hydraulic Engineering*, **110**, No. 4, 405-422.

Lau, Y.L. (1983) "Suspended Sediment Effect on Flow Resistance," *Journal of Hydraulic Engineering*, **109**, No. 5, 757-763.

Lawn, C.J. (1971) "The Determination of the Rate of Dissipation in Turbulent Pipe Flow," *Journal of Fluid Mechanics*, **48**, 477-505.

Lumley, J.L. (1976) "Two-Phase and Non-Newtonian Flows," in *Turbulence*, ed. P. Bradshaw, Springer-Verlag, Berlin, 289-324.

Lumley, J.L. and Panofsky, H.A. (1964) *The Structure of Atmospheric Turbulence*, Wiley-Interscience, New York.

McLaughlin, D.K. and Tiederman, W.G. (1973) "Biasing Correction for Individual Realization of Laser-Anemometer Measurements in Turbulent Flows," *Physics of Fluids*, **16**, No. 12, 2082-2088.

McQuivey, R.S. and Richardson, E.V. (1969) "Some Turbulence Measurements in Open-Channel Flow," *Journal of the Hydraulics Division, ASCE*, **95**, HY 1, 209-223.

McTigue, D.F. (1981) "Mixture Theory for Suspended Sediment Transport," *Journal of the Hydraulics Division, ASCE*, **107**, HY6, 659-673.

Millikan, C.B. (1939) "A Critical Discussion of Turbulent Flows in Channels and Circular Tubes," *Proceedings of the 5th International Congress of Applied Mechanics*, 386-392, Cambridge, Mass.

Monin, A.S. and Yaglom, A.M. (1971) *Statistical Fluid Mechanics*, v. 1, MIT Press, Cambridge, Mass.

Montes, J.S. and Ippen, A.T. (1973) *Interaction of Two-Dimensional Turbulent Flow with Suspended Particles*, Rept. 164, Ralph M. Parsons Laboratory for Water Resources and Hydrodynamics, Dept. of Civil Engineering, Massachusetts Institute of Technology, Cambridge, Mass.

Nakagawa, H. and Nezu, I. (1981) "Structure of Space-Time Correlations of Bursting Phenomena in an Open-Channel," *Journal of Fluid Mechanics*, **104**, 1-43.

Nezu, I. and Rodi, W. (1986) "Open Channel Flow Measurements with a Laser-Doppler Anemometer," *Journal of Hydraulic Engineering*, **112**, No. 5, 335-355.

Panofsky, H.A. (1974) "The Atmospheric Boundary Layer below 150 meters," *Annual Review of Fluid Mechanics* **6**, 142-177.

Perry, A.E. and Abell, C.J. (1975) "Scaling Laws for Pipe-Flow Turbulence," *Journal of Fluid Mechanics*, **67**, 257-271.

Raichlen, F. (1967) "Some Turbulence Measurements in Water," *Journal of the Engineering Mechanics Division, ASCE*, **93**, EM2, 73-97.

Rouse, H. (1937) "Modern Concepts of the Mechanics of Fluid Turbulence," *Transactions of the ASCE*, **102**, Paper No. 1965, 463-543.

Sabot, J. and Comte-Bellot, G. (1976) "Intermittency of Coherent Structures in the Core Region of Fully Developed Turbulent Pipe Flow," *Journal of Fluid Mechanics*, **74**, 767.

Sabot, J. and Comte-Bellot, G. (1977) "Effect of Roughness on the Intermittent Maintenance of Reynolds Shear Stress in Pipe Flow," *Physics of Fluids*, **20**, No. 10, S150-S155.

Saffman, P.G. (1962) "On the Stability of Laminar Flow of a Dusty Gas," *Journal of Fluid Mechanics*, **13**, 120-128.

Schlichting, H. (1979) *Boundary-Layer Theory*, 7th edition, McGraw-Hill, New York.

Tennekes, H. and Lumley, J.L. (1980) *A First Course in Turbulence*, MIT Press, Cambridge, Mass.

Tsuji, Y. and Morikawa, Y. (1982) "LDV Measurement of an Air-Solid Two-Phase Flow in an Horizontal Pipe," *Journnal of Fluid Mechanics*, **120**, 385-409.

van Ingen, C. (1981) *Observations in a Sediment-Laden Flow by Use of Laser-Doppler Velocimetry*, Rept. KH-R-42, W. M. Keck Laboratory of Hydraulics and Water Resources, California Institute of Technology, Pasadena, Calif.

van Ingen, C. (1983a) *Observations of Sediment-Laden Flows by Use of Laser-Doppler Velocimetry*, UCB/HEL-83/02, Hydraulic Engineering Laboratory, University of California, Berkeley, Calif.

van Ingen, C. (1983b) *A Signal-Processing System for Laser-Doppler Velocimetry in Solid-Liquid Flows*, UCB/HEL-83/03, Hydraulic Engineering Laboratory, University of California, Berkeley, Calif.

van Rijn, L.C. (1984) "Sediment Transport, Part II: Suspended Load Transport," *Journal of Hydraulic Engineering*, **110**, no. 11, 1613-1641.

Vanoni, V.A. (1946) "Transportation of Suspended Sediment by Water," *Transactions of the ASCE*, **111**, Paper no. 2267, 67-133.

Vanoni, V.A. (1953) "Some Effects of Suspended Sediment on Flow Characteristics," *Proceedings of the Fifth Hydraulics Conference*, Bulletin 34, State University of Iowa Studies in Engineering, Iowa City.

Vanoni, V.A. (1974) "Factors Determining Bed Forms of Alluvial Streams," *Journal of the Hydraulics Division*, Proceedings of the ASCE, **100**, HY3, 363-377.

Vanoni, V.A. (1977) "Suspension of Sediment" in *Sedimentation Engineering*, ed. V.A. Vanoni, American Society of Civil Engineers, New York, 66-91.

Vanoni, V.A. and Nomicos, G.N. (1960) "Resistance Properties of Sediment-Laden Streams," *Transactions of the ASCE*, **125**, Paper no. 3055, 1140-1175.

Whitham, G.B. (1974) *Linear and Nonlinear Waves*, Wiley-Interscience, New York.

Yalin, M.S. and Karahan, E. (1981) "On the Development of Turbulent Boundary Layers in Open-Channel Flows," *Proceedings of the Seventh Symposium in Turbulence*, University of Missouri-Rolla, Missouri-Rolla.

A.1 Quadrant analysis

Another indication of the structure of Reynolds-stresses, and hence of turbulence, is obtained from the so-called quadrant analysis introduced by Willmarth and Lu (1971) and Wallace et al. (1972). This analysis sorts the contribution to the total $u'v'$ according to the quadrant of the u'-v' plane in which the signal is found. From this, it has been shown that the bulk of the Reynolds' stress results from events in the second and, particularly, the fourth quadrants, termed sweeps and ejections. The concept of a "hole" in the u'-v' plane provides a further classification of contributions, taking into account the relative magnitude of the contributions (Willmarth, 1975). The fractional contribution to $u'v'$ from the individual quadrants was computed as

$$\frac{[u'v']_J(H)}{u'v'} = \frac{1}{u'v'} \sum_{i=1}^{N} (u'v')_i S_J(H), \qquad (A.1.1)$$

where the subscripts i refer to individual velocity realizations, J refers to the j^{th}-quadrant, H is the hole size, and

$$S_J(H) = \begin{cases} 1, & \text{if } |(u'v')_i| > H \cdot u'v', \text{ and the point, } (u'v') \\ & \text{in the } u' - v' \text{ plane is in the } j^{\text{th}}\text{-quadrant;} \\ 0, & \text{otherwise.} \end{cases} \qquad (A.1.2)$$

The results of this classification for the clear-water experiments at an elevation of $\eta \approx 0.4$ (the specific time series used for the spectral analysis of vertical velocity fluctuations were used here also) are shown in Fig. A.1.1. A comparison with other investigations show broad agreement, verifying that this type of statistics can be computed with the available data. A conventional definition of the "turbulent burst" is often made as those event swhich are found outside a hole size, $H = 4$, although Sabot and Comte-Bellot (1977) have suggested that $H \approx 3$ may be more appropriate for the core region of a pipe. A determination of the average time interval between bursts so defined was not found feasible with the available data because of the relatively slow data rate.

Fig. A.1.1 Quadrant analysis of Reynolds stresses: clear-water flows

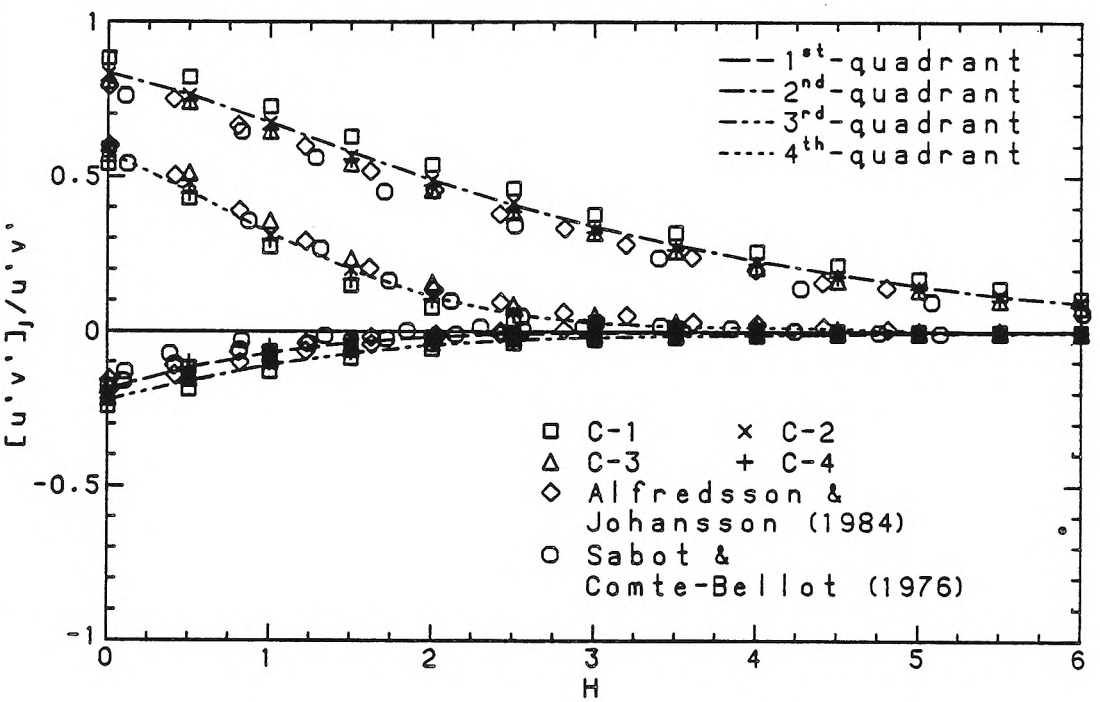

Fig. A.1.2 gives results for both equilibrium-bed and starved-bed cases. An effect of the aspect ratio is seen, particularly in the 2nd results. There is, however,

little sign of any difference from clear-water results that may be attributed to the presence of sediment.

References

Alfredsson, P. H. and Johansson, A. V. (1984) "On the Detection of Turbulence-Generating Events," *Journal of Fluid Mechanics*, **139**, 325-345.

Sabot, J. and Comte-Bellot, G. (1977) "Effect of Roughness on the Intermittent Maintenance of Reynolds Shear Stress in Pipe Flow," *Physics of Fluids*, **20**, No. 10, S150-S155.

Wallace, J.M., Eckelmann, H., Brodkey, R.S. (1972) "The Wall Region in Turbulent Shear Flow," *Journal of Fluid Mechanics*, **54**, 39-48.

Willmarth, W.W. (1975) "Structure of Turbulence in Boundary Layers," *Advances in Applied Mechanics*, **15**, 159-254.

Willmarth, W.W. and Lu, S.S. (1971) "Structure of the Reynolds Stress Near the Wall," *Journal of Fluid Mechanics*, **55**, 65-92.

Fig. A.1.2 Quadrant analysis of sediment-laden flows
a) equilibrium-bed , b) starved-bed flows

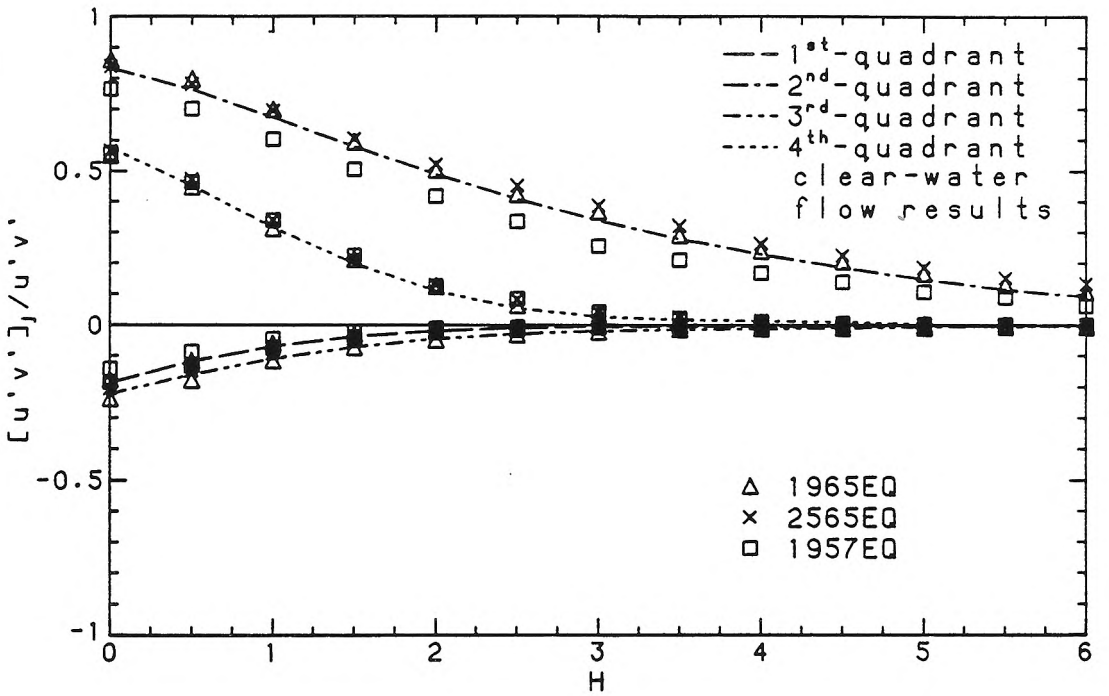

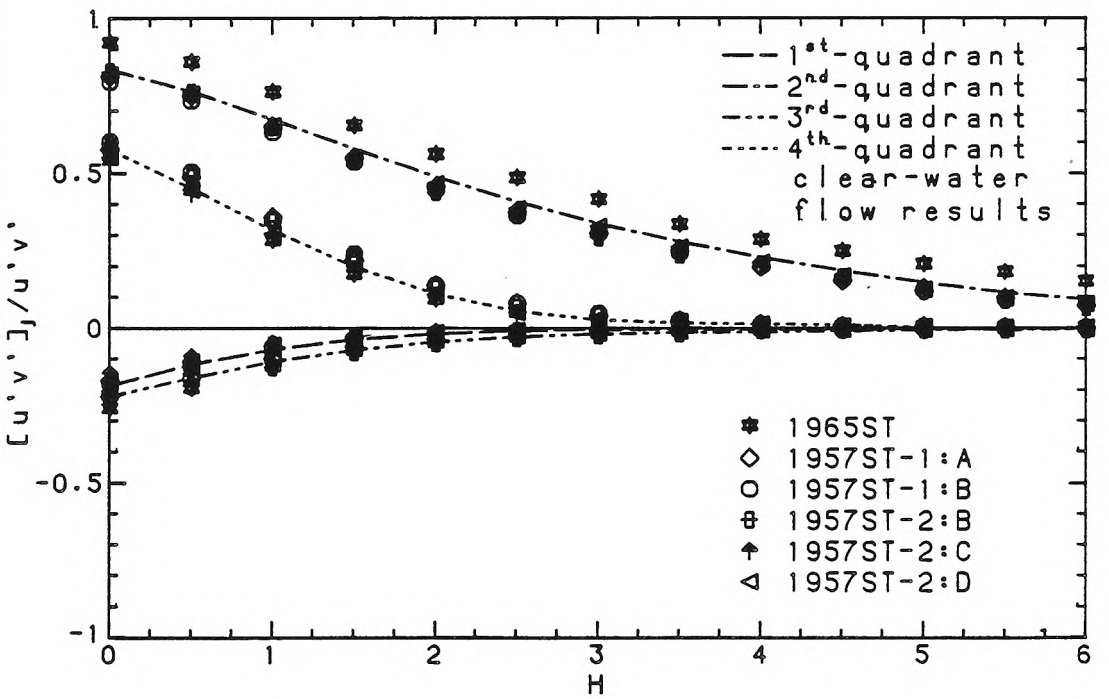

A.2 Gross flow characteristics

Table A.2.1 summarizes the gross flow characteristics, except the friction factor, of all sediment-laden flow experiments performed during this study. A similar table for clear-water flow experiments may be found in Table 5.1.2.

Table A.2.2 tabulates various estimates of the friction factors for the experiments discussed in §6.4. The labelling of the experiments follows that used in Chapters 5 and 6. For data from other sources, BRK refers to Brooks (1954), BL to Barton and Lin (1955), and GUY to Guy et al. (1966), and the accompanying number refers to the run number. In the case of data from the present experiments, EQ refers to equilibrium-bed flows, ST to starved-bed flows, and C to clear-water flows. For a series of starved-bed experiments, the suffix indicates the relative degree of suspended load; e.g., A has the most suspended load, then B, and so on. The comparison of friction factors, given in Fig. 6.4.1, between clear-water and sediment-laden flows was based on f_D and $(f_D)_{cw}$. The differences between f_D and the other estimates are typically less than 10%; moreover, f_D is not consistently larger or smaller than the other estimates. The qualitative conclusions of §6.4 do not, therefore, rely on any particular way of estimating the friction factor.

For additional definitions, the list of notation may be consulted.

Table A.2.1 Summary of flow characteristics: sediment-laden flows

	equilibrium-bed				starved-bed						
					1965ST	1957ST-1		1957ST-2			
	1565	1965	2565	1957		A	B	A	B	C	D
T (°C)	20.7	21.1	21.3	20.9	21.1	21.1	21.4	21.2	21.1	21.6	21.3
Q (l/s)	10.8	11.1	12.1	9.9	11.1	10.3	10.3	12.1	12.4	12.6	12.6
h (cm)	6.45	6.51	6.54	5.72	6.58	5.69	5.68	5.84	5.77	5.75	5.74
r_h (cm)	4.35	4.36	4.39	4.00	4.41	3.99	3.98	4.06	4.03	4.02	4.02
b/h	4.14	4.10	4.08	4.67	4.05	4.69	4.70	4.57	4.62	4.64	4.65
S ($\times 10^{-3}$)	2.44	2.51	2.96	2.95	2.49	2.99	2.98	4.00	3.95	4.00	4.00
$u_*^{\dagger}$ (cm/s)	3.58	3.75	4.25	3.95	3.57	3.74	3.69	4.25	4.31	4.28	4.34
$\sqrt{gSh}$ (cm/s)	3.93	4.00	4.36	4.07	4.01	4.08	4.07	4.78	4.73	4.75	4.74
$\sqrt{gSr_h}$ (cm/s)	3.23	3.28	3.57	3.40	3.28	3.42	3.42	3.99	3.95	3.97	3.97
$u_{\max}$ (cm/s)	75.7	77.7	85.9	79.3	78.0	83.3	84.9	95.8	98.8	100.4	100.4
$\langle u \rangle^{\dagger\dagger}$ (cm/s)	64.9	67.1	74.4	67.2	68.3	71.8	73.6	81.4	86.2	87.9	87.6
$\langle\langle u \rangle\rangle^{\dagger\dagger\dagger}$ (cm/s)	62.8	63.6	69.2	64.6	63.3	68.0	68.0	77.8	80.8	82.0	82.0
$c^{\ddagger}(\eta = 0.1)$ ($\times 10^{-3}$)	1.9	1.1	0.72	1.0	1.0	0.55	0.24	2.08	0.80	0.47	0.31
$c(\eta = 0.5)$ ($\times 10^{-4}$)	0.94	0.31	0.05	0.21	0.18	0.22	0.13	0.65	0.42	0.29	0.19
d_{50} (mm)	0.15	0.19	0.24	0.19	0.19	0.19	0.19	0.19	0.19	0.19	0.19
σ_g	1.12	1.20	1.18	1.20	1.20	1.20	1.20	1.20	1.20	1.20	1.20
w_{s0} (cm/s)	1.6	2.3	3.1	2.3	2.3	2.3	2.3	2.3	2.3	2.3	2.3
w_{s0}/u_*	0.45	0.61	0.73	0.58	0.64	0.61	0.62	0.54	0.53	0.54	0.54
$Fr \equiv \langle u \rangle / \sqrt{gh}$	0.82	0.84	0.93	0.90	0.85	0.96	0.99	1.08	1.15	1.17	1.17
$Re \equiv 4\langle u \rangle r_h/\nu$ ($\times 10^5$)	1.13	1.18	1.31	1.08	1.20	1.15	1.17	1.32	1.39	1.41	1.41
$Re_* \equiv u_* h/\nu$ ($\times 10^3$)	2.31	2.44	2.78	2.26	2.35	2.13	2.10	2.34	2.28	2.30	2.30

† estimated using Reynolds-stress profiles (except 1565)

†† numerically integrated from centerline measurements

††† based on bulk discharge and flow area

‡ concentrations at $\eta = 0.1$ and $\eta = 0.5$ estimated from interpolation of measured concentration profiles

Table A.2.2 Estimates of friction factors

Experiment	$f_D^{\dagger}$	$\langle\langle f_D\rangle\rangle^{\dagger\dagger}$	$\langle\langle f_D\rangle\rangle_{\text{swc}}^{\dagger\dagger\dagger}$	$(f_D)_B^{\ddagger}$	$(f_D)_{\text{cw}}^{\ddagger\ddagger}$
C-1	0.0170	0.0184	0.0188		0.0185
C-2	0.0179	0.0175	0.0177		0.0185
C-3	0.0182	0.0189	0.0195		0.0190
C-4	0.0186	0.0181	0.0186		0.0190
1565EQ	0.0243	0.0212	0.0228	0.0300	0.0180
1965EQ	0.0250	0.0213	0.0229	0.0320	0.0183
2565EQ	0.0254	0.0213	0.0231	0.0348	0.0192
1957EQ	0.0276	0.0222	0.0238	0.0330	0.0188
1965ST	0.0219	0.0217	0.0235		0.0183
1957ST-1:A	0.0211	0.0202	0.0214		0.0186
1957ST-1:B	0.0207	0.0202	0.0214		0.0186
1957ST-2:A	0.0218	0.0210	0.0225		0.0186
1957ST-2:B	0.0200	0.0193	0.0202		0.0186
1957ST-2:C	0.0190	0.0187	0.0194		0.0186
1957ST-2:D	0.0196	0.0187	0.0194		0.0186
BRK7	0.0182	0.0204	0.0220	0.0293	0.0180
BRK21	0.0197	0.0204	0.0220	0.0260	0.0178
BRK29	0.0176	0.0180	0.0185	0.0252	0.0177
BL36	0.0193	0.0176	0.0185	0.0256	0.0147
BL35	0.0190	0.0175	0.0186	0.0248	0.0146
BL31	0.0173	0.0176	0.0182	0.0255	0.0150
BL29	0.0282	0.0246	0.0275	0.0232	0.0148
BL26	0.0275	0.0257	0.0296	0.0227	0.0146
GUY46	0.0200	0.0184	0.0194	0.0267	0.0148
GUY26	0.0282	0.0252	0.0265	0.0338	0.0187
GUY25	0.0211	0.0177	0.0186	0.0276	0.0150
GUY15	0.0146	0.0159	0.0166	0.0238	0.0129

† $f_D \equiv 8(u_*/\langle u\rangle)^2$

†† $\langle\langle f_D\rangle\rangle \equiv 8gr_hS/\langle\langle u\rangle\rangle^2$

††† based on $\langle\langle f_D\rangle\rangle$ but incorporating a sidewall correction (Brooks, 1954)

‡ computed from the friction factor predictor for upper regime flow proposed by Brownlie (1981)

‡‡ friction factor for a clear-water flow of equal $Re = 4\langle\langle u\rangle\rangle r_h/\nu$ and a relative roughness, $d_{50}/4r_h$, estimated from Brownlie (1981)

#26018